2023

U.S. Department of Transportation Federal Highway Administration

NEBRASKA DEPARTMENT OF TRANSPORTATION

NEBRASKA TRANSPORTATION CENTER

Final Report SPR-FY22(010)

WBS Report #
26-1120-0117-001

Feasibility Study: Application of Steel Sheet-Piles for the Abutment of Water-Crossing Bridges in Nebraska

Seunghee Kim, PhD, PE
Associate Professor
Department of Civil and Environmental Engineering
University of Nebraska-Lincoln

Jongwan Eun, PhD, PE
Associate Professor

Chung R Song, PhD, AE
Associate Professor

Chungwook Sim, PhD
Associate Professor

Hung Van Phi, MS
Graduate Student

Basil Abualshar, MS
Graduate Student

Ramin Ziaei, MS
Graduate Student

Nebraska Department of Transportation Research
Headquarters Address
1400 Nebraska Parkway
Lincoln, NE 68509
ndot.research@nebraska.gov
(402) 479-4697
https://dot.nebraska.gov/business-center/research/

Nebraska Transportation Center
262 Prem S. Paul Research Center at Whittier School
2200 Vine Street
Lincoln, NE 68583-0851
(402) 472-1932
http://ntc.unl.edu

This report was funded in part through grant from the U.S. Department of Transportation Federal Highway Administration. The views and opinions of the authors expressed herein do not necessarily state or reflect those of the U.S. Department of Transportation.

TECHNICAL REPORT DOCUMENTATION PAGE

1. Report No. SPR-FY22(010)	**2. Government Accession No.**	**3. Recipient's Catalog No.**
4. Title and Subtitle Feasibility Study: Application of Steel Sheet-Piles for the Abutment of Water-Crossing Bridges in Nebraska		**5. Report Date** May 2023 **6. Performing Organization Code**
7. Author(s) Seunghee Kim, Jongwan Eun, Chung R. Song, Chungwook Sim, Hung Van Phi, Basil Abualshar, and Ramin Ziaei		**8. Performing Organization Report No.** If applicable, enter any/all unique numbers assigned to the performing organization.
9. Performing Organization Name and Address Board of Regents, University of Nebraska-Lincoln		**10. Work Unit No.** **11. Contract** SPR-FY22(010)
12. Sponsoring Agency Name and Address Nebraska Department of Transportation Research Section 1400 Hwy 2 Lincoln, NE 68502		**13. Type of Report and Period Covered** Final Report July 2021 – May 2023 **14. Sponsoring Agency Code**

15. Supplementary Notes
If applicable, enter information not included elsewhere, such as translation of (or by), report supersedes, old edition number, alternate title (e.g. project name), or hypertext links to documents or related information.

16. Abstract
The overall goal of this study is to investigate the anticipated performance of steel sheet-pile bridge abutments to encourage its wider application to not only new construction but also repair and replacement of existing water-crossing bridges in Nebraska. For this purpose, this study first reviewed several bridge cases with axially loaded sheet pile abutments, as well as previous in-depth studies related to the bearing capacity of sheet piles. Then, this study conducted the large-scale direct shear tests to better understand the interaction between sheet pile and soil. As a result, about four-fifths of the internal friction angle of fill sand was obtained as the interface friction angle. After that, this study conducted the static pile loading test with a down-sized test sheet pile. The ultimate bearing capacity of sheet piles obtained from three separate static pile loading tests was consistent. Analysis showed that the pile shaft carried most of the load (70% to 75%), while the tip resistance contributed up to 25% of the total bearing capacity. The CPT-based method resulted in an adequate match with the field test data, while the analytical method and SPT-based method appeared to slightly over- and under-estimate the side frictional resistance, respectively. Nonetheless, all predictions were comparable to the static loading test results. Upon the validation of the numerical simulation model, an extensive parametric study was conducted to investigate how various parameters may affect the performance of the sheet pile abutment system under the combined axial and lateral loading. After that, a summary of parametric numerical study results, including the maximum horizontal deflection, maximum vertical settlement, the factor of safety against shear failure, and the factor of safety against bending failure was prepared. Based on the study results, recommendations were made for follow-up research.

17. Key Words Sheet pile, sheet pile abutment bridge, bridge abutment, large-scale direct shear test, field test, numerical modeling, parametric study.	**18. Distribution Statement** No restrictions. This document is available through the National Technical Information Service. 5285 Port Royal Road Springfield, VA 22161

19. Security Classification (of this report) Unclassified	**20. Security Classification (of this page)** Unclassified	**21. No. of Pages** 216	**22. Price**

Form DOT F 1700.7 (8-72) Reproduction of completed page authorized

Disclaimer

The contents of this report reflect the views of the authors, who are responsible for the facts and the accuracy of the information presented herein. The contents do not necessarily reflect the official views or policies neither of the Nebraska Department of Transportations nor the University of Nebraska-Lincoln. This report does not constitute a standard, specification, or regulation. Trade or manufacturers' names, which may appear in this report, are cited only because they are considered essential to the objectives of the report.

The United States (U.S.) government and the State of Nebraska do not endorse products or manufacturers. This material is based upon work supported by the Federal Highway Administration under SPR-FY22(010). Any opinions, findings and conclusions or recommendations expressed in this publication are those of the author(s) and do not necessarily reflect the views of the Federal Highway Administration.

This report has been reviewed by the Nebraska Transportation Center for grammar and context, formatting, and 508 compliance.

Table of Contents

Disclaimer 3
Table of Contents 4
List of Figures 7
List of Tables 14
Chapter 1 Introduction 17
1.1 Background 17
1.2 Problem Statement 22
1.3 Objective of the Study 24
Chapter 2 Literature Review 27
2.1 Bridges with the Sheet Pile Abutments 27
2.1.1 Humber Road Bridge, Immingham, England 27
2.1.2 Canal Bridge, Stoke-on-Trent, England 28
2.1.3 A Bridge in Black Hawk County, IA 29
2.1.4 A Bridge in Tama County, IA 30
2.1.5 Route 4 Bridge in Sprout Brook, NJ 31
2.1.6 A Bridge over Klutuk Creek in Ekwok, AK 32
2.1.7 Summary - Bridges with the Sheet Pile Abutments 33
2.2 Bearing Capacity of Sheet Pile 36
2.2.1 Static Pile Load Test of Sheet Piles in Dense Sand (Durik, France) 36
2.2.2 Static Pile Load Test of Sheet Piles in Dense Clay (Merville, France) 37
2.2.3 Static Pile Load Test of Sheet Piles in Sand (Matthews, North Carolina) 40
2.2.4 Application of Sheet Piles as Permanent Building Foundations 43
2.2.5 Summary 46
Chapter 3 Large-Scale Direct Shear Tests 48
3.1 Testing Setup 48
3.2 Material 49
3.2.1 Steel plate 49
3.2.2 Fill Sand 50
3.3 Testing Procedure 53
3.4 Test Results 58
3.4.1 Internal Angle of Friction of Sand 58
3.4.2 Interface Friction Angle between Sand and Steel Plate 59
3.5 Interpretation 60
Chapter 4 Down-Sized Pile Load Tests 63
4.1 Estimate of Bearing Capacity of Sheet Pile: Analytical & Empirical Approaches 63
4.1.1 Analytical Approach 63
4.1.2 SPT-Based Estimate 65
4.1.3 CPT-Based Estimate 66
4.2 Estimate of Bearing Capacity: Axial Loading Test 67
4.3 Axial Loading Test of the Model Sheet Pile 69
4.3.1 Test Site 69
4.3.2 Fill Soil 72
4.3.3 Site Investigation of the Test Site 73

4.3.4 Summary: Site Investigation and Prediction of Bearing Capacity of the Test Sheet Pile 77
4.3.5 Preparation of Down-Sized Test Sheet-Pile 79
4.3.6 Setup of the Axial Loading Test 84
4.3.7 Test Procedure 86
4.4 Numerical Modeling of the Axial Loading Test 87
4.5 Test Results 89
4.6 Comparison and Discussion 91
Chapter 5 Numerical Studies: Validation of the Simulation Model 93
5.1 Introduction 93
5.2 Validation of Numerical Method: Axial Loading 94
5.2.1 Pile-Soil Interface Parameters 97
5.2.2 Numerical Simulation Model 97
5.2.3 Material Properties 98
5.2.4 Results 100
5.3 Validation of Numerical Method: Lateral Loading 100
5.3.1 Validation #1 101
5.3.2 Validation #2 106
5.4 Validation of Numerical Method: Axial + Lateral Loading (1) 110
5.4.1 Dimensions of the Bridge 110
5.4.2 Design Load 112
5.4.3 Material Properties 113
5.4.4 Numerical Simulation Model 115
5.4.5 Results 116
5.5 Validation of Numerical Method: Axial + Lateral Loading (2) 118
5.5.1 Dimension of the Bridge 119
5.5.2 Anchoring 120
5.5.3 Instrumentation and Monitoring 121
5.5.4 Design Load 123
5.5.5 Soil Properties 124
5.5.6 Material Properties 127
5.5.7 Cable Element 129
5.5.8 Numerical Simulation Model 131
5.5.9 Results 132
Chapter 6 Numerical Studies: A Parametric Study 134
6.1 Bridge Site Selected for Parametric Study 134
6.1.1 Bridge Dimension 135
6.1.2 Soil Properties 137
6.1.3 Pile-Soil Interface Parameters 141
6.1.4 The Base Model for Parametric Study 142
6.2 Case 1 143
6.2.1 Parameters 143
6.2.2 Results 144
6.3 Case 2 148
6.3.1 Parameters 148
6.3.2 Results 149

6.4 Case 3 153
6.4.1 Parameters 153
6.4.2 Results 154
6.5 Case 4 163
6.5.1 Parameters 163
6.5.2 Results 164
6.6 Case 5 168
6.6.1 Parameters 168
6.6.2 Results 170
6.7 Case 6 175
6.7.1 Parameters 175
6.7.2 Results 177
6.8 Case 7 181
6.8.1 Parameters 181
6.8.2 Results 182
6.9 Case 8 186
6.9.1 Parameters 186
6.9.2 Results 188
6.10 Case 9 192
6.10.1 Parameters 192
6.10.2 Results 194
6.11 Summary 200
Chapter 7 Conclusions and Recommendations 206
7.1 Conclusions 206
7.2 Recommendations for Future Work 209
References 212

List of Figures

Figure 1.1 (a) An example of design guidelines that include both bearing and sheet piling for scour protection, and (b) sheet pile abutment cap geometry (Sections 4.1 and 4.2 of BOPP; Nebraska Department of Roads, 2016)..... 17
Figure 1.2 The number: single- and multi-span bridges in Nebraska (left) and by span length (right). 18
Figure 1.3 Nebraska bridges: (a) the number of single-span bridges built by decade, and (b) the location of single-span bridges by counties in Nebraska. 18
Figure 1.4 A design example of the sheet pile cantilever wall (left) and anchored retaining wall acting as a bridge abutment (right). Images are from Yandzio (1998)..... 19
Figure 1.5 An example of sheet pile abutment bridges in Europe. (a) Humber Road bridge (Immingham, UK), and (b) Canal bridge (Stoke-on-Trent, UK). Images are from Yandzio (1998)..... 20
Figure 1.6 An example of a county bridge in Nebraska with solid planks and sheet pile abutments. 21
Figure 1.7 An example of sheet pile abutment bridges in the USA. (a) Small Creek bridge (Seward, Alaska), (b) Taghkanic Creek bridge (New York), (c) Banks Road bridge (New York), and (d) Black Hawk county bridge (Iowa). Images are from Evans et al. (2012). 22
Figure 1.8 Current semi-integral abutment bridge design in Nebraska. Note: black shades are where elastomeric paddings are used to allow horizontal movement between the superstructure and substructure. 24
Figure 2.1 Humber Road Bridge, Immingham, England (the image from Yandzio, 1998). 28
Figure 2.2 Canal bridge, Stoke-on-Trent, England (the image from Yandzio, 1998). 29
Figure 2.3 A plan view of the sheet pile abutment and backfill retaining system for demonstration projects in BHC, Iowa (Evans et al., 2011). 30
Figure 2.4 A plan view of the sheet pile abutment and backfill retaining system for demonstration projects in Tama County, Iowa (Evans et al., 2011). 31
Figure 2.5 A substructure redesign for Route 4 Bridge over Sprout Brook (from Nucor Skyline, 2021). 32
Figure 2.6 The cross sections of test sheet pile and box pile (Bustamante and Gianeselli, 1991). 36
Figure 2.7 An estimate of ultimate bearing capacity of the sheet pile walls and box piles from the pile load test (Bustamante and Gianeselli, 1991). 37
Figure 2.8 CPT and SPT soil profiles at the test site, Merville, France (Bustamante and Gianeselli, 1991)..... 38
Figure 2.9 A pile load test result of the sheet pile in clayey soil (Bustamante and Gianeselli, 1991). 39
Figure 2.10 The obtained *T-Z* function curves of the skin resistance for sheet pile elements (Bustamante and Gianeselli, 1991)..... 40
Figure 2.11 Site investigation data for the pile loading test site in Matthews, North Carolina (Sylvain, 2019). 42
Figure 2.12 A comparison of the static axial pile loading tests performed at a field site in Matthews, North Carolina (Sylvain, 2019). 43
Figure 2.13 An example of sheet piling as a permanent foundation (with a temporary soil berm) for the construction of below-grade precast concrete framing (Underwood, 2020). 44

Figure 2.14 Average ultimate skin friction values *vs*. relative density of granular soils estimated from PDA tests (Underwood, 2020). 45
Figure 3.1 A schematic diagram of the large-scale direct shear testing setup for this research. 49
Figure 3.2 Fabrication of the sheet pile sample for large-scale direct shear test. 50
Figure 3.3 The sample of steel plate for large-scale direct shear test. 51
Figure 3.4 The location where the research team acquired the fill sand. 52
Figure 3.5 The grain size distribution of the collected fill sand. 53
Figure 3.6 Fill sand in the shear box. 55
Figure 3.7 Load cell to measure the vertical normal stress. 55
Figure 3.8 The piston and vertical LVDT placed on top of the shear box. 56
Figure 3.9 The horizontal LVDT. 56
Figure 3.10 Clamping of the steel sample with the bottom shear box. 57
Figure 3.11 Implementation of the large-scale direct shear tests in (a) dry, and (b) submerge conditions. 57
Figure 3.12 The complete setup of the large-scale direct shear tests. 58
Figure 3.13 The shear stress-displacement curves for the sand only condition. 59
Figure 3.14 The shear stress-displacement curves for the sand-steel plate interface in dry condition. 60
Figure 3.15 The shear stress-displacement curves for the sand-steel plate interface in submerged condition. 60
Figure 3.16 The compiled normal stress-shear stress data to determine the friction angle. 61
Figure 4.1 Variation of α' with an embedment ratio of pile in sand: electric cone penetrometer (Das and Sivakugan, 2019). 67
Figure 4.2 The static pile loading test: (a) using kentledge, (b) using reaction pile, (c) load *vs*. total settlement plots, and (d) load *vs*. net settlement (image from Das and Sivakugan, 2019). 68
Figure 4.3 Davisson's method for the determination of Q_u (image from Das and Sivakugan, 2019). 69
Figure 4.4 The location of the test site at the Midwest Roadside Safety Facility (MwRSF). 70
Figure 4.5 A photo of the test pit after excavation. 71
Figure 4.6 The drawing and dimensions of the test pit with a sheet pile. 71
Figure 4.7 The fill sand used for the static pile loading test. 72
Figure 4.8 The grain size distribution of sand used for the static pile loading test. 73
Figure 4.9 Geoprobe 7822 DT used for the subsurface investigation of the test site. 74
Figure 4.10 Top view: the location of SPT and CPT tests on the test site. 75
Figure 4.11 SPT test conducted by the research team. 75
Figure 4.12 Original *N* values obtained from the SPT test. 76
Figure 4.13 CPT test conducted by the research team. 76
Figure 4.14 The tip resistance q_c, and skin resistance f_s (left to right) obtained from CPT tests. 77
Figure 4.15 A photo: the piece of test sheet piles (1 m long each), with the bearing plate. 79
Figure 4.16 The location of strain gauges (one electric resistive and vibrating wire strain gauge at each depth) attached on the test sheet pile. 80
Figure 4.17 Cleaning liquid and adhesive used for resistive strain gauge installation (from Micro-Measurements VPG). 81
Figure 4.18 Actual photo of resistive and vibrating strain gauges attached to the test sheet pile. 82
Figure 4.19 The protection kit for strain gauges (from GEOKON). 82

Figure 4.20 Welding of an outside cover for strain gauges. 83
Figure 4.21 An overall setup for the axial loading test with the model sheet pile..... 84
Figure 4.22 A photo of the axial loading test setup with the reaction beam (front view). 85
Figure 4.23 A photo of the axial loading test setup with the reaction beam (side view)..... 85
Figure 4.24 The vertical LVDT installed on the top of the bearing plate..... 86
Figure 4.25 A photo of the overall axial loading test setup. 87
Figure 4.26 Constructed numerical model in FLAC for the static axial loading test. 88
Figure 4.27 Applied axial load *vs*. displacement curves obtained from three static axial loading tests and complementary numerical simulation using FLAC..... 89
Figure 4.28 Load transfer along the pile length. Data is obtained from strain gauges attached to the test sheet pile (axial loading test #1)..... 90
Figure 4.29 Load transfer along the pile length. Data is obtained from strain gauges attached to the test sheet pile (axial loading test #2)..... 91
Figure 5.1 An example of maximum unbalanced force for the problem of sudden end-load application to a column (Itasca Consulting Group, 2019)..... 94
Figure 5.2 The combined axial and lateral loads imposed on the sheet pile abutment system. ... 94
Figure 5.3 The location and relationships of the pile element and beam element in the domain. 95
Figure 5.4 A numerical simulation model with the beam element (left), and the pile element (right). 97
Figure 5.5 The comparison of vertical settlements from the models that use either the beam element or pile element. Three level of axial loads (10 kN, 100 kN, and 1000 kN) is applied to the numerical simulation. Note: 1 inch = 2.54 cm. 100
Figure 5.6 A lane load applied over two infinite 3 m wide strips (Mullins et al., 2009)..... 101
Figure 5.7 A cross-section of the numerical model with layered zones (Mullins et al., 2009). . 102
Figure 5.8 The numerical simulation model on the sheet pile wall conducted by the project team at USF (from Mullins et al., 2009). 104
Figure 5.9 A contour of horizontal displacements after about 6.1 m (20 ft) excavation with no roadway (PZ-27 in stronger soil; Mullins et al., 2009). 104
Figure 5.10 The numerical simulation model made by the project team at UNL (PZ27 sheet pile with no roadway) for the validation of lateral load retainment. 105
Figure 5.11 The comparison of horizontal displacements of the sheet pile wall from the numerical model by the project team at UNL and literature (USF). 106
Figure 5.12 The geometry of the sheet pile retaining wall for numerical modeling (Day and Potts, 1993). 106
Figure 5.13 Finite element meshes constructed for the numerical simulation in the literature (Day and Potts, 1993). 108
Figure 5.14 A comparison of horizontal displacements of the low-modulus and high-modulus piles from the numerical simulations by the project team and in the literature (Day and Potts, 1993). 109
Figure 5.15 The dimensions of the bridge (Nucor Skyline, 2021) used for the validation of combined axial + lateral loading on the sheet pile abutment. 110
Figure 5.16 The cross-section and dimension of the bridge (Nucor Skyline, 2021) used for the validation of combined axial + lateral loading on the sheet pile abutment. 111
Figure 5.17 The side view of the sheet pile abutment (Nucor Skyline, 2021) used for the validation of combined axial + lateral loading on the sheet pile abutment. 111
Figure 5.18 The section of the reinforced concrete cap beam (Nucor Skyline, 2021). 112

Figure 5.19 The numerical simulation model reconstructed by the project team at UNL for the validation of combined vertical + lateral loads. 115
Figure 5.20 Simulation results: (a) vertical stress contour, and (b) horizontal stress contour in the model. 116
Figure 5.21 Simulation results: horizontal displacement of the sheet pile wall. 117
Figure 5.22 Simulation results: vertical settlement of the sheet pile wall. 118
Figure 5.23 As-built profile of bridge for the project in BHC, Iowa (Evans et al., 2011)..... 119
Figure 5.24 Precast abutment cap and contact between bridge deck, abutment cap, and sheet piling foundation in BHC, Iowa (from Evans et al., 2011). 120
Figure 5.25 Plan view of the sheet pile abutment and retaining backfill system for a demonstration project in BHC, Iowa (from Evans et al., 2011). 121
Figure 5.26 The installation of displacement transducers in the demonstration bridge project site (Evans et al., 2011). 122
Figure 5.27 Installation of Earth pressure cells behind the sheet pile abutment (Evans et al., 2011). 123
Figure 5.28 Soil boring log (SB 2) for the bridge demonstration project site in BHC, Iowa (Evans et al., 2011). 125
Figure 5.29 Direct shear test results on backfill material for the bridge demonstration project site in BHC, Iowa (Evans et al., 2011). 126
Figure 5.30 Conceptual mechanical representation of fully bonded reinforcement which accounts for the shear behavior of the grout annulus (Itasca Consulting Group, 2019). 130
Figure 5.31 The numerical simulation model in FLAC to compare the results with field data from the demonstration bridge site in IOWA. 131
Figure 5.32 Simulation results: (a) vertical stress contour, and (b) horizontal stress contour in the model. 132
Figure 5.33 Simulation results: horizontal deflection of the sheet pile wall. 133
Figure 6.1 Geological profile and elevation of the bridge located in Tarnov South, Platte County, Nebraska – selected bridge site for the parametric study of the sheet pile abutment system. 134
Figure 6.2 Pile Layout of the bridge in Tarnov South, Platte County, Nebraska – selected bridge site for the parametric study of the sheet pile abutment system. 135
Figure 6.3 Abutment cross section of the bridge in Tarnov South, Platte County, Nebraska. ... 137
Figure 6.4 The base numerical simulation model for the parametric study of this project. 143
Figure 6.5 Parametric study Case 1: Horizontal deflection of the sheet pile wall for different span lengths. 145
Figure 6.6 An expected P-Delta effect on the behavior of the sheet pile abutment that is subjected to the combined axial and lateral loads. 145
Figure 6.7 Parametric study Case 1: Vertical settlement of the sheet pile wall for different span lengths. 146
Figure 6.8 Parametric study Case 1: Shear force imposed on the sheet pile wall for different span lengths. 147
Figure 6.9 Parametric study Case 1: Bending moment imposed on the sheet pile wall for different span lengths. 148
Figure 6.10 Simulation of the sheet pile wall with different excavation depths: 0.5 m, 1.5 m, and 2.5 m (1.6, 4.9, and 8.2 ft). 149

Figure 6.11 Parametric study Case 2: Horizontal deflection of the sheet pile wall for different excavation levels..... 150
Figure 6.12 Parametric study Case 2: Vertical settlement of the sheet pile wall for different excavation levels..... 151
Figure 6.13 Parametric study Case 2: Shear force imposed on the sheet pile wall for different excavation levels..... 152
Figure 6.14 Parametric study Case 2: Bending moment imposed on the sheet pile wall for different excavation levels..... 153
Figure 6.15 Parametric study Case 3: Horizontal deflection of the sheet pile wall for different sheet pile sections (a base condition with a span length of 60 ft and excavation level of 4.9 ft (1.5 m)). 156
Figure 6.16 Parametric study Case 3: Vertical settlement of the sheet pile wall for different sheet pile sections (a base condition with a span length of 60 ft and excavation level of 4.9 ft (1.5 m)). 157
Figure 6.17 Parametric study Case 3: Shear force imposed on the sheet pile wall for different sheet pile sections (a base condition with a span length of 60 ft and excavation level of 4.9 ft (1.5 m)). 158
Figure 6.18 Parametric study Case 3: Bending moment imposed on the sheet pile wall for different sheet pile sections (a base condition with a span length of 60 ft and excavation level of 4.9 ft (1.5 m))..... 159
Figure 6.19 Parametric study Case 3: Horizontal deflection of the sheet pile wall for different sheet pile sections (an extreme condition with a span length of 100 ft and excavation level of 8.2 ft (2.5 m))..... 160
Figure 6.20 Parametric study Case 3: Vertical settlement of the sheet pile wall for different sheet pile sections (an extreme condition with a span length of 100 ft and excavation level of 8.2 ft (2.5 m)). 161
Figure 6.21 Parametric study Case 3: Shear force imposed on the sheet pile wall for different sheet pile sections (an extreme condition with a span length of 100 ft and excavation level of 8.2 ft (2.5 m))..... 162
Figure 6.22 Parametric study Case 3: Bending moment imposed on the sheet pile wall for different sheet pile sections (an extreme condition with a span length of 100 ft and excavation level of 8.2 ft (2.5 m)). 163
Figure 6.23 The summary of parametric study Case 4 with different pile lengths: 6.5 m, 8.5 m, and 10.5 m (21.3, 27.9, 34.4 ft). 164
Figure 6.24 Parametric study Case 4: Horizontal deflection of the sheet pile wall for different pile lengths..... 165
Figure 6.25 Parametric study Case 4: Vertical settlement of the sheet pile wall for different pile lengths..... 166
Figure 6.26 Parametric study Case 4: Shear force imposed on the sheet pile wall for different pile lengths..... 167
Figure 6.27 Parametric study Case 4: Bending moment imposed on the sheet pile wall for different pile lengths. 168
Figure 6.28 The summary of parametric study with hypothetical anchor and Deadman concrete: Case 5 with anchor lengths, 4 m (13.1 ft) or 8 m (26.2 ft). Note: the spacing is the same at 4.5 m (14.8 ft). 169

Figure 6.29 Parametric study Case 5: Horizontal deflection of the sheet pile wall for different anchor lengths (a base condition with a span length of 60 ft and excavation level of 4.9 ft (1.5 m)). 172
Figure 6.30 Parametric study Case 5: Horizontal deflection of the sheet pile wall for different anchor lengths (an extreme condition with a span length of 100 ft and excavation level of 8.2 ft (2.5 m)). 173
Figure 6.31 Parametric study Case 5: Shear force imposed on the sheet pile wall for different anchor lengths (an extreme condition with a span length of 100 ft and excavation level of 8.2 ft (2.5 m)). 174
Figure 6.32 Parametric study Case 5: Bending moment imposed on the sheet pile wall for different anchor lengths (an extreme condition with a span length of 100 ft and excavation level of 8.2 ft (2.5 m)). 175
Figure 6.33 The summary of parametric study with hypothetical anchor and Deadman concrete: Case 6 with anchor spacings, 2 m (6.6 ft) or 6 m (19.7 ft). Note: the length is the anchor at 6 m (19.7 ft). 176
Figure 6.34 Parametric study Case 6: Horizontal deflection of the sheet pile wall for different anchor spacings (a base condition with a span length of 60 ft and excavation level of 4.9 ft (1.5 m)). 178
Figure 6.35 Parametric study Case 6: Horizontal deflection of the sheet pile wall for different anchor lengths (an extreme condition with a span length of 100 ft and excavation level of 8.2 ft (2.5 m)). 179
Figure 6.36 Parametric study Case 6: Shear force imposed on the sheet pile wall for different anchor lengths (an extreme condition with a span length of 100 ft and excavation level of 8.2 ft (2.5 m)). 180
Figure 6.37 Parametric study Case 6: Bending moment imposed on the sheet pile wall for different anchor lengths (an extreme condition with a span length of 100 ft and excavation level of 8.2 ft (2.5 m)). 181
Figure 6.38 Parametric study Case 7: Horizontal deflection of the sheet pile wall with dry or submerged conditions. 183
Figure 6.39 Parametric study Case 7: Vertical settlement of the sheet pile wall with dry or submerged conditions. 184
Figure 6.40 Parametric study Case 7: Shear force imposed on the sheet pile wall with dry or submerged conditions. 185
Figure 6.41 Parametric study Case 7: Bending moment imposed on the sheet pile wall with dry or submerged conditions. 186
Figure 6.42 Case 8: Comparison of the end-bearing conditions on the sheet pile behavior. 187
Figure 6.43 Parametric study Case 8: Horizontal deflection of the sheet pile wall for different end-bearing (soil *vs*. rock) conditions. 189
Figure 6.44 Parametric study Case 8: Vertical settlement of the sheet pile wall for different end-bearing (soil *vs*. rock) conditions. 190
Figure 6.45 Parametric study Case 8: Shear force imposed on the sheet pile wall for different end-bearing (soil *vs*. rock) conditions. 191
Figure 6.46 Parametric study Case 8: Bending moment imposed on the sheet pile wall for different end-bearing (soil *vs*. rock) conditions. 192
Figure 6.47 Case 9: Comparison of the abutment types (conventional *vs*. semi-integral) and consequent temperature effect. 194

Figure 6.48 Parametric study Case 9: Horizontal deflection of the sheet pile wall for different abutment types (conventional *vs*. semi-integral) and consequent temperature effect (a base condition with a span length of 60 ft and excavation level of 4.9 ft (1.5 m)). 195
Figure 6.49 Parametric study Case 9: Horizontal settlement of the sheet pile wall for different abutment types (conventional *vs*. semi-integral) and consequent temperature effect (an extreme condition with a span length of 100 ft and excavation level of 8.2 ft (2.5 m)). 196
Figure 6.50 Parametric study Case 9: Shear force imposed on the sheet pile wall for different abutment types (conventional *vs*. semi-integral) and consequent temperature effect (a base condition with a span length of 60 ft and excavation level of 4.9 ft (1.5 m)). 197
Figure 6.51 Parametric study Case 9: Bending moment imposed on the sheet pile wall for different abutment types (conventional *vs*. semi-integral) and consequent temperature effect (a base condition with a span length of 60 ft and excavation level of 4.9 ft (1.5 m)). 198
Figure 6.52 Parametric study Case 9: Shear force imposed on the sheet pile wall for different abutment types (conventional *vs*. semi-integral) and consequent temperature effect (an extreme condition with a span length of 100 ft and excavation level of 8.2 ft (2.5 m)). 199
Figure 6.53 Parametric study Case 9: Bending moment imposed on the sheet pile wall for different abutment types (conventional *vs*. semi-integral) and consequent temperature effect (an extreme condition with a span length of 100 ft and excavation level of 8.2 ft (2.5 m)). 200
Figure 7.1 An example of the unplugged and plugged area in the sheet pile. 210

List of Tables

Table 2.1 Surveyed Bridge sites with sheet-pile abutments in Europe..... 34
Table 2.2 Surveyed Bridge sites with sheet-pile abutments in the USA. 35
Table 2.3 A summary of pile load tests in dense sand (Bustamante and Gianeselli, 1991). 37
Table 2.4 A summary of pile load tests in dense clay (Bustamante and Gianeselli, 1991). 39
Table 2.5 A summary of the bearing capacity estimates of two test piles, sheet pile and H-pile, based on PDA (Sylvain, 2019). 43
Table 2.6 A summary of ultimate skin friction values of sheet piles for various relative densities of granular soils - estimated from PDA tests (Underwood, 2020). 45
Table 2.7 Average ultimate skin friction values *vs*. relative density of granular soils estimated from PDA tests (from Underwood, 2020). 46
Table 2.8 Summary of literature review about axially loaded sheet pile test in the thesis. 47
Table 3.1 The properties and dimension of the test sheet pile sample. 51
Table 3.2 The properties of collected fill sand. 53
Table 3.3 Summary: Internal friction angle of sand and sand-steel plate interface friction angle. 62
Table 3.4 Summary: the elastic strain threshold of soil-steel plate interface. 62
Table 4.1 Classifications of sand used for the static pile loading test. 73
Table 4.2 Soil parameters used to estimate the bearing capacity of sheet pile. 78
Table 4.3 The properties of the model test sheet pile. 78
Table 4.4 A prediction of the bearing capacity from analytical, SPT-based, and CPT-based methods. 79
Table 4.5 Soil properties used for the complementary numerical simulation on static axial loading test. 88
Table 4.6 Soil-pile interface properties for the complementary numerical simulation on static axial loading test. 88
Table 4.7 The bearing capacity of the sheet pile: Comparison of the static pile loading test results with those from analytical, SPT-based, and CPT-based methods and numerical model. 92
Table 5.1 Material properties used for the validation of the beam element in case of axial loading. 98
Table 5.2 Soil-pile interface properties used for the validation of the beam element in case of axial loading. 99
Table 5.3 Input parameter for the pile element for the validation of the beam element in case of axial loading. 99
Table 5.4 Input properties for the sheet pile for the validation of the beam element in case of axial loading. 99
Table 5.5 Properties of materials used for the numerical simulation (Mullins et al., 2009)..... 103
Table 5.6 Properties of the sheet pile used for the numerical simulation (Mullins et al., 2009). 103
Table 5.7 Properties of the pile-soil interface used for the numerical simulation (adopted from Mullins et al., 2009). 103
Table 5.8 Properties of the sheet piles used for the numerical modeling (from Day and Potts, 1993). 107
Table 5.9 Properties of the soil used for the numerical modeling (from Day and Potts, 1993). 107
Table 5.10 Properties of the pile-soil interface used for the numerical modeling. 109

Table 5.11 A summary of applied service load reactions and loads used for the validation of combined axial + lateral loading on the sheet pile abutment (unit: tons). 113
Table 5.12 Material properties used for the validation of combination loads (1). 113
Table 5.13 Pile properties used for the validation of combined loads (1). 114
Table 5.14 Pile-soil interface properties used for the validation of combined loads (1). 115
Table 5.15 Monitored values of the backfill pressure and wall deflections in the demonstration bridge project site (Evans et al., 2011). 122
Table 5.16 Material properties used for the numerical simulation (from Evans et al., 2011). 127
Table 5.17 The property of sheet pile used for the numerical simulation (from Evans et al., 2011). 127
Table 5.18 The pile-soil interface property for each soil layer. 128
Table 5.19 The pile-soil interface properties used for the numerical simulation. 129
Table 5.20 Input parameters of the cable element used for the numerical simulation. 130
Table 5.21 Backfill pressure and deflections from the numerical simulation by the project team for the validation of the combined axial + lateral load (2). 133
Table 6.1 The dimension of the bridge selected for the parametric study in this project. 135
Table 6.2 Penetration resistance and soil properties based on SPT N-value for cohesionless soil (adapted by Rahman, 2019). 138
Table 6.3 Penetration resistance and soil properties based on SPT N-value for cohesive soil (adapted by Rahman, 2019). 138
Table 6.4 Selected elastic constants of soils (adapted by Itasca Consulting Group, 2019). 139
Table 6.5 Soil properties following SPT values – Parametric study for sheet pile abutment. 140
Table 6.6 Soil input parameters used for the parametric study of the sheet pile abutment system. 141
Table 6.7 Pile-soil interface properties for each soil layer. 141
Table 6.8 Pile-soil interface: input parameters used for the parametric study of the sheet pile abutment system. 142
Table 6.9 A summary of the simulations of the sheet pile abutment with different span lengths (Case 1). 144
Table 6.10 A summary of the simulations of the sheet pile abutment with different excavation depths (Case 2). 149
Table 6.11 Properties for different sheet pile sections. 154
Table 6.12 A summary of the simulations of the sheet pile abutment with different sheet pile sections (Case 3). 154
Table 6.13 A summary of the simulations of the sheet pile abutment with different sheet pile lengths (Case 4). 164
Table 6.14 Input parameters for the anchor-soil interface (from Itasca Consulting Group, 2019) for Case 5. 169
Table 6.15 A summary of the simulations of the sheet pile abutment and anchors with different anchor lengths (Case 5). 170
Table 6.16 Input parameters for the anchor-soil interface (from Itasca Consulting Group, 2019) for Case 6. 176
Table 6.17 A summary of the simulations of the sheet pile abutment and anchors with different anchor lengths (Case 6). 177
Table 6.18 A summary of the simulations of the sheet pile abutment with dry or submerged conditions (Case 7). 182

Table 6.19 Input parameters of material properties for Case 8..... 187
Table 6.20 A summary of the simulations of the sheet pile abutment with end-bearing conditions (Case 8)..... 188
Table 6.21 The summary of parametric case study results in this project..... 204

Chapter 1 Introduction

1.1 Background

Sheet piles are recommended to be installed for most water-crossing bridges, along with load-bearing piles (e.g., usually H-piles or pipe piles), to avoid the scouring problem and protect backfill soils in Nebraska (Section 4.1 of "Bridge office policies and procedures" (BOPP; Nebraska Department of Roads, 2016); Figure 1.1). Sheet piles have also been frequently applied to semi-integral abutment bridges in Nebraska. While sheet piling is not recommended for resisting any vertical load in the current BOPP, recent studies (Sylvain et al., 2017; Panchal et al., 2020) suggested that sheet piles could be employed for both axial load-bearing and backfill retaining lateral loads for either short-span or low-traffic volume road bridges. Nevertheless, there have been limited resources in terms of design, analysis (e.g., calculation of vertical and lateral load-bearing capacity of sheet piles under such superstructures), and construction strategies.

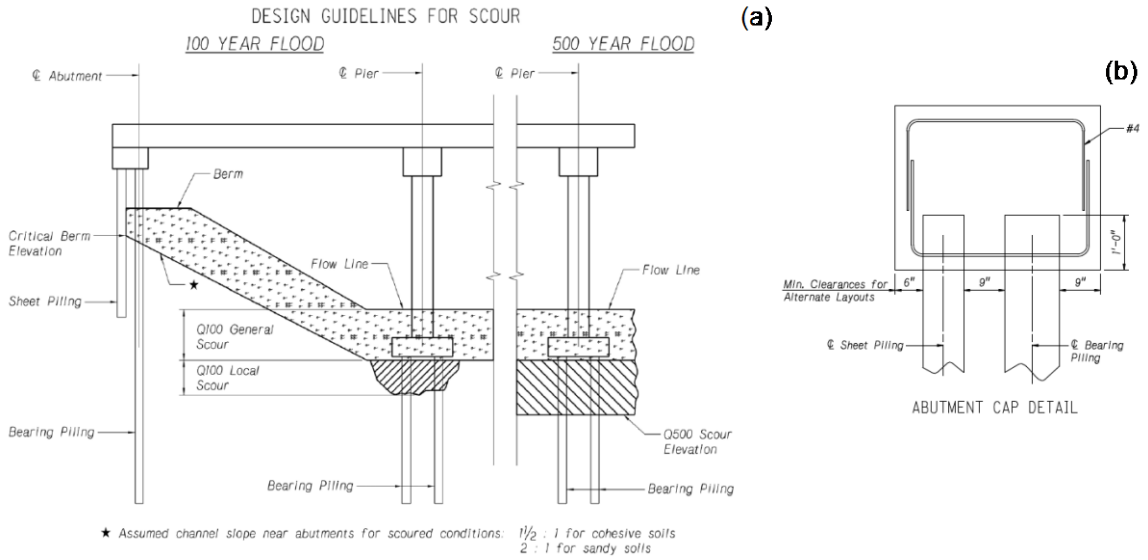

Figure 1.1 (a) An example of design guidelines that include both bearing and sheet piling for scour protection, and (b) sheet pile abutment cap geometry (Sections 4.1 and 4.2 of BOPP; Nebraska Department of Roads, 2016).

On the other hand, there are significant numbers of short-span bridges in Nebraska that may need repair or replacement in the near future. According to the Nebraska bridge data from the Datacenterhub (https://datacenterhub.org), there are 8,052 single-span bridges in Nebraska out of a total of 17,717 bridges surveyed (Figure 1.2). And 8,353 bridges' span length is shorter than 70 ft. Many of those bridges were built a long time ago. For instance, about 3,900 bridges were built in the 1930s and may require replacement or repair and strengthening (Figure 1.3(a)). It was also observed that a significant portion of those short-span bridges is located in the eastern part of the state due to smaller tributaries from the Missouri River (Figure 1.3(b)).

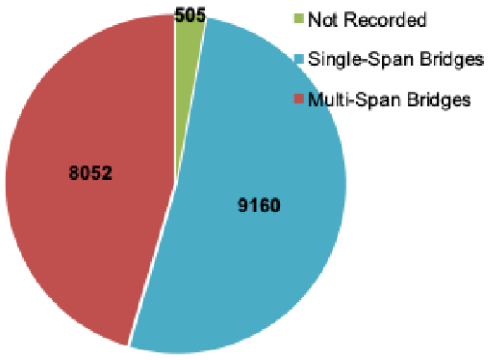

Span length (ft)	Number
<50	7,220
50-70	1,133
70-90	448
90-110	206
>110	153

Figure 1.2 The number: single- and multi-span bridges in Nebraska (left) and by span length (right).

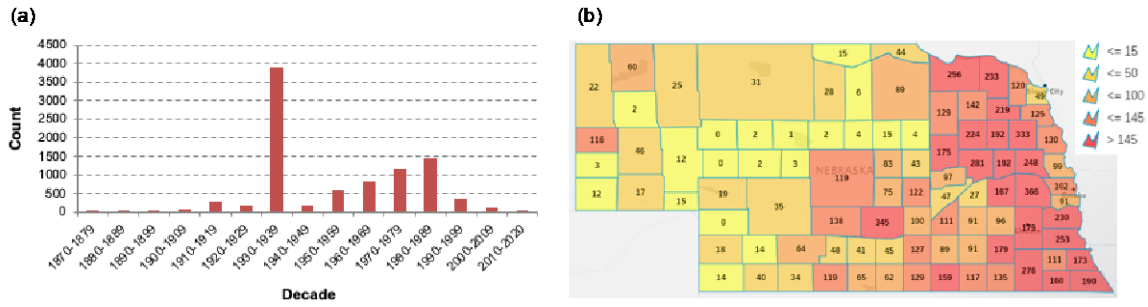

Figure 1.3 Nebraska bridges: (a) the number of single-span bridges built by decade, and (b) the location of single-span bridges by counties in Nebraska.

In this regard, Nebraska is expecting high needs in the near future for bridge repairs and replacements for short-span and low-traffic volume bridges, many of which are water-crossing bridges. Steel sheet piles have been identified as a possible option for two principal uses in the bridge abutment: as cantilever walls or anchored walls (Figure 1.4).

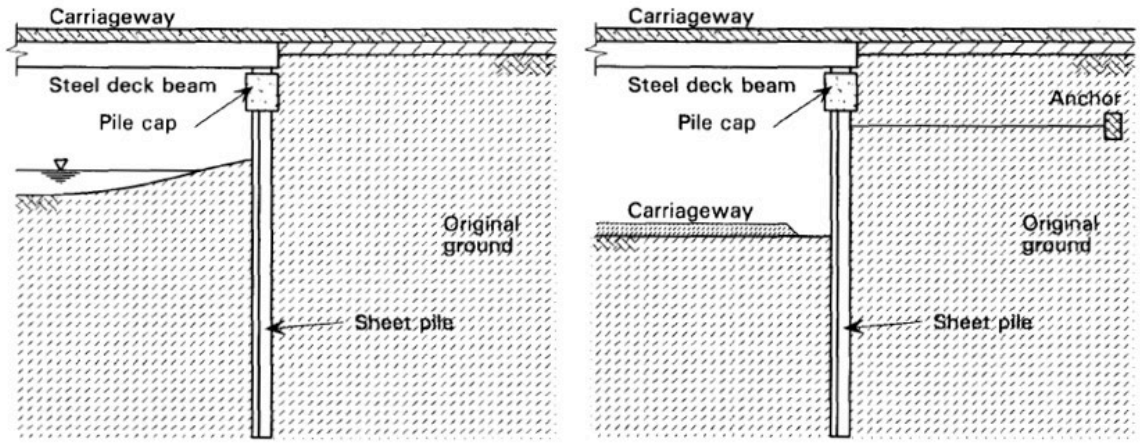

Figure 1.4 A design example of the sheet pile cantilever wall (left) and anchored retaining wall acting as a bridge abutment (right). Images are from Yandzio (1998).

It was reported that many bridges had been built using such a steel sheet pile abutment system, particularly in Europe (Yandzio, 1998). Examples include small span bridges (8 to 20 m; 26 to 65 feet) as well as medium-span bridges (20 to 35 m; 65 to 115 feet). Some of those examples are shown in Figure 1.5.

Figure 1.5 An example of sheet pile abutment bridges in Europe. (a) Humber Road bridge (Immingham, UK), and (b) Canal bridge (Stoke-on-Trent, UK). Images are from Yandzio (1998).

In contrast, there are not many projects in the US in which the axially loaded sheet piles were used in the bridge abutment. In Nebraska, counties have multi-beam (planks) bridges sitting on bearing piles with sheet piles used as abutments. However, these sheet piles are not necessarily carrying the beams or are used as axially loaded members. They are rather installed to protect backfill soils and avoid scouring, as shown in Figure 1.6.

Figure 1.6 An example of a county bridge in Nebraska with solid planks and sheet pile abutments.

A few examples found during the literature search include an 80-ft single-span bridge in Alaska, 42-ft and 65-ft single-span bridges in New York, and a 40-ft bridge (in Iowa). Their designs are summarized in Figure 1.7.

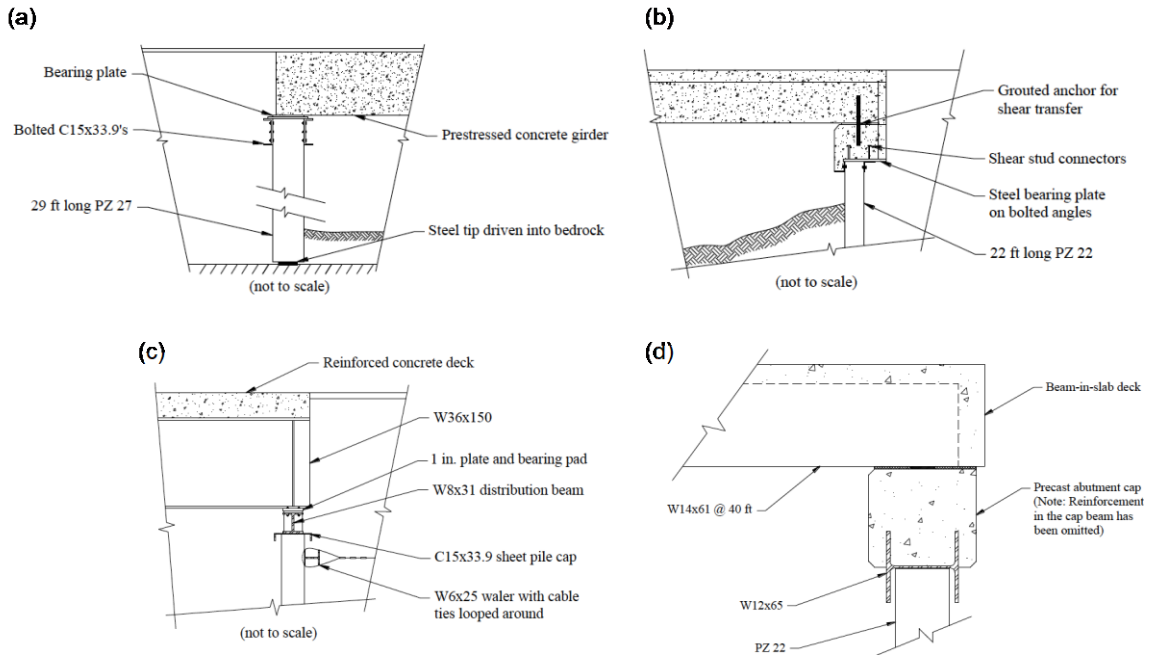

Figure 1.7 An example of sheet pile abutment bridges in the USA. (a) Small Creek bridge (Seward, Alaska), (b) Taghkanic Creek bridge (New York), (c) Banks Road bridge (New York), and (d) Black Hawk county bridge (Iowa). Images are from Evans et al. (2012).

It was noted that more in-depth research is needed due to the lack of experience in regard to the design, analysis (e.g., vertical and lateral load resistances), load test, and construction procedure in the recent project report by Iowa DOT (Evans et al., 2012). For example, it was noted that there is no specific design procedure in the US partly because the concept of axially loaded sheet piling is relatively new. Sheet piles are analyzed as a soil retaining structure in most design practices, as in Nebraska, which means the lateral soil pressure would control the design approach. The combined effect of axial and lateral loading needs to be considered when the axially loaded sheet pile abutment system is intended in the design.

1.2 Problem Statement

A specific design procedure related to the axially loaded sheet piling does not exist in most parts of the US (Evans et al. 2012). Accordingly, the research team perceived a lack of data

and experience in the design and analysis of vertical and lateral load resistance of the axially loaded sheet piling. For example, there is insufficient confidence in the estimate of bending and lateral stresses induced by the axial loading and lateral soil pressure, respectively. There is also uncertainty on how lateral load could be transferred from the superstructure to the sheet pile during a seasonal temperature variation. In terms of the side frictional resistance, it is unknown how the skin frictional resistance of the sheet pile could be mobilized in the different passive and active zones. Moreover, the side frictional resistance could be noticeably different between the dry and submerged soil conditions. For the end bearing resistance, the soil plugging effect may improve the end bearing capacity. Those uncertainties may result in a too-conservative design, and thus, an unnecessary increase in the construction cost.

In addition to those general challenges, there are additional research needs perceived by engineers in Nebraska. First, the load transfer from the superstructure to the substructure could be substantially different in other states depending on the connection design. For example, the Nebraska DOT design for semi-integral abutment bridges is unique and may differ from other states' conventional abutment bridge or semi-integral abutment bridge designs. Typical Nebraska semi-integral abutment details are shown in Figure 1.8. This created a joint at the approach span, in the furthest location from the deck. Due to the difference in details at the end of the deck, the total horizontal force created by temperature loading from the superstructure is different, which should interact with the lateral soil loads and create a moment. Second, the tie-rod anchor may be avoided depending on the soil condition and bridge design. With that, the reduction or elimination of the anchor will bring the cost and construction time down. Lastly, there is a research need that investigates the feasible length of the superstructure that is compatible with the axially loaded sheet pile abutment system of a short-span bridge for general geologic

conditions and construction practices in Nebraska. In summary, those general and Nebraska-specific questions are to be addressed by the proposed research project.

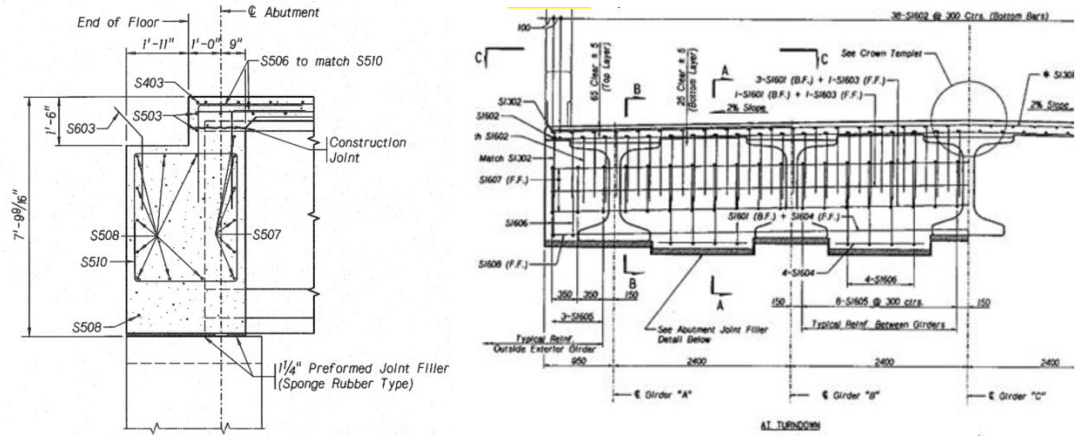

Figure 1.8 Current semi-integral abutment bridge design in Nebraska. Note: black shades are where elastomeric paddings are used to allow horizontal movement between the superstructure and substructure.

1.3 Objective of the Study

The overall goal of this study is to investigate the anticipated performance of steel sheet-pile bridge abutments to encourage its wider application to not only new construction but also repair and replacement of existing water-crossing bridges in Nebraska. To achieve this goal, we set several objectives as follows:

- Suggest an improved analysis method that incorporates the combined effect of axial and lateral loads that are imposed on the sheet pile walls and considers the following aspects:
    - Skin frictional resistance in active/passive zones for either dry or submerged soil conditions
    - Soil plugging effects
    - Different cross-sections of the sheet piles
    - Design configurations (cantilever vs. anchored walls)

    - Effect of seasonal temperature variations
- Elucidate the moment generated by the forces between the horizontal movement of the superstructure of semi-integrals in Nebraska vs. loads caused by the soil behind (e.g., active/passive pressures, the friction of backfill on superstructure end or the shearing resistance of backfill, which could play a role if the bridge has skew and lateral bearings are not provided).
- Assess the feasibility of avoiding the tie-rod anchoring for various design parameters.
- Suggest a range of superstructure length and skew angle that can be supported by the axially loaded sheet pile abutment system.
- Provide the research summary and design recommendations that can be used by engineers and contractors for water-crossing bridges in Nebraska.

The research team aims to provide input parameters of soil-sheet pile interactions for the design and analysis of the axially loaded sheet pile walls. The end results of this research project will contain a summary table/chart of the soil-sheet pile interaction properties and design parameters with the selected sets of soil conditions, dry/saturated water conditions, and the types of sheet piles. The end results of this research project will also include the performance charts of the sheet pile abutment systems from numerical studies with various input parameters. Based on those summary tables and charts, the design recommendations of the sheet pile abutment system will be provided. For example, the team will suggest a range of feasible lengths of the superstructure that can be compatible with the sheet pile abutment system for different conditions, including the superstructure-substructure connection design, soil/rock bearing, cross-section of sheet piles, abutment height, etc. The team will also suggest in which conditions the cantilever sheet pile walls (i.e., without the tie-rod anchor) could be considered. Moreover, a

suggestion for an improved analysis method to determine the bearing capacity of the axially loaded sheet pile walls will be included in the end results.

Chapter 2 Literature Review

The research team surveyed project reports and research articles published in the USA, Europe, and other parts of the world to review the state-of-the-art design and analysis practices related to the sheet pile abutment system. This chapter provides several bridge cases with axially loaded sheet pile abutments. This chapter also provides a review of previous in-depth studies related to the bearing capacity of sheet piles.

2.1 Bridges with the Sheet Pile Abutments

2.1.1 Humber Road Bridge, Immingham, England

The Humber Road Bridge is located in Immingham, England, and docks on Humberside. It was built on Humber Road near the west gate (Figure 2.1), situated in a heavy industrial area with substantial construction. The bridge span is 36 m (116 ft), having an 8 m (26 ft) height atop the abutment. The bridge goes over the railroad track at a skew angle of 25°. The abutments were designed by combining box piles of Larssen 32W and 20W sections. A reinforced concrete backseat abutment was built on granular soil to distribute bridge loading better and avoid settlement. High-build, isocyanate-cured epoxy pitch coating was applied to protect the steel.

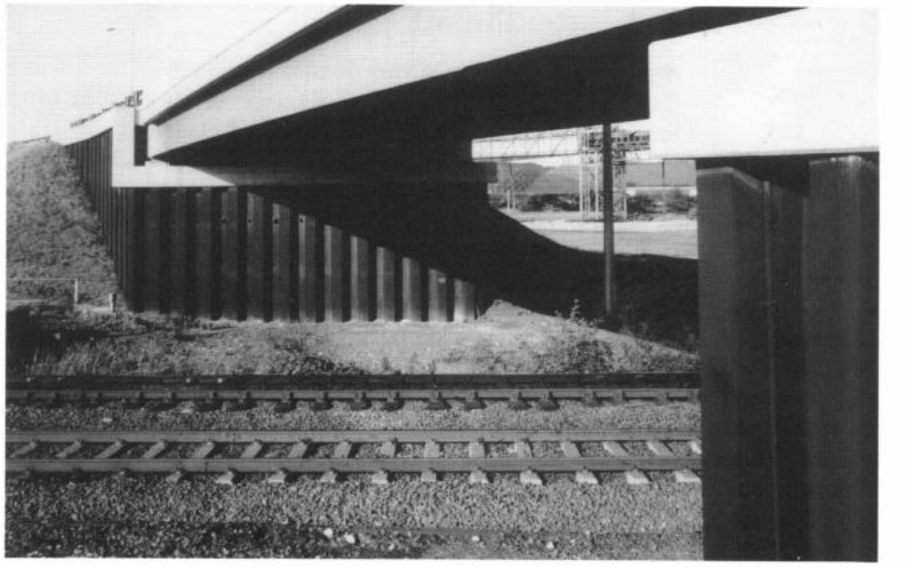

Figure 2.1 Humber Road Bridge, Immingham, England (the image from Yandzio, 1998).

2.1.2 Canal Bridge, Stoke-on-Trent, England

This bridge was constructed to replace a Victorian wrought iron beam and "brick jack bridge" in Stoke-on-Trent, England. The bridge is located on busy routes, and its primary function is maintaining two-way traffic streams. The foundation and abutment were combined by sheet piles, driven in a single operation to reduce construction time. Frodingham 3N and 4N sections also consisted of sheet piles, which were driven into an embedded depth by a 1-ton hydraulic hammer. The wing walls were protected by brickwork, and the abutment faces underneath the bridge deck were painted for aesthetics.

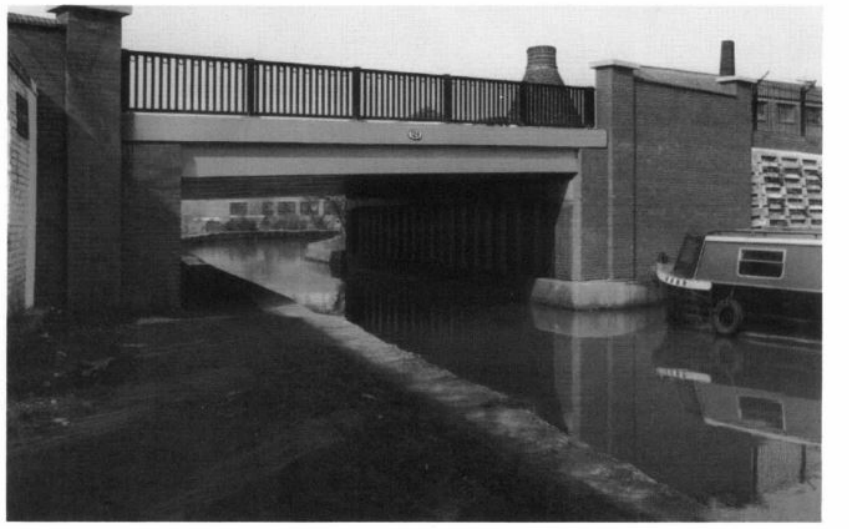

Figure 2.2 Canal bridge, Stoke-on-Trent, England (the image from Yandzio, 1998).

2.1.3 A Bridge in Black Hawk County, IA

A research team from Iowa State University and the Iowa Department of Transportation constructed three bridges using a sheet pile as an axial bearing pile of the abutment. This project aimed to investigate the practicability of using sheet piling as the primary foundation as well as the retaining backfill system. The research team employed various instrumentation tools, including strain gauges, deflection transducers, pressure cells, and piezometers, to assess the effects of lateral and live loads on the abutment. The first bridge site among them was located in Black Hawk County (BHC), Iowa.

The selected site was a low-volume bridge crossing Spring Creek (a tributary of the Cedar River) on Bryan Road near La Porte City, Iowa. The newly built bridge was a two-lane single-span beam-in-slab structure 9.4 m (31 ft) wide and 11.9 m (39 ft) long. The Engineer's Office in BHC utilized previous precast elements to complete the superstructure design. The sheet piles were PZ22 sections, and the 64 sheet piles were installed at both abutments. The main wall of the abutment required 20 sheet pile elements, with each wing wall consisting of six parts

(every 4.6 m (15 ft) long). The main wall was reinforced with two 2.54-cm-diameter (1 in.) tie rods connected to a 4.3 m × 1.2 m × 0.6 m (14.1 ft × 3.9 ft × 2.0 ft) cast-in-place reinforced concrete Deadman anchor. The wing walls were joined using a 14 m (46 ft) long and 2.54-cm-diameter tie rod (non-epoxy coated). The abutment cap was a precast element designed and fabricated by BHC engineers that consisted of a W12×65 steel beam cast in reinforced concrete.

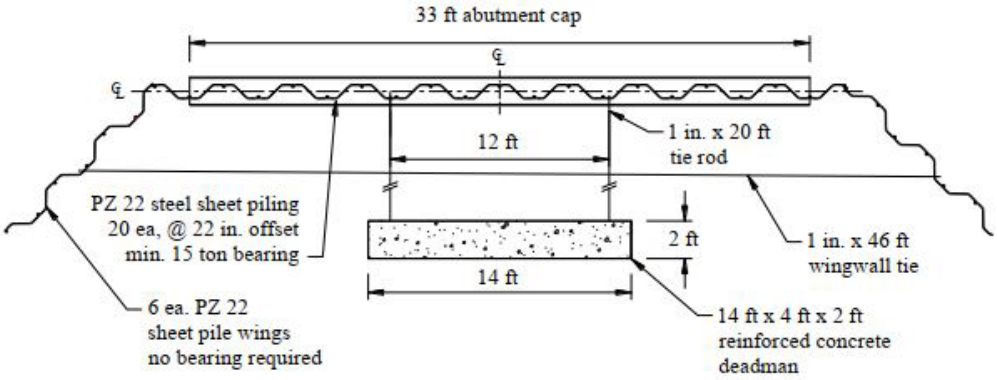

Figure 2.3 A plan view of the sheet pile abutment and backfill retaining system for demonstration projects in BHC, Iowa (Evans et al., 2011).

2.1.4 A Bridge in Tama County, IA

The same research team continued constructing another project in Tama County, Iowa. A low-volume bridge was built on MM Avenue near 380th Street, crossing Richland Creek. The substructure for the bridge utilized geosynthetic reinforced soil (GRS) with a steel sheet pile and scoured retaining wall. The bridge structure in Tama County employed two 27.1 m (89 ft) long railroad flatcars for the superstructure. This project used PZC13 sheet pile sections that were lighter and stronger than the traditional PZ22 section. The research team also combined an anchor system with the sheet piles to hold all loads (including bridge and backfill surcharge). The research team claimed the contribution of the GRS system to restrict lateral loads being

applied to the abutment over the extent of the GRS system. Seven layers of BX1200 geogrid were constructed with approximately 6.1 m (20 ft) × 12.2 m (40 ft) in the plan.

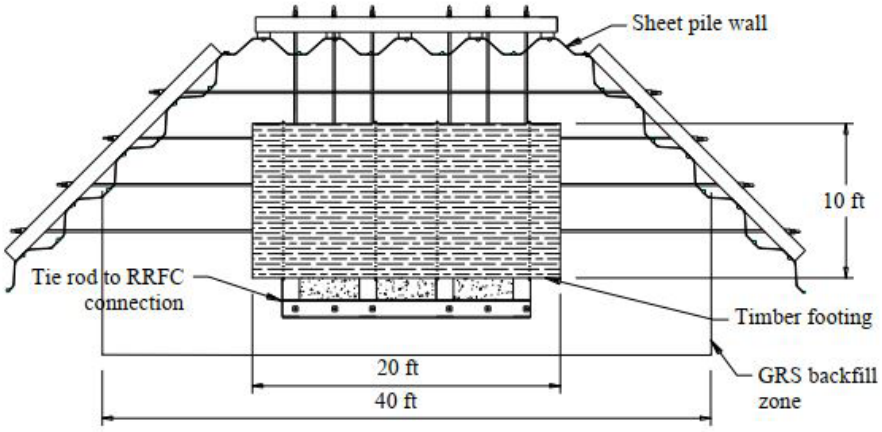

Figure 2.4 A plan view of the sheet pile abutment and backfill retaining system for demonstration projects in Tama County, Iowa (Evans et al., 2011).

2.1.5 Route 4 Bridge in Sprout Brook, NJ

The sheet pile abutment was applied to construct a 14.6 m (48 ft) long bridge along Route 4 over Sprout Brook in Paramus, New Jersey. Using sheet pile abutments eliminated the need for cofferdams by utilizing tied-back steel sheet pile systems capped with concrete to form the abutment and wing walls. ASTM A572, Gr 50, AZ 36 steel sheet piles were combined with a reinforced concrete cap beam to support the load from the bridge. The permanent steel sheet and wing walls were designed following AASHTO Standard Specification for Highway Bridges and included provisions for seismic events. A double corrosion protection system was employed on the tie rods to satisfy design life requirements. The sheet piles were embedded in sandstone to maximize the tip resistance.

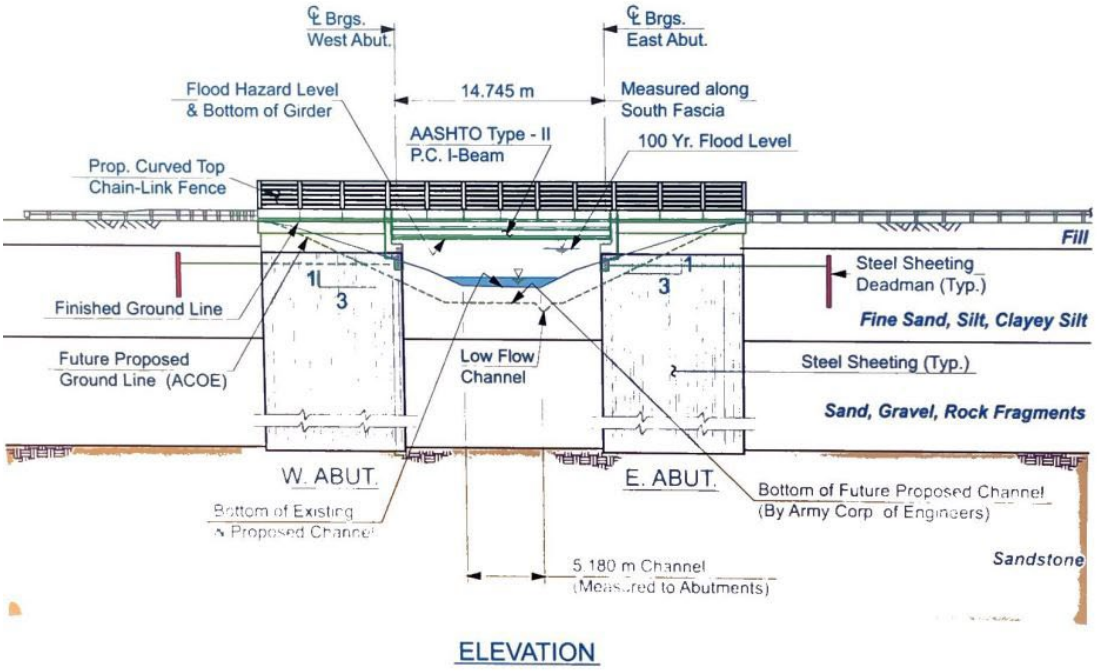

Figure 2.5 A substructure redesign for Route 4 Bridge over Sprout Brook (from Nucor Skyline, 2021).

2.1.6 A Bridge over Klutuk Creek in Ekwok, AK

A new bridge was constructed over Klutuk Creek in Ekwok, Alaska, due to the village's demand to expand the current landfill. The first design called for a bin wall with significant riprap. There were restrictions on the volume of material that could be carried along the Nushagak River, and the extremely remote location of the job site proved to be a challenge. It was expensive to transport the needed rock to the area. In this background, a value-engineered design called for a sheet pile abutment. The bridge abutment used ASTM A572, Gr. 50, 40 double AZ19-700 steel sheet piles 12.2 m (40 ft) long, installed by a vibratory hammer. The soil behind the wall was excavated to install anchor D18 tie rods with deadman concrete. After installation, the backfill was placed and compacted behind the abutment wall. The sheet pile abutments eliminated the need to drill, blast, and produce riprap. The value-engineered solution utilizing sheet pile abutments claimed to save the Ekwok Village Council $1.1M, thus putting the

total cost within their budget and saving the project nearly two months construction time (Nucor Skyline, 2021).

2.1.7 Summary - Bridges with the Sheet Pile Abutments

Table 2.1 Surveyed Bridge sites with sheet-pile abutments in Europe.

Bridge site	Location	Details on sheet-piles	Length of pile	Length of span	Ref.
Humber Road bridge	Immingham, England	between Larssen 32W and 20W	8 m	36 m	1
Canal bridge	Stoke-on-Trent, England	Frodingham3N and 4N	N/A	N/A	1
Holes Bay bridge	Poole, England	Frodingham 3N and universal beam, concrete anchorage	N/A	16 m	1
Stockman's Lane flyover	Belfast, England	boxed Larssen 4/20 piles, concrete anchorage	N/A	20 m	1
Simwhite bridge	Grimsby, England	Larssen 25W	16 m	N/A	1
Capel St Mary A12 underpass bridge	near Ipswich, England	High modulus piles, ground anchor	N/A	10 m	1
Railway underline bridge	Shrivenham, England	Larssen sheet piles, universal beam	N/A	N	1

(1) Yandzio (1998)
(2) Carle & Whitaker (1989)
(3) Evans et al. (2011)
(4) Lichtenstein Consulting Engineers (2001)
(5) Nucor Skyline (2021)

Table 2.2 Surveyed Bridge sites with sheet-pile abutments in the USA.

Bridge site	Location	Details on sheet-piles	Length of pile	Length of span	Ref.
Small Creek Bridge	Seward, Alaska	PZ27	9m	24m	2
Taghkanic Creek Bridge	New York City, New York	PZ22	7m	13m	2
Banks road bridge	New York City, New York	-	-	20m	2
On Bryan Road	Black Hawk County, Iowa	PZ22 and concrete deadman	5m	12m	3
Avenue near 380th Street crossing Richland Creek	Tama County (TC), Iowa	PZC13, tie-rod, and GRS method	12m	27m	3
Route 4, Sprout brook	Paramus, New Jersey	AZ36, and reinforced concrete cap beam	N/A	15m	4
Klutuk Creek	Ekwok, Alaska	AZ 19-700	12m		5
CR 1013 Long Stretch Road, over Turtle Creek	Bracken County, Kentucky	PZC26 with pile points, reinforced concrete cap beam	N/A	18m	5

(1) Yandzio (1998)
(2) Carle & Whitaker (1989)
(3) Evans et al. (2011)
(4) Lichtenstein Consulting Engineers (2001)
(5) Nucor Skyline (2021)

2.2 Bearing Capacity of Sheet Pile

2.2.1 Static Pile Load Test of Sheet Piles in Dense Sand (Durik, France)

Bustamante and Gianeselli (1991) conducted a field load test with four sheet piles of Larssen IIS and IIN section (Figure 2.6) at Durik, France, to evaluate the bearing capacity of the sheet pile wall. The embedded depth was 7.42 m (24 ft) for the sheet piles. The reference piles were closed-end box piles (embedded depth - 12.2 m (40 ft)) and open-end box piles (embedded depths - 7.72 to 12.2 m). The research team conducted a standard penetration test (SPT), cone penetration test (CPT), pressure meter test (PMT), and self-boring pressure meter test to estimate soil strength. The in-situ sand was dense, with the tip resistance (q_c) reaching 40 MPa (5,801 psi) at 10 m (32.8 ft) depth (from the CPT-based estimate). A dynamic cone penetration test (DCP) was also conducted to measure the sheet pile element's skin friction and tip-bearing capacity. A pile load test was applied up to 2,400 kN (540 kips) to assess the total capacity of sheet piles and reference piles. Following the pile load test, the sheet pile settled by 73 mm (2.9 in.) at the full load of 2,400 kN (540 kips). The sheet pile yielded better ultimate bearing capacity (Q_u), compared to the box pile (Q_u = 2,050 kN (460 kips) at 12.5 m depths).

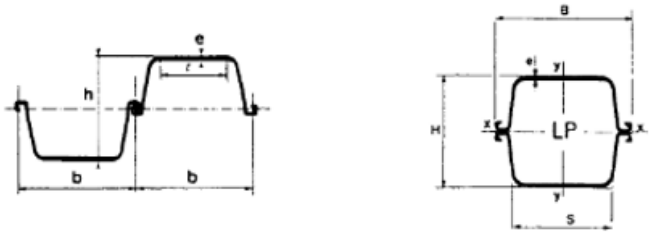

Figure 2.6 The cross sections of test sheet pile and box pile (Bustamante and Gianeselli, 1991).

Table 2.3 A summary of pile load tests in dense sand (Bustamante and Gianeselli, 1991).

Pile Type	Test	Embedment Depth (m)	Ultimate Capacity (kN)	Shaft Resistance (kN)	Tip Resistance (kN)
Sheet pile wall	1	7.42	2400	1880	520
Open-end box-pile	1	7.76	2000	720	1280
	2	7.76	2250	1410	840
	3	7.76	1060	1060	-
	4	7.76	>1950	>1260	>690
Closed-end box-pile	1	7.72	1140	660	480
	2	12.22	1500	1033	467
	3	12.22	700	700	-
	4	12.22	1650	1150	500
	5	12.22	1200	885	315

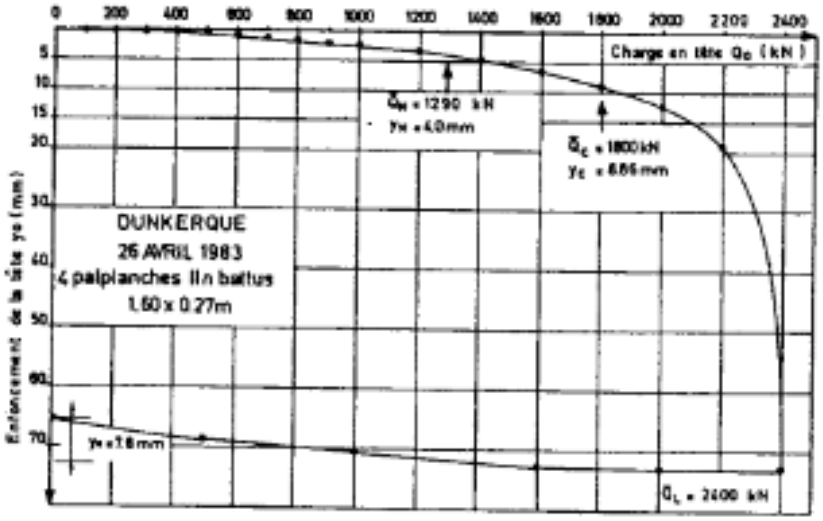

Figure 2.7 An estimate of ultimate bearing capacity of the sheet pile walls and box piles from the pile load test (Bustamante and Gianeselli, 1991).

2.2.2 Static Pile Load Test of Sheet Piles in Dense Clay (Merville, France)

Bustamante and Gianeselli (1991) conducted five pile-load tests for sheet piles in clay.

The test pile consisted of four sections of Larssen II2S or II2N steel at 7.5 m (25 ft) and 12 m (39

ft) depths. The topsoil was clayey silt around 2-3 m (6.6-9.9 ft) deep, and the underlying soil was Flanders Clay. According to the laboratory test, the soil density was about 18.2 to 19.1 kN/m^3 (117 to 123 pcf); water content was from 30 to 41; and the liquid limit was from 72 to 92. The tip resistance (q_c) from the CPT test increased with depth and reached 6 MPa at around 15 m (49 ft) depth. The N_{60} value from the SPT test reached a maximum of 42 blow counts at the same depth (Figure 2.8). The research team also conducted the dynamic cone penetration test to estimate the skin and tip resistance, and devised the *T-Z* function curve (Figure 2.10). A pile-load test applied up to 3,000 kPa (62.7 ksf) to evaluate the full bearing capacity of sheet piles in dense clay. The pile-load test indicated that the bearing capacity of sheet-pile sections (3,000 kN/m^2) was much higher compared to that of the box pile (1,300 kN/m^2) at the same depth (Table 2.4).

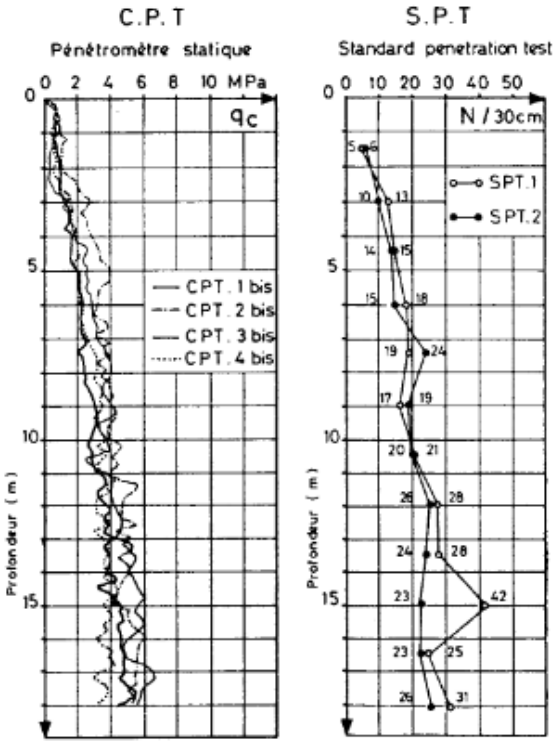

Figure 2.8 CPT and SPT soil profiles at the test site, Merville, France (Bustamante and Gianeselli, 1991).

Table 2.4 A summary of pile load tests in dense clay (Bustamante and Gianeselli, 1991).

Pile type	Test	Embedment Depth (m)	Ultimate Capacity (kN)	Shaft Resistance (kN)	Tip Resistance (kN)
Closed end box pile CF	1	7.5	625	475	150
	2	12.0	1,300	1,057	243
Sheet pile wall element 4PPIIs	1	7.5	1,750	1,465	285
	2	12.0	3,000	2,491	509
Sheet pile wall element 4PPIIn	1	7.5	1,300	1,025	275

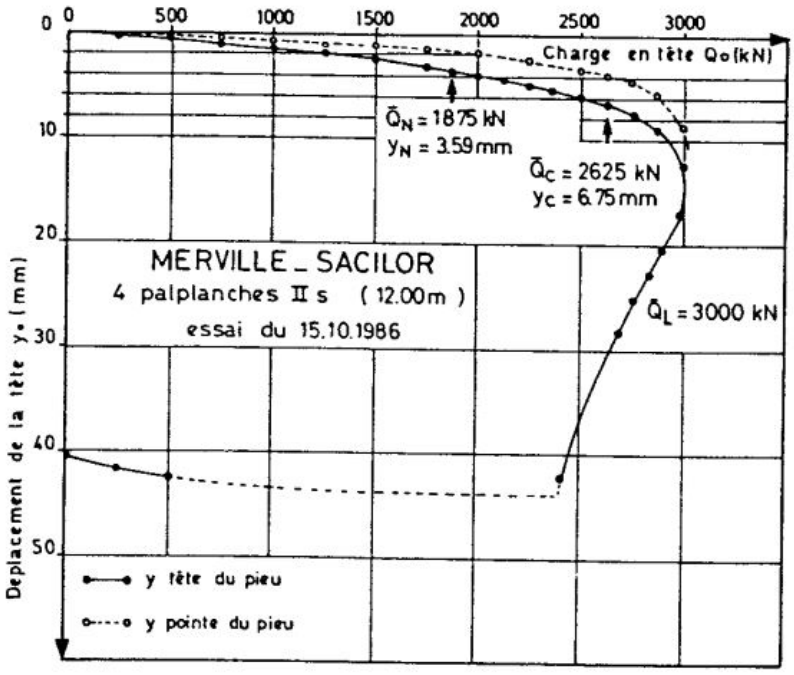

Figure 2.9 A pile load test result of the sheet pile in clayey soil (Bustamante and Gianeselli, 1991).

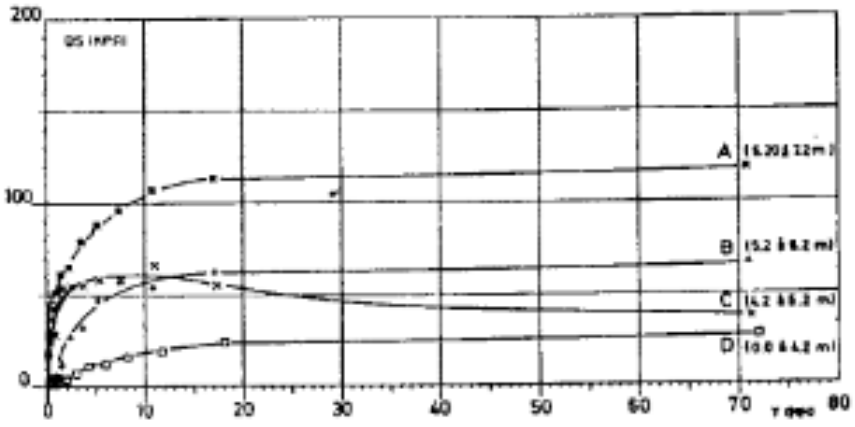

Figure 2.10 The obtained *T-Z* function curves of the skin resistance for sheet pile elements (Bustamante and Gianeselli, 1991).

2.2.3 Static Pile Load Test of Sheet Piles in Sand (Matthews, North Carolina)

The research team conducted axial load tests for sheet pile and H-pile in Matthews, North Carolina, in the yard of the International Construction Equipment (ICE). One of the main objectives was to compare the total bearing capacity between these two pile types. In detail, PZ-27 was used for sheet pile pairs and HP 12×73 for H-pile, with the same length of 5.2 m (17 ft). Before the loading test, the research team conducted a site investigation, including four conventional hollow stem auger borings with SPT testing and sampling, two SCPTu tests, MASW geophysical testing, and the installation of a standpipe for monitoring groundwater elevation (Figure 2.11), along with laboratory tests. Consequently, the subsurface profile was divided into four layers, based on the N_{60} from the SPT test and q_c from the CPT test. From the dynamic pile load test, the ultimate bearing capacity of the sheet pile was observed to be almost five times higher than that of the H-pile, according to the Case Restrike Method, or two times higher with the CAPWAP (Case Pile Wave Analysis Program) Restrike method (Table 2.5). In addition, the static pile load test showed that the ultimate bearing capacity of the Sheet pile was

152.5 kN (34.3 kips), while that of the H-pile was 100.1 kN (22.5 kips) when vertical settlement at the pile head hit 6.5 mm (1/4 inches) (Figure 2.12).

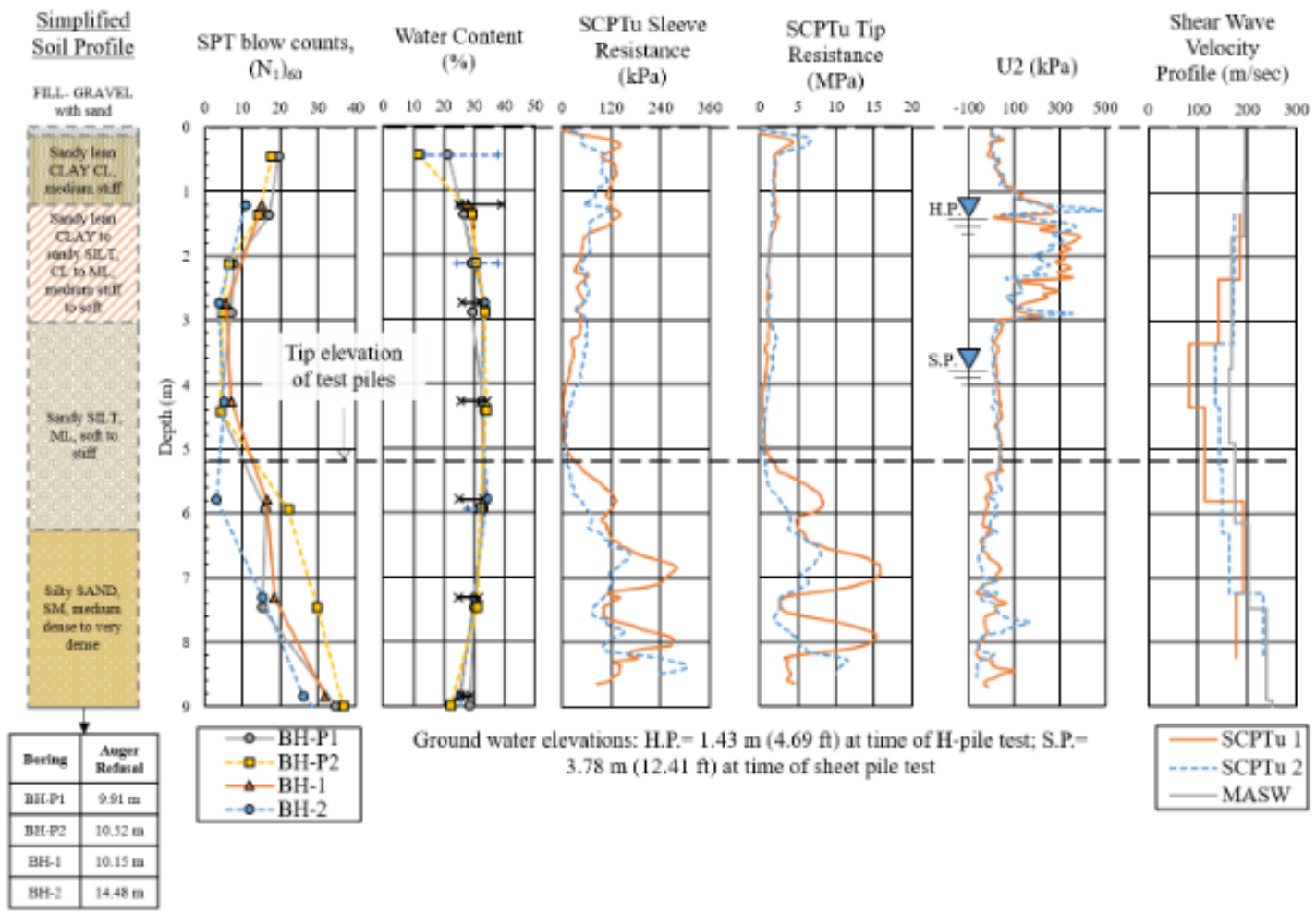

Figure 2.11 Site investigation data for the pile loading test site in Matthews, North Carolina (Sylvain, 2019).

Table 2.5 A summary of the bearing capacity estimates of two test piles, sheet pile and H-pile, based on PDA (Sylvain, 2019).

Method	Capacity Provided	Sheet pile (two PZ-27 sections)	H-pile (one HP 12×53 section)
Case EOD	Total	Not available	Not available
Case Restrike	Total	195.7 kN	40 kN
CAPWAP* Restrike	Shaft	76.1 kN	54.7 kN
	Toe	98.3 kN	24.5 kN
	Total	174.4 kN	79.2 kN

* CAPWAP: Case Pile Wave Analysis Program

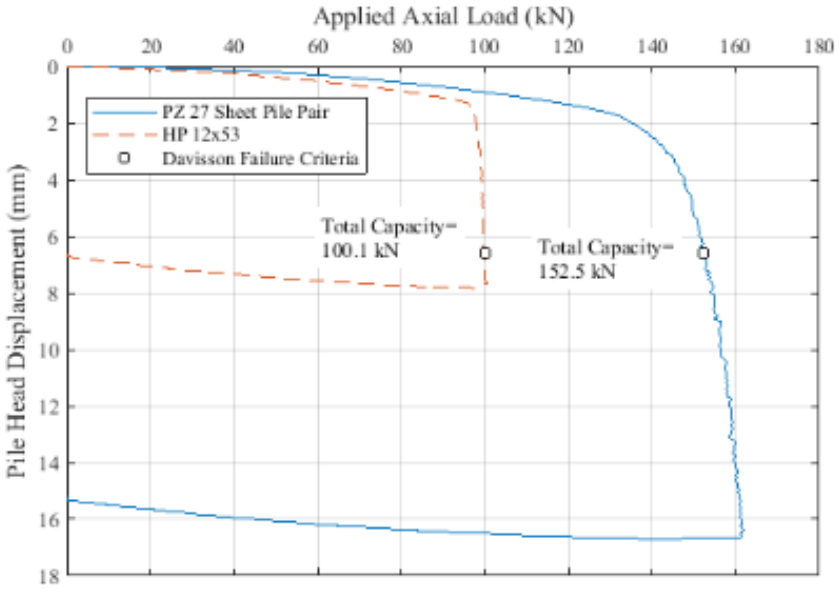

Figure 2.12 A comparison of the static axial pile loading tests performed at a field site in Matthews, North Carolina (Sylvain, 2019).

2.2.4 Application of Sheet Piles as Permanent Building Foundations

A group of engineers at Engineering Partners International LLC applied the sheet pile as a permanent foundation for about 30 projects in the USA since 2005 (Figure 2.13). Those buildings supported by sheet piles have one to three floors below the surface and up to 16 floors

above. The maximum point load was up to 380 kips (172.3 tons), and the wall load was up to 12 klf (175 kN/m). Most sheet piles in those projects were designed as friction piles in sand. For a few projects, however, sheet piles were designed either as end-bearing piles on bedrock or as a combination of side friction-end bearing piles.

Figure 2.13 An example of sheet piling as a permanent foundation (with a temporary soil berm) for the construction of below-grade precast concrete framing (Underwood, 2020).

Underwood (2020) conducted 35 PDA (Pile Driving Analyzer) tests on 30 project sites to verify the axial bearing capacity of sheet piles. One to eight PDA tests were conducted per site, depending on the size of the projects. CAPWAP (Case Pile Wave Analysis Program) was used for test data to estimate the total bearing capacity and distribution of skin frictional resistance along the pile shaft. The tip resistance was neglected in this effort unless sheet piles were laid on bedrock for conservative purposes. Test results indicated similar ultimate skin friction values above and below the groundwater table for similar soil types. And the unit skin friction showed a good correlation with the relative density and SPT blow counts. When relative density of soil

ranged from very loose to loose, the unit skin friction ranged 0.08 to 0.59 ksf (3.83 to 28.2 kPa); from medium dense to dense, the unit skin friction ranged 0.1 to 1.34 ksf (4.8 to 64.2 kPa) (Table 2.6, Figure 2.14).

Table 2.6 A summary of ultimate skin friction values of sheet piles for various relative densities of granular soils - estimated from PDA tests (Underwood, 2020).

Soil Type		Granular											
Relative Density		Very Loose		Loose		Medium Dense				Dense			
(N-Values)		0-4		5-10		11-20		21-30		31-40		41-50	
Groundwater *(1)*		N	Y	N	Y	N	Y	N	Y	N	Y	N	Y
Ultimate Unit Skin Friction (ksf)	Min.	0.09	0.15	0.08	0.11	0.10	0.12	0.10	0.24	0.35	- -	0.34	- -
	Max.	0.34	0.34	0.57	0.59	0.71	0.74	0.77	0.47	1.07	- -	1.34	- -
	Range	0.25	0.19	0.49	0.48	0.61	0.62	0.67	0.23	0.72	- -	1.00	- -
	Avg.	0.20	0.21	0.24	0.24	0.35	0.36	0.39	0.37	0.59	- -	0.97	- -

Footnotes: (1) "N" = data from soil profile above the estimated groundwater elevation. "Y" = data from soil profile below the estimated groundwater elevation.

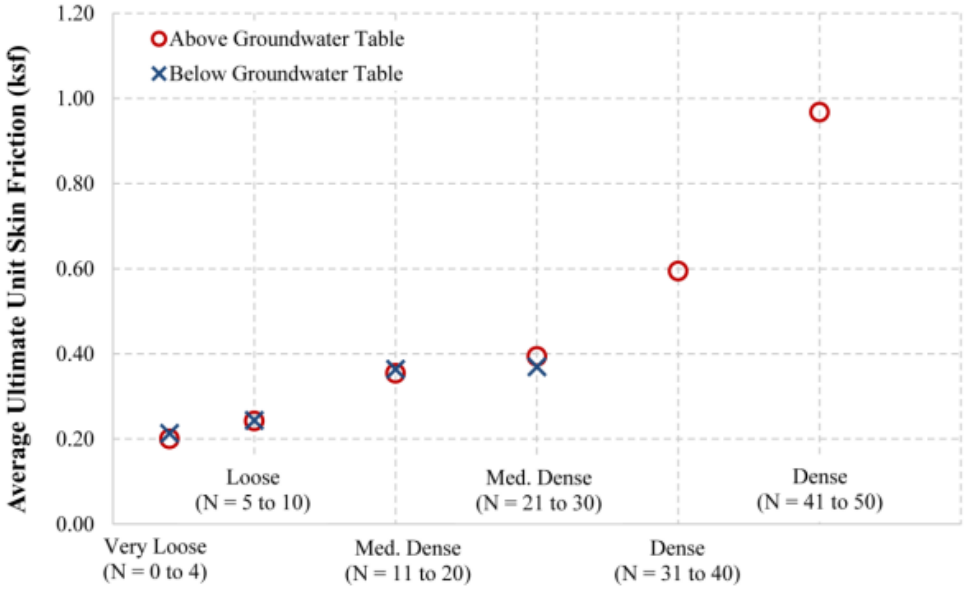

Figure 2.14 Average ultimate skin friction values *vs*. relative density of granular soils estimated from PDA tests (Underwood, 2020).

Table 2.7 Average ultimate skin friction values *vs*. relative density of granular soils estimated from PDA tests (from Underwood, 2020).

Project Name[(1)]	Test Pile Length (ft)	CAPWAP Ultimate Capacity		Avg. Ultimate Unit Skin Friction Resistance (ksf)	Final Pile Embed. Depth [(2)] (ft)	Ultimate Pile Capacity per Unit Wall Length [(3)] (klf)
		Skin (kips)	End (kips)			
Blue Apts.	37	197	19	0.6	15	27
	32	617	12	1.4	17	71
St. Cloud Police Station	32	161	9	0.8	20	44
Lake & Knox Apts. [(4)]	21	42	33	0.3	19	16
	23	29	11	0.2	19	10

Footnotes:

(1) Dynamic pile testing was completed only at sites where axial capacity was obtained entirely from skin friction.

(2) Embedded portion of pile below lowest floor slab elevation (uniform wall load condition only – deeper pile embedment was used at point load conditions where greater capacity was required.

(3) Ultimate pile capacity based on skin friction values estimated from load test data, before taking into account active and passive zone horizontal stress redistribution.

(4) Preliminary pile capacities prior to completing final CAPWAP analyses.

2.2.5 Summary

A review on several bridges with the sheet-pile abutment and field loading tests on the sheet pile suggests that the sheet-pile abutment system is capable of supporting a short-span bridge. However, there are several knowledge gaps identified during the review. For example, there is uncertainty on the side frictional resistance between the sheet pile and soil. It is rather complex with active and passive states of soils near the sheet pile, so a better understanding is needed to gain more confidence in the design of the axially loaded sheet pile wall. Besides, the plugged condition is highly uncertain. When it occurs, the shaft resistance may be reduced while the tip resistance is increased. More importantly, there has been no systematic study that investigated the effect of main factors, such as the bridge span length, excavation level, sheet-pile type and embedment depth, the presence of anchoring, groundwater level, end-bearing conditions, and seasonal temperature fluctuations.

Table 2.8 Summary of literature review about axially loaded sheet pile test in the thesis.

Measurement	Soil characterization	Type of soil	Test scale	Type of pile	Length of pile (m)	Perimeter and cross section	Ultimate load	Compared pile	Length of compared pile	Ultimate load of compared pile	Ref.
PDA	SPT	Sand	Full scale	AZ	11.2	N/A	(Q_u=216kips, Q_s=197 kips, Q_t= 19 kips)	N/A	N/A	N/A	1
Pile load test, PDA	SPT, CPT, DMT, Laboratory tests (Triaxial test, direct shear test, etc.)	Sand	Down scale	PZ27	2.2		(Q_u=1218.9 kN, Q_s=1130.3 kN, Q_t= 88.6 kN)	N/A	N/A	N/A	2
			Full scale	PZ27	5	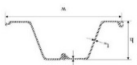	(Q_u=152.6 kN, Q_s=136.6 kN, Q_t= 16.0 kN)	H-pile 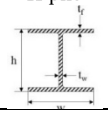	5	Q_u=100.1 kN	
Pile load test, PDA	SPT, CPT, PM, PAF, CPD, Laboratory test	Clay	Full scale	LP2S	7.4	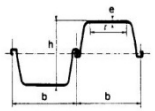	(Q_u=2400 kN, Q_s=1880 kN, Q_t= 520 kN)	Open end and closed end box-pile 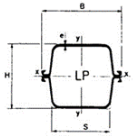	12.2	Q_u=2250 kN	3
		Sand		2S	12		(Q_u=3000 kN, Q_s=2491 kN, Q_t= 509 kN)		12.2	Q_u=1300 kN	
Pile load test, PDA	SPT	Sand, silt, gravel	Full scale	N/A	11.2		Q_u=3500 kN	Open end box pile 	11.2	Q_u=2100 kN	4
Pile load test	CPT	fine, medium and coarse sand	Full scale	AZ37	15		Q_u=2500 kN	Composite pile 4×GU16-400 	13	Q_u=2654 kN	5

(1) Underwood & Greenlee (2010)
(2) Sylvain (2019)
(3) Bustamante & Gianeselli (1991)
(4) Taenaka et al. (2006)
(5) Rybak & Zyrek (2013)

Chapter 3 Large-Scale Direct Shear Tests

The project team conducted the large-scale direct shear tests to better understand the interaction between sheet pile and soil, particularly the interface friction angle and the elastic threshold at the large scale. The test results, including the interface friction angle between sand and sheet piles, are one of the primary properties for estimating the bearing capacity of sheet piles.

3.1 Testing Setup

The shear box design was set up following ASTM D5321-12 (2021) to ascertain the interface friction angle and elastic threshold under both dry and wet conditions at a large scale. All the items were fabricated at a local plant in Omaha, Nebraska. The direct shear box design by the project team, shown in Figure 3.1, consists of the top and bottom boxes. The large-scale direct shear box was constructed with 0.5 m wide, 0.5 m long, and 0.25 m tall internal dimensions. The top box moves under the force of the hydraulic cylinder. The air cylinder sits on the top of the box to generate normal stress. It stands on a roller plate during the shear process. The vertical load was applied by a pneumatic cylinder and air pump (Figure 3.8). The vertical pressure was determined when the piston touched the load cell. The maximum air pressure that the piston can create for the test specimen was 50 kPa (7.3 psi), similar to the stress of 3 m (~10 ft) depths of dry sand. The hydraulic piston was installed horizontally and moved by the energy from the hydraulic pump. The capacity of the hydraulic piston was 17,200 kPa (2,500 psi). The maximum shear stress that can apply to the box is 45 kPa (6.5 psi).

The needle valves were installed on both sides to control the flow rate of the oil. This function controls the shearing velocity of the test within 0-5 cm/min following ASTM D5321-12 (2021). During the test, the research team continually monitored the pressure on the gauges

because pressure intensification may happen and exceed the allowable value of the equipment. A spring-type linear variable differential transformer (LVDT) was also installed from a fixed bar next to the piston to the top box. It measures the displacement of the box every second. The shearing rate is interpolated from these displacements. Two vertical LVDTs were applied from the extension rods (Figure 3.8) to measure vertical displacement during the shearing process.

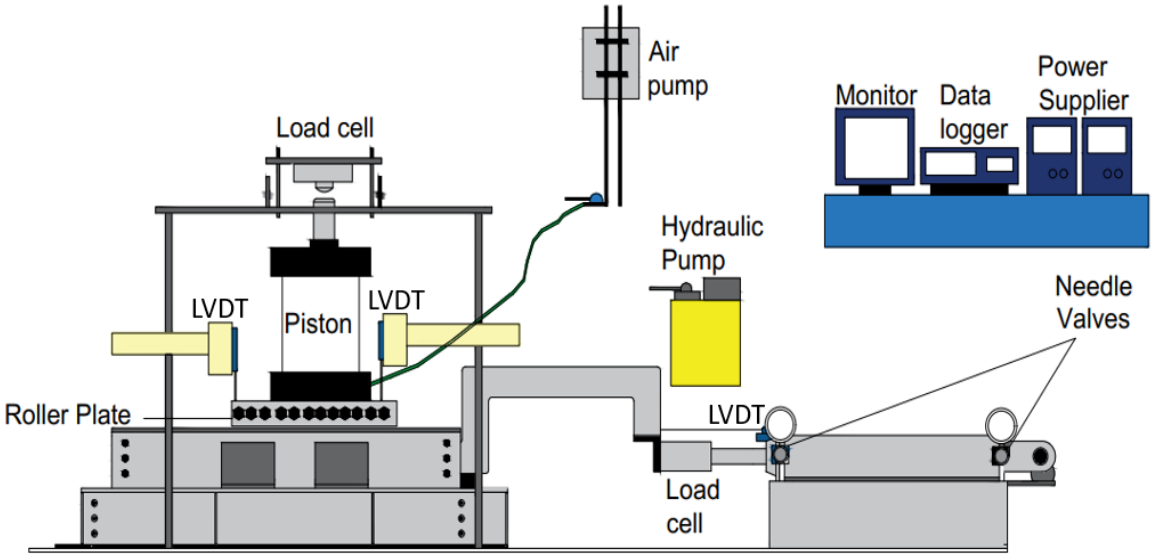

Figure 3.1 A schematic diagram of the large-scale direct shear testing setup for this research.

3.2 Material

3.2.1 Steel plate

The material used in this research is the same as that used for sheet pile PZ27. It was ordered from McMaster-Carr, a private USA supplier of hardware, tools, raw materials, industrial materials, and maintenance equipment. The plate size was 0.5 m by 0.5 m (~20 inches), and the thickness was 9.5 mm (0.37 inches), almost the same as the thickness of the actual sheet pile. The steel was produced and tested following ASTM A572/A572M-12 (2017).

A572 steel has a low carbon content and is easy to weld. Its yield strength is 50,000 psi (345 MPa), and it can handle heavy loads without fracturing. When it was delivered, the size of the plate was bigger than the size of the sheet pile wall, so it went through additional fabrication to fit into the box (Figures 3.2 and 3.3).

3.2.2 Fill Sand

The fill sand was acquired from a location south of Omaha, Nebraska, between the towns of South Bend and Louisville, north of the Platte River (Figure 3.4). The soil was brought back to Peter Kiewit Institute by a pick-up truck. The 50-gallon drums were used to store the fill sand in the laboratory.

Figure 3.2 Fabrication of the sheet pile sample for large-scale direct shear test.

Figure 3.3 The sample of steel plate for large-scale direct shear test.

Table 3.1 The properties and dimension of the test sheet pile sample.

Material	ASTM A 572 GRADE 50
Size	0.5 m × 0.5 m (20 inches)
Thickness	9.5 mm (0.37 inches)

Figure 3.4 The location where the research team acquired the fill sand.

The properties of collected fill sand are summarized in Table 3.2. The grain size distribution is shown in Figure 3.5.

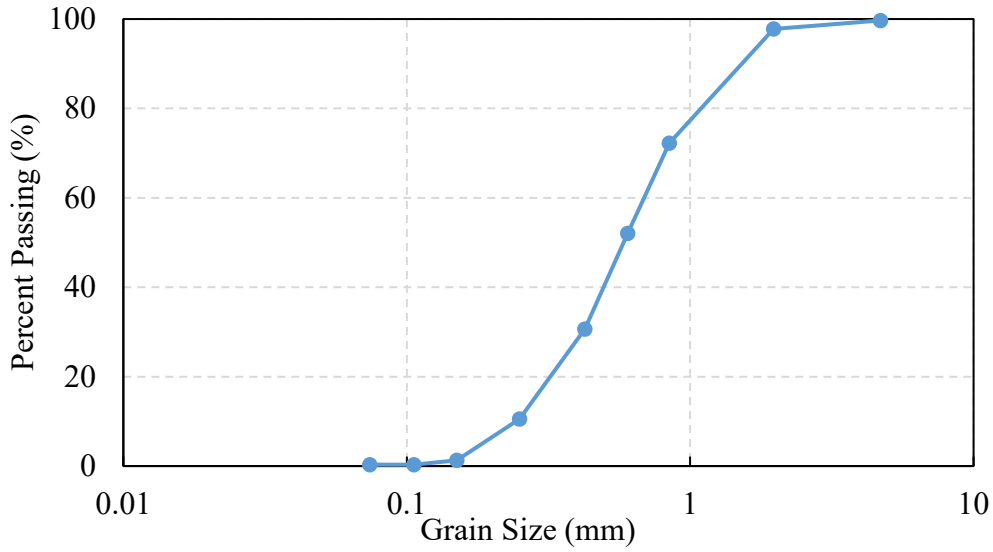

Figure 3.5 The grain size distribution of the collected fill sand.

Table 3.2 The properties of collected fill sand.

Soil property	Classification
$D_{60} = 0.69$, $D_{30} = 0.41$	USCS: SP
Uniform Coefficient, $C_u = 3.14$	AASHTO: A-1-b
Coefficient of Curvature $C_c = 1.11$	

3.3 Testing Procedure

The collected fill sand was air-dried initially, and then water was added to the soil to reach an optimum moisture content of 9%. Then, the sand was poured into the shear box, one sub-layer at a time. There were two layers—one below the sample of steel sheet pile and the other above it. Each layer was compacted into two sub-layers, each with a height of 2.54 cm (1 in.). Each sub-layer was compacted by dropping a 0.2 m × 0.2 m square steel tamper from the same height. The sub-layer was deemed adequate after the soil had reached 70% relative compaction (Figure 3.6). After the soil level reached the proper thickness, it was covered with a

~5.1 cm (2 in.) thick wooden plate. This wooden plate was stiff enough to transfer the uniform load from the air piston to the samples while also fitting within the inner wall of the top shear box. The air piston and roller plate were then placed on top of the plate (Figures 3.7 and 3.8). When applying the load, the pneumatic piston touched the load cell. The bottom of the piston was bolted with a steel roller plate to ensure it did not move during the shearing process. The cylinder provided almost consistent pressure during the shearing process. All the normal stress values during the shearing process were recorded by the vertical load cell. Three levels of vertical stress were applied to the sample (10 kPa, 30 kPa, 45 kPa; 1.45 psi, 4.35 psi, 6.5 psi), each with corresponding maximum horizontal pressure. The level of vertical stress was controlled by an air regulator. After the vertical pressure was stabilized, the upper box was sheared at a rate of 1 mm/minute to 5 mm/minute. Testing was stopped when the displacement reached ten percent (10%) of the inner dimension (Figure 3.9). The shear force was measured with a 15-ton capacity load cell. For the data acquisition system, a data logger from Keysight DAQ970A with a 20-channel multiplexer was used to read data from the load cells and the LVDTs.

Figure 3.6 Fill sand in the shear box.

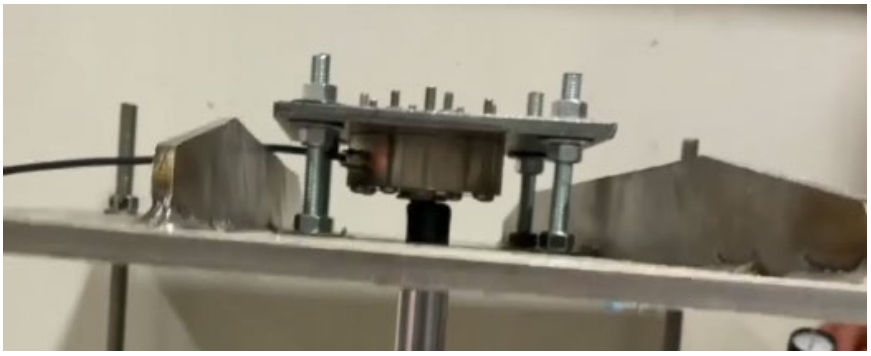

Figure 3.7 Load cell to measure the vertical normal stress.

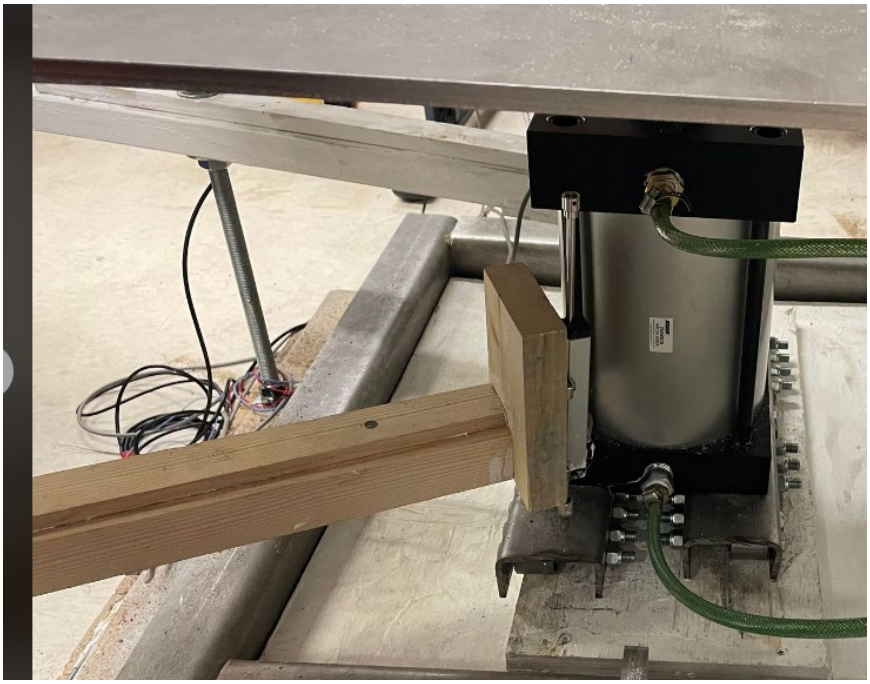

Figure 3.8 The piston and vertical LVDT placed on top of the shear box.

Figure 3.9 The horizontal LVDT.

The steel plate was clamped at one side and sheared to another, so the boundary did not affect the test result (Figure 3.10). The steel plate was placed between the two shear boxes.

Both submerged and dry conditions were examined in the tests. The sheet pile abutment functions to prevent scouring, so the submerged condition could be more probable environment.

The outside wall was applied to contain the water (Figure 3.11). The complete testing setup is shown in Figure 3.12.

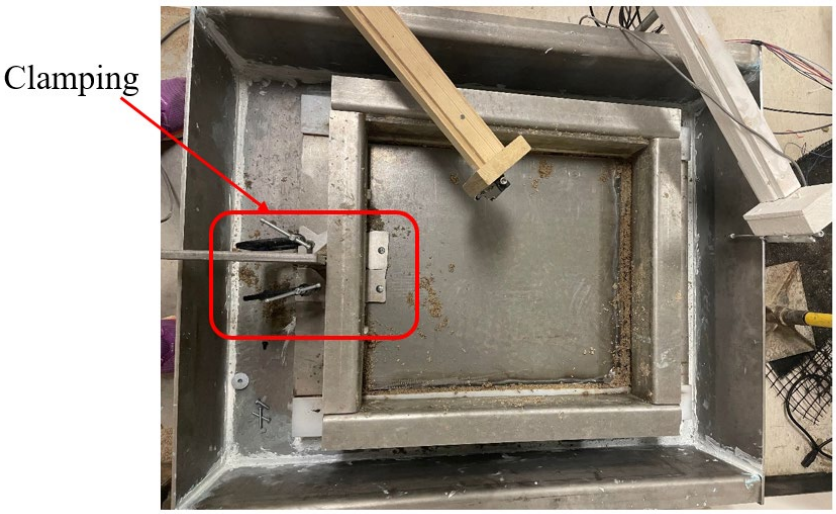

Figure 3.10 Clamping of the steel sample with the bottom shear box.

Figure 3.11 Implementation of the large-scale direct shear tests in (a) dry, and (b) submerge conditions.

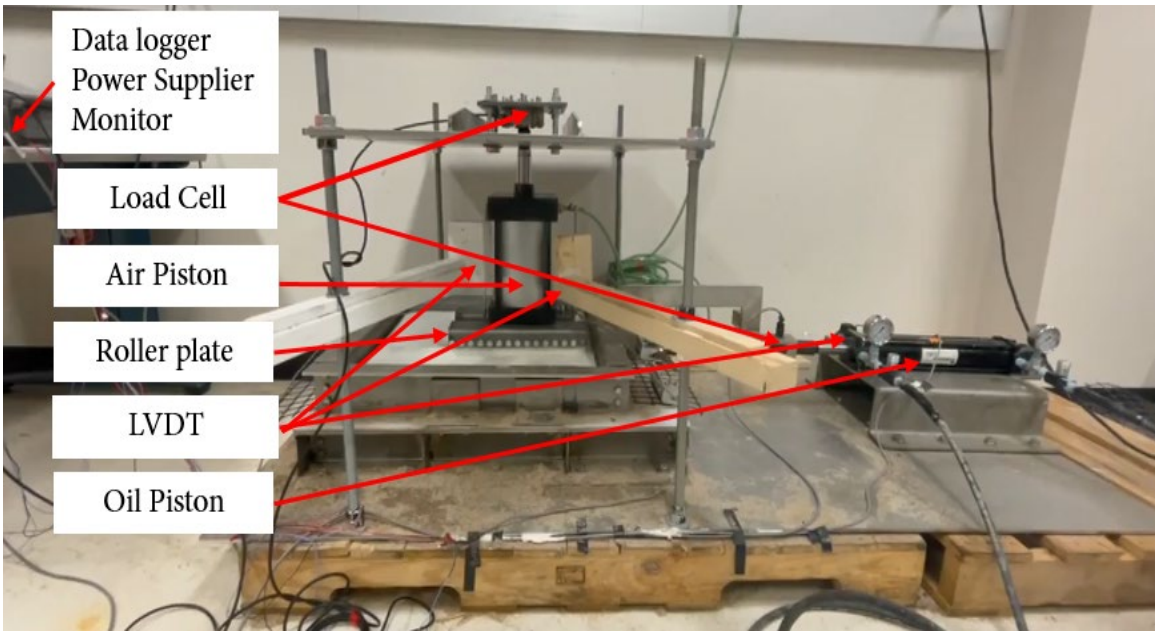

Figure 3.12 The complete setup of the large-scale direct shear tests.

3.4 Test Results

3.4.1 Internal Angle of Friction of Sand

Figure 3.13 shows the test results for sand only with three different normal stress values of 13, 25, and 41 kPa. Once the shear stress reached its maximum, it remained fairly stable during the extended duration of the shearing process.

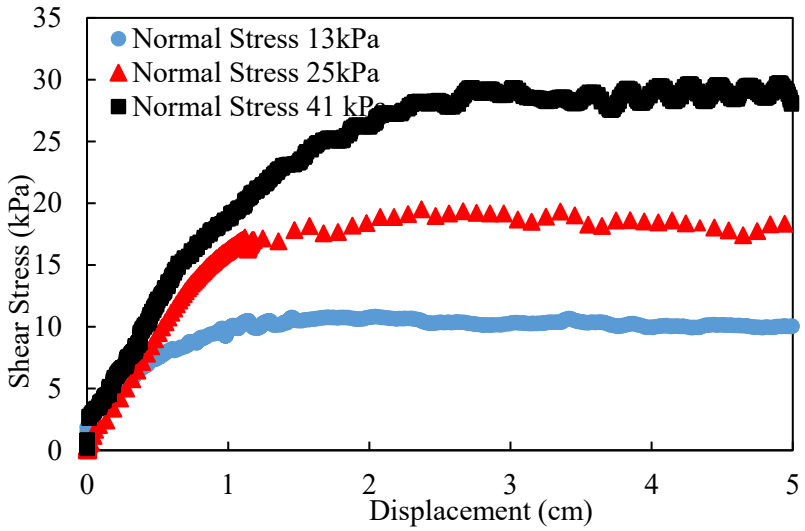

Figure 3.13 The shear stress-displacement curves for the sand only condition.

3.4.2 Interface Friction Angle between Sand and Steel Plate

Figures 3.14 and 3.15 show the shear stress-displacement curves for the sand-steel plate interface in the dry and submerged conditions, respectively. In general, the higher the confining stresses, the higher the maximum shear stresses observed. The shape of each shear stress-displacement curve was consistent between the dry and submerged conditions. The peak shear stresses were recorded at higher shear displacement as the confinement stress increased.

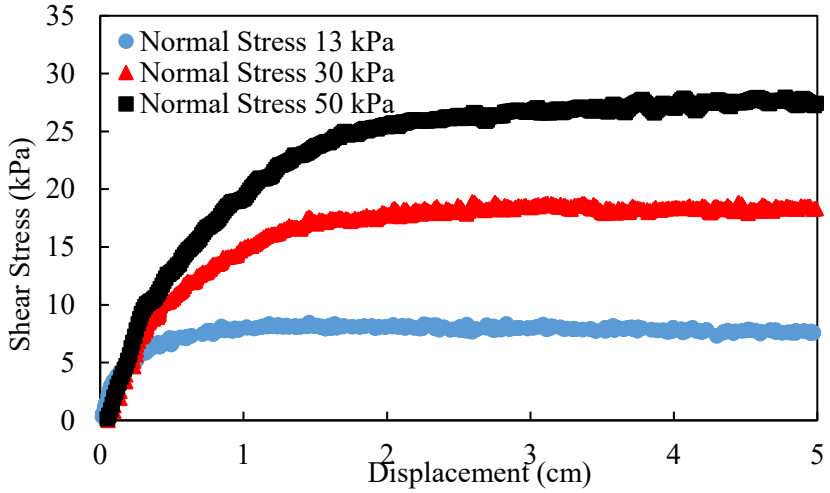

Figure 3.14 The shear stress-displacement curves for the sand-steel plate interface in dry condition.

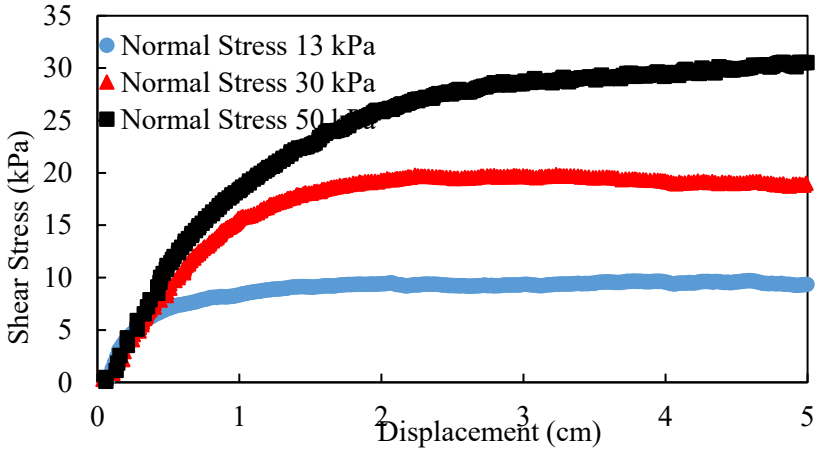

Figure 3.15 The shear stress-displacement curves for the sand-steel plate interface in submerged condition.

3.5 Interpretation

The sample was tested under three levels of confining stress, and the friction angles were determined based on Mohr-Coulomb criteria (Figure 3.16). This criterion was widely used among geotechnical engineers in practice because it was simple to understand and analyze. For sand only, the peak shear stresses were 10 kPa, 17 kPa, and 27 kPa, for confinement stresses of

10 kPa, 25 kPa, and 41 kPa, respectively. As a result, the internal angle of friction was obtained as 34°. At the same relative density, the friction angle of the interface between sand and steel plate was 27°, which was almost four-fifths (4/5) of the internal friction angle of sand (Table 3.3). In general, geotechnical engineers adopt two-thirds of the internal friction angle for the interface friction angle. As expected, the interface friction angles were not significantly different between the submerged and dry conditions. These results were in good agreement with the study reported by Underwood et al. (2020). This obtained friction angle of the interface is used for the numerical study of the sheet pile abutment in the following chapters.

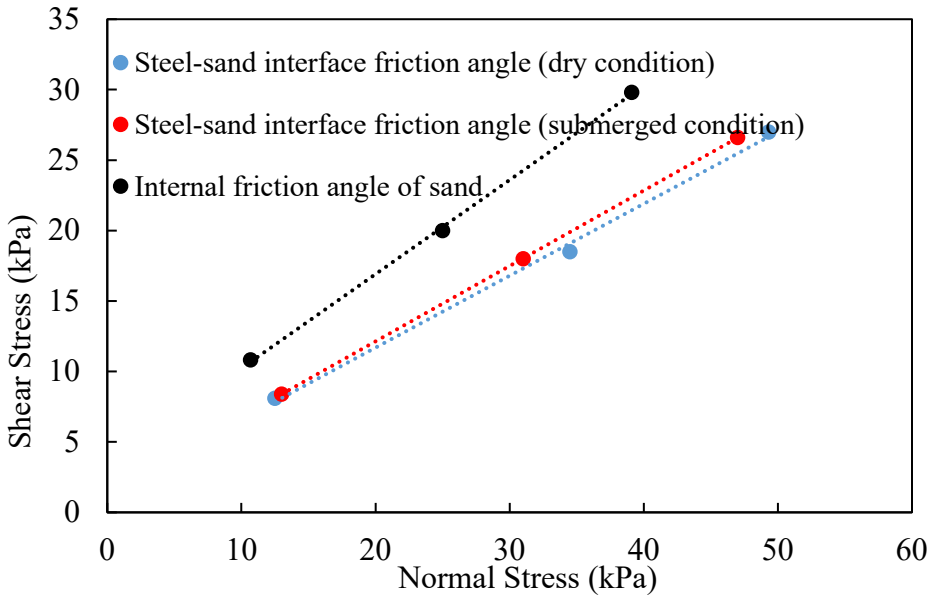

Figure 3.16 The compiled normal stress-shear stress data to determine the friction angle.

Table 3.3 Summary: Internal friction angle of sand and sand-steel plate interface friction angle.

Material	Friction angle (°)
Sand-steel plate interface (dry condition)	27
Sand-steel plate interface (submerge condition)	28
Sand only	34

The elastic strain threshold was the point where the behavior of the soil in the stress-strain curve transitioned from elastic to plastic. During the shearing process, the elastic strain threshold of the sand-steel plate interface was reached at different levels corresponding to varying magnitudes of confining stresses (Table 3.4).

Table 3.4 Summary: the elastic strain threshold of soil-steel plate interface.

Confining stress (kPa)	Elastic strain threshold (dry condition)	Elastic strain threshold (submerged condition)
13	0.06 of D	0.07 of D
30	0.26 of D	0.26 of D
50	0.36 of D	0.40 of D

D: Diameter or width of the sample.

Chapter 4 Down-Sized Pile Load Tests

This chapter presents the setup and results of the static pile loading test with a down-sized test sheet pile. The static pile load test yields the load-displacement curve of the test sheet pile in a particular soil condition.

4.1 Estimate of Bearing Capacity of Sheet Pile: Analytical & Empirical Approaches

Total bearing capacity consists of skin friction along the side and the bearing capacity at the tip. With that, the ultimate bearing capacity (Q_u) can be expressed as follows (Das and Sivakugan, 2019), similar to the previous studies introduced in Chapter 2:

$$Q_u = Q_p + Q_s \tag{4.1}$$

where Q_p is the point bearing capacity and Q_s is the frictional resistance (skin friction) along the shaft of the pile. Each approach has a calculation method for (a) Point Resistance and (b) Side Resistance.

4.1.1 Analytical Approach

(a) Point Resistance

Point bearing capacity in clay (φ=0) is estimated following Meyerhof's method (Meyerhof, 1976). With that, the end bearing capacity of the sheet piles in this research is estimated using the following equation:

$$Q_p = 9c_u A_p \tag{4.2}$$

where c_u is the undrained shear strength of soil and A_p is the cross-sectional area at the tip of the pile.

(b) Side Resistance

The following equation is used to evaluate the side resistance of the sheet pile surrounded by granular soils:

$$Q_s = \sum p \Delta L f \tag{4.3}$$

where p is the perimeter of the pile, ΔL is the length of the pile at each sub-layer, and f is the unit frictional resistance. Many factors can affect the distribution of side resistance of the sheet piles, such as pile installation methods, soil density, and pile types (e.g., low-displacement or high-displacement piles). The unit frictional resistance is known to reach its maximum at $L'=15D$, with D being the diameter of the pile:

$$f = K\sigma_0' tan\delta' \tag{4.4}$$

where σ_0' is the effective vertical stress at the point of interest. In general, effective stress is the average value for the area of mobilized side resistance. The magnitude of K, the coefficient of Earth pressure, depends on many factors. It varies with depth, and it can be the passive or active coefficient depending on whether the pile moves towards or away from the soil. Sheet pile is a low-displacement pile, so the K value varies from 1-sinφ' to 1.4(1-sinφ') (Das and Sivakugan,

2019). Based on the load test results, Mansur & Hunter (1970) reported the following average values of K:

- H-piles: K = 1.65
- Steel pipe piles: K = 1.25
- Precast concretes piles: K = 1.5

δ' is the interface friction angle between soil and pile. For design purposes, geotechnical engineers adopt two-thirds of the internal friction angle of soil as the interface friction angle in general. In this project, the friction angle between soil and pile was obtained as 27°, while the internal friction angle of soil was 34° from the laboratory tests.

4.1.2 SPT-Based Estimate

(a) Point Resistance

Meyerhof (1967) suggested the unit point bearing capacity (q_p) in sand can be evaluated based on the standard penetration test (SPT) results as follows:

$$q_p = 0.4 p_a N_{60} \frac{L}{D} \leq 4 p_a N_{60} \tag{4.5}$$

where N_{60} is the average number of blow counts near the pile tip (about 10D below and 4D above the pile tip), L is the length and D is the diameter of the pile, and p_a is the atmospheric pressure (= 100 kN/m^2 = 14.5 psi).

(b) Side Resistance

For low-displacement piles, the unit side resistance (f) based on the SPT results is:

$$f = 0.01 p_a (N_{60}) \tag{4.6}$$

The number of blow counts needs to be corrected because it is affected by the effective overburden stress. N_{60} is corrected following Equation 4.7:

$$(N_1)_{60} = C_N N_{60} \tag{4.7}$$

where $(N_1)_{60}$ is the value of blow counts after correcting from N_{60}, and C_N is the correction factor. In this project, C_N is estimated following Liao & Whitman (1986):

$$C_N = \left[\frac{1}{\left(\frac{\sigma'_o}{p_a}\right)}\right]^{0.5} \tag{4.8}$$

4.1.3 CPT-Based Estimate

(a) Point Resistance

The method suggested by Meyerhof (1956) is as follows:

$$q_p \approx q_c \tag{4.9}$$

where q_c is the penetration resistance at the tip of the CPT cone.

(b) Side Resistance

Unit skin resistance (f) is calculated from the cone penetration test (CPT) following Nottingham & Schmertmann (1975) and Schmertmann (1978):

$$f = \alpha' f_c \tag{4.10}$$

α' depends on the pile type and L/D ratio, as shown in Figure 4.1.

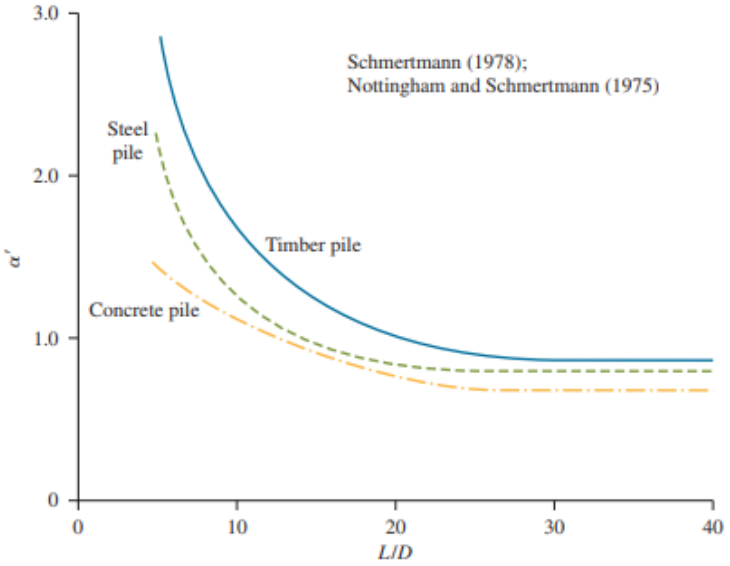

Figure 4.1 Variation of α' with an embedment ratio of pile in sand: electric cone penetrometer (Das and Sivakugan, 2019).

4.2 Estimate of Bearing Capacity: Axial Loading Test

The static axial loading test is a widely used field test approach used to evaluate the bearing capacity of deep foundations prior to the construction of a superstructure. The test measures the displacement of a pile under an applied axial load. There are two different pile load test arrangements. The first arrangement utilizes heavy kentledge weights, and the second

employs reaction piles (Figure 4.2). A continuous load transfer from the reaction frame to the pile head causes the pile to settle until it reaches the ultimate load, determined by failure criteria.

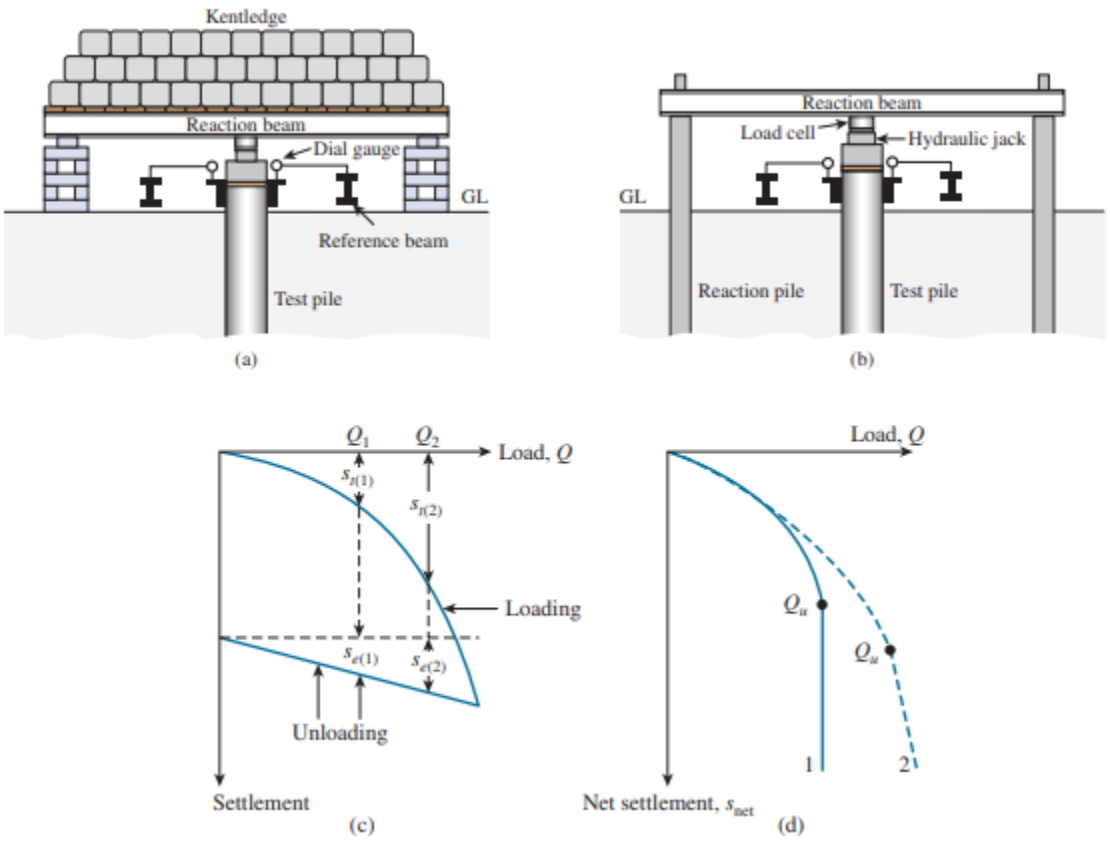

Figure 4.2 The static pile loading test: (a) using kentledge, (b) using reaction pile, (c) load *vs*. total settlement plots, and (d) load *vs*. net settlement (image from Das and Sivakugan, 2019).

Davisson's method (Davisson, 1973) is used as the failure criteria for the static pile loading tests in this project. The ultimate load occurs at a total settlement level (S_u) of:

$$S_u(mm) = 4 + \frac{D}{120} + \frac{Q_u L}{A_p E_p} \tag{4.11}$$

where Q_u is the ultimate load (kN), D is the pile diameter or width (mm), L is the pile length (mm), A_p is the area of the pile cross section (mm^2), and E_p is the elastic modulus of the pile (kN/mm^2).

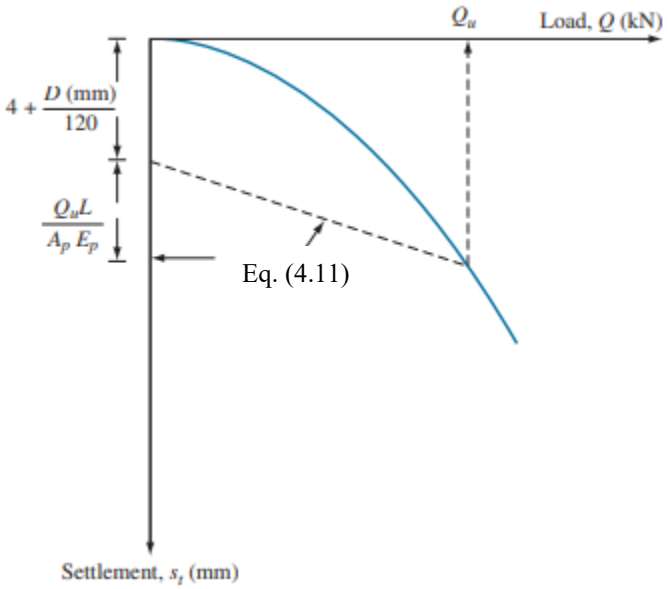

Figure 4.3 Davisson's method for the determination of Q_u (image from Das and Sivakugan, 2019).

4.3 Axial Loading Test of the Model Sheet Pile

To comprehend the axial bearing capacity of sheet piles, a down-sized static pile loading test was conducted at the University of Nebraska-Lincoln. Tests were conducted to determine the side and tip resistances and the results were compared with analytical and empirical predictions. The test results can help to better understand how sheet piles behave under axial loads.

4.3.1 Test Site

The test was conducted at the Midwest Roadside Safety Facility (MwRSF) testing site near the Lincoln municipal airport in Lincoln, Nebraska (Figure 4.4). The size of the test pit was

1.8 m (~6 ft) by 1.8 m (Figures 4.5 and 4.6). The excavated depth of the test pit was about 3 m (~10 ft).

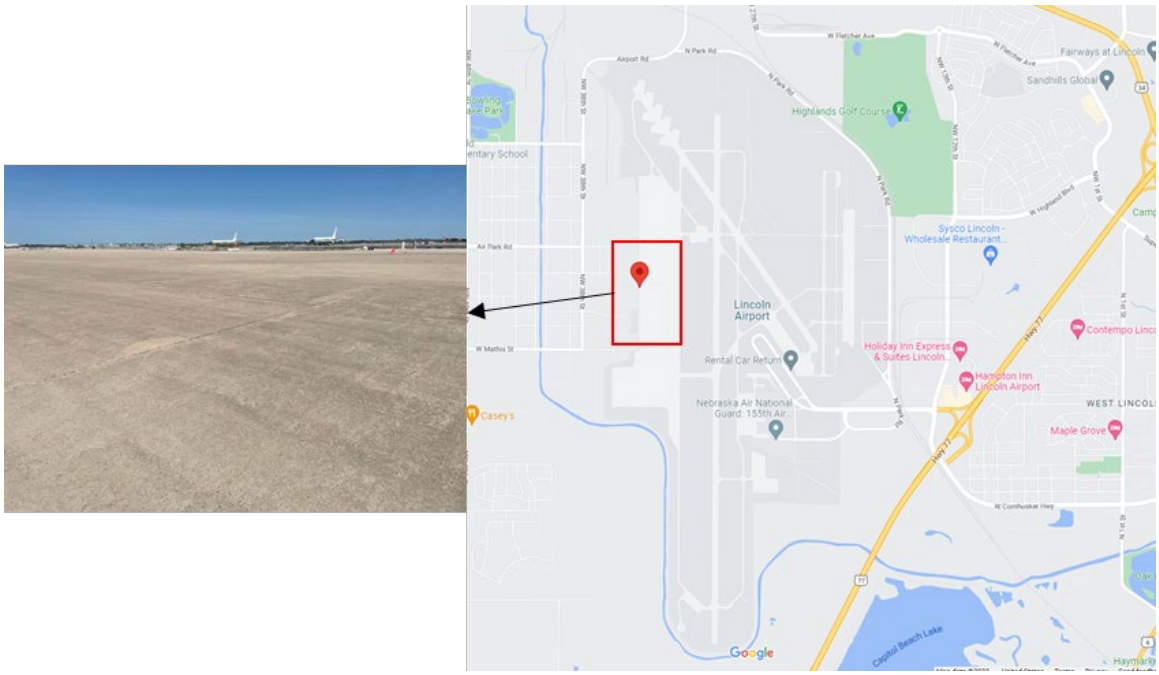

Figure 4.4 The location of the test site at the Midwest Roadside Safety Facility (MwRSF).

Figure 4.5 A photo of the test pit after excavation.

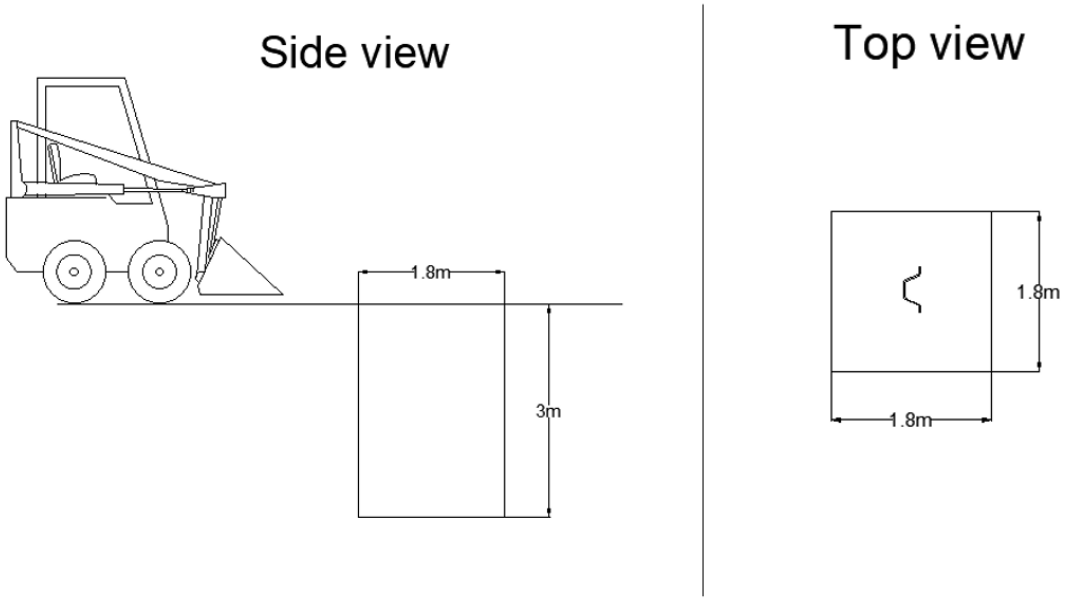

Figure 4.6 The drawing and dimensions of the test pit with a sheet pile.

4.3.2 Fill Soil

The fill sand, shown in Figure 4.7, was purchased from Martin Marietta, a company that supplies aggregates and heavy building materials in the USA. Figure 4.8 and Table 4.1 show the properties and grain size distribution of this sand. The soil was poorly graded, with gravelly sands and little or no fines.

Figure 4.7 The fill sand used for the static pile loading test.

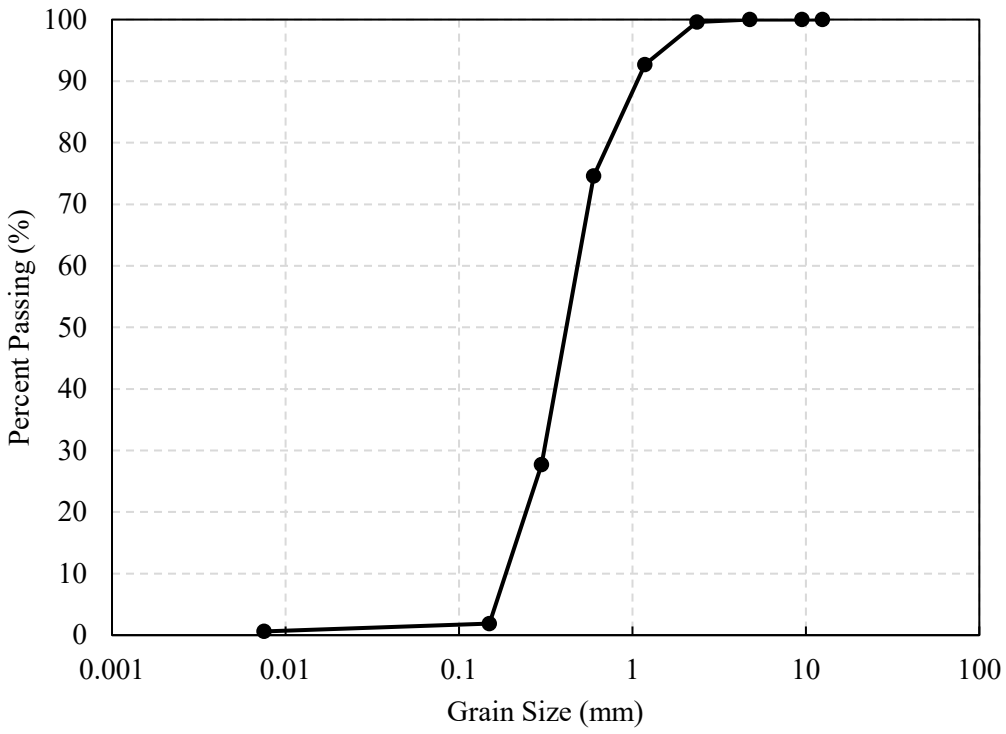

Figure 4.8 The grain size distribution of sand used for the static pile loading test.

Table 4.1 Classifications of sand used for the static pile loading test.

Property of soil	Classification
$D_{60} = 0.51$, $D_{30} = 0.31$, $D_{10} = 0.20$ Uniform Coefficient, $C_u = 2.6$ Coefficient of Curvature, $C_c = 1.0$	USCS: SP AASHTO: A-1-b

4.3.3 Site Investigation of the Test Site

The SPT and CPT tests were conducted using Geoprobe 7822 DT (owned by the project team; Figure 4.9), based on ASTM D1586/D1586M-18e1 (2022). The location of the SPT and CPT tests was near the sheet pile installation location (Figure 4.10).

The SPT test was conducted using an automatic hammer (Figure 4.11), and the field N-values were corrected for energy and overburden to obtain $(N_1)_{60}$ values. $(N_1)_{60}$ increased

gradually from 1 to 5 from the surface to the bottom of the test pit (3 m), and then jumped to 9 at 3.5 m where the in-situ soil underlayed the test pit (Figure 4.12).

The CPT test was conducted up to a 4 m (~13 ft) depth (Figure 4.13). CPT data included the tip resistance, skin resistance, and pore pressure. As depth increased from 0 to 2.5 m (8.2 ft), q_c (tip resistance) and f_s (skin resistance) values increased (Figure 4.14).

Figure 4.9 Geoprobe 7822 DT used for the subsurface investigation of the test site.

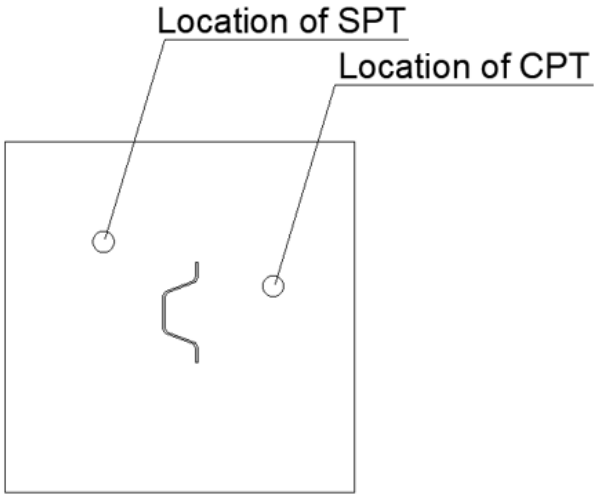

Figure 4.10 Top view: the location of SPT and CPT tests on the test site.

Figure 4.11 SPT test conducted by the research team.

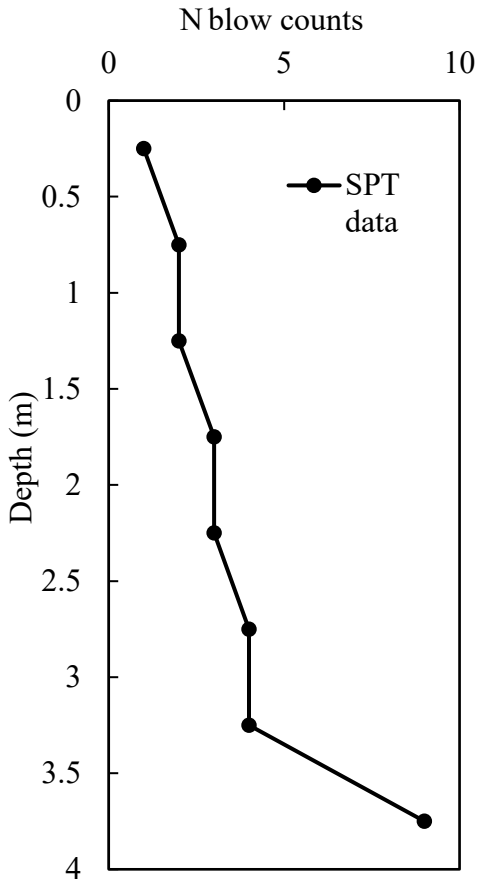

Figure 4.12 Original *N* values obtained from the SPT test.

Figure 4.13 CPT test conducted by the research team.

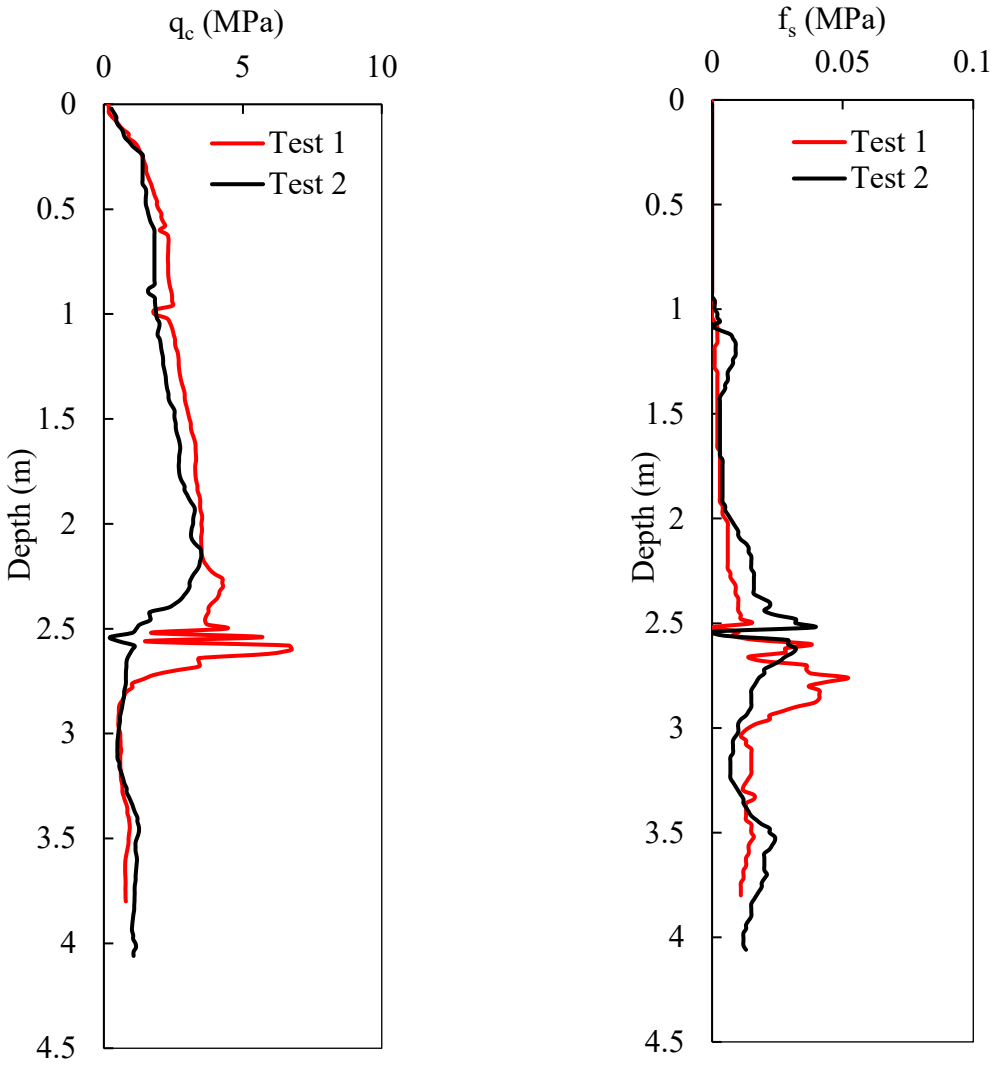

Figure 4.14 The tip resistance q_c, and skin resistance f_s (left to right) obtained from CPT tests.

4.3.4 Summary: Site Investigation and Prediction of Bearing Capacity of the Test Sheet Pile

Tables 4.2 and 4.3 present a summary of the properties of soil and test sheet pile, respectively. Table 4.4 shows a summary of the prediction on the side resistance, tip resistance, and total bearing capacity of the test sheet pile from the analytical, SPT-based, and CPT-based

methods. The SPT-based method yielded a smaller bearing capacity than the other two approaches.

Table 4.2 Soil parameters used to estimate the bearing capacity of sheet pile.

Soil Parameter				
γ (kN/m^3)	ϕ (°)	C (kN/m^2)	θ(°)	K=1-sinϕ
18	30	0	24	0.5

Table 4.3 The properties of the model test sheet pile.

Pile designation		Sheet pile
Type		PZ27
Width, W (m)		0.457
Depth, h (m)		0.153
Thickness	Flange, t_f (m)	0.0095
	Wall, t_w (m)	0.0095
Cross sectional area (m^2)		0.005
Perimeter surface area (m)		1.28
Young's modulus (Pa)		$2x10^{11}$

Table 4.4 A prediction of the bearing capacity from analytical, SPT-based, and CPT-based methods.

Method	Length (m)	Q_{shaft} (kN)	Q_{tip} (kN)	$Q_{ultimate}$ (kN)
Analytical method	2.7	28.8	8.7	37.4
SPT-based method	2.7	15.1	10.4	25.6
CPT-based method	2.7	20.5	12.4	32.9

4.3.5 Preparation of Down-Sized Test Sheet-Pile

The test model sheet pile was designed based on the dimensions of PZ27 sections. However, in order to accommodate the project team's test capacity, the width and height of the test sheet pile was reduced by 50%. Its total length was 3 m (~10 ft). The test sheet pile was fabricated using the same material for general PZ27.

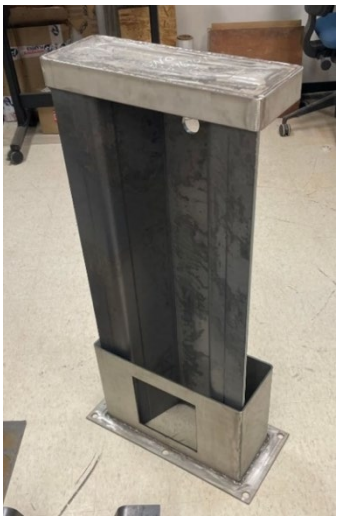

Figure 4.15 A photo: the piece of test sheet piles (1 m long each), with the bearing plate.

For the instrumentation, the project team installed strain gauges along its length, as shown in Figure 4.16. Two types of strain gauges, electric resistive strain gauges (Micro-

Measurements VPG Brand) and vibrating wire strain gauges (4150, GEOKON) were attached at each location to collect data, following the instructions from the manufacturers.

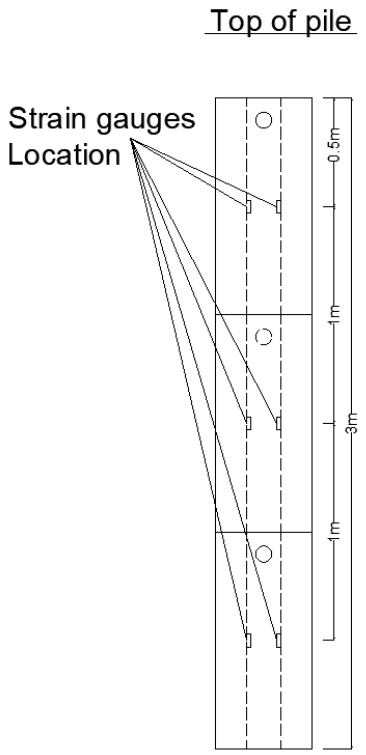

Figure 4.16 The location of strain gauges (one electric resistive and vibrating wire strain gauge at each depth) attached on the test sheet pile.

To begin installation of the resistive strain gauges, sandpaper was used to smooth out the rough surface. A cleaning liquid was then applied to degrease the surface. After that, the M-Bond 200 Catalyst C was applied to control the reactivity rate of the M-Bond 200 adhesive (Figure 4.17). These precautions helped to minimize the effects of poor bond strength, age-embrittlement of the adhesive, and poor glue line thickness control.

For the vibrating strain gauge installation, on the other hand, engineers needed to adjust the coins to the nominal mid-range position of 2500μ using a small wrench. Then, after locating

the strain gauge at the desired position, engineers held the sensor with the V-positioning tool and welded the flange of strain gauges to the sheet pile using a spot-welding machine. Note that gauge wire tension could not be readjusted after welding down. Then, users applied collar shim to distribute strains evenly on the strain gauges.

Two types of covers were employed for the strain gauges in this project. The first type of protection was a gauge protection kit from GEOKON (Figure 4.19). The second type of protection was the use of metal pieces across the sheet pile to fully isolate the strain gauge from the soil. These metal pieces were welded by the project team (Figure 4.20).

Figure 4.17 Cleaning liquid and adhesive used for resistive strain gauge installation (from Micro-Measurements VPG).

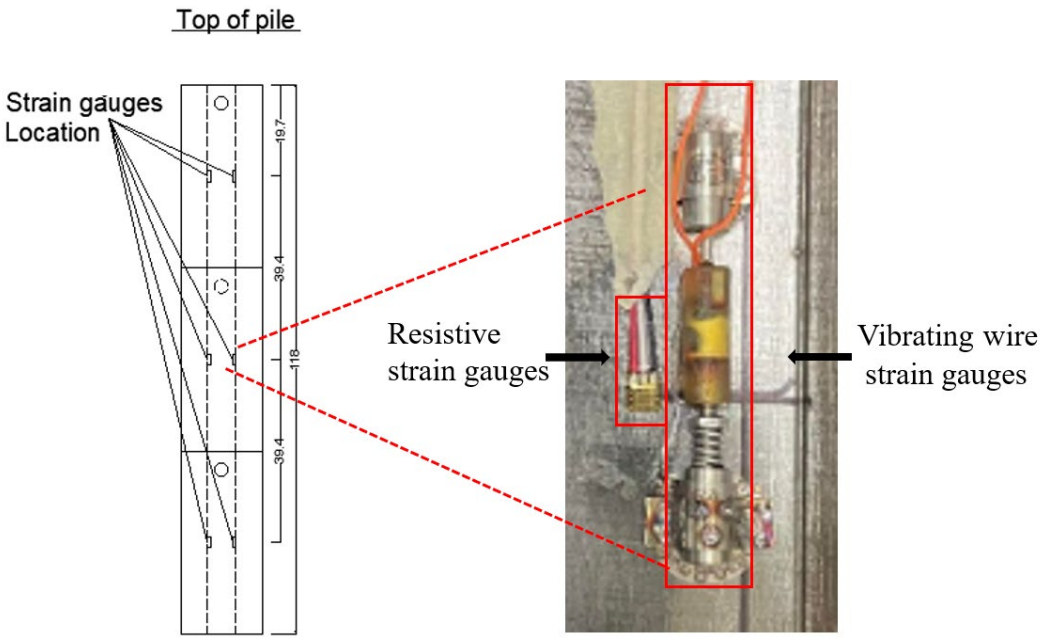

Figure 4.18 Actual photo of resistive and vibrating strain gauges attached to the test sheet pile.

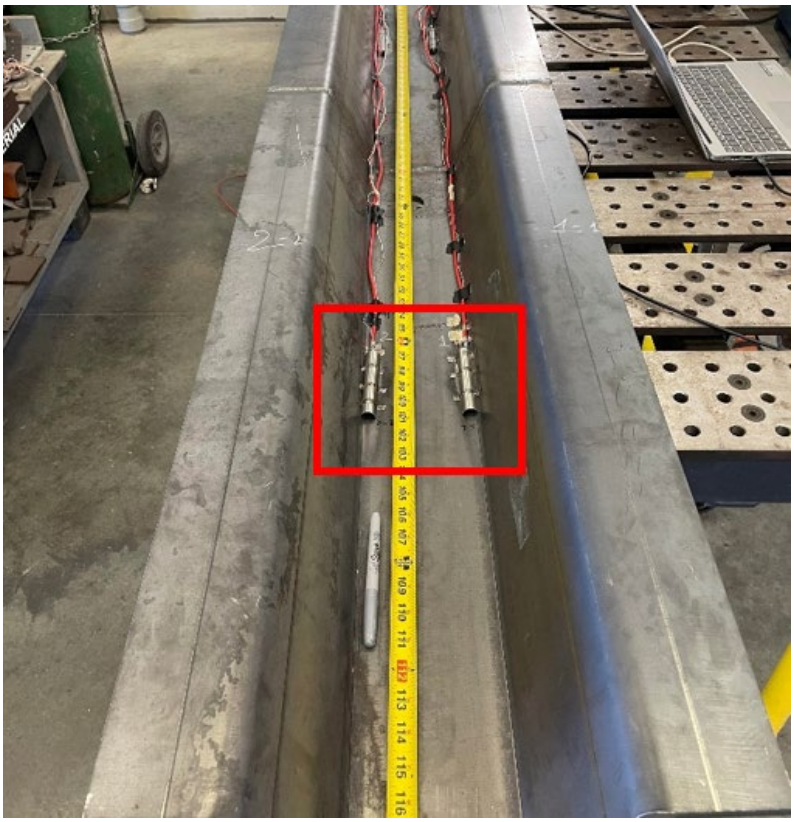

Figure 4.19 The protection kit for strain gauges (from GEOKON).

Figure 4.20 Welding of an outside cover for strain gauges.

Strain gauges measured strains (ε) or deformations of the test sheet pile. Stresses were also calculated by multiplying the measured strain by the Young's modulus of steel (E_s), which varied between 190 to 206 GPa. Then, loads (F) at the pile-soil interface were computed by multiplying the stress by the cross-sectional area (A_g) of the test sheet pile as follows:

$$F = \varepsilon E_s A_g \tag{4.12}$$

4.3.6 Setup of the Axial Loading Test

The static pile loading test design followed ASTM D1143/D 1143M – 07 (2020). This test aimed to estimate the axial bearing capacity of the model test sheet pile. In this project, the research team used the anchor method with concrete blocks (Figures 4.21 to 4.23) to apply the necessary reaction force. Given the sheet pile's estimated bearing capacity from the analytical, SPT-based, and CPT-based methods was in the range of 23.4 kN to 43.1 kN, this setup was deemed sufficient. The load cell (ATO) with a capacity of 20 tons was installed between the test sheet pile and the bearing plate to monitor the applied load during the test. The LVDT was also installed on top of the bearing plate to read the vertical displacement of the pile head (Figure 4.24).

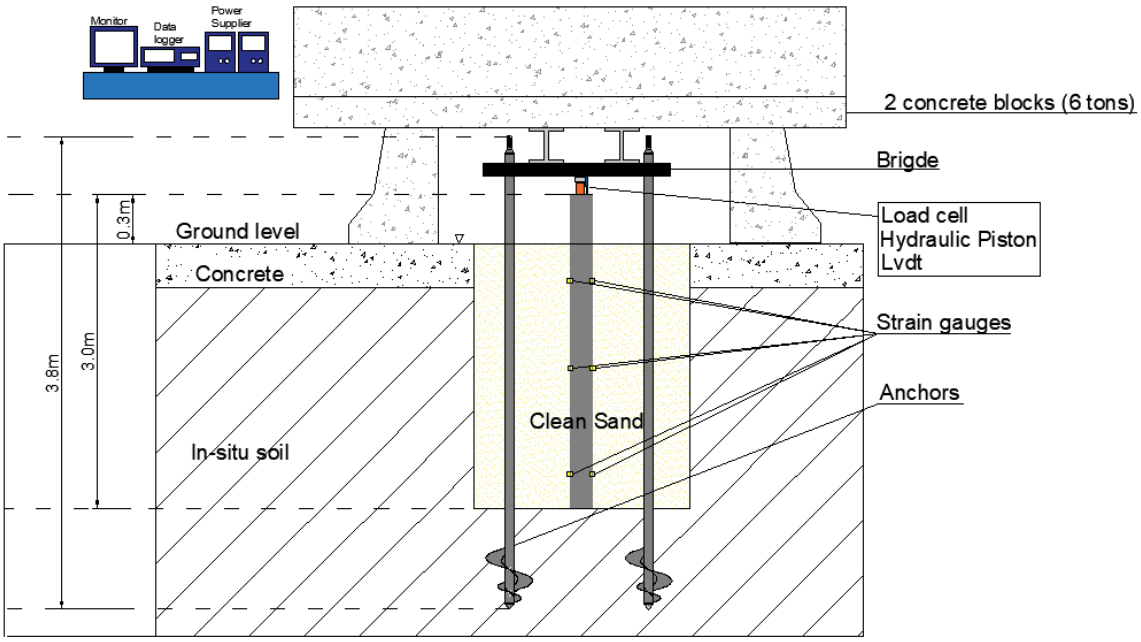

Figure 4.21 An overall setup for the axial loading test with the model sheet pile.

Figure 4.22 A photo of the axial loading test setup with the reaction beam (front view).

Figure 4.23 A photo of the axial loading test setup with the reaction beam (side view).

Figure 4.24 The vertical LVDT installed on the top of the bearing plate.

4.3.7 Test Procedure

To begin, all sensors, including strain gauges, loadcell, and LVDT, were connected to the data logger, power supply, and computer (Figure 4.25). The research team also checked the vertical alignment of the LVDT and the horizontal alignment of the reaction beam before each loading test. The applied force was controlled by using the load cell and hand pump (Figure 4.25). The load increment was 10% of the estimated ultimate bearing capacity. The team kept each loading stage constant for a time interval between 4 minutes and 15 minutes, complying with ASTM D1143/D 1143M – 07 (2020).

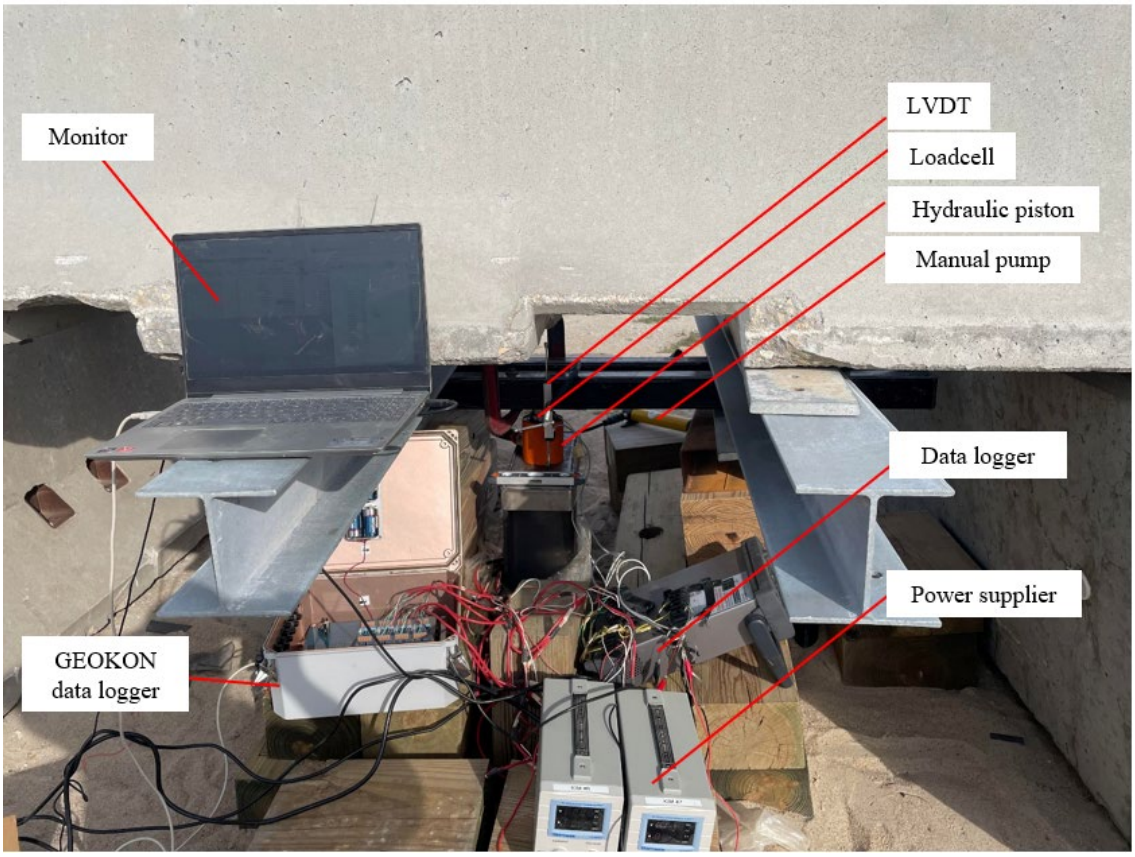

Figure 4.25 A photo of the overall axial loading test setup.

4.4 Numerical Modeling of the Axial Loading Test

Numerical simulation using FLAC on the static axial loading condition was conducted as a complementary analysis based on the site investigation data (Figure 4.26). Adopted soil and soil-pile interface properties are summarized in Tables 4.5 and 4.6, respectively. Details on the numerical modeling are provided in Chapter 5.

Table 4.5 Soil properties used for the complementary numerical simulation on static axial loading test.

Material	Unit weight (kg/m^3)	K (Pa)	G (Pa)	Friction angle (^{o})	Cohesion, c (Pa)	Model
Sand	1,800	5.30E6	3.20E6	30	2000	Mohr-Couloumb
Clay	1,700	2.00E7	4.30E6	0	50000	Mohr-Couloumb

Table 4.6 Soil-pile interface properties for the complementary numerical simulation on static axial loading test.

Interface properties for beam element's model	
Interface normal stiffness (Pa/m)	3.83E8
Interface shear stiffness (Pa/m)	3.83E8
Interface cohesion (Pa)	0
Interface friction angle (^{o})	24

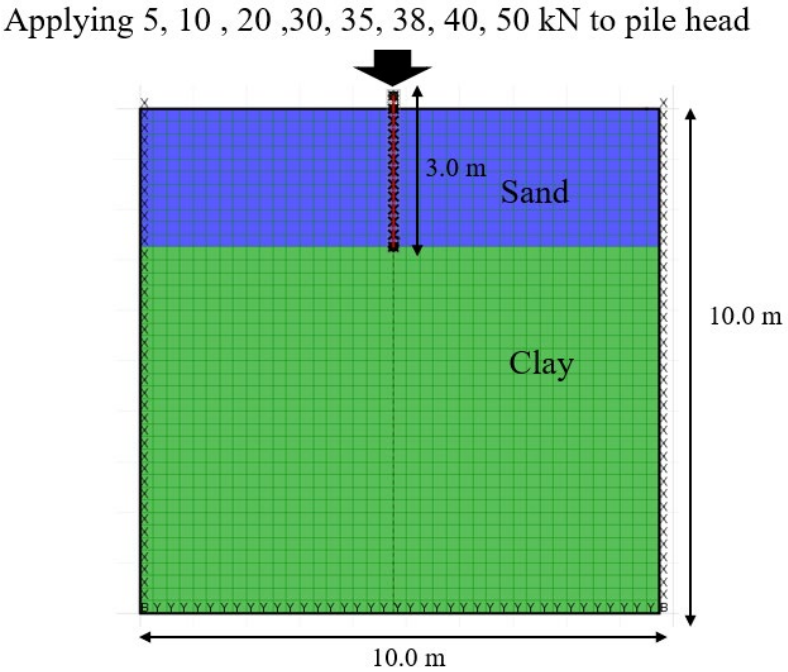

Figure 4.26 Constructed numerical model in FLAC for the static axial loading test.

4.5 Test Results

Three separate static axial loading tests were conducted, and the obtained results were quite consistent (Figure 4.27). The research team also obtained the load transfer curves along the pile length by analyzing the data from strain gauges attached to the test sheet pile (Tests #1 and #2 – Figures 4.28 and 4.29).

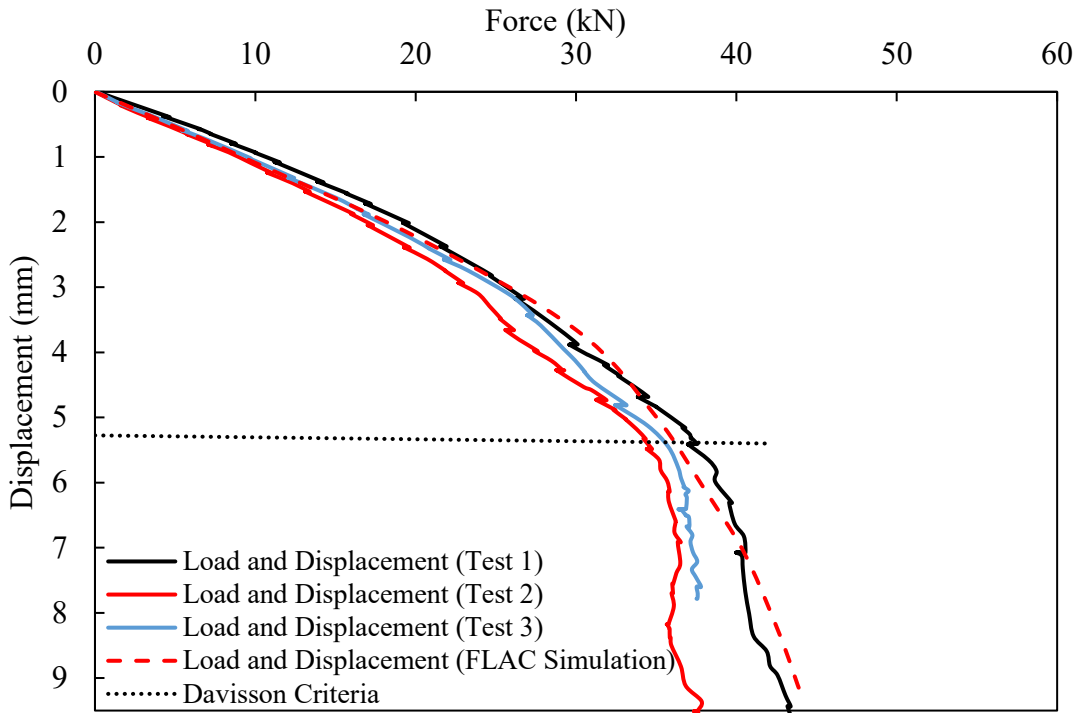

Figure 4.27 Applied axial load *vs*. displacement curves obtained from three static axial loading tests and complementary numerical simulation using FLAC.

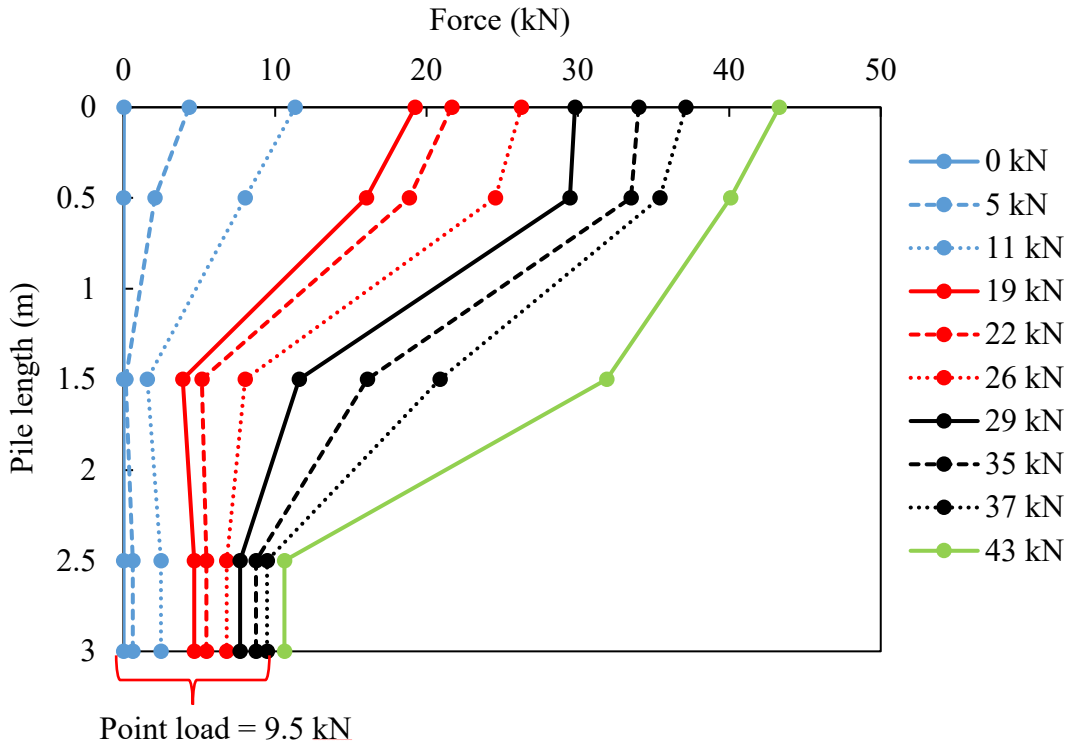

Figure 4.28 Load transfer along the pile length. Data is obtained from strain gauges attached to the test sheet pile (axial loading test #1).

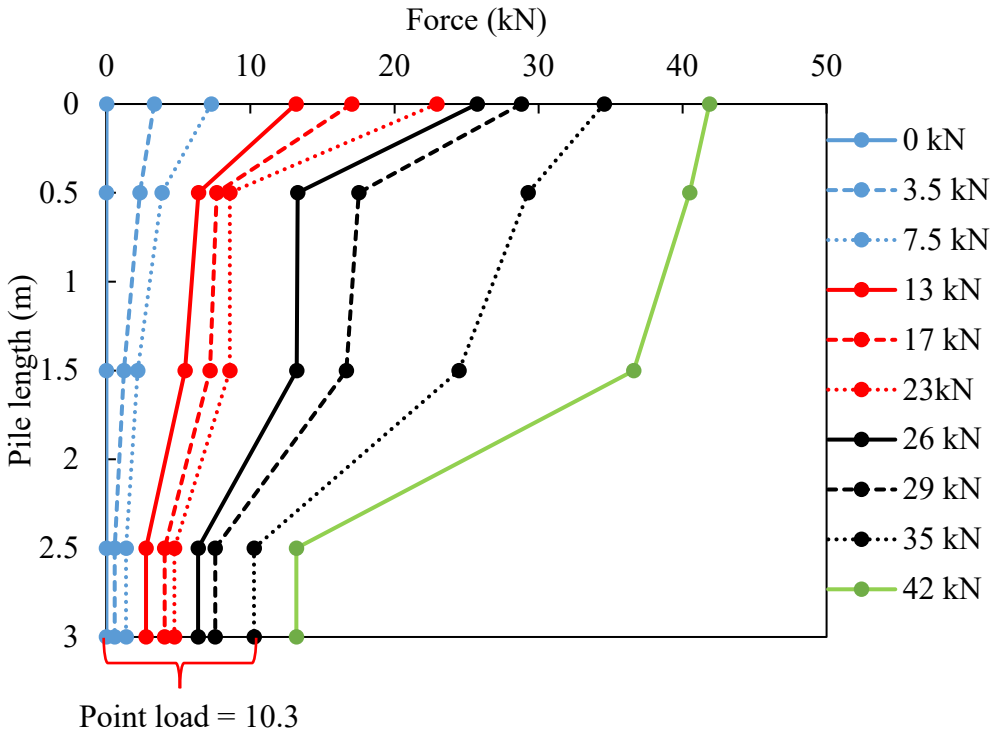

Figure 4.29 Load transfer along the pile length. Data is obtained from strain gauges attached to the test sheet pile (axial loading test #2).

4.6 Comparison and Discussion

The ultimate bearing capacity of sheet piles obtained from three separate static pile loading tests was consistently in the range of 35 kN to 37 kN. Analysis based on the strain gauge measurements showed that the pile shaft carried most of the load (70% to 75%), while the tip resistance contributed up to 25% of the total bearing capacity. The CPT-based method resulted in an adequate match with the field test data, while the analytical method and SPT-based method appeared to slightly over- and under-estimate the side frictional resistance, respectively. Nonetheless, all predictions were comparable to the static loading test results. The result from the numerical modeling was also in agreement with the field test data.

Table 4.7 The bearing capacity of the sheet pile: Comparison of the static pile loading test results with those from analytical, SPT-based, and CPT-based methods and numerical model.

Method	Length (m)	Q_{shaft} (kN)	Q_{tip} (kN)	$Q_{ultimate}$ (kN)
Analytical method	2.7	28.8	8.7	37.4
SPT-based method	2.7	15.1	10.4	25.6
CPT-based method	2.7	20.5	12.4	32.9
Static pile loading test #1	2.7	27.5	9.5	37.0
Static pile loading test #2	2.7	24.7	10.3	35.0
Static pile loading test #3	2.7	N/A	N/A	35.2
Numerical simulation	2.7	29.4	6.6	36.0

Chapter 5 Numerical Studies: Validation of the Simulation Model

5.1 Introduction

The numerical simulation software, FLAC (Fast Lagrangian Analysis of Continua), was utilized in this project to investigate the performance of the sheet pile abutment system for various parametric conditions. FLAC uses finite difference and constitutive equations to simulate the relationship between displacement and stress. The quadrilateral grid represents materials like soil or concrete. The domain is the combination of the grid with the coordinate of *i* and *j* in the direction of *x* (horizontal) and *y* (vertical). The finite difference grid assembles one or more finite difference zones relating to a physical problem. The relationship between the reinforcement and unbalanced force is derived according to the equilibrium conditions. The equations of motion must be damped to provide the static solution. The direction of the damping force is such that energy is continuously dissipated. The magnitude of the damping force should converge to zero to reach a static status (Figure 5.1).

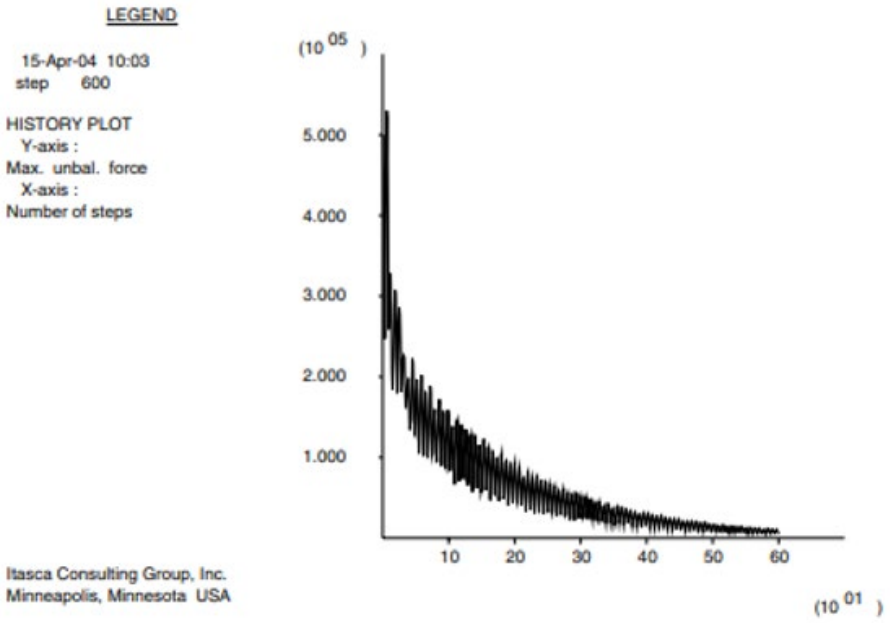

Figure 5.1 An example of maximum unbalanced force for the problem of sudden end-load application to a column (Itasca Consulting Group, 2019).

The sheet pile abutment system is subjected to a combination of lateral and vertical loads. The lateral load is mostly from excavating activities, while the vertical load comes from the superstructure and live loads (Figure 5.2). In this chapter, the validation of the numerical model is presented before an actual parametric study.

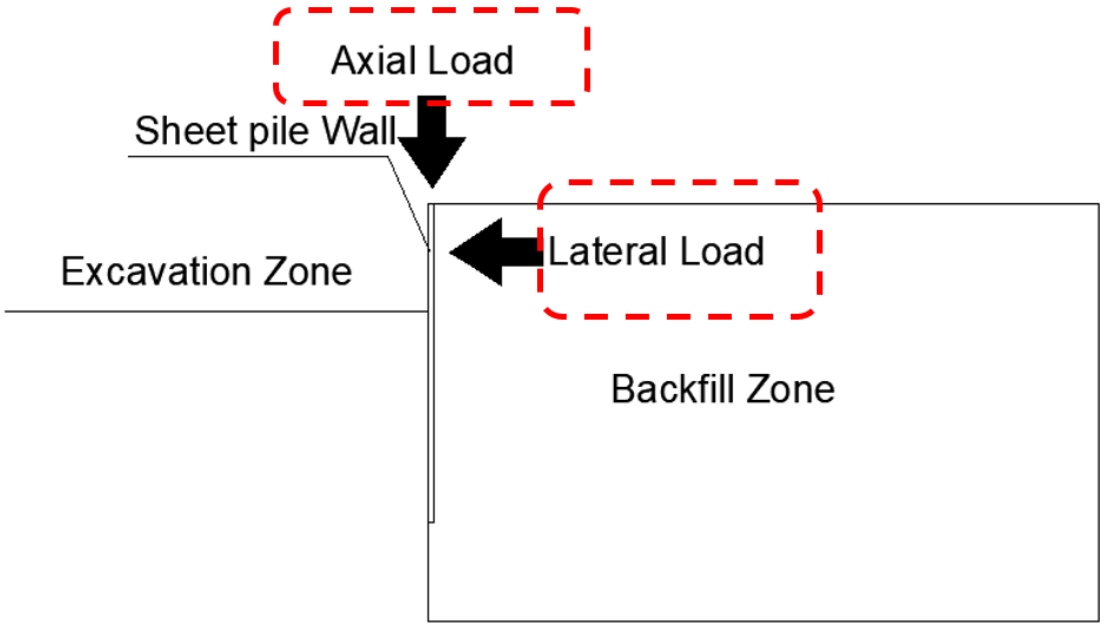

Figure 5.2 The combined axial and lateral loads imposed on the sheet pile abutment system.

5.2 Validation of Numerical Method: Axial Loading

FLAC has structural elements that represent soil and structure interaction (such as tunnel, pile foundation, anchor, and cable bolts). They include beam element, liner element, cable element, pile element, rock bolt element, strip element, and support member. Each tool has different geo-mechanical aspects, and what the engineers could choose depends on the purpose

of numerical simulation. In this project, the beam element is adopted to simulate the sheet pile abutment system, even though the pile element is generally used for other geotechnical simulations to examine the performance of axially-loaded piles.

The beam element has two-dimensional components with three degrees of freedom (x-translation, y-translation, rotation). Beam elements interact with the grid via the interface. The grid-grid interface is separated initially by command, and the beam element is added between two grids. A new interface between two grids is applied via friction angle, cohesion, normal stiffness, and horizontal stiffness (Figure 5.3). The beam elements are widely used to model supports like struts in an open-cut excavation and yield arches in a tunnel or retaining wall.

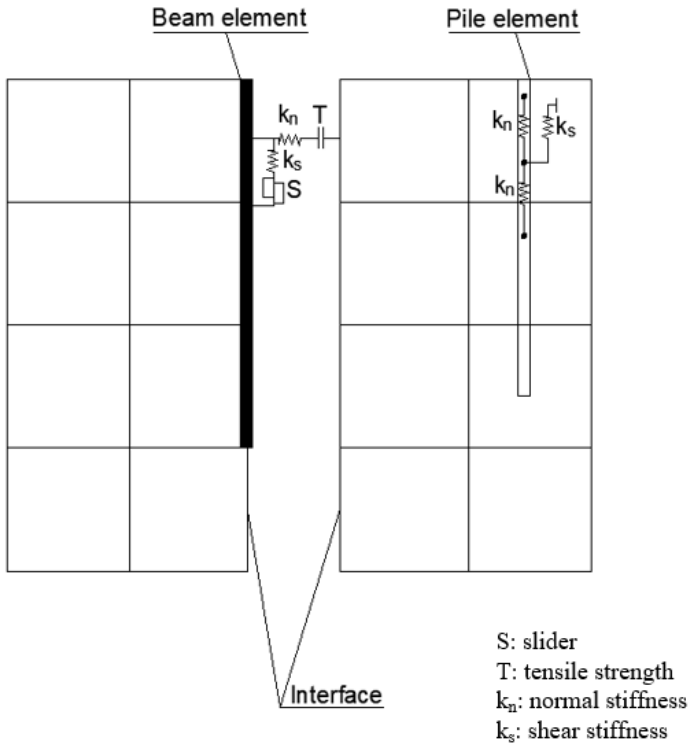

Figure 5.3 The location and relationships of the pile element and beam element in the domain.

The pile element is also a two-dimensional element that can transfer normal forces, shear forces, and bending moments to the grid. The pile element is the combination of beam element and cable element features. The three-dimensional result between the soil and grid is simulated by input parameters such as the normal stiffness of the coupling spring, the shear stiffness of the coupling spring, and the frictional resistance of the normal coupling spring. Pile elements are created to represent the behavior of the pile foundation.

The beam element and pile element need different input parameters. The pile element uses normal stiffness and shear stiffness for the soil-pile interaction. The beam element's shear stiffness (k_s) is the same as the pile element's shear stiffness (k_s). Normal stiffness (k_n) of the pile element can be estimated using the following equation (Itasca Consulting Group, 2019):

$$k_n = \frac{E_S A}{L} \tag{5.1}$$

where E_s is Young's modulus of a pile, A is the cross-sectional area of a pile, and L is the length of a sheet pile. Similarly, the bending stiffness (k_r) of the pile is calculated as follows:

$$k_r = \frac{E_S I}{L} \tag{5.2}$$

where I is the inertia of a pile.

5.2.1 Pile-Soil Interface Parameters

Following the FLAC manual, k_n and k_s for the beam element should be set to ten times the equivalent stiffness of the stiffest neighboring zone (Itasca Consulting Group, 2019). The apparent stiffness (expressed in stress-per-distance units) of a zone in the normal direction is:

$$k_n = k_s = 10\left(\frac{K+\frac{4}{3}G}{\Delta z}\right) \tag{5.3}$$

where K and G are the bulk and shear moduli, respectively, and Δz is the smallest width of an adjoining zone in the normal direction.

5.2.2 Numerical Simulation Model

Two simple models with the beam element and pile element are constructed, as shown in Figure 5.4, to confirm the ability of axial resistance of the beam element.

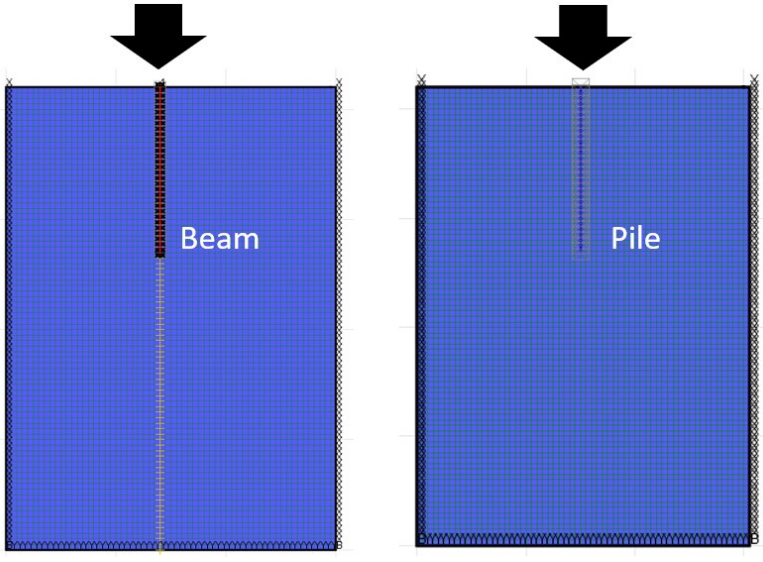

Figure 5.4 A numerical simulation model with the beam element (left), and the pile element (right).

5.2.3 Material Properties

(a) Soil-Pile Interface

Normal and shear stiffness at the soil-pile interface is estimated as follows (Itasca, 2016):

$$k_n = k_s = 10\left(\frac{K+\frac{4}{3}G}{\Delta z}\right) = 10\left(\frac{4.2E7 + \frac{4}{3}1.92E7}{0.5}\right) = 1.35\text{E}9\left(\frac{\text{Pa}}{\text{m}}\right) \quad (5.4)$$

Where the size of the mesh is Δz = 0.5 m for this model. The friction angle of sand is 30° and cohesion is 0 for both beam and pile elements. As mentioned above, the coupling-spring constants normal - stiffness (Pa/m) is estimated based on Equation 5.1. The shear stiffness at the soil-pile interface and friction angle of the beam element is the same as the coupling-spring constants shear - stiffness (Pa/m) and friction angle of the pile element (Tables 5.2 and 5.3).

$$k_{n(pile\ element)} = \frac{E_S A}{L} = \frac{2E11\times 0.01681}{15} = 2.24E8(Pa/m) \quad (5.5)$$

Table 5.1 Material properties used for the validation of the beam element in case of axial loading.

Material	Unit weight (kg/m^3)	K (Pa)	G (Pa)	Friction angle (°)	c (kPa)	Model
Sand	2,000	4.20E7	1.92E7	33	10	Mohr-Couloumb

Table 5.2 Soil-pile interface properties used for the validation of the beam element in case of axial loading.

Soil-pile interface properties for the beam element	
Interface normal stiffness (Pa/m)	1.35E9
Interface shear stiffness (Pa/m)	1.35E9
Interface cohesion (Pa)	0
Interface friction angle (°)	30

Table 5.3 Input parameter for the pile element for the validation of the beam element in case of axial loading.

Input parameters for the pile element	
Coupling-spring constants normal - stiffness (Pa/m)	2.24E8
Coupling-spring constants normal - Friction angle (°)	0
Coupling-spring constants normal - Cohesion (Pa)	0
Coupling-spring constants shear - stiffness (Pa/m)	1.35E9
Coupling-spring constants shear - Friction angle (°)	30
Coupling-spring constants shear - Cohesion (Pa)	0

(b) Pile

The input properties used for the sheet pile are summarized in Table 5.4.

Table 5.4 Input properties for the sheet pile for the validation of the beam element in case of axial loading.

Properties	PZ27
Elastic modulus (Pa)	2.00E11
Cross-section area (m^2)	0.01681
Inertia (m^4)	2.52E-04
length of the pile (m)	15

5.2.4 Results

As shown in Figure 5.5, the results using the beam element showed a good match with those using the pile element. As mentioned above, the pile element is designed for a deep foundation and so mainly deals with the vertical load. That is, the pile element cannot properly simulate the horizontal load from excavating activities because it is not connected with the domain. Thus, in terms of combining both axial and vertical loads, beam elements work better. With the installment of the interface properties, the beam element becomes a part of the domain.

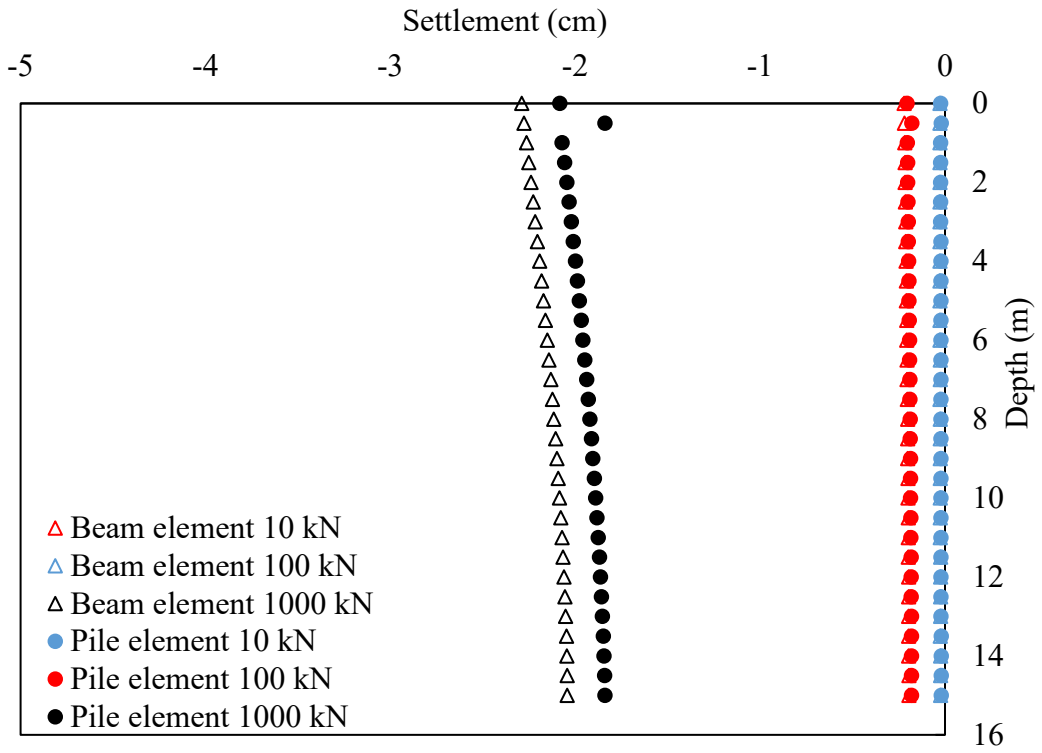

Figure 5.5 The comparison of vertical settlements from the models that use either the beam element or pile element. Three level of axial loads (10 kN, 100 kN, and 1000 kN) is applied to the numerical simulation. Note: 1 inch = 2.54 cm.

5.3 Validation of Numerical Method: Lateral Loading

Next, the project team used data in the literature to validate the simulation model with the beam element in the case of lateral loading.

5.3.1 Validation #1

The project in the literature (Influence of Cantilever Sheet Pile Deflection On Adjacent Roadway; Mullins and Stokes, 2009) mainly focuses on simulating sheet-pile wall retaining soil and preventing damage to nearby structures during construction. When the road was constructed next to the sheet-pile wall, the excessive horizontal load could result in the loss of confinement underneath the roadway, thereby causing the vertical displacement and longitudinal cracking of the asphalt layer in the wheel path. The project team at the University of South Florida (USF) used the same numerical simulation software, FLAC, to model the problem (Mullins and Stokes, 2009; Figures 5.6 and 5.7).

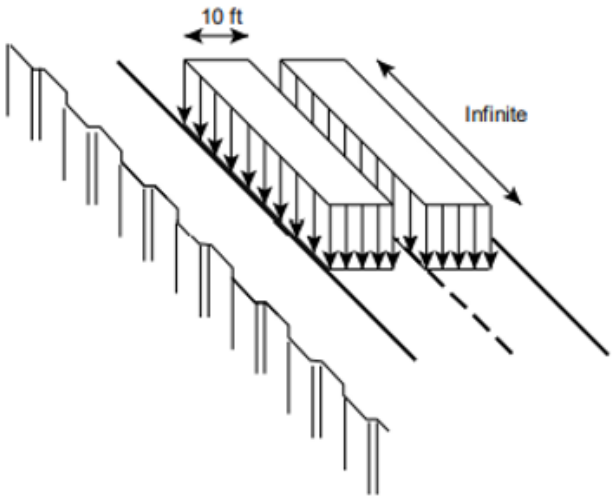

Figure 5.6 A lane load applied over two infinite 3 m wide strips (Mullins et al., 2009).

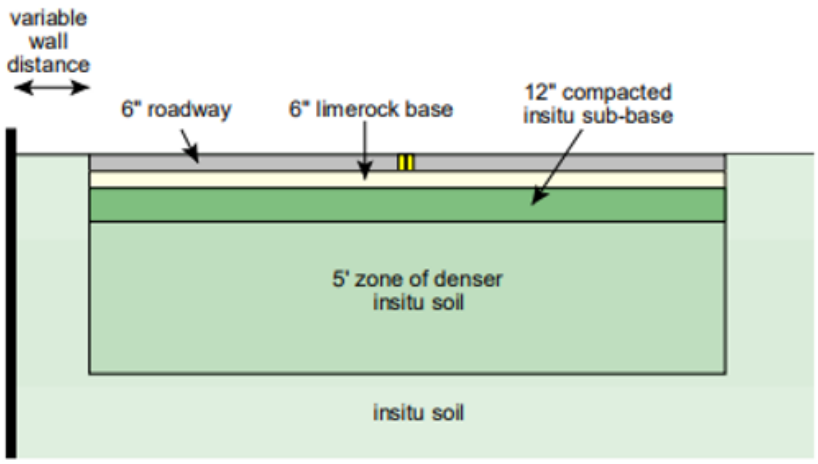

Figure 5.7 A cross-section of the numerical model with layered zones (Mullins et al., 2009).

The size of the numerical model was 46 m wide and 14.6 m deep, combining more than 4,700 elements for the whole grid. The road lane was 7.3 m wide with 0.15 m of asphalt, 0.15 m of lime rock base, and 0.3 m of compacted in-situ sub-base soil. Soil properties and other materials, such as asphalt and aggregate, were provided by the Florida Department of Transportation (FDOT) State Material Office (SMO). Triaxial tests were also performed to define these material parameters. The in-situ soil parameter was determined from the SPT test (Table 5.5).

Two types of sheet piles, PZ27 and PZ40, were used for the simulation (Figures 5.8 and 5.9). The cross-section of PZ40 was about 1.5 times larger than that of PZ27, while the inertia of PZ40 was 2.7 times higher. The UNL project team only used the PZ27 data for validation purposes (Figure 5.10). The pile properties of PZ27 are provided in Table 5.6.

The interface between the soil and pile was applied when the beam element was employed to simulate the sheet pile wall. The interface parameters are summarized in Table 5.7.

Table 5.5 Properties of materials used for the numerical simulation (Mullins et al., 2009).

Material	Unit weight (kg/m^3)	K (Pa)	G (Pa)	Friction angle (°)	c (kPa)
Asphalt	2,323	9.34E7	5.61E7	49.7	457
Base	2,067	3.90E7	2.34E7	44.4	86.2
Subbase	1,922	2.56E7	1.53E7	33	0
Weak Soil	1,722	9.60E6	5.80E6	30	0
Strong Soil	1,882	2.00E7	1.00E7	33	0

Table 5.6 Properties of the sheet pile used for the numerical simulation (Mullins et al., 2009).

Pile properties	PZ27
Elastic modulus (Pa)	2.00E11
Cross-section area (m^2/m)	0.01681
Inertia (m^4/m)	2.52E-4

Table 5.7 Properties of the pile-soil interface used for the numerical simulation (adopted from Mullins et al., 2009).

Interface properties	
Normal stiffness (Pa/m)	1.57E9
Shear stiffness (Pa/m)	1.57E9
Cohesion (Pa)	0
Friction angle (°)	10

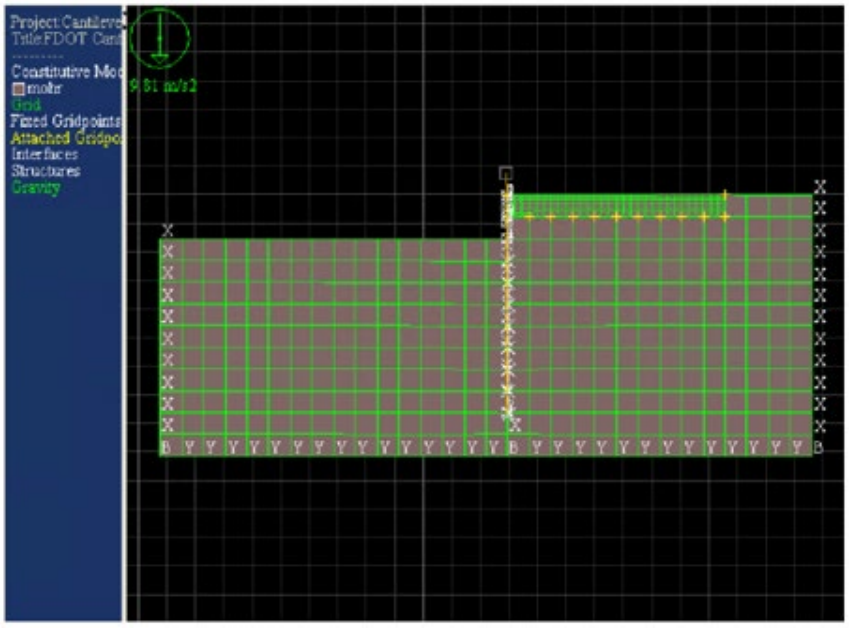

Figure 5.8 The numerical simulation model on the sheet pile wall conducted by the project team at USF (from Mullins et al., 2009).

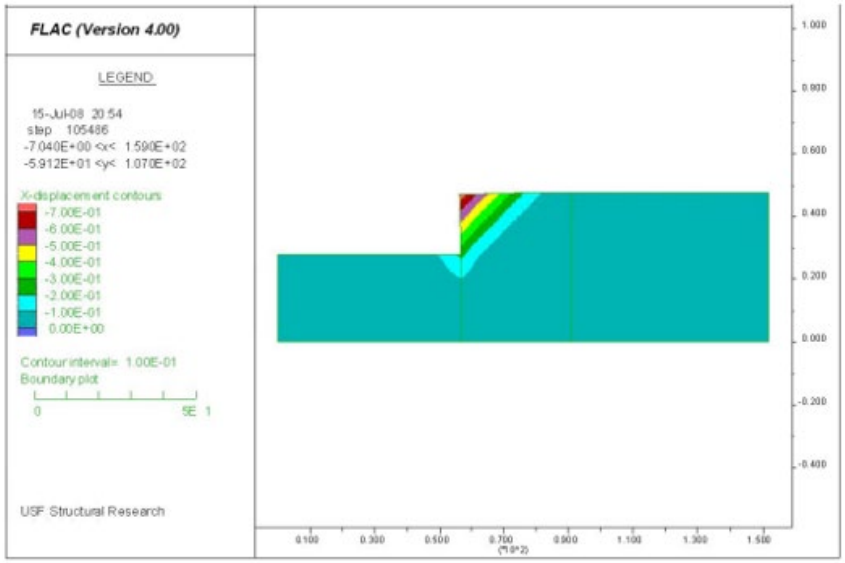

Figure 5.9 A contour of horizontal displacements after about 6.1 m (20 ft) excavation with no roadway (PZ-27 in stronger soil; Mullins et al., 2009).

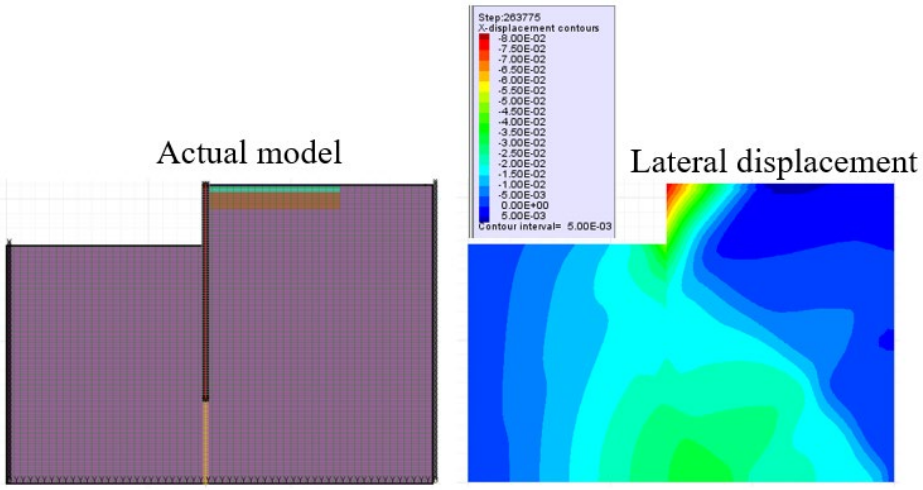

Figure 5.10 The numerical simulation model made by the project team at UNL (PZ27 sheet pile with no roadway) for the validation of lateral load retainment.

The simulation results were in good agreement, as shown in Figure 5.11. The minor differences were due to uncertainty in the overall dimensions of the simulation model and some input parameters not being specified in the literature. Nonetheless, both models showed a minimal deflection when the excavation level was 0.5 m (1.6 ft). When the excavation level increased to 5 m (16 ft), both models delivered a maximum displacement of around 8.3 cm (~3.27 inches).

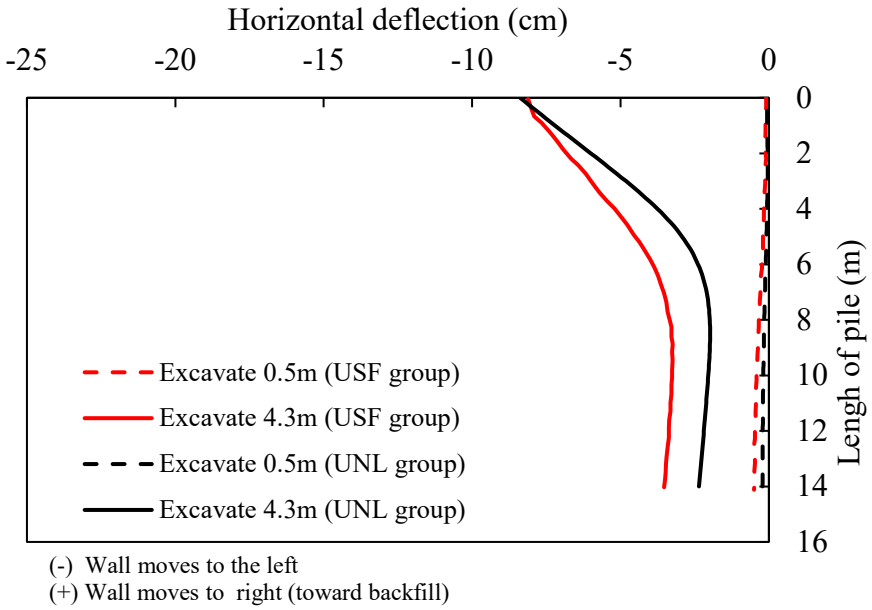

Figure 5.11 The comparison of horizontal displacements of the sheet pile wall from the numerical model by the project team at UNL and literature (USF).

5.3.2 Validation #2

The second model used for validation was of a sheet pile retaining wall from a research group at the Imperial College of Science (ICL). The numerical model was a simple case with a 10 m sheet pile wall, and the embedment depth was 5 m from the top surface (Day and Potts, 1993).

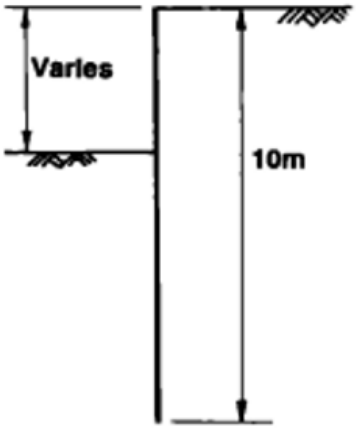

Figure 5.12 The geometry of the sheet pile retaining wall for numerical modeling (Day and Potts, 1993).

The low-modulus pile wall was Frodingham 3NA with an inertia of $I = 2.568\times10^{-4}$ m^4/m and a cross-sectional area of 1.65×10^{-2} m^2/m. For a high-modulus pile, its inertia was about 19 times, and its cross-sectional area was 3.2 times, that of the low-modulus pile. The elastic modulus was 2.1×10^8 kPa for both piles (Table 5.8).

Table 5.8 Properties of the sheet piles used for the numerical modeling (from Day and Potts, 1993).

Sheet Pile type	Moment Inertia, I (10^{-4} m^4/m)	Cross- Sectional Area, A (10^{-2} m^2/m)	Young's Modulus, E (kN/m^2)
Frodingham 3NA	2.568	1.65	2.10E8
High Modulus 610×305×149 + Frod 5N	46.85	5.26	2.10E8

For the soil parameters, Young's modulus was interpolated along with depth from the equation $E = 5000 + 5000z$ [kN/m^2], and Poisson's ratio was 0.2. Those values were used to calculate the bulk and shear moduli (Table 5.9).

Table 5.9 Properties of the soil used for the numerical modeling (from Day and Potts, 1993).

Material	Unit weight (kg/m^3)	K (MPa)	G (MPa)	Friction angle (^{o})	c (Pa)	Angle of Dilation (^{o})
Sand	20	31	23	25	0	13

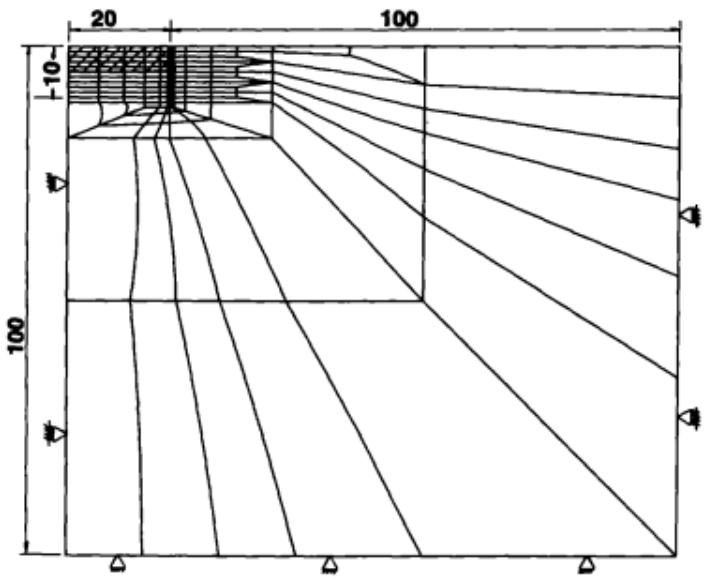

Figure 5.13 Finite element meshes constructed for the numerical simulation in the literature (Day and Potts, 1993).

The project team reconstructed the original numerical simulation model (Figure 5.13) with the same length and properties of the piles. The pile-soil interface properties were interpolated using values in Tables 5.8 and 5.9, as shown in Table 5.10.

Table 5.10 Properties of the pile-soil interface used for the numerical modeling.

Interface properties	
Normal stiffness (Pa/m)	1.20E9
Shear stiffness (Pa/m)	1.20E9
Cohesion (Pa)	0
Friction angle (°)	25

Once again, the simulation results were in good agreement for both low-modulus and high-modulus sheet piles, as shown in Figure 5.14. The high-modulus pile was deflected less than the low-modulus pile and tended to rotate at a point near the bottom. The minor differences were due to the assumptions made for several missing input parameters.

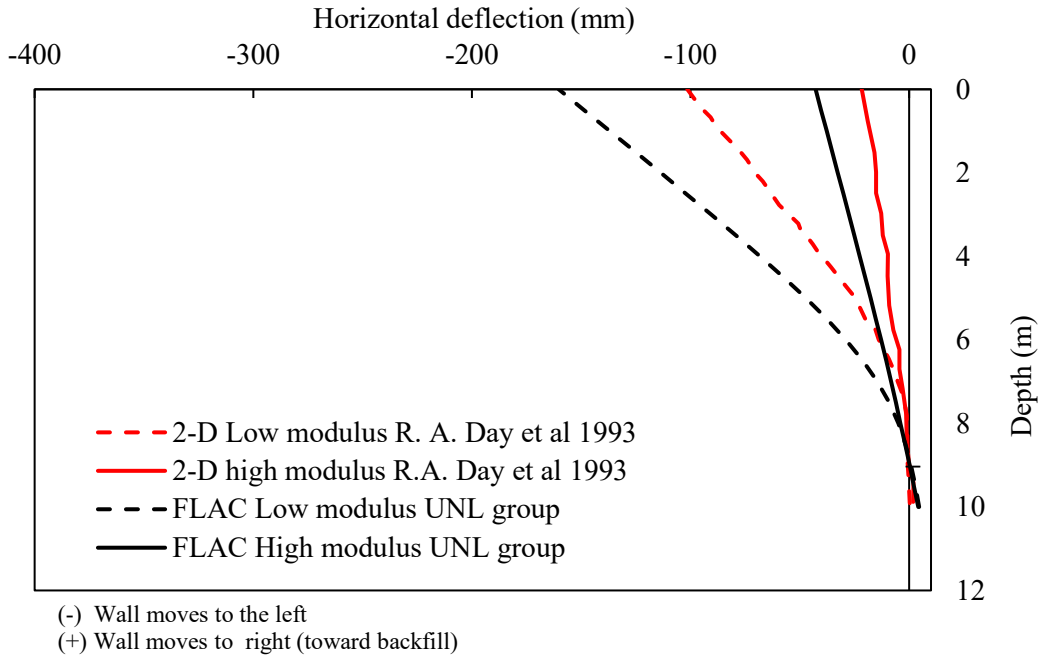

Figure 5.14 A comparison of horizontal displacements of the low-modulus and high-modulus piles from the numerical simulations by the project team and in the literature (Day and Potts, 1993).

5.4 Validation of Numerical Method: Axial + Lateral Loading (1)

The project team adopted the case in which sheet pile abutments were driven into sandy soil in the literature (Nucor Skyline, 2021) for the validation of combined axial + lateral loading on the sheet pile wall.

5.4.1 Dimensions of the Bridge

The bridge span was 26.8 m (88 ft). The bridge had a 0.2 m thick concrete slab supported by five girders (W403199). The piles were designed according to the Load and Resistance Factor Design (LFRD). Each pile had a total length of 12.2 m (40 ft), with 3 m (~10 ft) of unbraced length. The entire length of the pile cap was 9.1 m (30 ft), and the cap beam width and height were 1.2 m and 0.9 m, respectively. The water table was located around the dredge line (Figures 5.15 to 5.17).

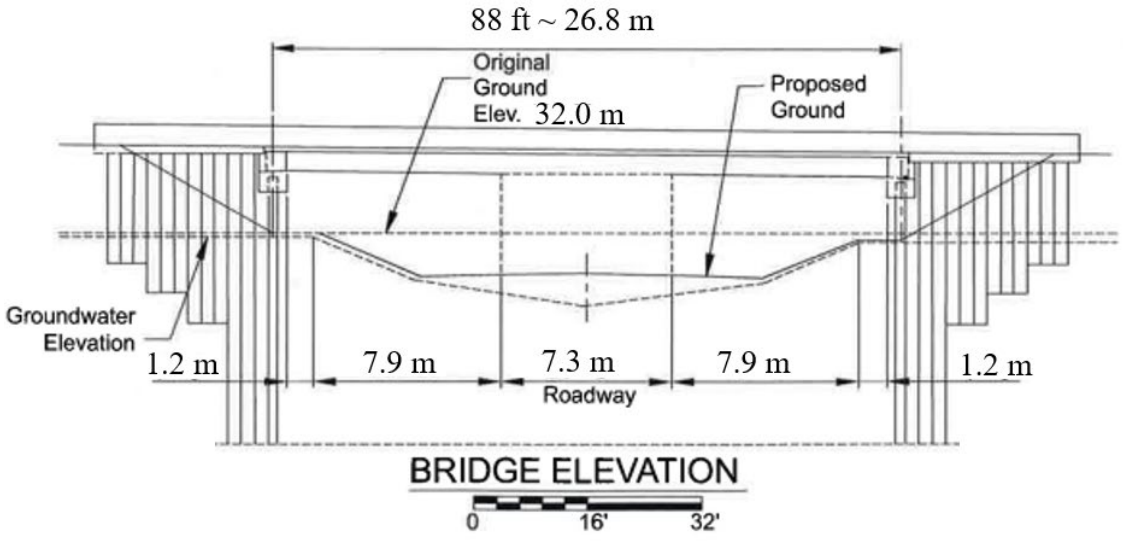

Figure 5.15 The dimensions of the bridge (Nucor Skyline, 2021) used for the validation of combined axial + lateral loading on the sheet pile abutment.

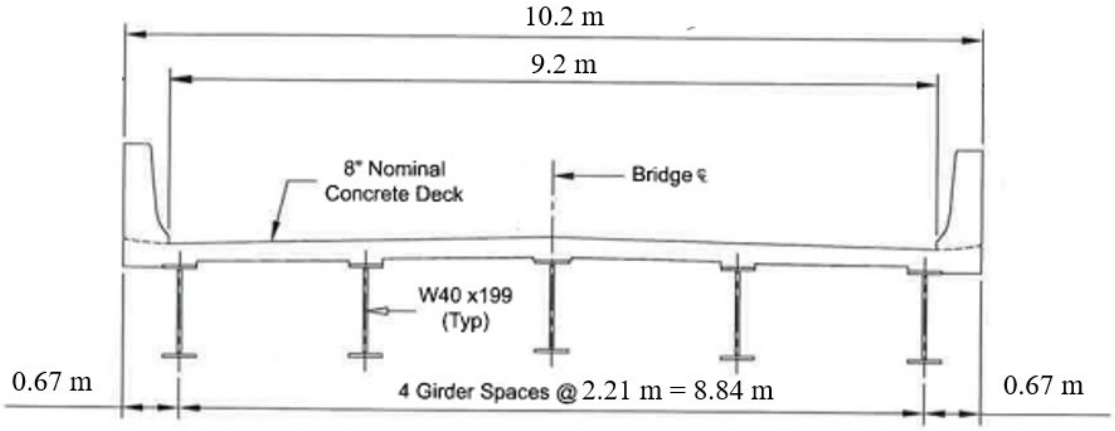

Figure 5.16 The cross-section and dimension of the bridge (Nucor Skyline, 2021) used for the validation of combined axial + lateral loading on the sheet pile abutment.

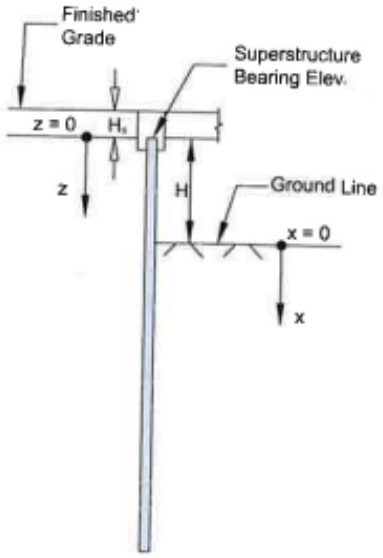

Figure 5.17 The side view of the sheet pile abutment (Nucor Skyline, 2021) used for the validation of combined axial + lateral loading on the sheet pile abutment.

The actual design of the cap beam was 0.91 m in depth and 1.2 m in width in the literature and made of reinforced concrete (Figure 5.18). The sheet pile was assumed to be

connected to the center of the cap beam. For simplicity, the cap beam with size 1 m × 1 m is modeled here.

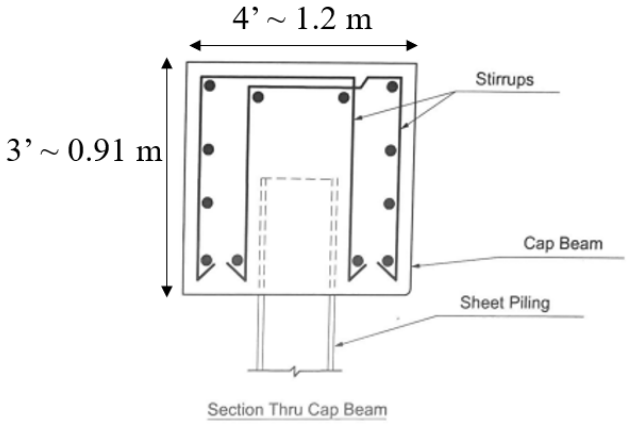

Figure 5.18 The section of the reinforced concrete cap beam (Nucor Skyline, 2021).

5.4.2 Design Load

The dead and live loads consider for the numerical simulation are summarized in Table 5.11. The loads were estimated based on the LRFD design approach. The dead load was the total weight transferred from five beams multiplied by the dead load factor (1.2), which equaled 296 tons. The total live load was the combination of superstructure reaction and slab reaction multiplied by the live load factor (1.6), which equaled 173 tons. With a 9.1 m length of the cap, the live and dead load transmitted to each abutment was as follows:

$$P_{uDL} = (269 + 173)\frac{1}{2\times 9.1} = 24.3\frac{tons}{m} = 242.4kN/m \quad 5.6$$

Table 5.11 A summary of applied service load reactions and loads used for the validation of combined axial + lateral loading on the sheet pile abutment (unit: tons).

Type	Component	Beam 1	Beam 2	Beam 3	Beam 4	Beam 5
DC1	Non-Composite Dead Load	18.0	21.3	21.3	21.3	18.0
DC2	Composite Dead Load	5.1	5.1	0.0	5.1	5.1
DW	Future Wearing Surface	3.5	3.5	3.5	3.5	3.5
DC1	Beam Length Beyond Bearing	0.1	0.1	0.1	0.1	0.1
DC1	½ of Approach Slab	7.5	7.5	7.5	7.5	7.5
DC1	End Diaphragm	6.3	7.8	7.8	7.8	6.3
DC1	Cap beam Self weight	4.7	5.9	5.9	5.9	4.7
DC2	Barrier on Approach Slab	1.1	1.1	1.1	1.1	1.1
DW	Approach Slab future Wearing Surface	0.8	0.8	0.8	0.8	0.8
LL+IM	Superstructure Reaction	51.0 tons/ loaded lane				
LL+IM	Approach Slab Reaction	3.6 tons/loaded lane				

5.4.3 Material Properties

Concrete was assumed to behave elastically, while soils followed the Mohr-Coulomb model. The input parameters for concrete were obtained from Razmi et al. (2014), while soil properties were from the Nucor Skyline manual (Table 5.12). The pile properties are summarized in Table 5.13.

Table 5.12 Material properties used for the validation of combination loads (1).

Material	Sand (fill material)	Silty sand	Concrete (abutment)
Unit weight (kg/m^3)	2000	1760	2322
K (Pa)	1.0E7	5.6E6	1.4E10
G (Pa)	6.0E6	4.2E6	1.1E10
Friction angle (°)	33	31	-
c (Pa)	0	0	-
Model	Mohr-Coulomb	Mohr-Coulomb	Elastic

Table 5.13 Pile properties used for the validation of combined loads (1).

Pile properties	As-Driven AZ 28-700	Deteriorated AZ 28-700
Elastic modulus (Pa)	2.0E11	2.0E11
Cross-section area (m^2/m)	0.02	0.012
Inertia (m^4/m)	6.4E-04	3.7E-04

The project team used the beam element to simulate the sheet pile abutment. The normal stiffness (k_n) and shear stiffness (k_s) at the pile-soil interface were calculated using Equation 5.3, as shown below. The interface frictional angle was assumed as 27°, following the result from laboratory tests.

For fill material:

$$k_{n1} = k_{s1} = 10\left(\frac{K+\frac{4}{3}G}{\Delta z}\right) = 0.36E9 \tag{5.7}$$

For silty sand:

$$k_{n2} = k_{s2} = 10\left(\frac{K+\frac{4}{3}G}{\Delta z}\right) = 0.23E9 \tag{5.8}$$

For the average value:

$$k_n = k_s = \frac{(k_1 x t_1 + k_2 x t_2)}{t_1 + t_2} = 0.32E9 \tag{5.9}$$

where t_1 and t_2 is the thickness of the fill material and silty sand, respectively.

Table 5.14 Pile-soil interface properties used for the validation of combined loads (1).

Interface properties	
Normal stiffness (Pa/m)	0.32E9
Shear stiffness (Pa/m)	0.32E9
Cohesion (Pa)	0
Friction angle (°)	27

5.4.4 Numerical Simulation Model

The numerical model reconstructed by the project team is shown in Figure 5.19.

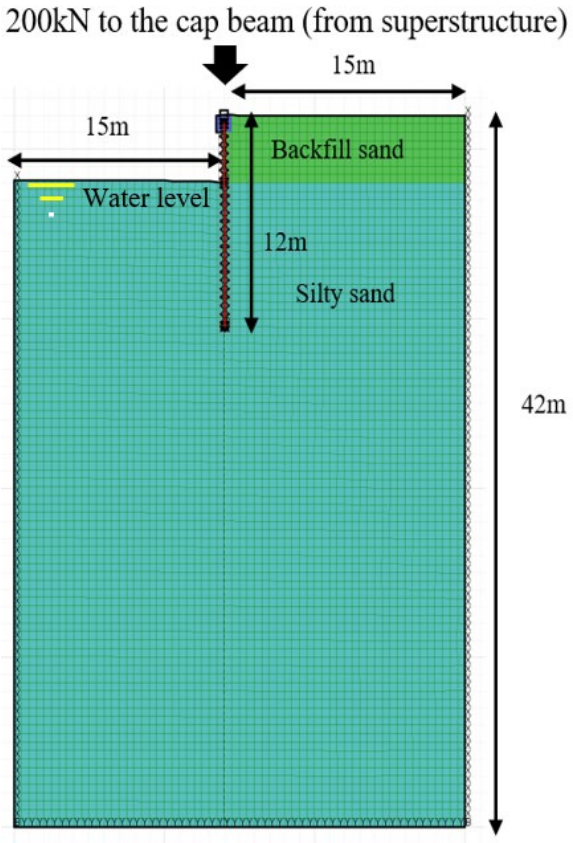

Figure 5.19 The numerical simulation model reconstructed by the project team at UNL for the validation of combined vertical + lateral loads.

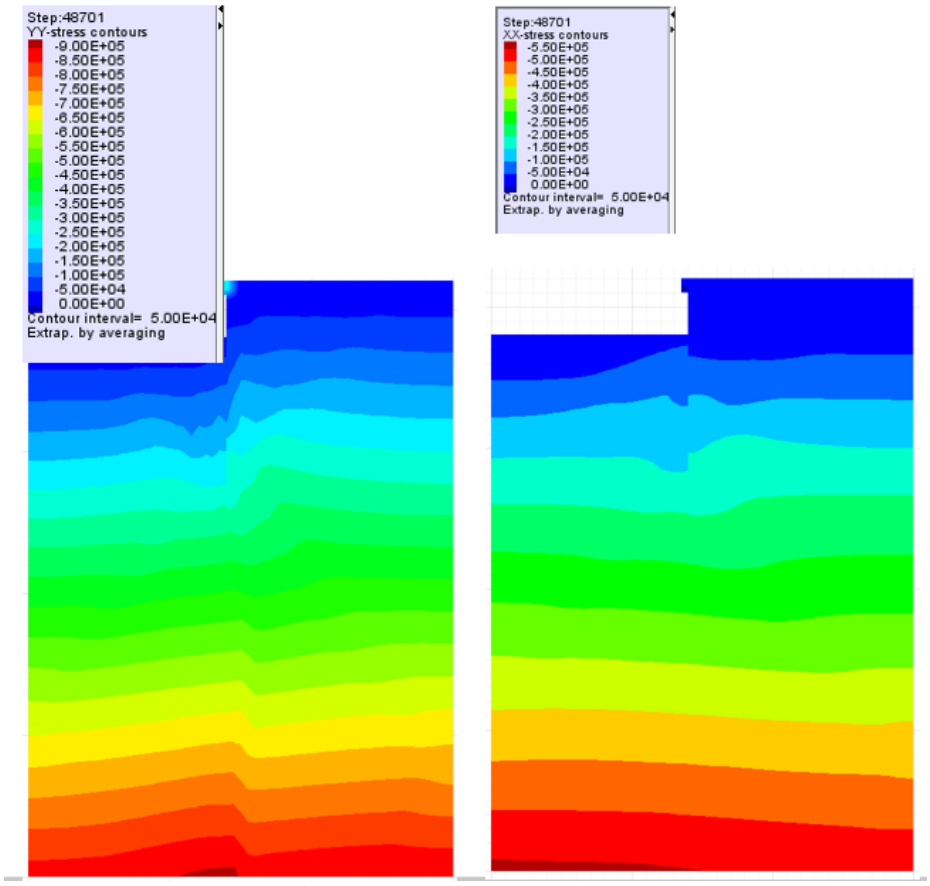

Figure 5.20 Simulation results: (a) vertical stress contour, and (b) horizontal stress contour in the model.

5.4.5 Results

The simulation results, including the contours of vertical and horizontal stresses in the simulation model, horizontal deflection of the sheet pile wall, and vertical settlement of the sheet pile wall, are displayed in Figures 5.20, 5.21, and 5.22, respectively. In the literature, the maximum horizontal deflection and vertical settlement were computed as 11 cm (~4.3 inches) and 0.3 cm (~0.1 inches), respectively, for the given loading condition (Nucor Skyline, 2021). The maximum horizontal deflection and vertical settlement obtained by the project team at the UNL group were 8.5 cm (~3.3 inches) and 0.4 cm (0.15 inches), respectively, which showed a good agreement with the literature.

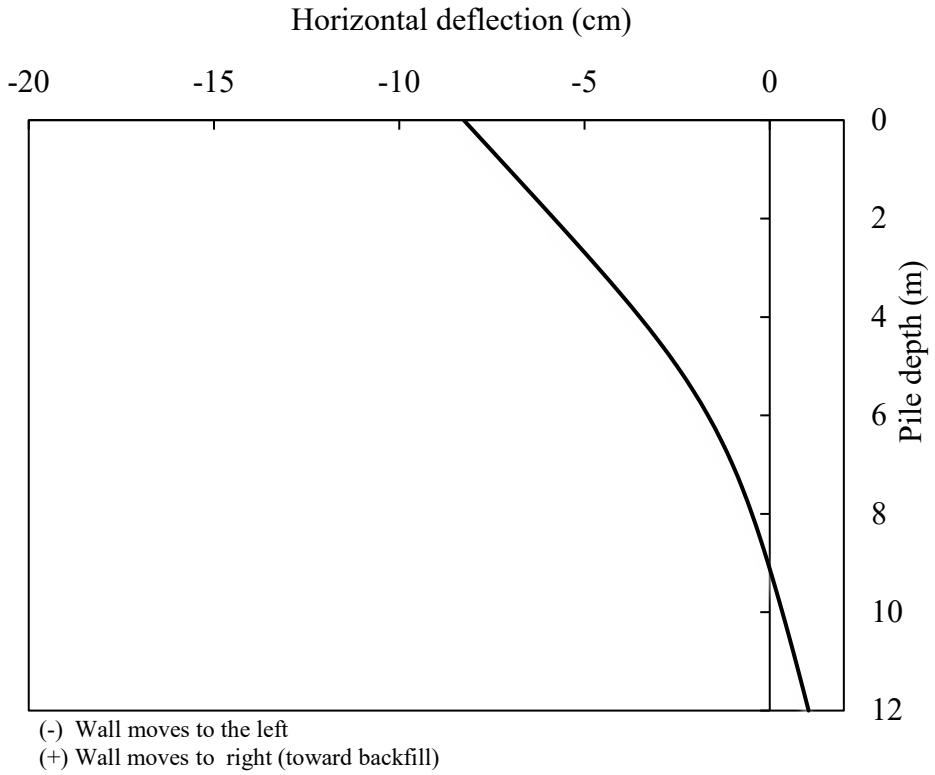

Figure 5.21 Simulation results: horizontal displacement of the sheet pile wall.

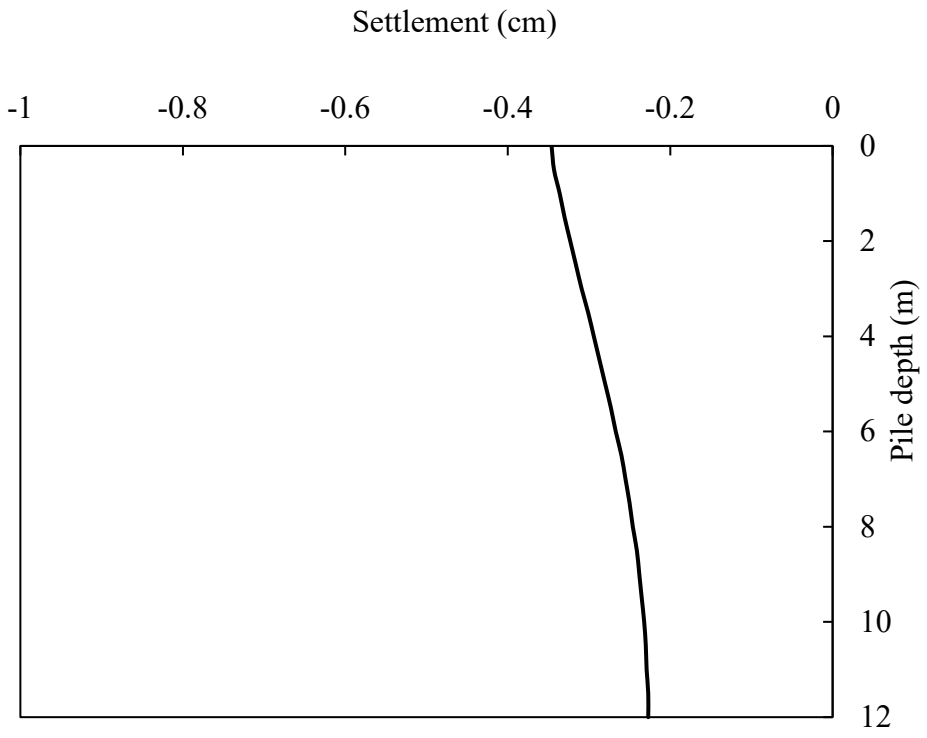

Figure 5.22 Simulation results: vertical settlement of the sheet pile wall.

5.5 Validation of Numerical Method: Axial + Lateral Loading (2)

The second case adopted for the validation of the combined axial + lateral loading was the bridge site constructed in Black Hawk County (BHC), Iowa, by a research team at Iowa State University (ISU) and the Iowa Department of Transportation. This project investigated the feasibility of employing sheet piling as the primary abutment foundation and retaining a backfill system. Instrumentation of the bridge foundation system and superstructure was performed, and data were continuously collected. The project team at UNL constructed a numerical simulation model based on the information provided in the project report.

5.5.1 Dimension of the Bridge

This new bridge site was a joint research effort between BHC and ISU. The design of the superstructure was performed by the BHC Engineer's Office and utilized precast elements previously developed. The bridge span was 10.3 m (Figure 5.23). Each pile had a total length of 12.2 m, with 3 m of unbraced length. The total size of the pile cap was 10.1 m, and the cap beam width and height were 1.2 m and 0.9 m, respectively. All parts of the pile, including wing walls, handle the lateral load from backfill soil.

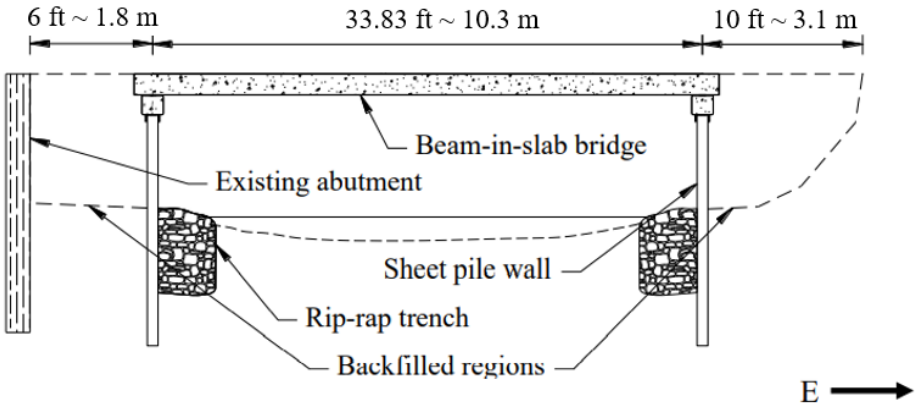

Figure 5.23 As-built profile of bridge for the project in BHC, Iowa (Evans et al., 2011).

The pile cap was a precast element created and fabricated by BHC that consisted of a W12×65 steel beam cast in reinforced concrete (Figure 5.24). The dimensions of the cap was 1 m × 1 m, and the pile head length in the cap was 0.5 m.

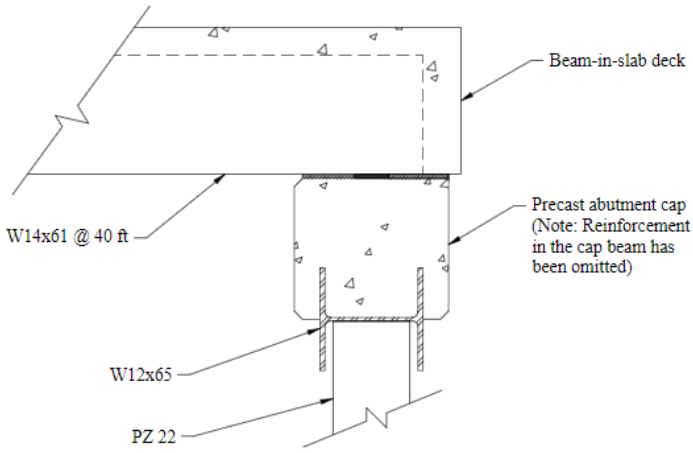

Figure 5.24 Precast abutment cap and contact between bridge deck, abutment cap, and sheet piling foundation in BHC, Iowa (from Evans et al., 2011).

5.5.2 Anchoring

The anchor system consisted of a cast-in-place concrete Deadman that supported the wall by two 25.4 mm (1 inch) threaded rods (non-epoxy coated) connected to a steel channel waler. An overview of the anchor system is presented in Figure 5.25. The Deadman was cast in a trench excavated from the existing soil, and the concrete was 4.3 m × 1.2 m × 0.6 m. Another rod was placed parallel to the wall to tie the wing walls together.

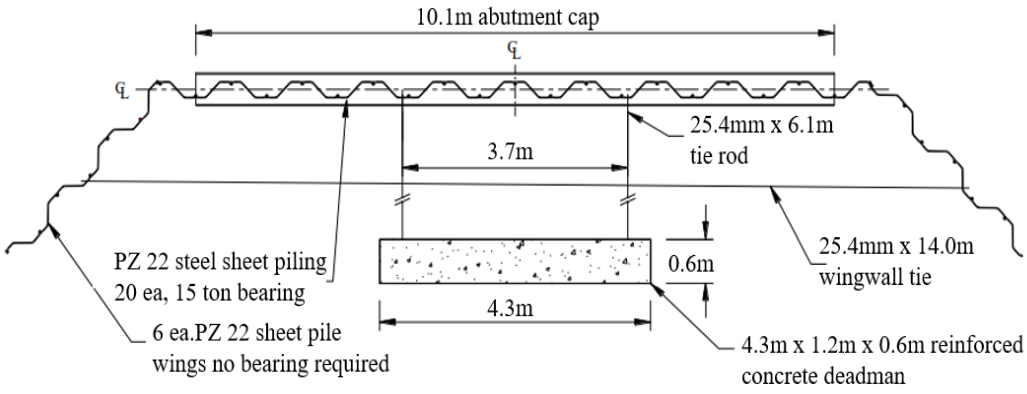

Figure 5.25 Plan view of the sheet pile abutment and retaining backfill system for a demonstration project in BHC, Iowa (from Evans et al., 2011).

5.5.3 Instrumentation and Monitoring

The bridge was instrumented with vibrating wire instruments and strain, displacement, and earth pressure cell transducers for long-term monitoring. Three displacement transducers were installed in front of the wall to measure the maximum deflection of the sheet pile wall (Figure 5.26). Three earth pressure cells were installed in the back of the sheet pile wall at depths of 0.3 m, 0.9 m, and 1.5 m from the cap (Figure 5.27). Data from these transducers, as shown in Table 5.15, was used to validate the numerical simulation model by the project team at UNL. Here, the project team considered only the simulation's dead load to compare with field data.

Table 5.15 Monitored values of the backfill pressure and wall deflections in the demonstration bridge project site (Evans et al., 2011).

Pressure or deflection	Estimated Total
Earth pressure (0.3m below TOC)	6.66 kPa (0.97 psi)
Earth pressure (0.9m below TOC)	12.16 kPa (1.76 psi)
Earth pressure (1.5 m below TOC)	16.04 kPa (2.33 psi)
Wall deflection	0.33 cm (0.13 inches)

TOC: Top of Cap

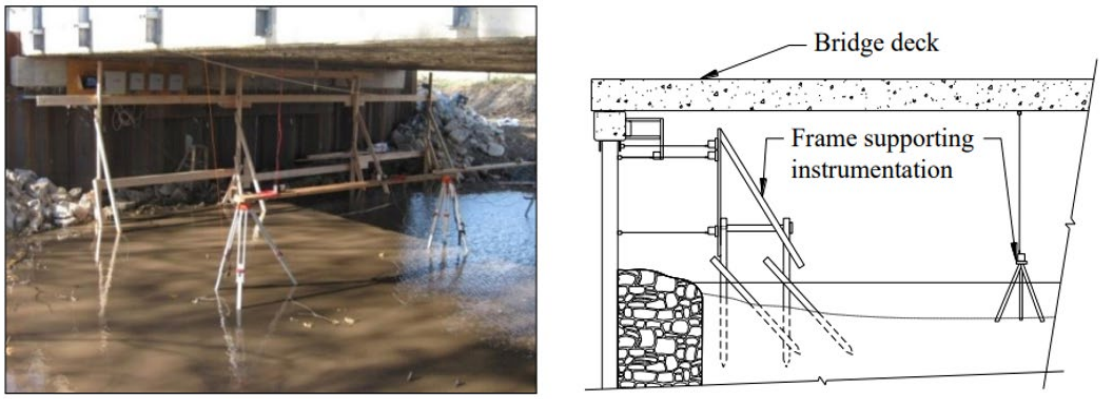

a.) View of west abutment b.) Side view of west abutment and midpsan

Figure 5.26 The installation of displacement transducers in the demonstration bridge project site (Evans et al., 2011).

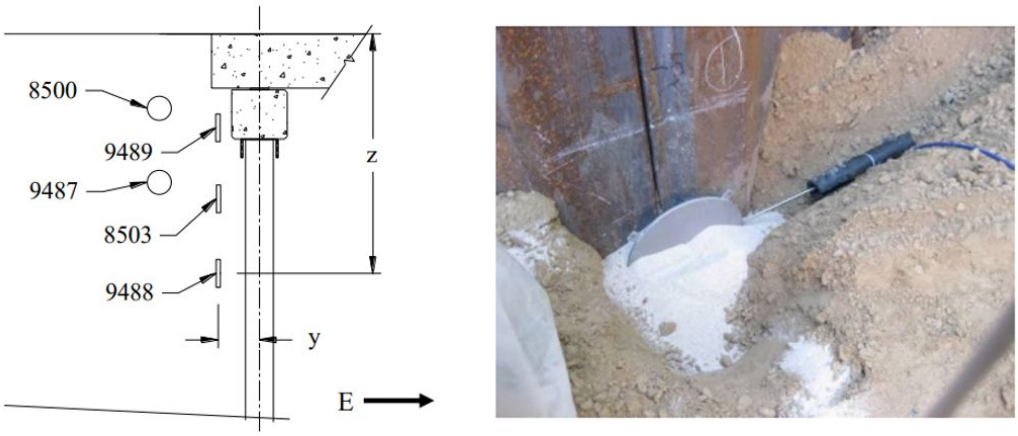

Figure 5.27 Installation of Earth pressure cells behind the sheet pile abutment (Evans et al., 2011).

5.5.4 Design Load

The dead load on the abutment was calculated based on the design. The weight of the deck elements (assuming a reinforced concrete weight of 2400 kg/m^3) was calculated to be 7.42 tons/m. For analysis, the dead load was distributed evenly across the 12 beams (2 beams per deck element). The beam-in-slab deck elements had 12 W14×61 beams, which were set on the abutment cap. Assuming 149 kg/m for guardrail weight, the total distributed dead load on the bridge (per beam) was calculated as follows:

$$W = \frac{7.42\ tons/m}{12\ beams} + \frac{0.149 tons/m}{12\ beams} + 0.091\frac{tons}{m} = 0.73\ tons/m \quad (5.10)$$

Using the length of the bridge (12.4 m), each girder was determined to deliver a concentrated force of 4.53 tons) per abutment. The factored dead load is as follows:

$$P_{uDL} = 1.2(4.53) = 5.44\ tons\ (per\ girder, per\ abutment) \quad (5.11)$$

The dead load was assumed to distribute evenly across the sheet pile wall (10.1 m wide abutment cap):

$$P_{uDL} = 5.44 \times (12\ beams) \times \frac{1}{10.1} = \frac{6.46 tons}{m} = 64.4\ kN/m \tag{5.12}$$

In order to compare results with field instrumentation data, only dead loads were considered in the numerical simulation model.

5.5.5 Soil Properties

The property of soils used for the numerical simulation was obtained from the project report, as shown in Figures 5.28 (soil boring log) and 5.29 (direct shear test). Based on the soil data, the unconfined stress, q_u, was estimated as:

$$q_u = \frac{1.35+2.25+1.3}{3} = 1.63\ tsf = 175\ kPa \tag{5.13}$$

The internal angle of friction of backfill material was 45° from Figure 5.29.

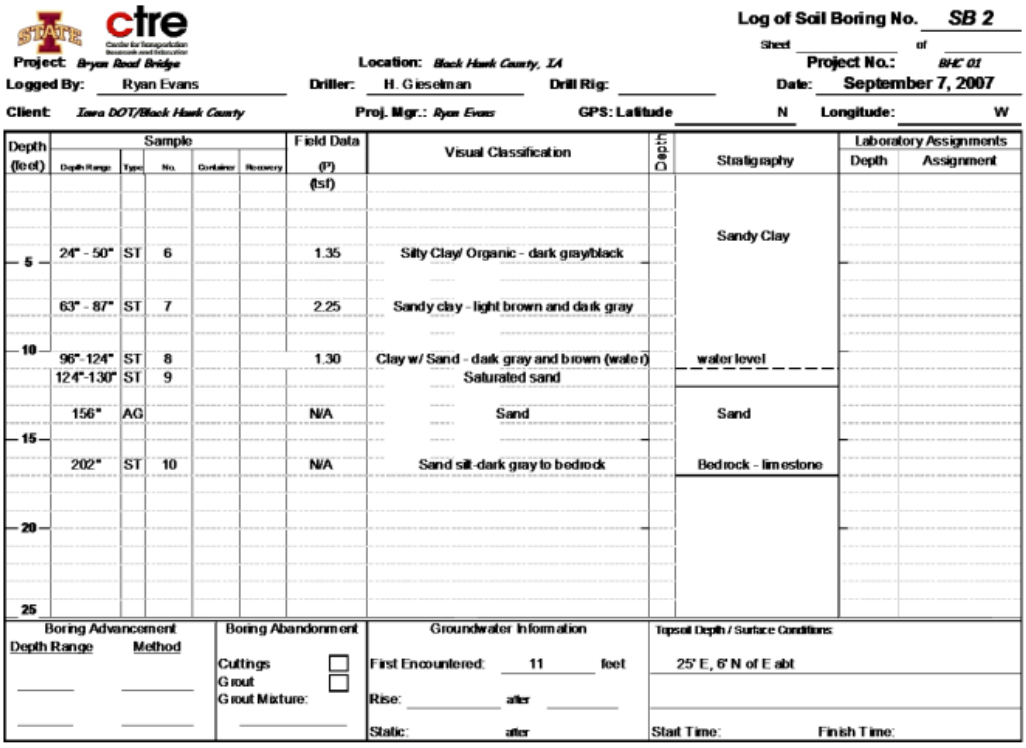

Log of Soil Boring No. SB 2

Sheet ____ of ____

Project: Bryan Road Bridge | Location: Black Hawk County, IA | Project No.: BHC 01

Logged By: Ryan Evans | Driller: H. Gieselman | Drill Rig: ____ | Date: September 7, 2007

Client: Iowa DOT/Black Hawk County | Proj. Mgr.: Ryan Evans | GPS: Latitude ____ N | Longitude: ____ W

Depth (feet)	Sample: Depth Range	Type	No.	Container	Recovery	Field Data (ft) (tsf)	Visual Classification	Depth	Stratigraphy	Laboratory Assignments: Depth	Assignment
									Sandy Clay		
5	24" - 50"	ST	6			1.35	Silty Clay/ Organic - dark gray/black				
	63" - 87"	ST	7			2.25	Sandy clay - light brown and dark gray				
10	96"-124"	ST	8			1.30	Clay w/ Sand - dark gray and brown (wet)		water level		
	124"-130"	ST	9				Saturated sand				
	156"	AG				N/A	Sand		Sand		
15	202"	ST	10			N/A	Sand silt-dark gray to bedrock		Bedrock - limestone		
20											
25											

Boring Advancement — Depth Range / Method

Boring Abandonment — Cuttings ☐ Grout ☐ Grout Mixture:

Groundwater Information — First Encountered: 11 feet; Rise: ____ after ____; Static: ____ after ____

Topsoil Depth / Surface Conditions: 25' E, 6' N of E abt

Start Time: ____ Finish Time: ____

Figure A9. Log of soil boring SB 2 for demonstration project in BHC, Iowa

Figure 5.28 Soil boring log (SB 2) for the bridge demonstration project site in BHC, Iowa (Evans et al., 2011).

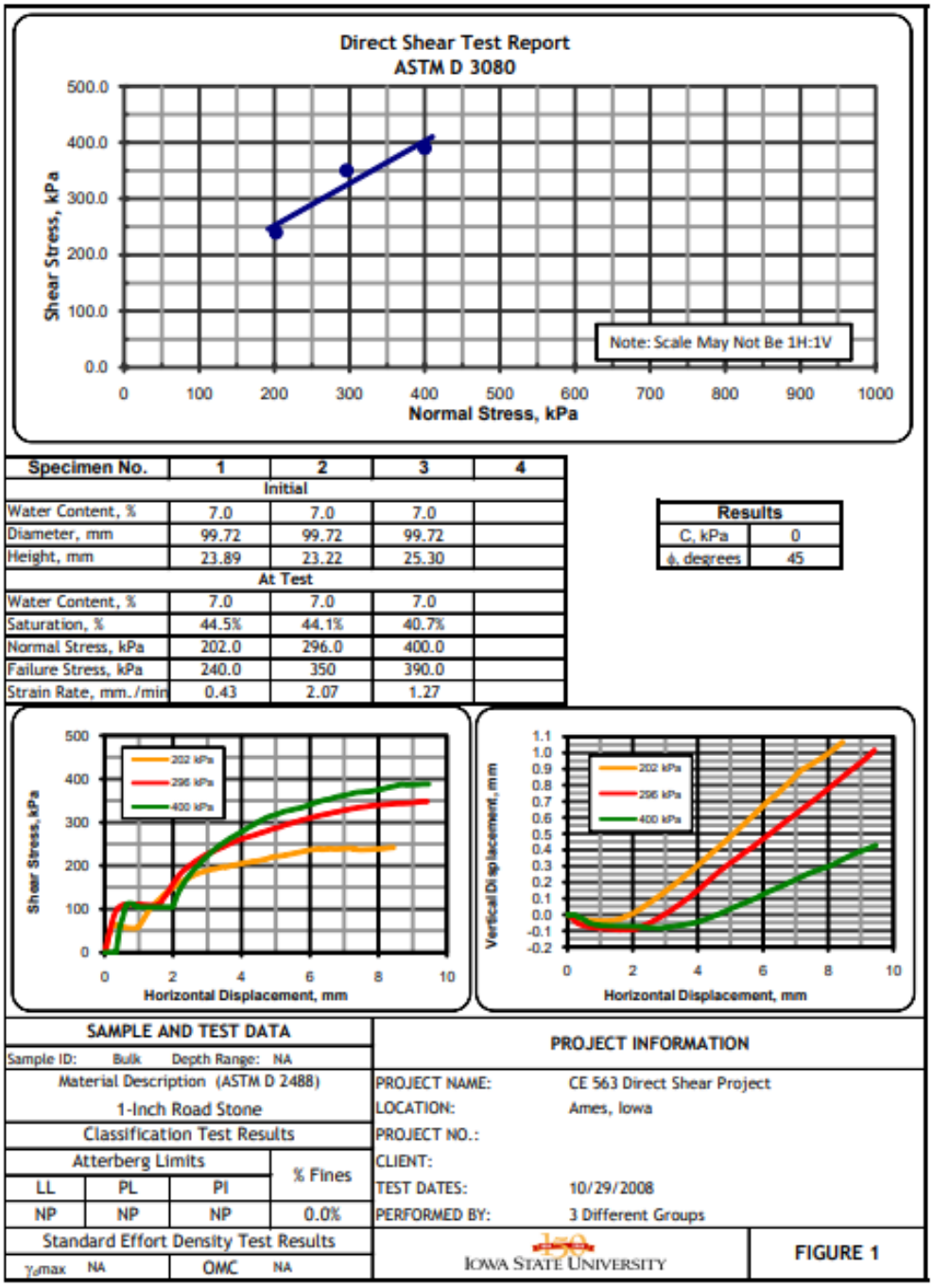

Figure 5.29 Direct shear test results on backfill material for the bridge demonstration project site in BHC, Iowa (Evans et al., 2011).

5.5.6 Material Properties

The properties of materials and the sheet pile wall used for the numerical simulation are summarized in Tables 5.16, and 5.17, respectively.

Table 5.16 Material properties used for the numerical simulation (from Evans et al., 2011).

Material	Sand (fill material)	Concrete (abutment)	Sandy clay	Bed rock
Unit weight (kg/m^3)	2002	2322	1730	2300
K (Pa)	3.3E7	1.4E10	1.7E7	2.3E10
G (Pa)	1.5E7	1.1E10	8.3E6	1.2E10
Friction angle (°)	45	-	0	-
c (Pa)	0	-	85000	-
Model	Mohr-Coulomb	Elastic	Mohr-Coulomb	Elastic

Table 5.17 The property of sheet pile used for the numerical simulation (from Evans et al., 2011).

Pile properties	PZ22
Elastic modulus (Pa)	2.00E11
Cross-section area (m^2/m)	0.0137
Inertia (m^4/m)	1.20E-04

The normal and shear stiffness of each soil layer was calculated in the same approach for the combined loading case (1). The friction interface between the sand and sheet pile was 27° following the laboratory test. The cohesion between clay and sheet pile was two thirds of the internal cohesion of clay.

Table 5.18 The pile-soil interface property for each soil layer.

Thickness	Interface properties	Friction angle (°)	C (Pa)	k_n=k_s
1.5	Sand and pile	27	0	1.4E9
3.0	Sandy clay and pile	0	57000	6.7E8

The normal and shear stiffness of each soil layer:

For sand (fill material):

$$k_{n1} = k_{s1} = 10\left(\frac{K+\frac{4}{3}G}{\Delta z}\right) = 1.4E9 \tag{5.14}$$

For sandy clay:

$$k_{n2} = k_{s2} = 10\left(\frac{K+\frac{4}{3}G}{\Delta z}\right) = 6.7E8 \tag{5.15}$$

Then the representative values are calculated as the average:

$$k_n = k_s = \frac{(k_1 x t_1 + k_2 x t_2)}{t_1 + t_2} = 0.85E9 \tag{5.16}$$

$$\varphi = \frac{(\varphi_1 x t_1 + \varphi_2 x t_2)}{t_1 + t_2} = 9^o \tag{5.17}$$

$$c = \frac{(c_1 x t_1 + c_2 x t_2)}{t_1 + t_2} = 38kPa \tag{5.18}$$

where t_1, t_2 are the thickness of backfill sand and sandy clay; k_{n1}, k_{s1}, k_{n2}, k_{s2} are normal and shear stiffness of backfill sand and sandy clay; φ_1, φ_2 are friction angle of backfill sand and sandy clay; and c_1, c_2 are friction angle of backfill sand and sandy clay.

Table 5.19 The pile-soil interface properties used for the numerical simulation.

Soil and pile	Interface properties
Normal stiffness (Pa/m)	0.85E9
Shear stiffness (Pa/m)	0.85E9
Cohesion (Pa)	38000
Friction angle (^{o})	9

5.5.7 Cable Element

A cable element in FLAC was used to model the Deadman anchor. Cable elements were one-dimensional axial elements that were able to be anchored at a specific point in the grid (point-anchored) or grouted so that the cable element developed forces along its length as the grid deformed. Cable elements can yield tension or compression but cannot sustain a bending moment (Figure 5.30). If desired, cable elements may have been initially pre-tensioned. Cable elements were used to model various supports for which tensile capacity was essential, including rock bolts, cable bolts, and tiebacks. The cable elements used in FLAC required the following input parameters: (1) cross-sectional area [length^2] of the cable; (2) density [mass/volume] of the cable (optional - used for dynamic analysis and gravity loading); (3) elastic modulus [stress] of the cable; (4) spacing [length] (optional - if not specified, cables were considered continuous in the out-of-plane direction); (5) tensile yield strength [force] of the cable (if not specified, the tensile yield strength was zero); (6) compressive yield strength [force] of the cable (if not specified, the compressive yield strength was zero); (7) exposed perimeter [length] of the cable; (8) stiffness of the grout [force/cable length/displacement]; (9) cohesive strength of the grout [force/cable length]; (10) frictional resistance of the grout [degrees]; and (11) thermal expansion

coefficient (optional - used for thermal analysis). The input parameters used for this simulation are summarized in Table 5.20.

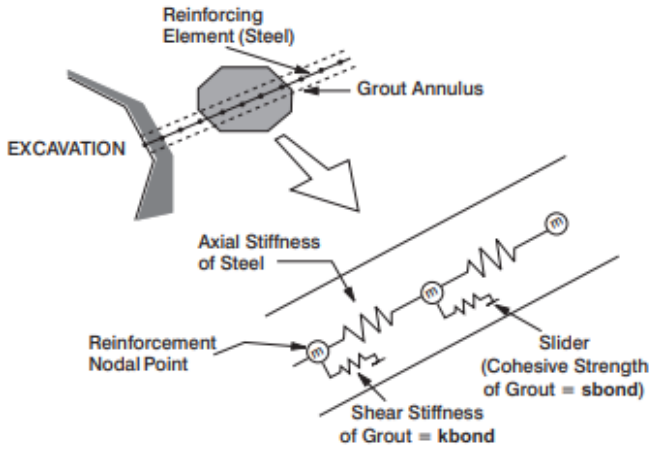

Figure 5.30 Conceptual mechanical representation of fully bonded reinforcement which accounts for the shear behavior of the grout annulus (Itasca Consulting Group, 2019).

Table 5.20 Input parameters of the cable element used for the numerical simulation.

Soil and cable	
Shear stiffness kbond (N/m/m)	1.50E10
Cohesive strength sbond (Pa/m)	0
Elastic modulus E (GPa)	98.6
Yield (N)	5.48E5
Area (m^2)	5.00E-04
Shear friction (^{o})	30
Spacing (m)	3.5
Perimeter (m)	6

5.5.8 Numerical Simulation Model

The numerical model constructed by the project team is shown in Figure 5.31.

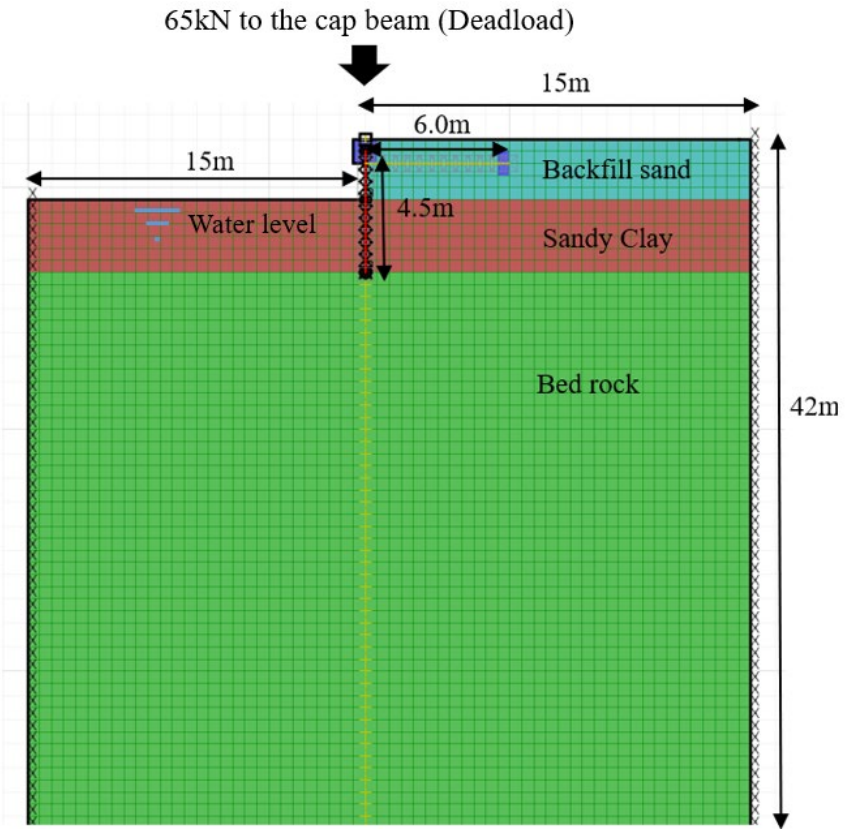

Figure 5.31 The numerical simulation model in FLAC to compare the results with field data from the demonstration bridge site in IOWA.

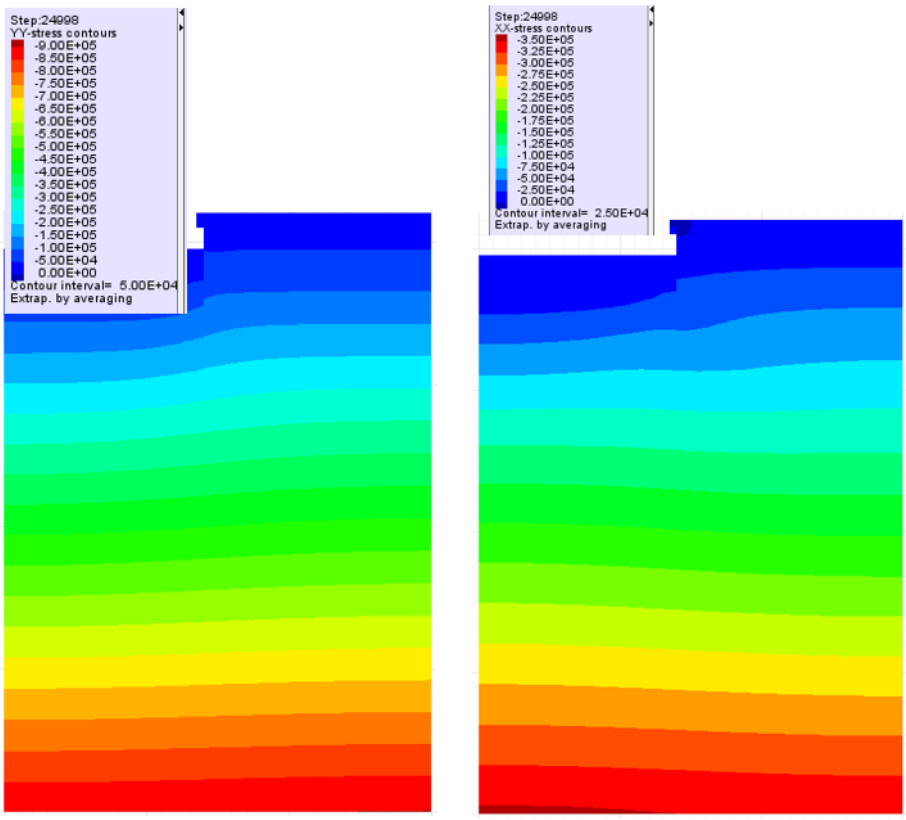

Figure 5.32 Simulation results: (a) vertical stress contour, and (b) horizontal stress contour in the model.

5.5.9 Results

The deflection of the sheet pile wall from the numerical simulation was about 0.49 cm (0.19 inches; Figure 5.33), which was slightly larger than the wall deflection from field monitoring data (0.33cm). The Earth pressure from the cap to 1.5 m below (7.0 kPa to 19.2 kPa) was similar to the field observations (6.66 kPa to 16.04 kPa), as shown in Table 5.21.

In summary, the good comparison of the numerical simulation results with the data an literature for the combined axial + lateral loading (cases 1 and 2) validate the reliability of the modeling approach by the project team at UNL.

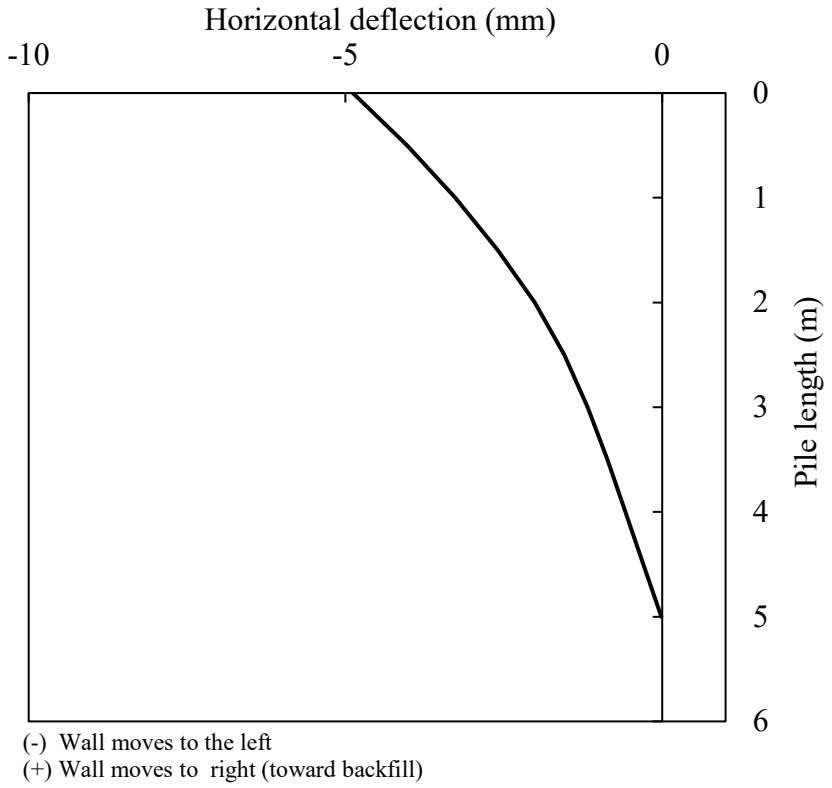

Figure 5.33 Simulation results: horizontal deflection of the sheet pile wall.

Table 5.21 Backfill pressure and deflections from the numerical simulation by the project team for the validation of the combined axial + lateral load (2).

Pressure or deflection	Estimated Total
Earth pressure (0.5 m below TOC)	7.0 kPa
Earth pressure (1.0m below TOC)	10.9 kPa
Earth pressure (1.5 m below TOC)	19.2 kPa
Earth pressure (2.0m below TOC) - Dredge line & Clay Stratum	15.8 kPa
Earth pressure (2.5 m below TOC)	15.9 kPa
Earth pressure (3.0m below TOC)	21.0 kPa
Earth pressure (3.5m below TOC)	29.9 kPa
Wall deflection	0.49 cm

Chapter 6 Numerical Studies: A Parametric Study

6.1 Bridge Site Selected for Parametric Study

An extensive parametric study was conducted for this project to investigate how various parameters may affect the performance of the sheet pile abutment system under the combined axial and lateral loading. The project team selected a bridge site in the state of Nebraska for this parametric study. The selected bridge was located in Tarnov South, Platte County, Nebraska, which was a two-lane single-span beam-in-slab structure 12.4 m (~40 ft) wide and 18.3 m (60 ft) long (Figure 6.1; Table 6.1). The employed design combined 15 driven piles for axial-load bearing. The sheet piles used for the bridge were PZ22 sections. All 76 sheet pile sections were driven for both abutments to prevent scouring and handle the lateral load from backfill (Figure 6.2). In this parametric study, the project team examined a hypothetical case where the axial-load bearing piles were not driven, and thus, the sheet piles supported both the axial and lateral loads.

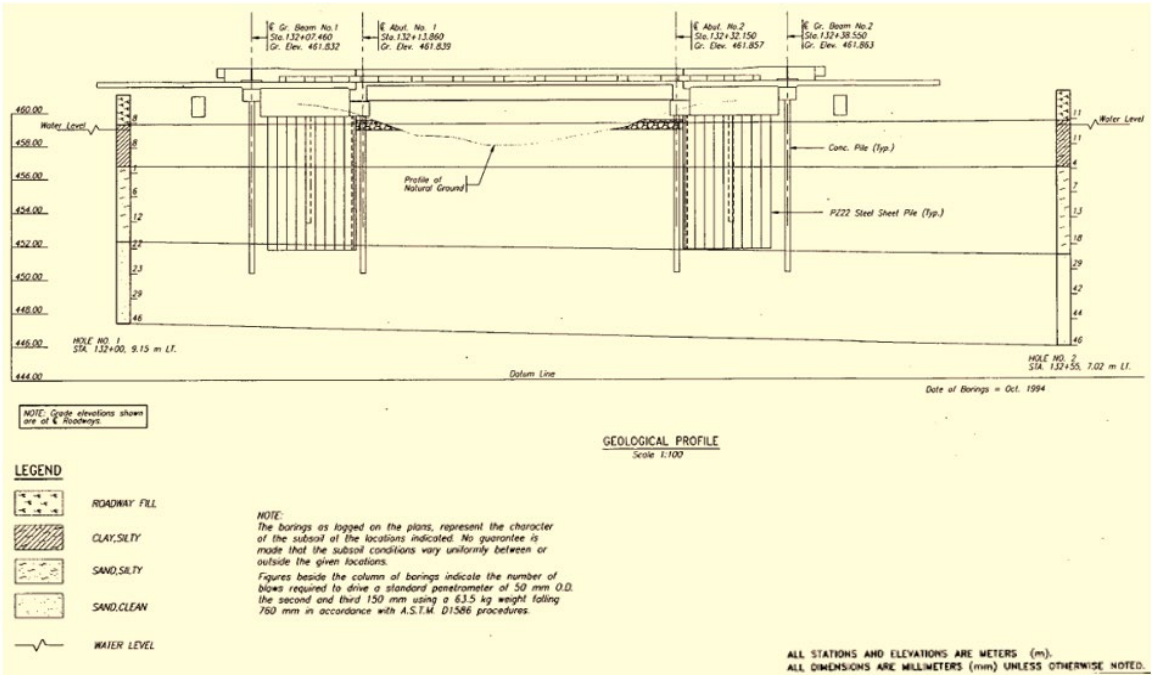

Figure 6.1 Geological profile and elevation of the bridge located in Tarnov South, Platte County, Nebraska – selected bridge site for the parametric study of the sheet pile abutment system.

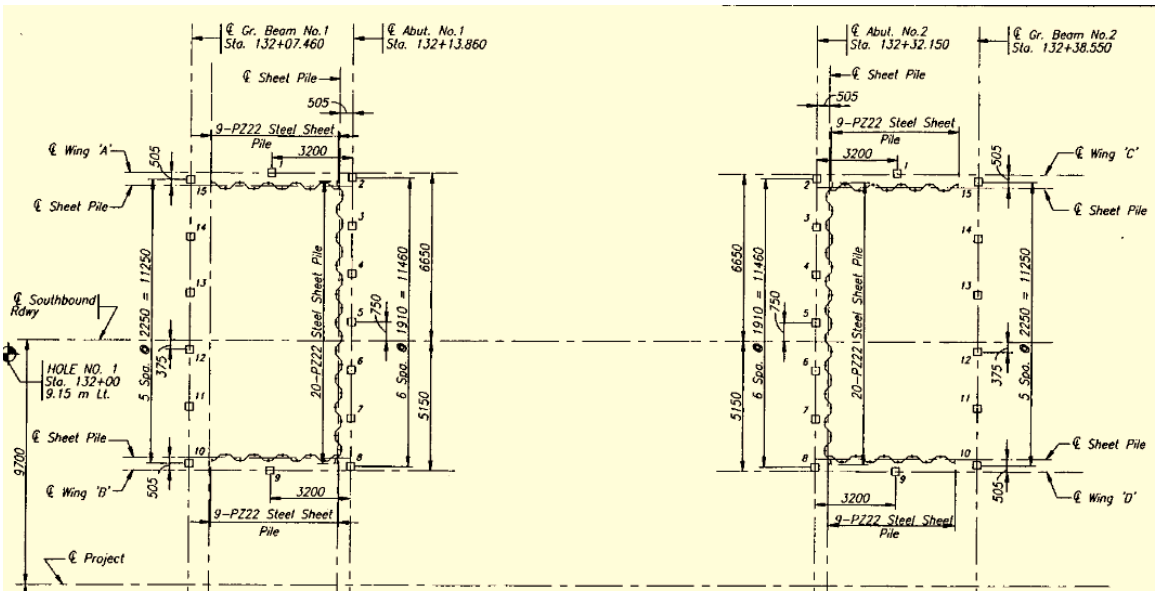

Figure 6.2 Pile Layout of the bridge in Tarnov South, Platte County, Nebraska – selected bridge site for the parametric study of the sheet pile abutment system.

Table 6.1 The dimension of the bridge selected for the parametric study in this project.

Properties	
Length of bridge	18.3 m (60 ft)
Width of bridge	12.4 m (40 ft)
Slab thickness	190 mm (7.5 inches)
Number of Girders (W920 x253) Steel grade 50	5
Concrete weight	2,403 kg/m^3

6.1.1 Bridge Dimension

The project team considered only the dead load in this parametric study. The CSI bridge was employed to estimate the total dead load from the superstructure. CSiBridge executed a parametric object-based modeling technique when designing analytical bridge systems. This software enabled engineers to assign bridge composition as an assemblage of objects (roadway

superstructure, substructure, abutments, piers, foundation system). From the dimensions in Table 6.1, the total dead load was calculated as 121 tons for each abutment. The factored dead load was calculated following Load and Resistance Factor Design (LFRD):

$$\mathrm{DL} = 1.2(121) = 145.2\ tons\ (per\ girder, per\ abutment) \tag{6.1}$$

Assuming the cap length was the same as width at 12.4 m, the dead load was:

$$P_{uDL} = \frac{DL}{12.4} = 11.7\frac{tons}{m} \approx 120\mathrm{kN/m} \tag{6.2}$$

In the actual design, the sheet pile walls were combined with the load-bearing piles into an integral abutment. The separate load-bearing piles were not simulated in this parametric study to evaluate the feasibility of sheet piles in sustaining both lateral and axial loads. For simplicity, the cap beam size was assumed as 1 m × 1 m, and 0.5 m of the pile head was set into the cap.

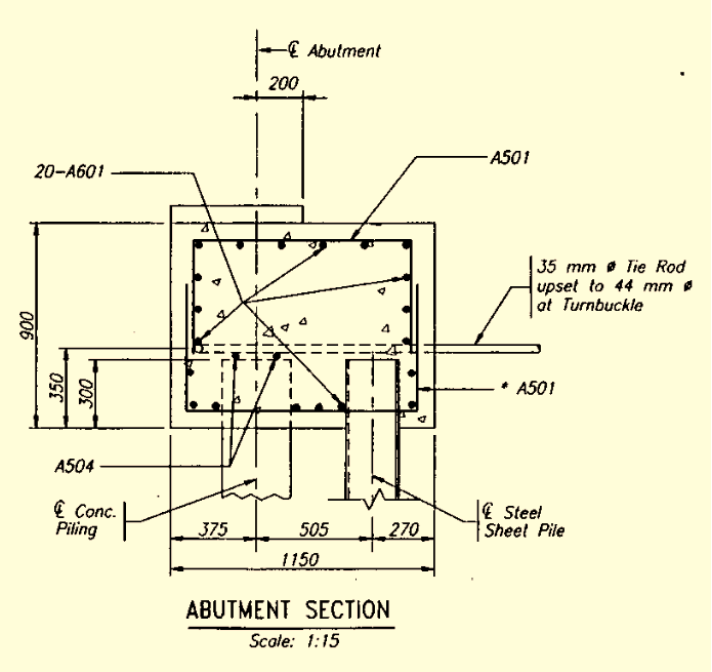

Figure 6.3 Abutment cross section of the bridge in Tarnov South, Platte County, Nebraska.

6.1.2 Soil Properties

The soil properties, including unit weight, Young's modulus, Poisson's ratio, and cohesion for each soil layer were estimated, using the SPT values in the soil profile (Tables 6.2, 6.3, and 6.4). $N_{(60)}$ was corrected to $N_{(60)1}$ using Liao and Whitman's relationship (1986).

Table 6.2 Penetration resistance and soil properties based on SPT N-value for cohesionless soil (adapted by Rahman, 2019).

SPT N-value		0 to 4	4 to 10	10 to 30	30 to 50	>50
Compactness		very loose	loose	medium	dense	very dense
Relative density, D_r (%)		0 to 15	15 to 35	35 to 65	65 to 85	85 to 100
Internal angle of friction, φ(°)		<28	28 to 30	30 to 36	36 to 41	>41
Unit weight (moist)	pcf	<100	95 to 125	110 to 130	110 to 140	>130
	kN/m^3	<15.7	14.9 to 19.6	17.3 to 20.4	17.3 to 22.0	>20.4
Submerged unit weight	pcf	<60	55 to 65	60 to 70	65 to 85	>75
	N/m^3	<9.4	8.6-10.2	9.4 to 11.0	10.5 to 13.4	>11.8

Table 6.3 Penetration resistance and soil properties based on SPT N-value for cohesive soil (adapted by Rahman, 2019).

SPT N-value		0 to 2	2 to 4	4 to 8	8 to 16	16 to 32	>32
Consistency		very soft	soft	medium	stiff	very stiff	hard
Unit weight (moist)	pcf	0 to 250	250 to 500	500 to 1000	1000 to 2000	2000 to 4000	>4000
	kPa	0 to 25	25 to 50	50 to 100	100 to 200	200 to 400	>400
Submerged unit weight	Pcf	<100	100 to 120	110 to 125	115 to 130	120 to 140	>130
	N/m^3	<15.7	15.7 to 18.8	17.3 to 19.6	18.1 to 20.4	18.8 to 22.0	>20.4

Table 6.4 Selected elastic constants of soils (adapted by Itasca Consulting Group, 2019).

	Dry density (kg/m^3)	Elastic modulus E(MPa)	Poisson's ratio
Loose uniform sand	1470	10 to 26	0.2 to 0.4
Dense uniform sand	1840	34 to 69	0.3 to 0.45
Loose, angular-grained, silty sand	1630		
Dense, angular-grained, silty sand	1940		0.2 to 0.4
Stiff clay	1730	6 to 14	0.2 to 0.5
Soft clay	1170 - 1490	2 to 3	0.15 to 0.25
Loess	1380		
Soft organic clay	1610 - 820		
Glacial till	2150		

The input properties for the soil layers are summarized in Tables 6.5 and 6.6. The Mohr-Coulomb model was applied to all materials, while the sheet pile abutment was simulated using the beam elements.

Table 6.5 Soil properties following SPT values – Parametric study for sheet pile abutment.

Material	Thickness (m)	N_{60}	Effective stress σ' (kPa)	C_N	$N_{(60)1}$	Unit weight (kN/m^3)	Young modulus (Pa)	Poisson ratio	Friction angle (°)	c (kPa)
Roadway fill	2	8	40	1.58	13	20	1.15E7	0.3	30	0
Silty clay	2.5	8	52.25	N/A	N/A	14.9	1.00E7	0.4	0	50
Silty Sand	4	7	123.65	0.9	6	17.85	8.00E6	0.3	30	0
Sand Clean	4	31	203.65	0.7	22	20	3.00E7	0.3	36	0

Table 6.6 Soil input parameters used for the parametric study of the sheet pile abutment system.

Material	Friction angle (°)	c (kPa)	B (Pa)	G (Pa)	Model
Roadway fill	30	0	9.6E6	4.6E6	Mohr-Coulomb
Silty clay	0	50	1.7E7	3.6E6	Mohr-Coulomb
Silty Sand	30	0	6.7E6	3.1E6	Mohr-Coulomb
Sand Clean	36	0	2.5E7	1.2E7	Mohr-Coulomb

6.1.3 Pile-Soil Interface Parameters

The normal and shear stiffness at the sheet pile-soil interface were calculated using Equation 5.3. Properties for each soil layer are summarized in Table 6.7. From those properties, the average interface properties—the input parameters for the beam element—were estimated as shown in Table 6.8.

Table 6.7 Pile-soil interface properties for each soil layer.

Material	Thickness of layer (m)	Stiffness $k_n=k_s$ (Pa)	Interface friction angle (°)	Interface cohesion (kPa)
Roadway fill and pile	2	3.2E8	27	0
Silty clay and pile	2.5	4.4E8	0	31
Silty sand and pile	4	2.2E8	27	0
Clean sand and pile	4	8.2E8	27	0

Table 6.8 Pile-soil interface: input parameters used for the parametric study of the sheet pile abutment system.

Soil and pile	Interface properties
Normal stiffness (Pa/m)	3.6E8
Shear stiffness (Pa/m)	3.6E8
Cohesion (kPa)	8
Friction angle (°)	20

6.1.4 The Base Model for Parametric Study

The base numerical simulation model was constructed as shown in Figure 6.4. Then, nine parametric case studies relating to the sheet pile abutment system were investigated as follows (underline: original design):

- Case 1: Span length (40, 60, 80, 100 ft)
- Case 2: Excavation depth (0.5, 1.5, 2.5 m; 1.6, 4.9, 8.2 ft)
- Case 3: Sheet-pile type (PZ22, PZ27, PZ35)
- Case 4: Sheet-pile length (6.5, 8.5, 10.5 m; 21.3, 27.9, 34.4 ft)
- Case 5: Anchors + Deadman concretes (different anchor lengths)
- Case 6: Anchors + Deadman concretes (different anchor spacings)
- Case 7: Submerged *vs*. dry condition
- Case 8: End-bearing conditions (soil *vs*. rock)
- Case 9: Temperature effects with abutment type (conventional *vs*. semi-integral)

Each case study employed different scenarios described above as input parameters to examine how those variables affected the performance of the sheet pile abutment system, which was intended to assume both the axial and lateral loads. The main outcome under investigation included horizontal deflections and vertical settlement of the sheet pile wall, as well as the shear force and bending moment imposed on the sheet pile wall.

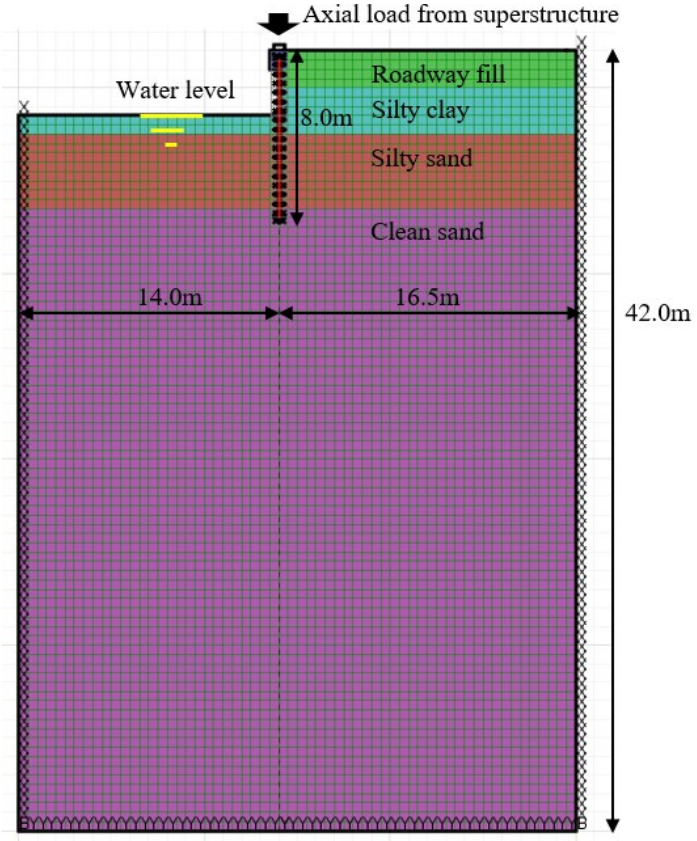

Figure 6.4 The base numerical simulation model for the parametric study of this project.

6.2 Case 1

6.2.1 Parameters

The dead load increased with an increase in bridge-span length. The project team investigated a bridge-span length range of 40 to 100 ft (12.2 to 30.5 m) for the selected bridge

site. Equation 6.3 below was used to calculate the dead load. For example, a span length of 60 ft (18.3 m) generated a total dead load of 120 kN/m. The corresponding dead load for each span length is summarized in Table 6.9. The excavation level of the abutment was the same at 1.5 m (4.9 ft) for all span lengths in the simulations.

$$DL_{(100ft\ span)} = \frac{DL_{(60ft\ span)}}{L_{(60ft\ span)}} L_{(100ft\ span)} \tag{6.3}$$

Table 6.9 A summary of the simulations of the sheet pile abutment with different span lengths (Case 1).

Number of simulation	**Span length**	**Dead load (kN/m)**	Pile type	Excavation	Note
1	40 ft (12.2 m)	80	PZ 22	1.5 m (4.9 ft)	Actual design
2	60 ft (18.3m)	120	PZ 22	1.5 m (4.9 ft)	
3	80 ft (24.4 m)	160	PZ 22	1.5 m (4.9 ft)	
4	100 ft (30.5 m)	200	PZ 22	1.5 m (4.9 ft)	

6.2.2 Results

Figure 6.5 shows that the maximum horizontal deflection for span lengths of 40 to 100 ft ranged from 1.8 cm (0.7 in.) to 4.8 cm (1.9 in.). As mentioned previously, an increase in the span length contributed to the dead load increase, leading to a larger horizontal deflection of the sheet pile. In the presence of the lateral load from the backfill soil, the sheet pile was deflected toward the excavation zone. Furthermore, the combined effect of the axial load imposed on the pile top and the lateral load magnified the horizontal deflection (i.e., P-Delta (P-Δ) effect; Figure 6.6).

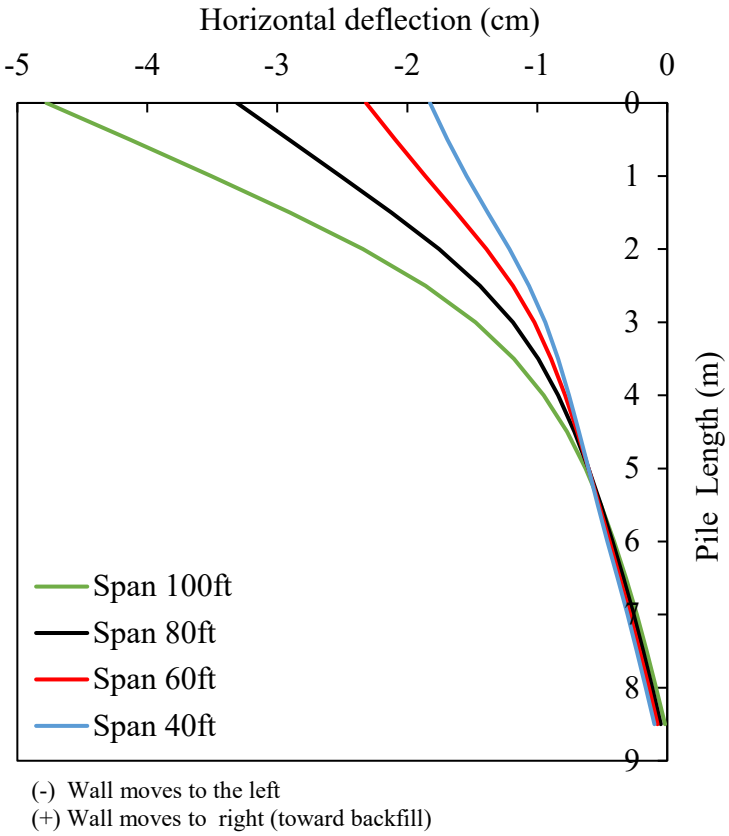

Figure 6.5 Parametric study Case 1: Horizontal deflection of the sheet pile wall for different span lengths.

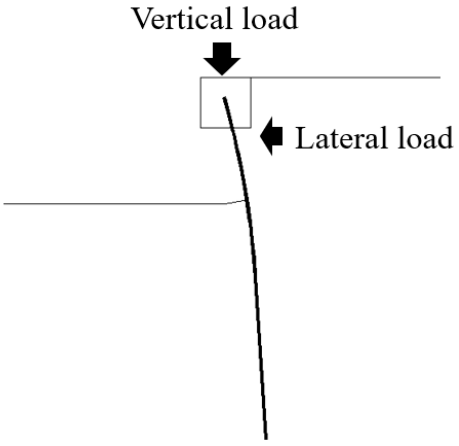

Figure 6.6 An expected P-Delta effect on the behavior of the sheet pile abutment that is subjected to the combined axial and lateral loads.

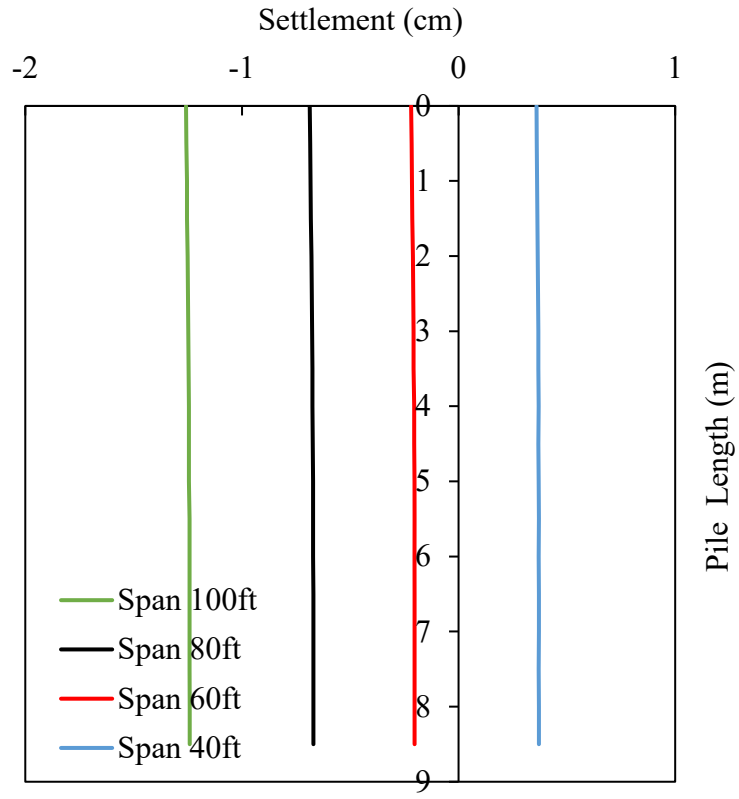

Figure 6.7 Parametric study Case 1: Vertical settlement of the sheet pile wall for different span lengths.

An increase in the span length also resulted in larger vertical settlements. Figure 6.7 shows that the maximum vertical settlement of the sheet pile was 1.3 cm (0.5 inches) in the case of a 100 ft span length. Similarly, the maximum values of shear force and bending moment imposed on the sheet pile increased with the span length, as shown in Figures 6.8 and 6.9, respectively. With these simulated cases, it can be inferred that the shear force and bending moment also followed a similar trend with the span length as that of horizontal deflection and vertical settlement of the sheet pile. The calculated factors of safety (*FS*) in terms of the shear force and bending moment were presented in the summary Table 6.21. For a 100 ft bridge-span

length, the calculated factor of safety was $FS_{shear} = 23.7$ and $FS_{bend} = 3.1$ for the shear force and bending moment, respectively.

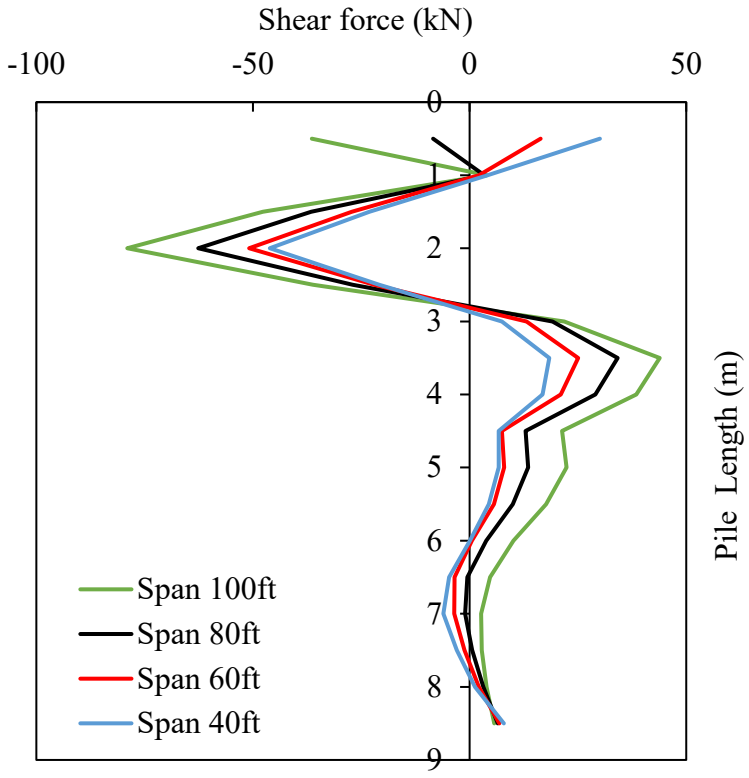

Figure 6.8 Parametric study Case 1: Shear force imposed on the sheet pile wall for different span lengths.

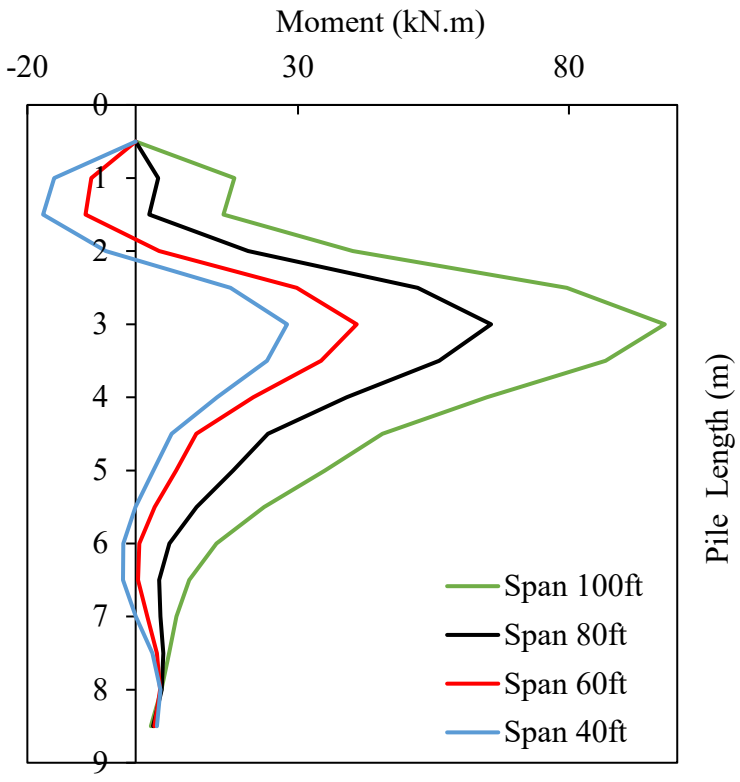

Figure 6.9 Parametric study Case 1: Bending moment imposed on the sheet pile wall for different span lengths.

6.3 Case 2

6.3.1 Parameters

In general, each bridge had a specific excavation level depending on the superstructure's height and the site's topography (Figure 6.10). An extension of the excavation level may have led to an increase in the horizontal deflection, shear force, and a bending moment of the sheet pile. Three excavation levels (0.5 m, 1.5 m, and 2.5 m; 1.6, 4.9, and 8.2 ft) were applied to a 60 ft span bridge for the Case 2 parametric study here (Table 6.10). The actual excavation level in the original design was approximately 0.5 m to 1.5 m. Besides, the riprap gravel was applied in front of the wall to lessen the horizontal displacement of the sheet pile in the actual design. This

material provided the counterforce to the backfill lateral force to enhance the stabilization of the sheet pile. However, such riprap gravel was not considered in the numerical simulation for simplicity.

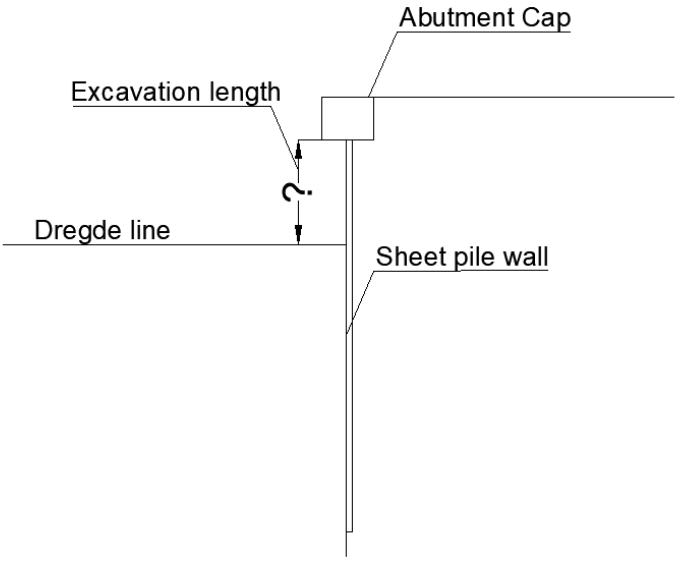

Figure 6.10 Simulation of the sheet pile wall with different excavation depths: 0.5 m, 1.5 m, and 2.5 m (1.6, 4.9, and 8.2 ft).

Table 6.10 A summary of the simulations of the sheet pile abutment with different excavation depths (Case 2).

Number of simulation	Span length	Dead load (kN/m)	Pile type	**Excavation**	
1	60 ft (18.3m)	120	PZ22	0.5 m (1.6 ft)	
2	60 ft (18.3m)	120	PZ22	1.5 m (4.9 ft)	Actual design
3	60 ft (18.3m)	120	PZ22	2.5 m (8.2 ft)	

6.3.2 Results

An increase in the level of excavation resulted in an increase in the lateral load, which magnified the horizontal deflection of the sheet pile, as shown in Figure 6.11. The maximum

deflection observed from this parametric study was 5 cm (~2 inches) for the 2.5 m excavation level. On the other hand, there was no direct correlation between the excavation level and vertical settlement of the sheet pile (Figure 6.12).

An increase in the excavation level also led to an increase in the shear force and bending moment imposed on the sheet pile, as a result of the P-Delta effect. The location of maximum shear force and bending moment also moved downward as the excavation level increased (see Figures 6.13 and 6.14). For a 60 ft span bridge with 2.5 m excavation, FS_{shear} was 38.4 and FS_{bend} was 4.6. All FS values are listed in Table 6.21.

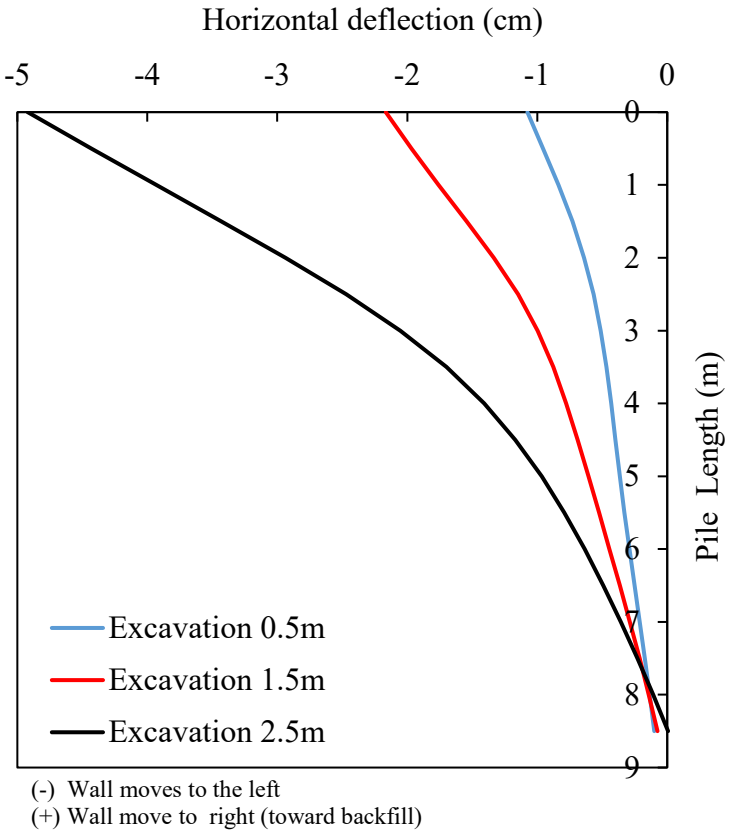

Figure 6.11 Parametric study Case 2: Horizontal deflection of the sheet pile wall for different excavation levels.

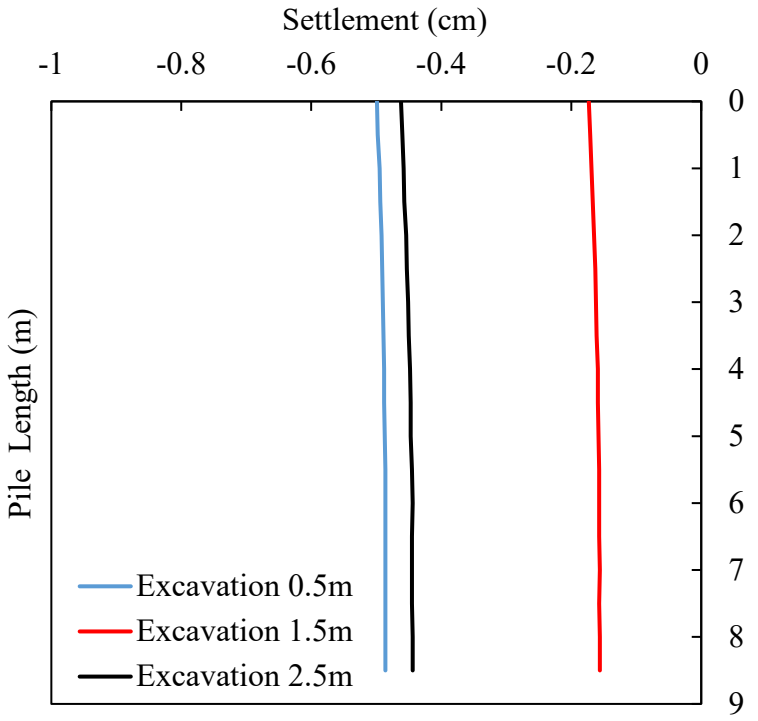

Figure 6.12 Parametric study Case 2: Vertical settlement of the sheet pile wall for different excavation levels.

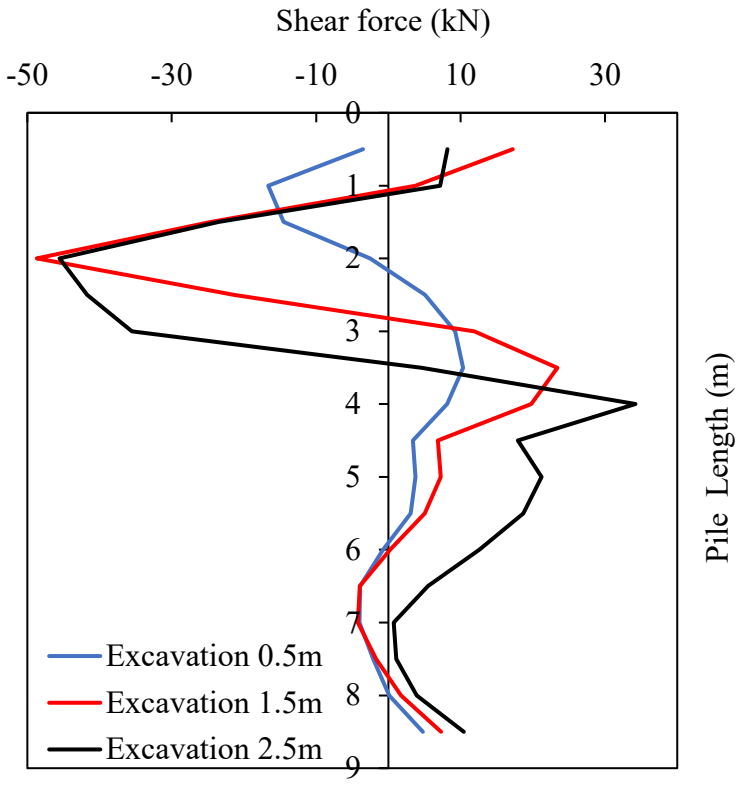

Figure 6.13 Parametric study Case 2: Shear force imposed on the sheet pile wall for different excavation levels.

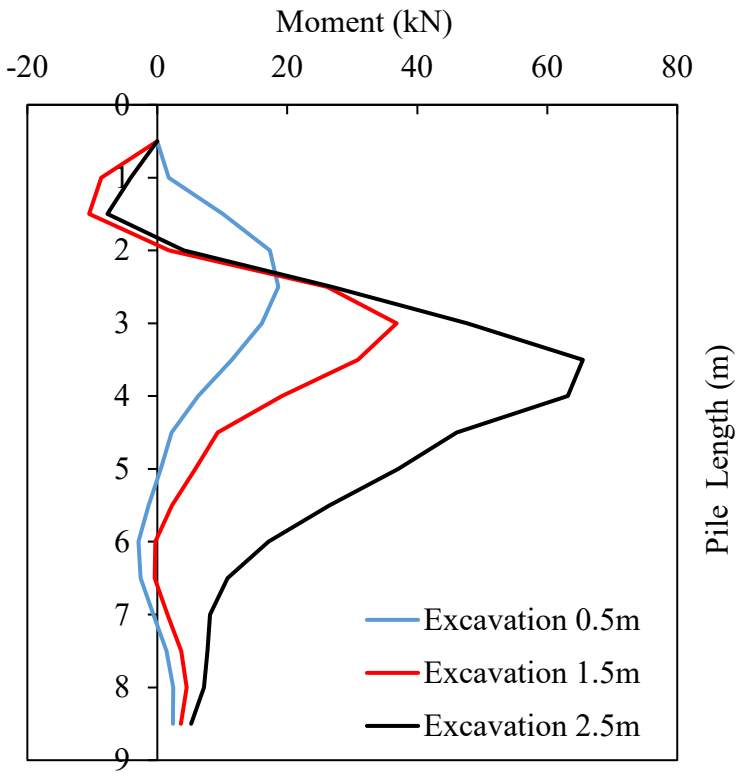

Figure 6.14 Parametric study Case 2: Bending moment imposed on the sheet pile wall for different excavation levels.

6.4 Case 3

6.4.1 Parameters

A different sheet pile section may impact the performance of a sheet pile wall under the combined axial and lateral loads. The sheet pile sections considered for this parametric study were PZ22, PZ27, and PZ35 (Table 6.11). With that, the project team selected two conditions: a base condition with the original design (span length: 60 ft, excavation level: 4.9 ft (1.5 m)) and an extreme condition with a span length of 100 ft and excavation level of 8.2 ft (2.5 m), as summarized in Table 6.12.

Table 6.11 Properties for different sheet pile sections.

Pile properties	PZ22	PZ27	PZ35
Elastic modulus (Pa)	2.0E11	2.0E11	2.0E11
Cross-section area (m^2/m)	0.0137	0.01681	0.022
Inertia (m^4/m)	1.20E-04	2.52E-04	4.93E-04
Section modulus (m^3/m)	0.000973	0.00162	0.002608

Table 6.12 A summary of the simulations of the sheet pile abutment with different sheet pile sections (Case 3).

Number of simulation	Span length	Dead load (kN/m)	**Pile type**	Excavation	
1	60 ft (18.8 m)	120	PZ22	1.5 m (4.9 ft)	Actual design
2	60 ft (18.8 m)	120	PZ27	1.5 m (4.9 ft)	
3	60 ft (18.8 m)	120	PZ35	1.5 m (4.9 ft)	
4	100 ft (30.5 m)	200	PZ22	2.5 m (8.2 ft)	
5	100 ft (30.5 m)	200	PZ27	2.5 m (8.2 ft)	
6	100 ft (30.5 m)	200	PZ35	2.5 m (8.2 ft)	

6.4.2 Results

It was observed that sheet piles with higher inertia yielded smaller horizontal deflection, as shown in Figures 6.15 and 6.19. That is, the sheet pile with the highest inertia, PZ35, showed the smallest maximum horizontal deflection, 2.1 cm (0.83 inches) for a 60 ft span (Figure 6.15) and 6.5 cm (2.56 inches) for a 100 ft span (Figure 6.19), respectively. Meanwhile, the sheet pile with the lowest inertia, PZ22, exhibited the largest maximum deflection, 2.3 cm (0.91 inches) for a 60 ft span (Figure 6.15) and 10.7 cm (4.21 inches) for a 100 ft span (Figure 6.19), respectively.

Such a trend was the opposite for vertical settlement: the sheet pile with higher inertia yielded larger vertical settlement, as shown in Figures 6.16 and 6.20. In detail, the sheet pile with PZ35 showed the largest vertical settlement, 0.27 cm (0.11 inches) for a 60 ft span (Figure 6.16) and 2.1 cm (0.83 inches) for a 100 ft (Figure 6.20), respectively. On the other hand, the sheet pile with PZ22 showed 0.22 cm (0.09 inches) for a 60 ft span and 1.6 cm (0.63 inches) for a 100 ft span, respectively.

Lastly, the sheet pile with higher inertia showed a higher factor of safety against the shear force and bending moment failure (Figures 6.17, 6.18, 6.21, and 6.22). For example, the sheet pile with PZ22 exhibited the lowest safety factor, $FS_{shear} = 24.0$ and $FS_{bend} = 2.0$ when the span length was 100 ft. All FS values are listed in Table 6.21.

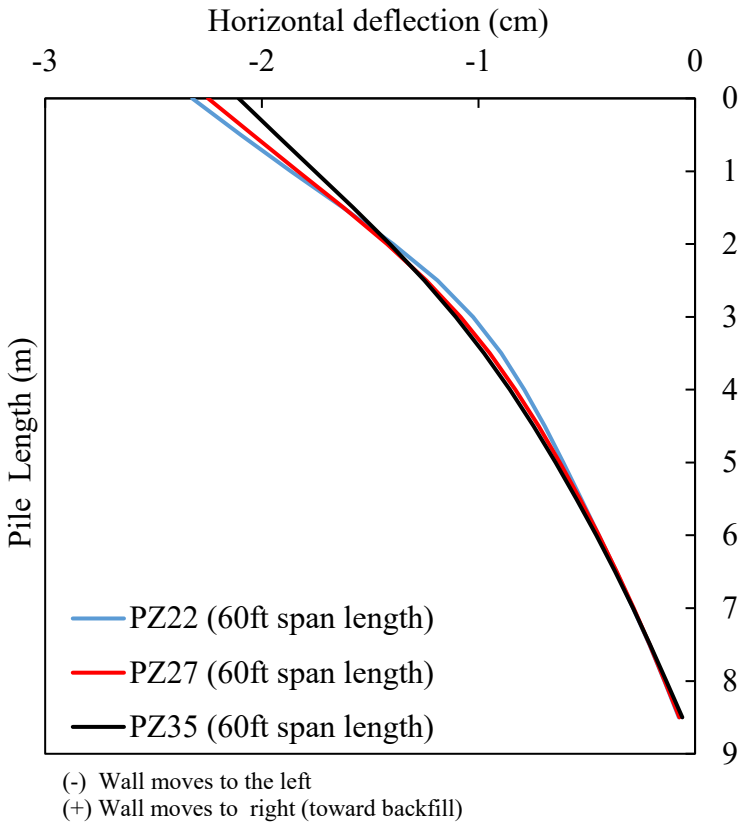

Figure 6.15 Parametric study Case 3: Horizontal deflection of the sheet pile wall for different sheet pile sections (a base condition with a span length of 60 ft and excavation level of 4.9 ft (1.5 m)).

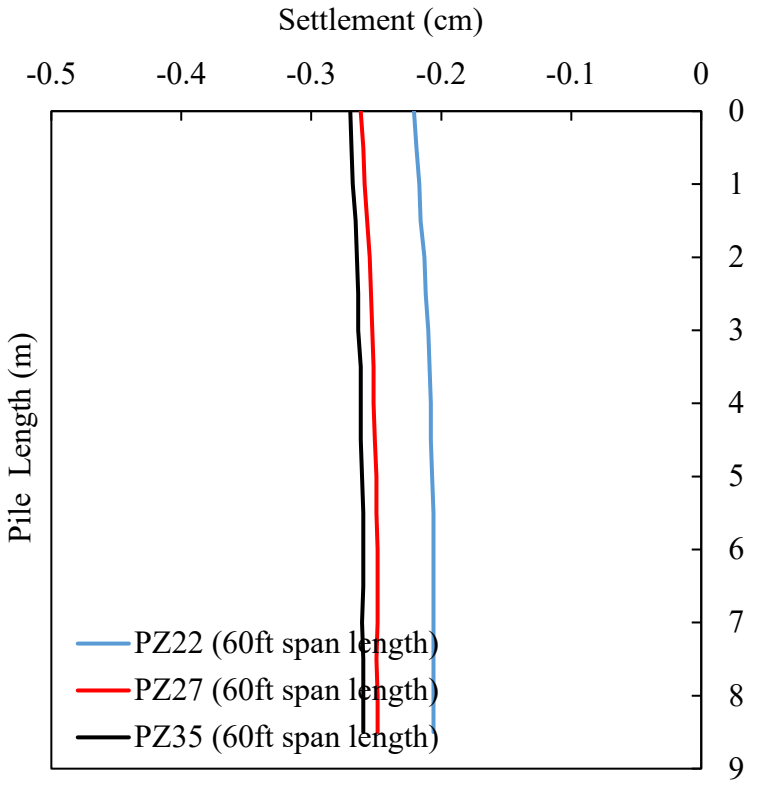

Figure 6.16 Parametric study Case 3: Vertical settlement of the sheet pile wall for different sheet pile sections (a base condition with a span length of 60 ft and excavation level of 4.9 ft (1.5 m)).

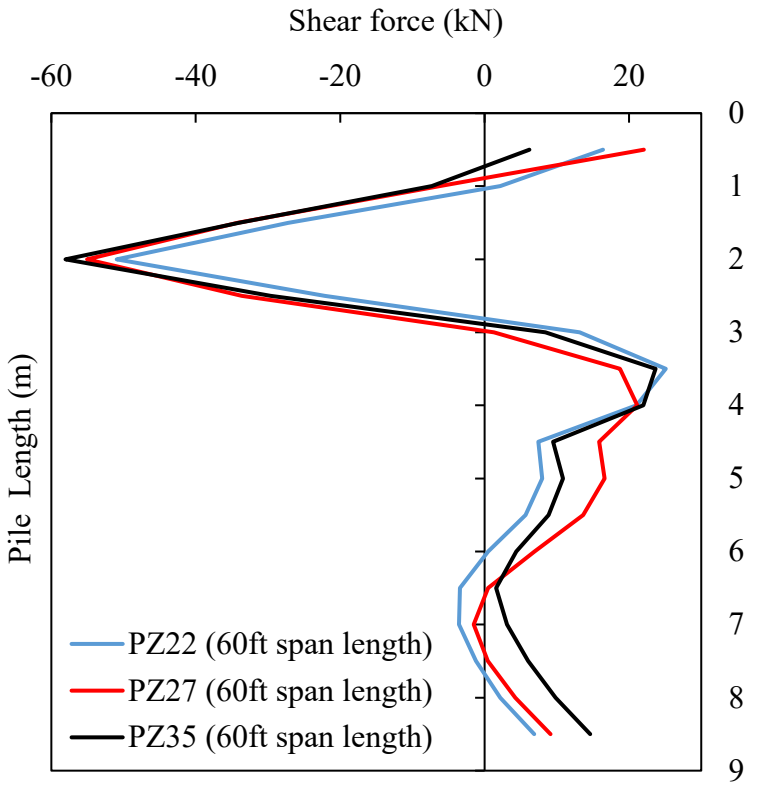

Figure 6.17 Parametric study Case 3: Shear force imposed on the sheet pile wall for different sheet pile sections (a base condition with a span length of 60 ft and excavation level of 4.9 ft (1.5 m)).

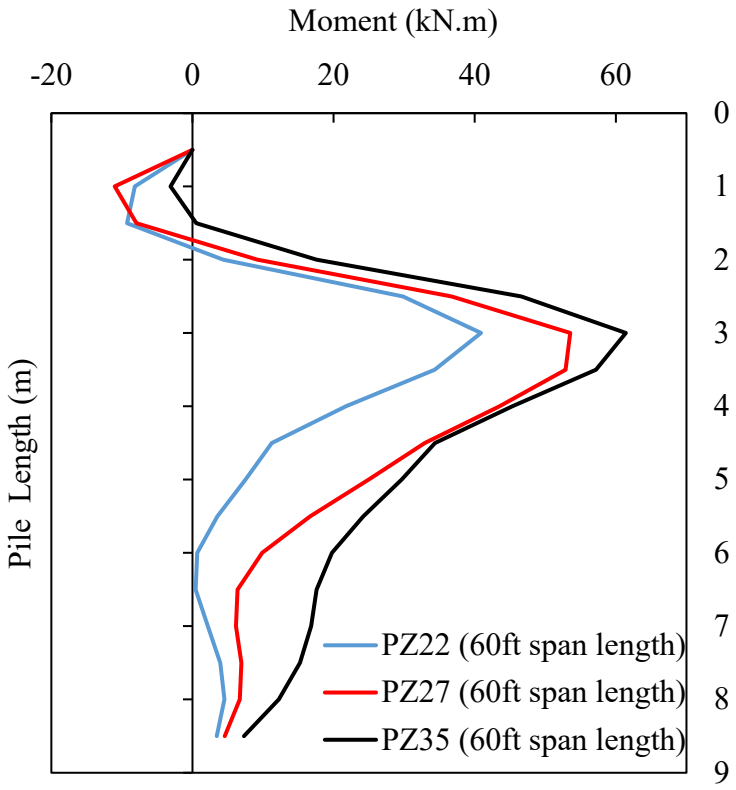

Figure 6.18 Parametric study Case 3: Bending moment imposed on the sheet pile wall for different sheet pile sections (a base condition with a span length of 60 ft and excavation level of 4.9 ft (1.5 m)).

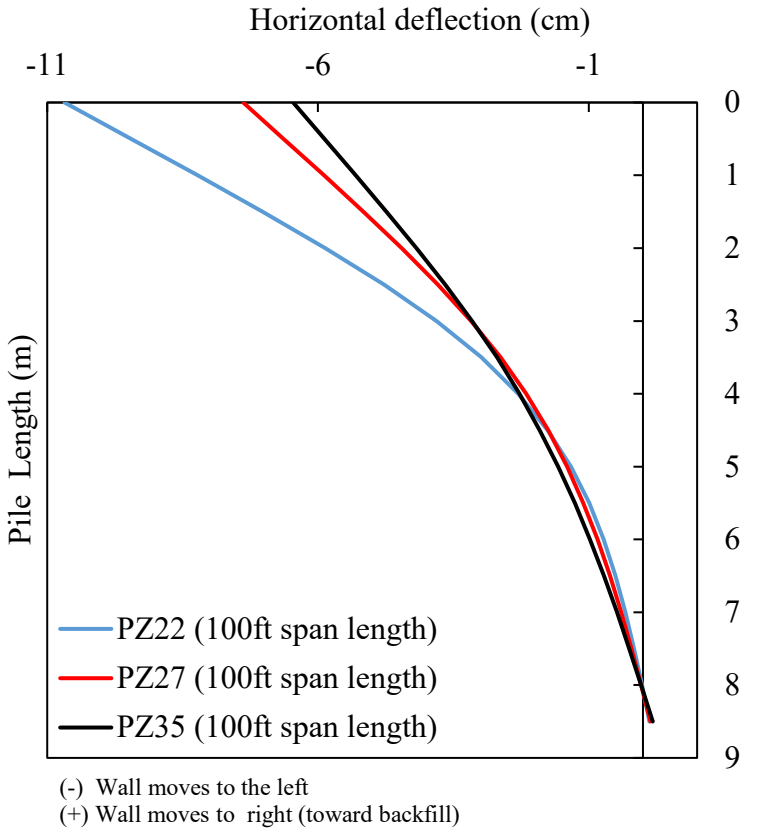

Figure 6.19 Parametric study Case 3: Horizontal deflection of the sheet pile wall for different sheet pile sections (an extreme condition with a span length of 100 ft and excavation level of 8.2 ft (2.5 m)).

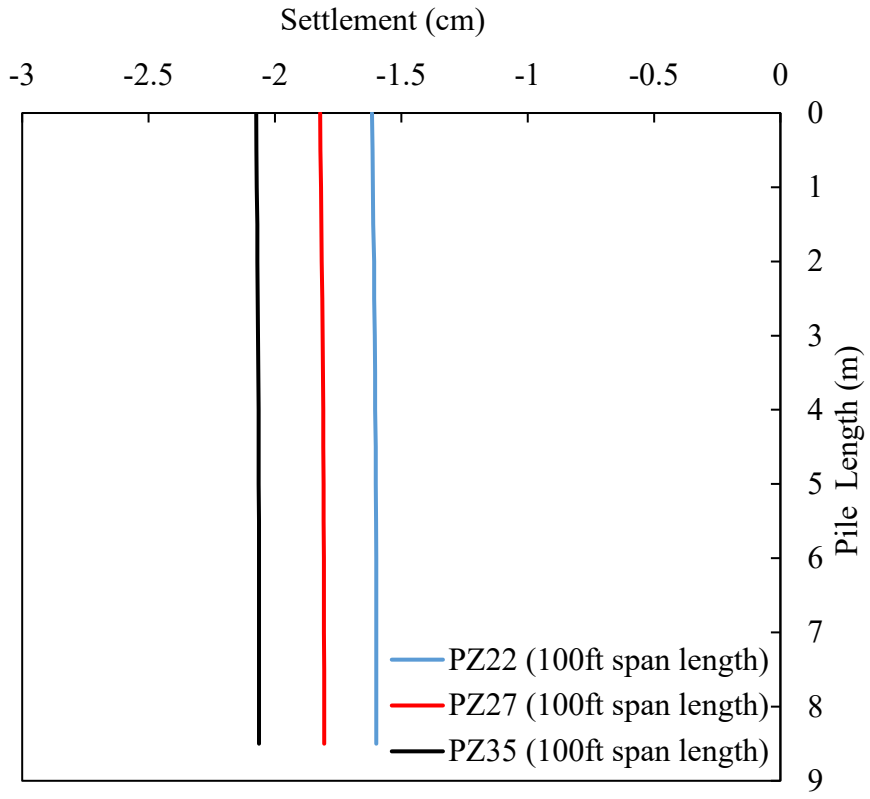

Figure 6.20 Parametric study Case 3: Vertical settlement of the sheet pile wall for different sheet pile sections (an extreme condition with a span length of 100 ft and excavation level of 8.2 ft (2.5 m)).

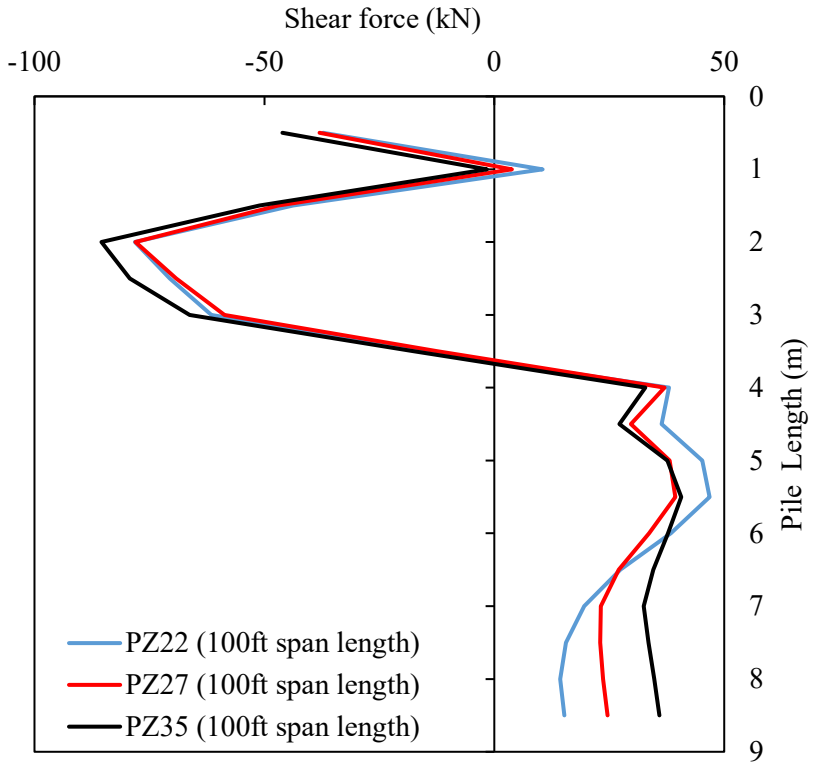

Figure 6.21 Parametric study Case 3: Shear force imposed on the sheet pile wall for different sheet pile sections (an extreme condition with a span length of 100 ft and excavation level of 8.2 ft (2.5 m)).

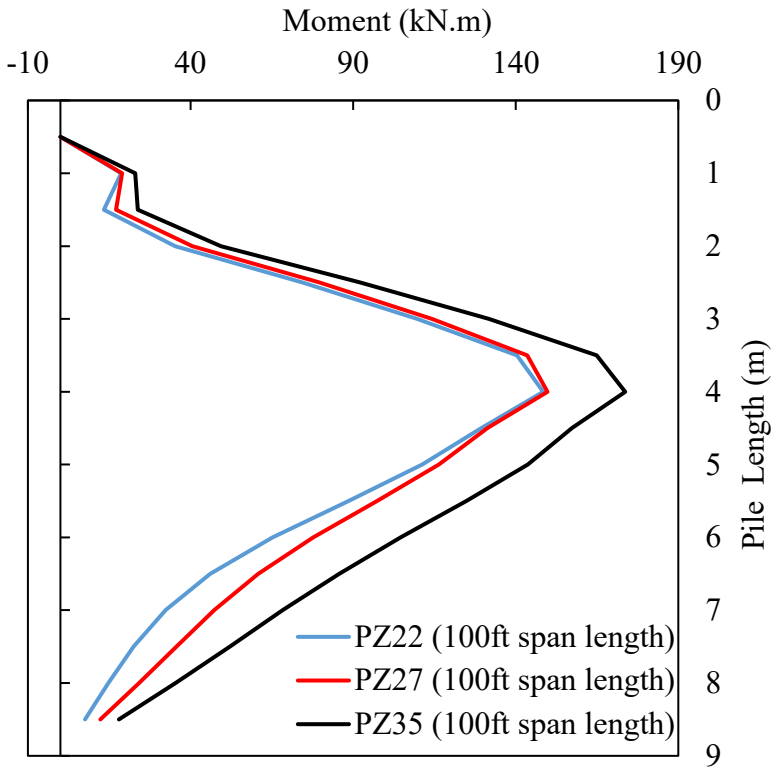

Figure 6.22 Parametric study Case 3: Bending moment imposed on the sheet pile wall for different sheet pile sections (an extreme condition with a span length of 100 ft and excavation level of 8.2 ft (2.5 m)).

6.5 Case 4

6.5.1 Parameters

For this case, the project team investigated the effect of different lengths of sheet piles (6.5 m, 8.5 m, 10.5 m; 21.3, 27.9, 34.4 ft) for a 60 ft span-length bridge. The sheet pile with a 6.5 m length had a tip in loose sand, while the sheet pile with an 8.5 m and 10.5 m length had a tip in dense sand (Figure 6.23). All other parameters, such as pile section, dead load, and excavation level, were the same as the actual design (Table 6.13).

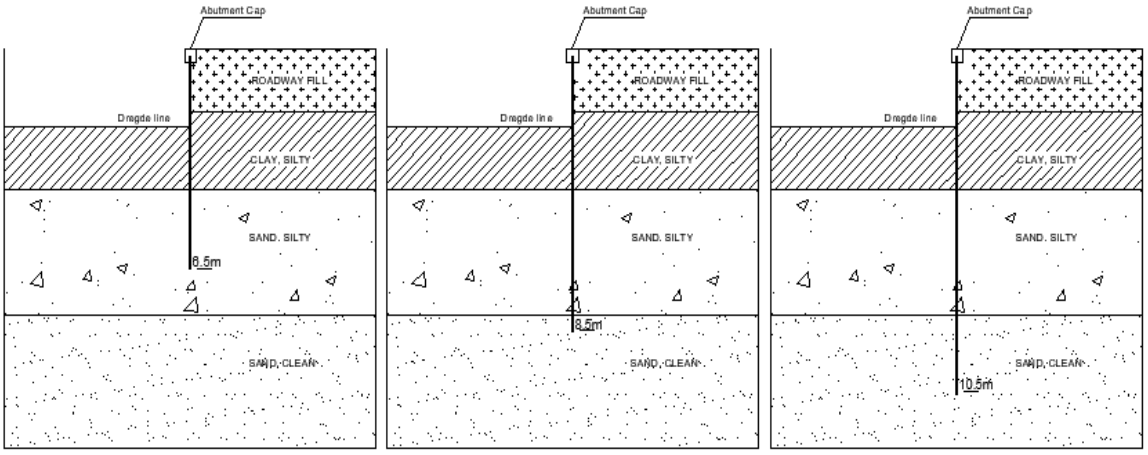

Figure 6.23 The summary of parametric study Case 4 with different pile lengths: 6.5 m, 8.5 m, and 10.5 m (21.3, 27.9, 34.4 ft).

Table 6.13 A summary of the simulations of the sheet pile abutment with different sheet pile lengths (Case 4).

Number of simulation	Span length	Dead load (kN/m)	Pile type	Excavation level (m)	**Pile length (m)**	
1	60 ft (18.8 m)	80	PZ22	1.5	6.5	
2	60 ft (18.8 m)	120	PZ22	1.5	8.5	Actual design
3	60 ft (18.8 m)	160	PZ22	1.5	10.5	

6.5.2 Results

It was observed that a shorter pile yielded larger horizontal deflection (Figure 6.24). In detail, a 6.5 m long pile showed a maximum horizontal deflection of 3.3 cm (1.3 inches), while a 10.5 m long pile showed a maximum horizontal deflection of 2 cm (0.79 inches) for a 60 ft span bridge. It could have been attributable to the more prominent P-Delta effect for the shorter length pile, associated with the worse end-bearing capacity of the loose soil.

In addition, a shorter pile exhibited a larger vertical settlement (Figure 6.25). The maximum settlement for the 6.5 m pile was 1.5 cm (0.59 inches), while the 8.5 m and 10.5 m piles settled only 0.27 cm (0.11 inches).

A shorter pile also experienced higher shear force and bending moment, compared to longer ones (Figures 6.26 and 6.27). But still, the safety factor of shear force and moment appeared sufficient, being FS_{shear} = 33.1 and FS_{bend} = 5.6 for the 6.5 m pile, respectively. All FS values are listed in Table 6.21.

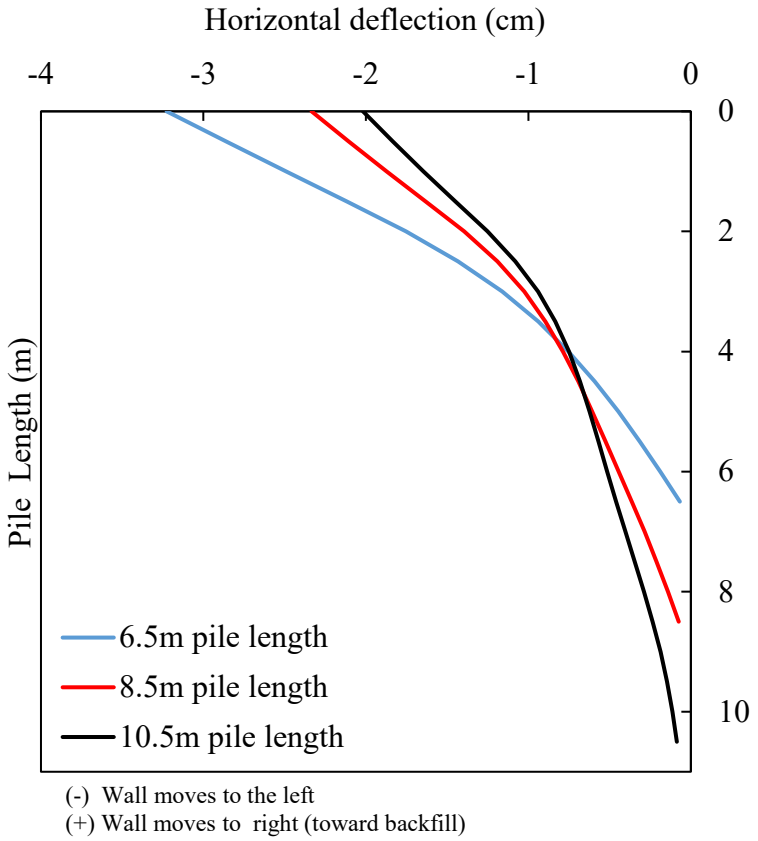

Figure 6.24 Parametric study Case 4: Horizontal deflection of the sheet pile wall for different pile lengths.

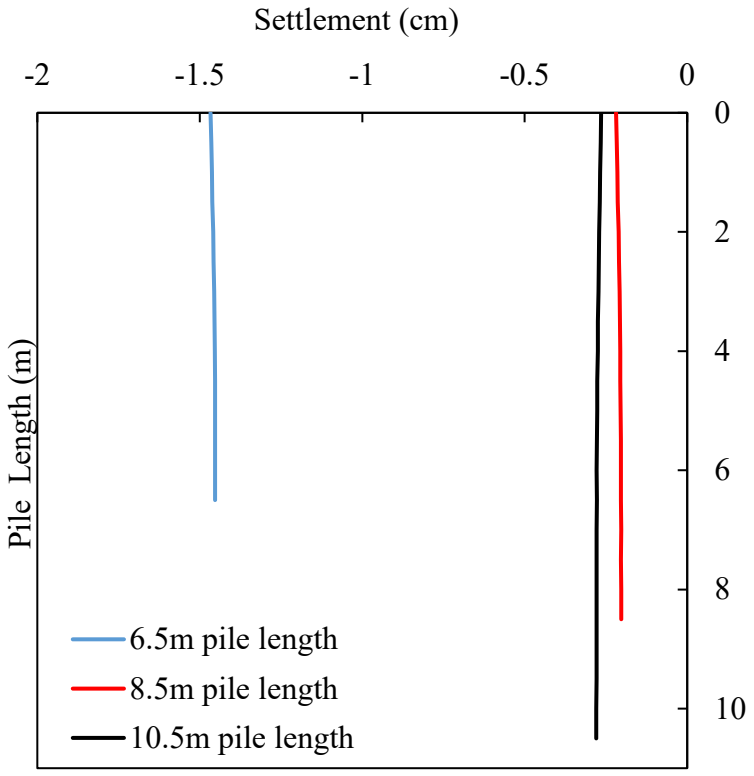

Figure 6.25 Parametric study Case 4: Vertical settlement of the sheet pile wall for different pile lengths.

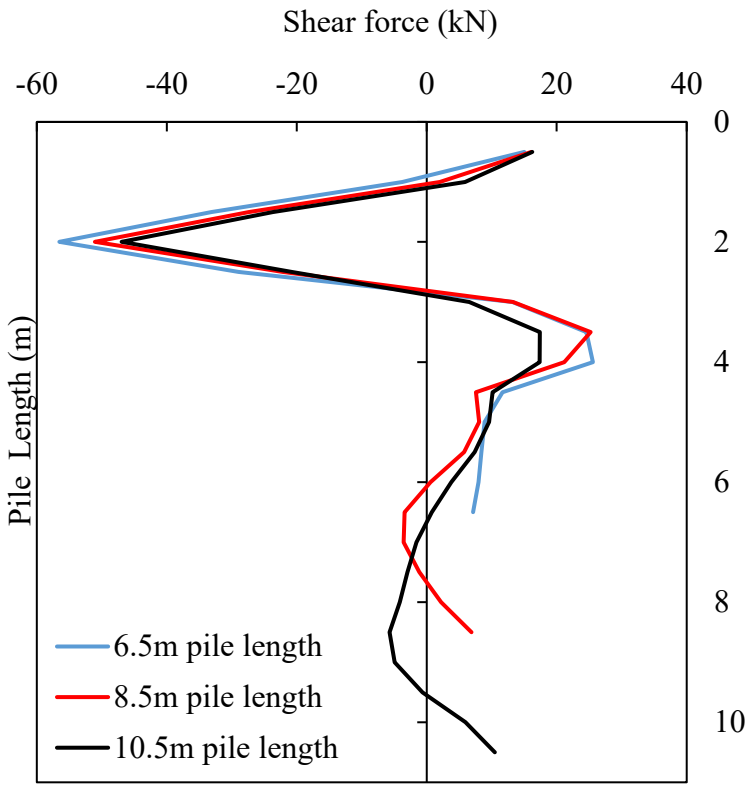

Figure 6.26 Parametric study Case 4: Shear force imposed on the sheet pile wall for different pile lengths.

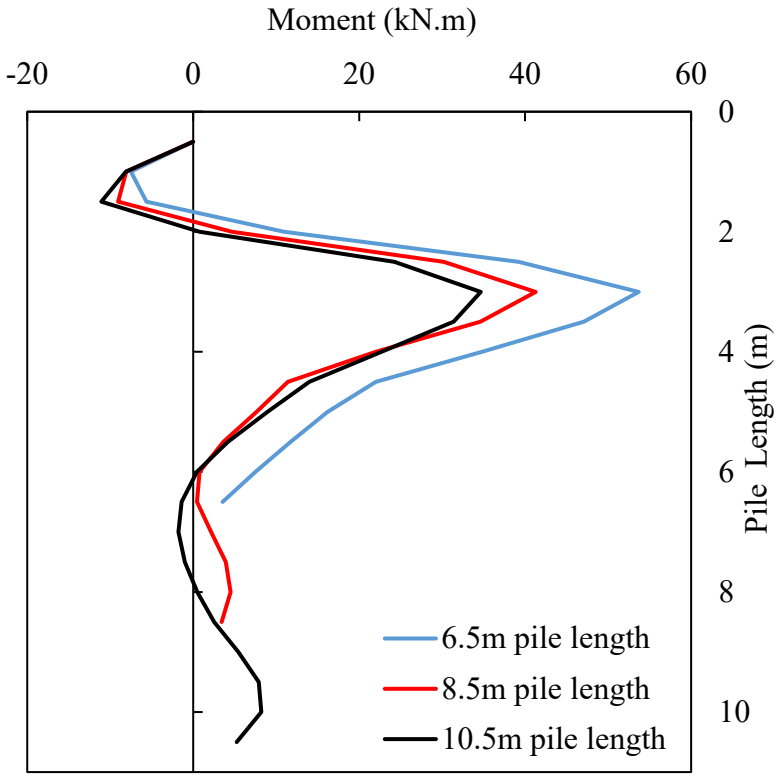

Figure 6.27 Parametric study Case 4: Bending moment imposed on the sheet pile wall for different pile lengths.

6.6 Case 5

6.6.1 Parameters

The anchor with Deadman concrete is an excellent solution to reduce deflection, shear force, and bending moment acting on sheet piles (Evans et al., 2011). The application of such an anchor and Deadman concrete method is examined in this parametric study Case 5 and Case 6. The Deadman concrete's size and the anchor's diameter are the same as the case from the preceding project by the research team in Iowa State (Evans et al., 2011). For Case 5, the spacing of anchors is fixed at 4.5 m, while the length of the anchor varies between 4 m (13.1 ft) and 8 m (26.2 ft) (Figure 6.28 and Table 6.14). Similar to Case 3, the project team selected two

conditions: a base condition with the original design (span length: 60 ft, excavation level: 4.9 ft (1.5 m)) and an extreme condition with a span length of 100 ft and excavation level of 8.2 ft (2.5 m), as summarized in Table 6.15.

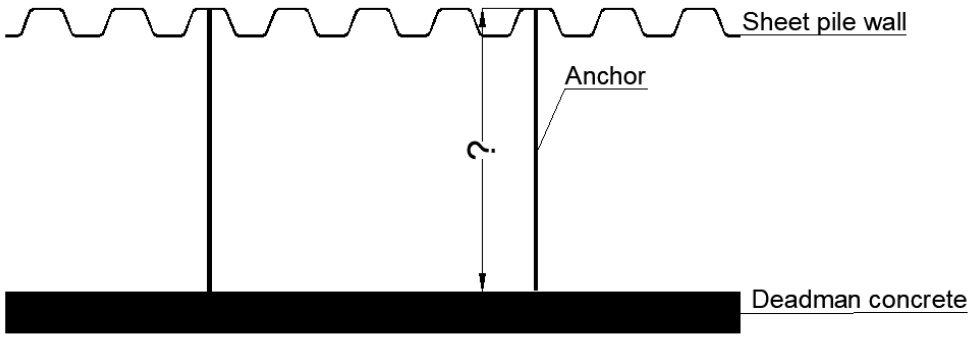

Figure 6.28 The summary of parametric study with hypothetical anchor and Deadman concrete: Case 5 with anchor lengths, 4 m (13.1 ft) or 8 m (26.2 ft). Note: the spacing is the same at 4.5 m (14.8 ft).

Table 6.14 Input parameters for the anchor-soil interface (from Itasca Consulting Group, 2019) for Case 5.

Soil and cable	
Shear stiffness, kbond (N/m/m)	1.50E10
Cohesive strength, sbond (Pa/m)	0
Elastic modulus, E (GPa)	98.6
Yield (N)	5.48E+05
Area (m^2)	5.00E-04
Shear friction (^{o})	20
Spacing (m)	4.5
Perimeter (m)-anchor length	4 m or 8 m

Table 6.15 A summary of the simulations of the sheet pile abutment and anchors with different anchor lengths (Case 5).

Number of simulation	Span length	Pile type	Excavation (m)	Anchors + Deadman concrete	
				Length (m)	Spacing (m)
1	60 ft (18.8 m)	PZ22	1.5	N/A	N/A
2	60 ft (18.8 m)	PZ22	1.5	4 m	4.5
3	60 ft (18.8 m)	PZ22	1.5	8 m	4.5
4	100 ft (30.5 m)	PZ22	2.5	N/A	N/A
5	100 ft (30.5 m)	PZ22	2.5	4 m	4.5
6	100 ft (30.5 m)	PZ22	2.5	8 m	4.5

6.6.2 Results

Figures 6.29 and 6.30 show the horizontal deflections of the sheet pile with the anchor and Deadman method, for the base and extreme conditions, respectively. For the base condition (a 60 ft span and 1.5 m excavation level), the anchor method did not show a significant reduction in the horizontal deflection because the lateral and axial loads were not big enough to activate the anchors and Deadman concrete's function (Figure 6.29). In detail, the sheet pile wall deflected by a maximum of 2.3 cm (0.91 inches) without the support, while its maximum deflection was about 2.1 cm (0.83 inches) when the 4 m and 8 m lengths of anchors with Deadman concrete were applied. On the other hand, for the extreme condition (a 100 ft span and 2.5 m excavation level), the anchor and Deadman concrete method was shown to reduce the maximum deflection of the sheet pile quite effectively (Figure 6.30). For example, the maximum horizontal deflection of the sheet pile was 10.7 cm (4.21 inches) without the support, while the 4 m and 8 m lengths of the anchors with Deadman concrete reduced the deflection of the sheet pile to 7.5 cm (2.95 inches) and 6.5 cm (2.56 inches), respectively.

Similarly, the shear force and bending moment imposed on the sheet pile wall was reduced significantly when the anchor and Deadman concrete method was applied, particularly for the extreme condition (100 ft span and 2.5 m excavation level; Figures 6.31 and 6.32). In detail, the factor of safety against shear failure (FS_{shear}) increased from 23.9 to 35.9. The factor of safety against bending failure (FS_{bend}) also increased from 2.0 to 3.6. All FS values are listed in Table 6.21.

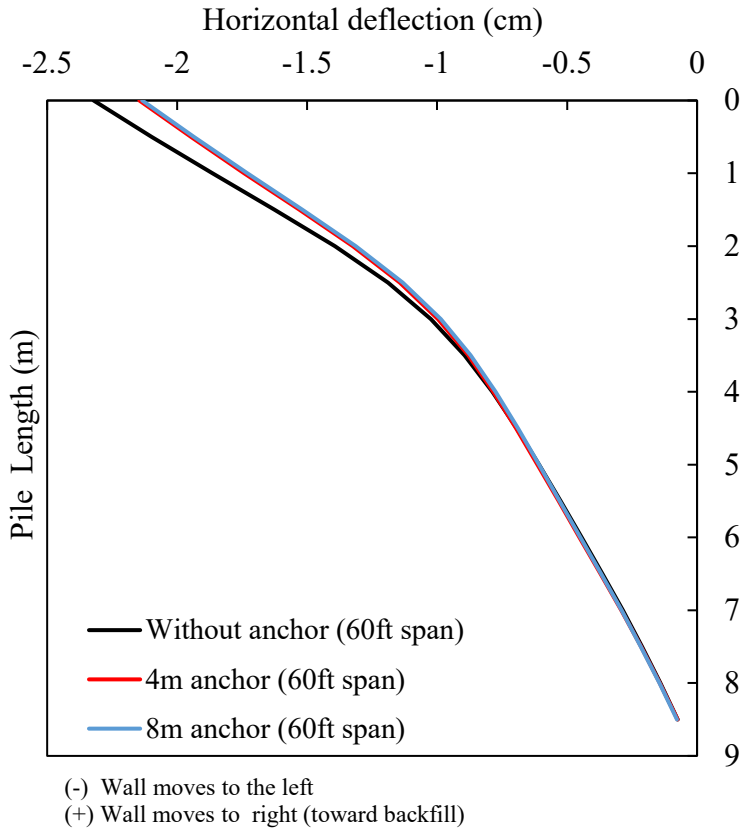

Figure 6.29 Parametric study Case 5: Horizontal deflection of the sheet pile wall for different anchor lengths (a base condition with a span length of 60 ft and excavation level of 4.9 ft (1.5 m)).

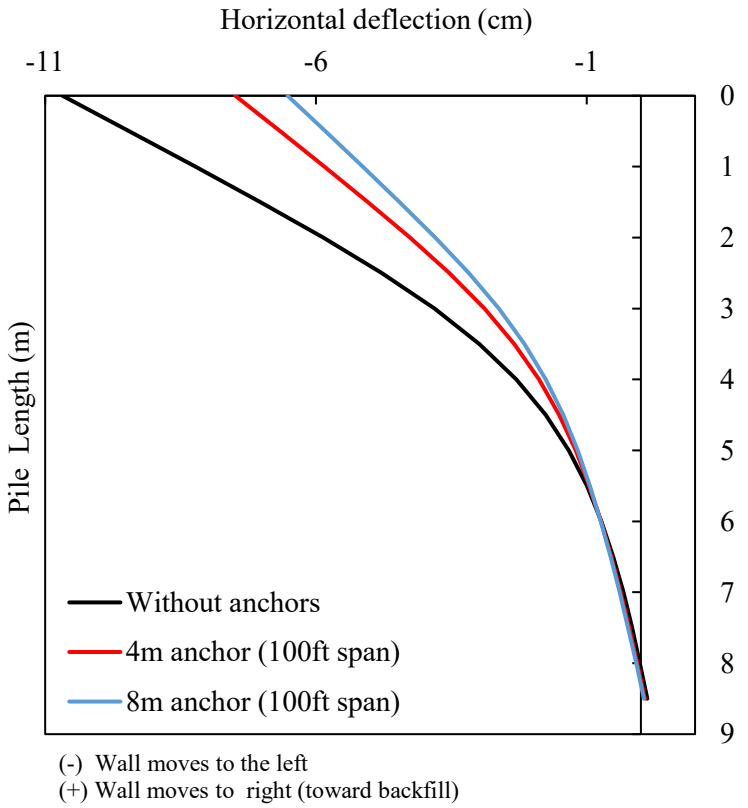

Figure 6.30 Parametric study Case 5: Horizontal deflection of the sheet pile wall for different anchor lengths (an extreme condition with a span length of 100 ft and excavation level of 8.2 ft (2.5 m)).

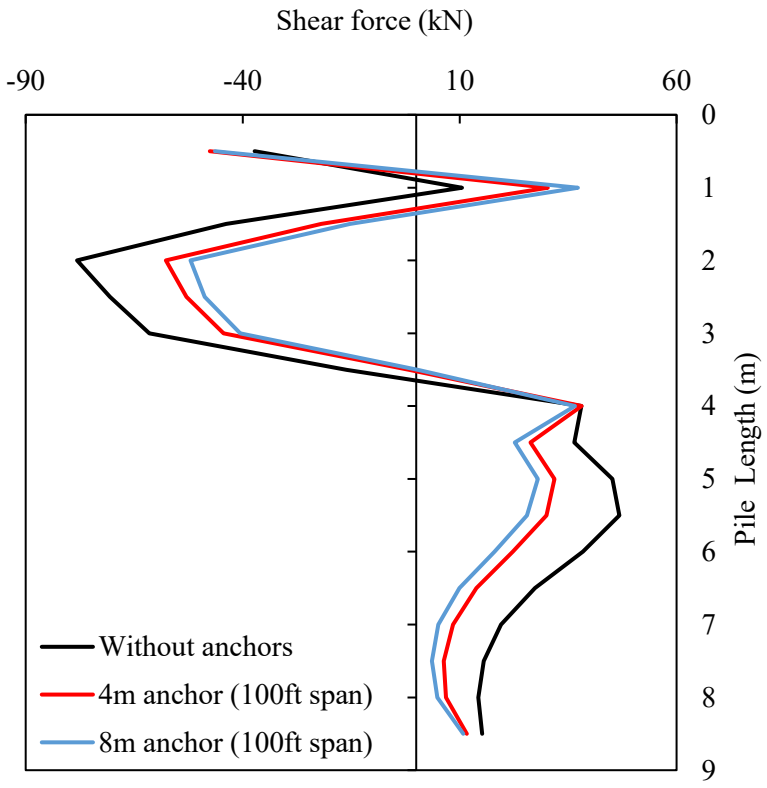

Figure 6.31 Parametric study Case 5: Shear force imposed on the sheet pile wall for different anchor lengths (an extreme condition with a span length of 100 ft and excavation level of 8.2 ft (2.5 m)).

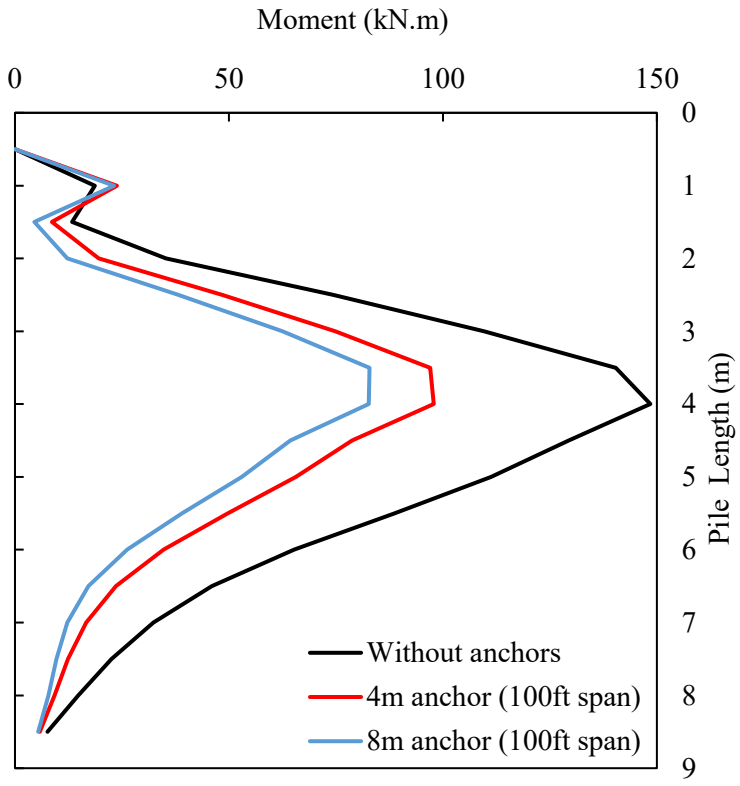

Figure 6.32 Parametric study Case 5: Bending moment imposed on the sheet pile wall for different anchor lengths (an extreme condition with a span length of 100 ft and excavation level of 8.2 ft (2.5 m)).

6.7 Case 6

6.7.1 Parameters

Case 6 was a parallel study to Case 5. For Case 6, the length of the anchors remained at 6 m, while the spacing between the anchors varied between 2 m (6.6 ft) and 6 m (19.7 ft) (Figure 6.33 and Table 6.16). Similar to Case 3, the project team selected two conditions: a base condition with the original design (span length: 60 ft, excavation level: 4.9 ft (1.5 m)) and an extreme condition with a span length of 100 ft and excavation level of 8.2 ft (2.5 m), as summarized in Table 6.17.

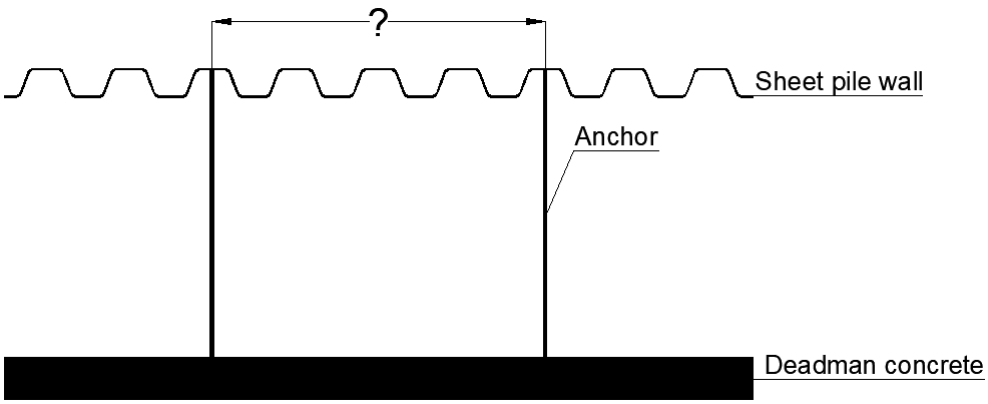

Figure 6.33 The summary of parametric study with hypothetical anchor and Deadman concrete: Case 6 with anchor spacings, 2 m (6.6 ft) or 6 m (19.7 ft). Note: the length is the anchor at 6 m (19.7 ft).

Table 6.16 Input parameters for the anchor-soil interface (from Itasca Consulting Group, 2019) for Case 6.

Soil and cable	
Shear stiffness kbond (N/m/m)	1.50E+10
Cohesive strength sbond (Pa/m)	0.00E+00
Elastic modulus E (GPa)	98.6
Yield (N)	5.48E+05
Area (m^2)	5.00E-04
Shear Friction (^{o})	30
Spacing (m)	2 m, 6 m
Perimeter (m)-anchor length	6 m

Table 6.17 A summary of the simulations of the sheet pile abutment and anchors with different anchor lengths (Case 6).

Number of simulation	Span length	Dead load (kN/m)	Pile type	Excavation (m)	Anchors + Deadman concrete	
					Length (m)	**Spacing (m)**
1	60 ft (12.2 m)	120	PZ22	1.5	N/A	N/A
2	60 ft (18.8 m)	120	PZ22	1.5	6 m	2
3	60 ft (24.4 m)	120	PZ22	1.5	6 m	6
4	100 ft (30.5 m)	200	PZ22	2.5	N/A	N/A
5	100 ft (30.5 m)	200	PZ22	2.5	6 m	2
6	100 ft (30.5 m)	200	PZ22	2.5	6 m	6

6.7.2 Results

Figure 6.34 and 6.35 show the horizontal deflections of the sheet pile with the anchor and Deadman method, for the base and extreme conditions, respectively. Similar to Case 5, for the base condition (60 ft span and 1.5 m excavation level), the anchor method did not show a significant reduction in the horizontal deflection because the lateral and axial loads were not big enough to activate the anchors and Deadman concrete's function (Figure 6.34). For the extreme condition (100 ft span and 2.5 m excavation level), the anchor and Deadman concrete method reduced the maximum deflection of the sheet pile quite effectively (Figure 6.35). In detail, the maximum horizontal deflection of the sheet pile was 10.7 cm (4.21 inches) without the support, while the 2 m and 6 m spacings of the anchors with Deadman concrete reduced the deflection of the sheet pile to 6.6 cm (2.6 inches) and 7.3 cm (2.87 inches), respectively.

Similarly, the shear force and bending moment imposed on the sheet pile wall was reduced significantly when the anchor and Deadman concrete method was applied, particularly for the extreme condition (100 ft span and 2.5 m excavation level; Figures 6.36 and 6.37). In detail, the factor of safety against shear failure (FS_{shear}) increased from 23.9 to 33 and 36.2 when

6 m and 2 m spacings of the anchors with Deadman concrete were applied. The factor of safety against bending failure (FS_{bend}) also increased from 2.0 to 3.2 and 3.7 when 6 m and 2 m spacings of the anchors with Deadman concrete were applied. All FS values are listed in Table 6.21.

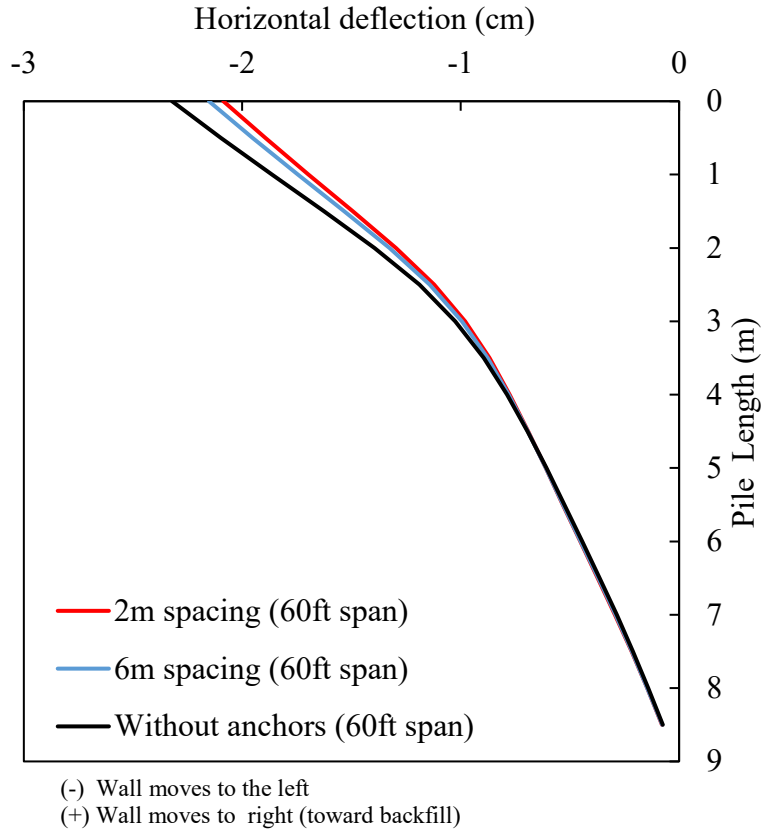

Figure 6.34 Parametric study Case 6: Horizontal deflection of the sheet pile wall for different anchor spacings (a base condition with a span length of 60 ft and excavation level of 4.9 ft (1.5 m)).

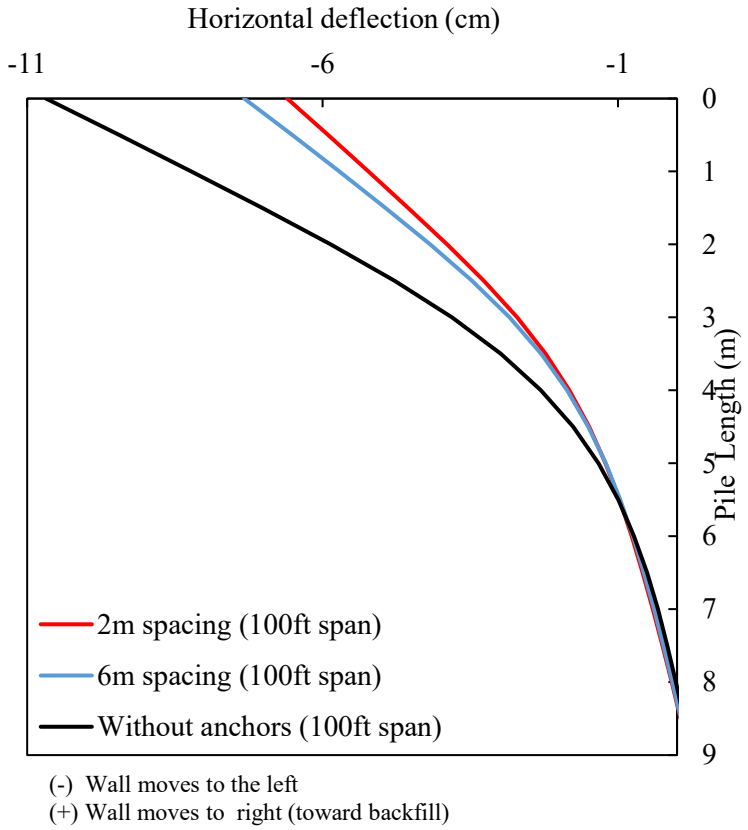

Figure 6.35 Parametric study Case 6: Horizontal deflection of the sheet pile wall for different anchor lengths (an extreme condition with a span length of 100 ft and excavation level of 8.2 ft (2.5 m)).

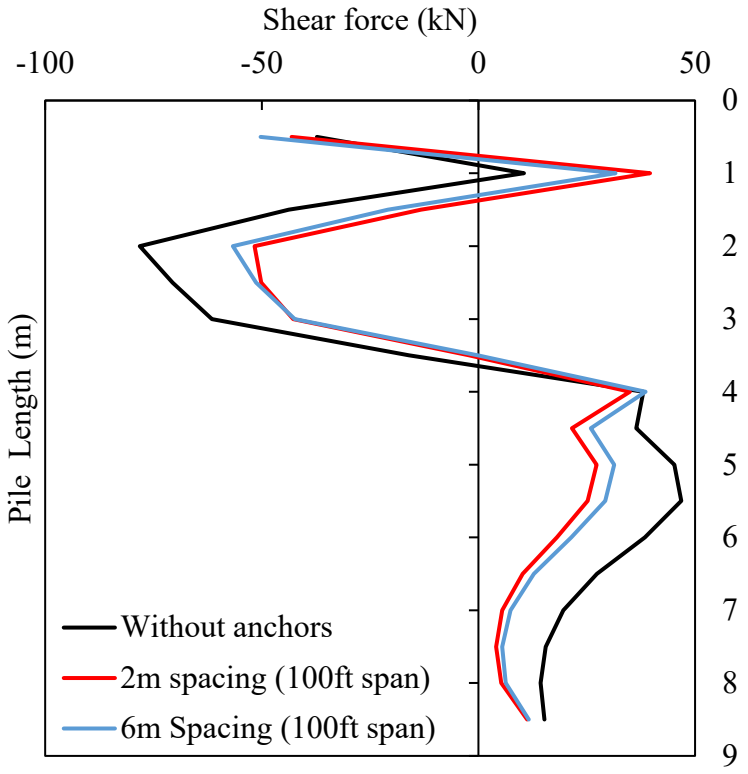

Figure 6.36 Parametric study Case 6: Shear force imposed on the sheet pile wall for different anchor lengths (an extreme condition with a span length of 100 ft and excavation level of 8.2 ft (2.5 m)).

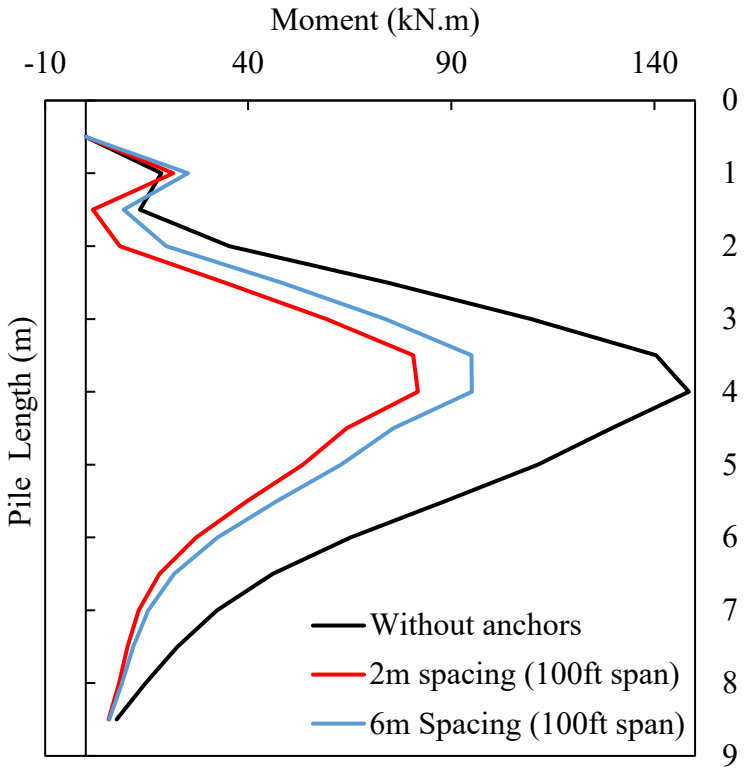

Figure 6.37 Parametric study Case 6: Bending moment imposed on the sheet pile wall for different anchor lengths (an extreme condition with a span length of 100 ft and excavation level of 8.2 ft (2.5 m)).

6.8 Case 7

6.8.1 Parameters

All simulations for the parametric study above were modeled with the water level at the dredge line. For Case 7, the project team examined the dry condition to compare the results with those from the submerged condition (water level at the dredge line). Similar to Case 3, the project team selected two conditions: a base condition with the original design (span length: 60 ft, excavation level: 4.9 ft (1.5 m)) and an extreme condition with a span length of 100 ft and excavation level of 8.2 ft (2.5 m), as summarized in Table 6.18.

Table 6.18 A summary of the simulations of the sheet pile abutment with dry or submerged conditions (Case 7).

Number of simulation	Span Length	Pile Type	Excavation (m)	**Water level (m)**	
1	60 ft (18.8 m)	PZ22	1.5	at dredge line	Actual design
2	60 ft (18.8 m)	PZ22	1.5	not considered	
3	100 ft (30.5 m)	PZ22	1.5	at dredge line	
4	100 ft (30.5 m)	PZ22	1.5	not considered	

6.8.2 Results

It was observed that the groundwater level (i.e., submerged *vs*. dry) did not meaningfully affect the maximum horizontal deflection of the sheet pile, as shown in Figure 6.38. For instance, the maximum deflection of the sheet pile for a hypothetical 100 ft span bridge was 5 cm (1.97 inches) and 4.8 cm (1.89 inches) for dry and submerged conditions, respectively. On the other hand, it was shown that the vertical settlement of the sheet pile increased with the submerged condition (Figure 6.39). The maximum vertical observed for the Case 7 study was 1.3 cm (0.51 inches) for a 100 ft span.

Noticeably, the shear force and moment acting on the sheet pile were higher in the dry condition due to the lack of pore pressure on the excavation side (Figures 6.40 and 6.41). For example, the factor of safety against shear failure was FS_{shear} = 23.7 in the submerged condition while it was FS_{shear} = 19.1 in the dry condition for a 100 ft span bridge. All FS values are listed in Table 6.21.

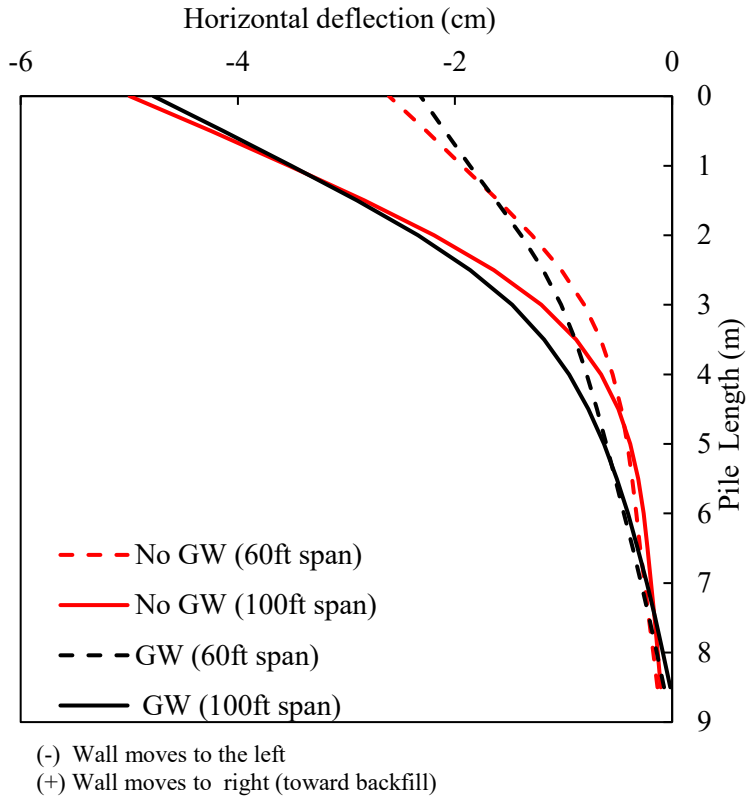

Figure 6.38 Parametric study Case 7: Horizontal deflection of the sheet pile wall with dry or submerged conditions.

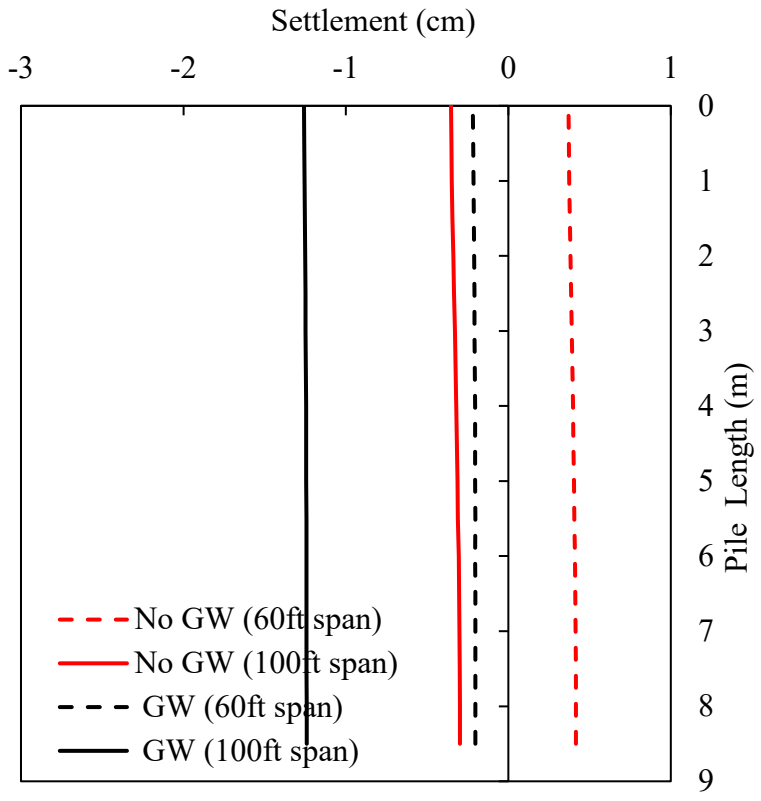

Figure 6.39 Parametric study Case 7: Vertical settlement of the sheet pile wall with dry or submerged conditions.

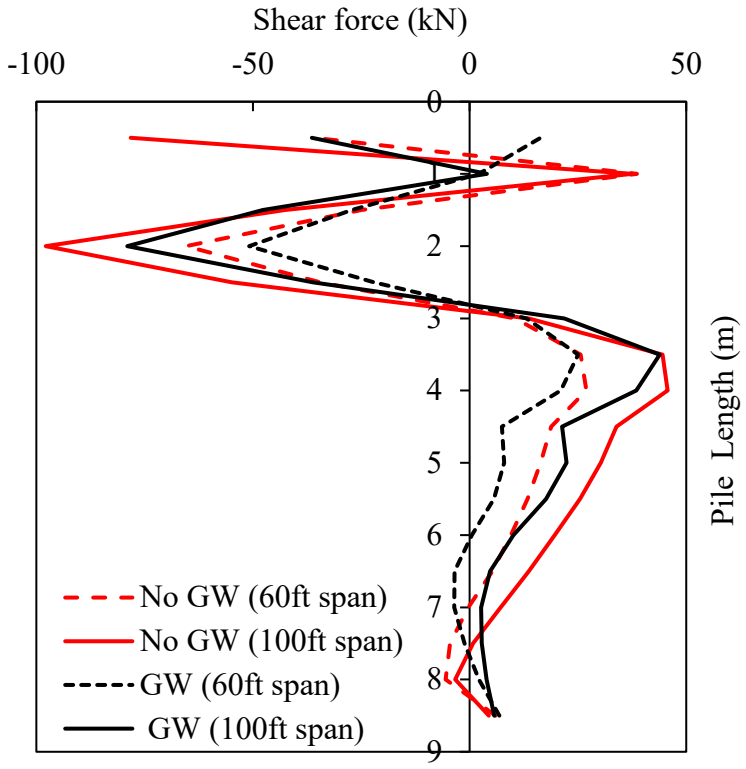

Figure 6.40 Parametric study Case 7: Shear force imposed on the sheet pile wall with dry or submerged conditions.

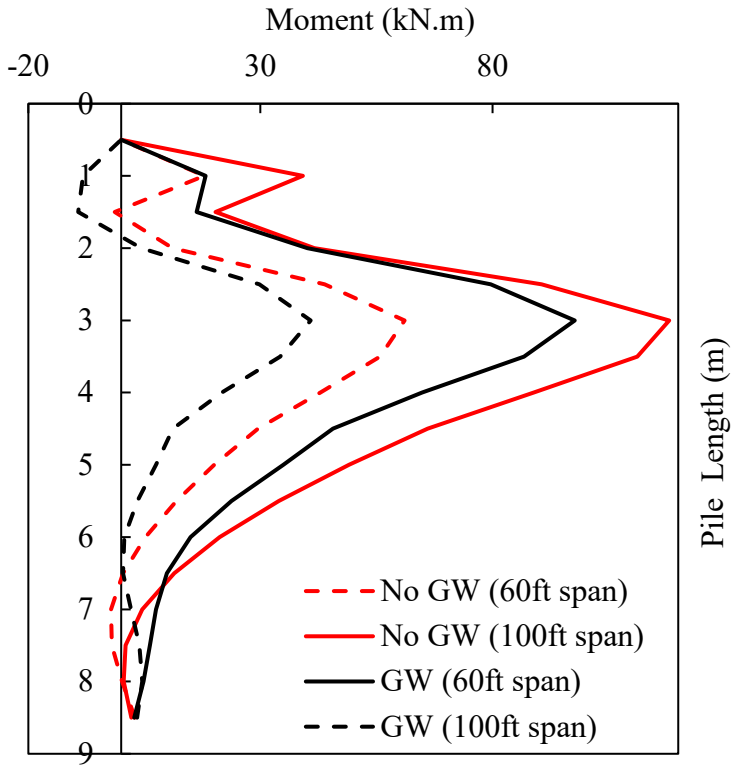

Figure 6.41 Parametric study Case 7: Bending moment imposed on the sheet pile wall with dry or submerged conditions.

6.9 Case 8

6.9.1 Parameters

For Case 8, the project team modelled the sheet pile sitting on the rock layer and compared the results with those from the original soil profile in which the sheet pile sat on sand (Figure 6.42). Similar to Case 3, the project team selected two conditions: a base condition with the original design (span length: 60 ft, excavation level: 4.9 ft (1.5 m)) and an extreme condition with a span length of 100 ft and excavation level of 8.2 ft (2.5 m), as summarized in Table 6.20.

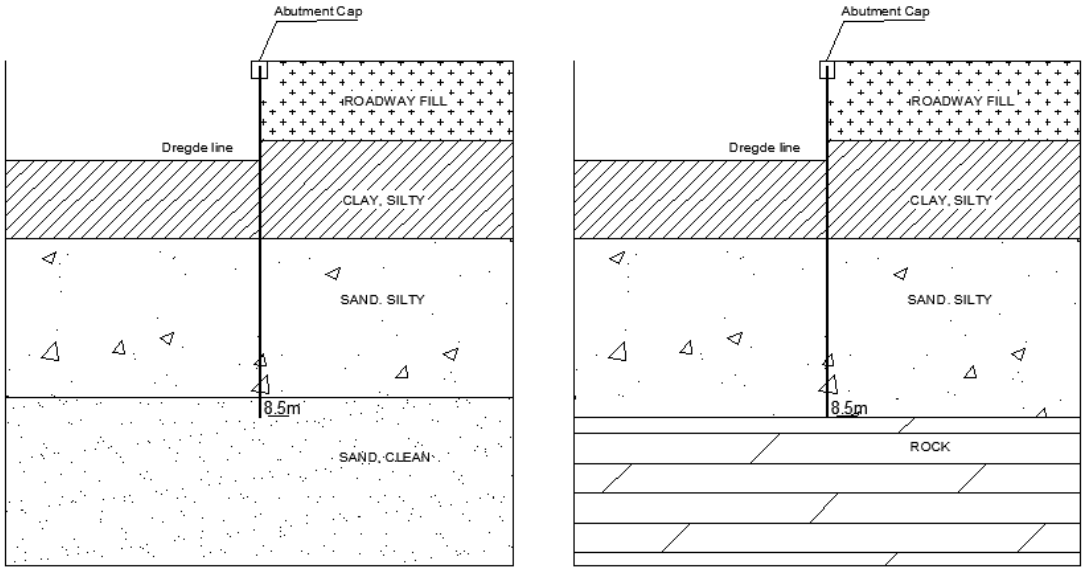

Figure 6.42 Case 8: Comparison of the end-bearing conditions on the sheet pile behavior.

Table 6.19 Input parameters of material properties for Case 8.

Material	Thickness	Unit weight (kN/m^3)	Friction angle (^{o})	c (kPa)	Bulk modulus (Pa)	Shear modulus (Pa)	Model
Roadway fill	2	20	30	0	9.60E6	4.60E6	Mohr - Coulomb
Silty clay	2.5	14.9	0	50	1.70E7	3.60E6	Mohr - Coulomb
Silty sand	4	17.85	30	0	6.70E6	3.10E6	Mohr - Coulomb
Rock	5	23	-	-	2.30E10	1.20E10	Elastic

Table 6.20 A summary of the simulations of the sheet pile abutment with end-bearing conditions (Case 8).

Number of simulation	Span length	Pile type	Excavation (m)	**Soil condition**	
1	60 ft (18.8 m)	PZ22	1.5	sand	Actual design
2	60 ft (18.8 m)	PZ22	1.5	rock	
3	100 ft (30.5 m)	PZ22	1.5	sand	
4	100 ft (30.5 m)	PZ22	1.5	rock	

6.9.2 Results

As expected, the vertical settlement of the sheet pile wall decreased when it sat on top of the rock layer (Figure 6.44). In contrast, the horizontal deflection of the sheet pile wall increased with the rock end-bearing condition (Figure 6.43). For example, for a 100 ft span-length, the maximum horizontal deflection of the sheet pile on the rock was 7.6 cm (2.99 inches), while the maximum horizontal deflection of the sheet pile on the sand was only 4 cm (1.57 inches). Similarly, for the 60 ft span-length, the maximum horizontal deflections of the sheet pile were 4.1 cm (1.61 inches) and 2.3 cm (0.91 inches) for the rock and sand end-bearing conditions, respectively. Overall, it was observed that the maximum horizontal deflection of the sheet pile on the sand was about 50% less than that on the rock condition. One possible explanation was that the horizontal deflection may have increased when the sheet pile sat on the rock layer because the rock layer would have allowed negligible vertical settlement of the sheet pile, and consequently, the firm end-bearing condition would have magnified the P-Delta effect when the sheet pile was subjected to the combined axial and lateral loads.

The shear force and bending moment imposed on the sheet pile also increased for the rock end-bearing condition, being consistent with the observation for the horizontal deflection. In detail, the factor of safety against bending failure for a 60 ft span length was FS_{bend} = 7.4 for sand and FS_{bend} = 3.9 for rock end-bearing conditions. The factor of safety for a 100 ft span length was FS_{bend} = 3.1 and FS_{bend} = 2.5, for soil and rock end-bearing conditions, respectively. All FS values are listed in Table 6.21.

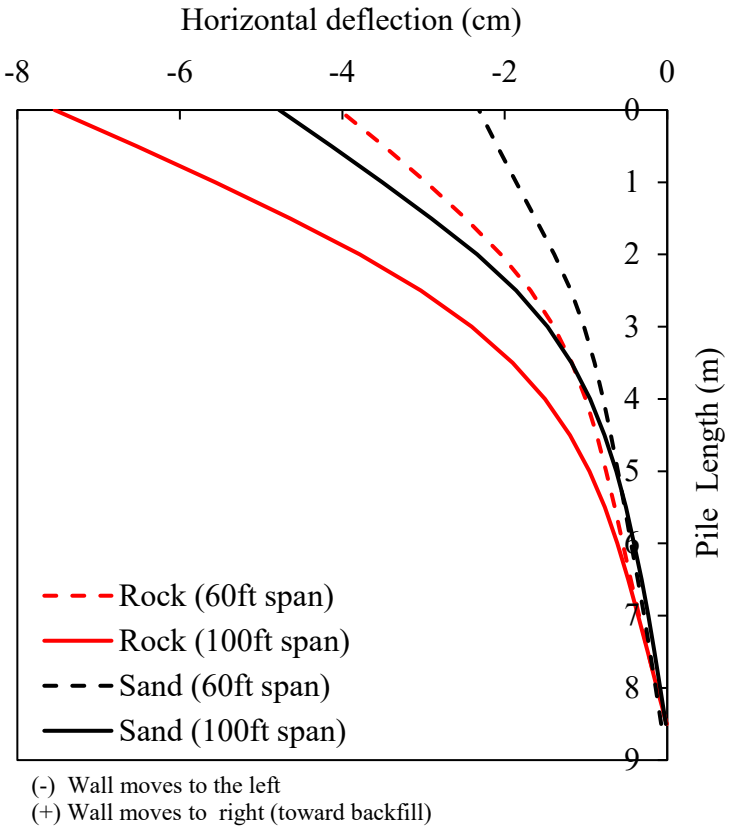

Figure 6.43 Parametric study Case 8: Horizontal deflection of the sheet pile wall for different end-bearing (soil *vs*. rock) conditions.

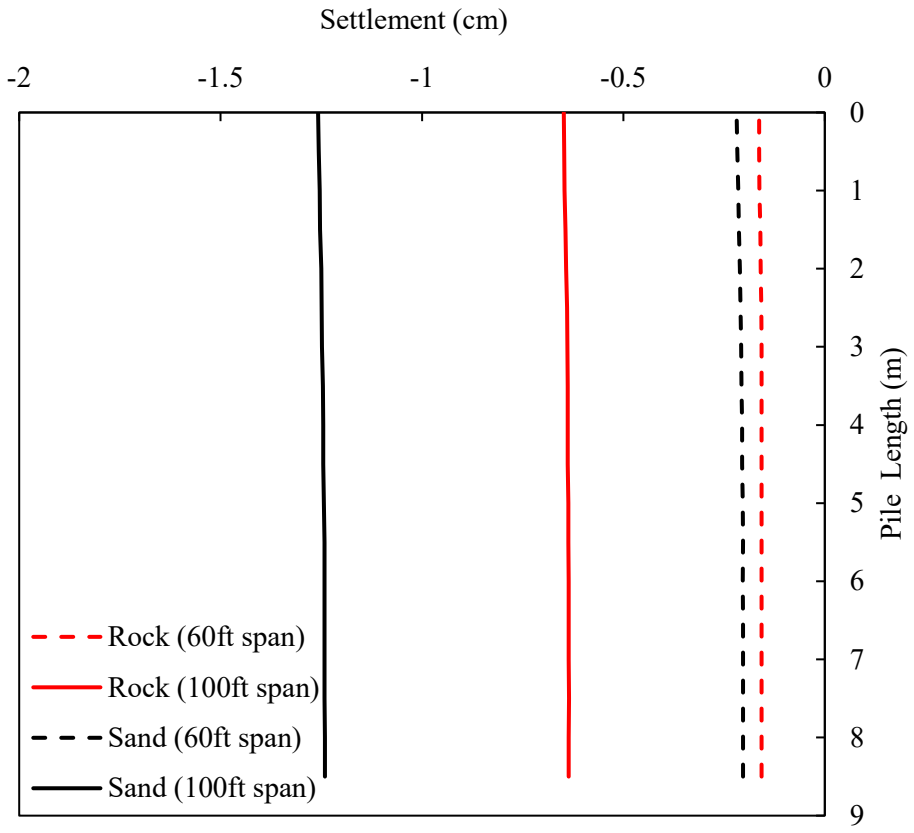

Figure 6.44 Parametric study Case 8: Vertical settlement of the sheet pile wall for different end-bearing (soil *vs*. rock) conditions.

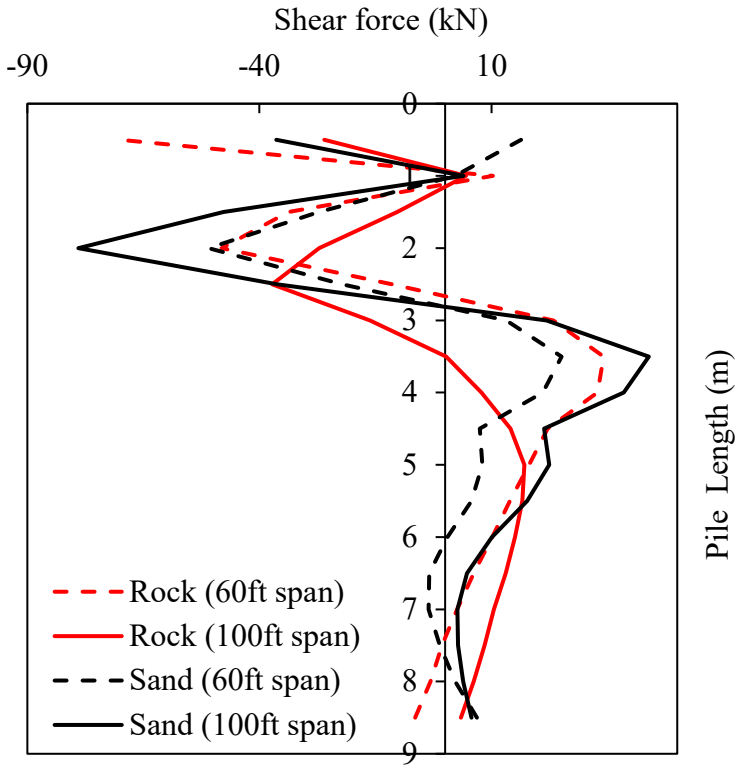

Figure 6.45 Parametric study Case 8: Shear force imposed on the sheet pile wall for different end-bearing (soil *vs*. rock) conditions.

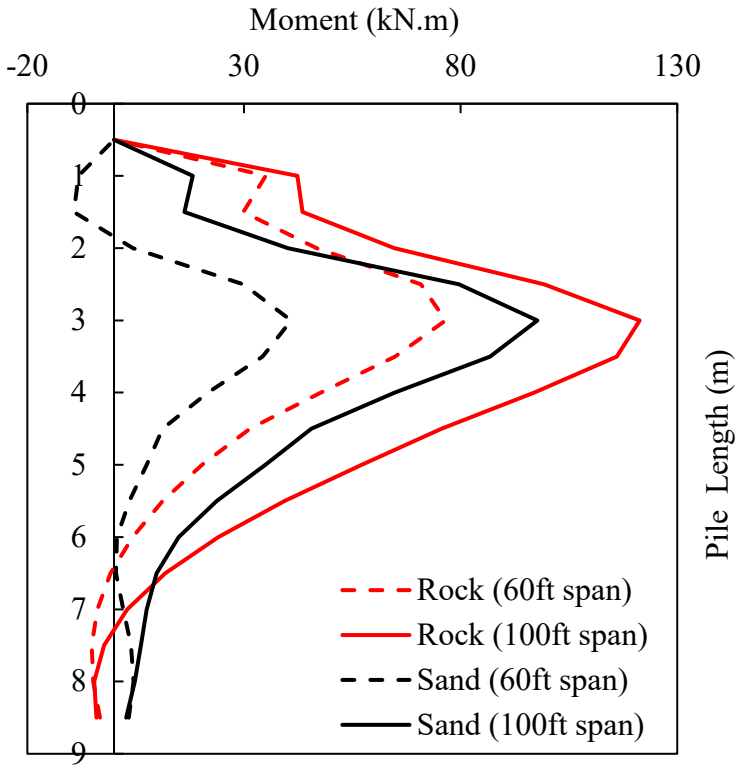

Figure 6.46 Parametric study Case 8: Bending moment imposed on the sheet pile wall for different end-bearing (soil *vs*. rock) conditions.

6.10 Case 9

6.10.1 Parameters

The type of bridge abutment system, that is either conventional or semi-integral bridge abutment, could significantly affect the horizontal load imposed on the sheet pile wall during seasonal temperature fluctuations. In this regard, the project team conducted additional modeling for the semi-integral bridge abutment case. Note that all the previous Cases 1-8 considered the traditional bridge abutment system in which seasonal temperature fluctuation and consequent thermal loading were neglected owing to the presence of an expansion joint. In contrast, if the superstructure and sheet pile wall was connected in a semi-integral way, additional thermal

loading may have been imposed on the sheet pile wall, as shown in Figure 6.47. In detail, thermal loading in the opposite direction of the lateral load from the backfill soil may develop in summer (that is, expansion cycle), while thermal loading may develop in the same direction as the lateral load from the backfill soil in winter (contraction cycle).

Similar to Case 3, the project team selected two conditions: a base condition with the original design (span length: 60 ft, excavation level: 4.9 ft (1.5 m)) and an extreme condition with a span length of 100 ft and excavation level of 8.2 ft (2.5 m). The thermally-induced displacement (ΔL; Figure 6.47) that can develop as a result of the seasonal thermal fluctuations was calculated as follows:

$$\Delta L = \alpha_L \Delta T \frac{L_{span}}{2} \tag{6.4}$$

where α_L is the coefficient of thermal expansion, ΔT is the temperature change between the summer and winter seasons, and L_{span} is the bridge span-length. With $\alpha_L = 5.5 \times 10^{-6}$ /°F for concrete and $\Delta T = 84$°F for the selected bridge site, the calculation resulted in $\Delta L = 4$ mm (0.16 inches) and $\Delta L = 7$ mm (0.28 inches) for 60 ft and 100 ft span length, respectively. Such thermally-induced displacement was applied to the top of the concrete cap in the numerical model, and thus, mimicked the expansion and contraction cycles throughout the seasons.

The project team also considered both configurations, a cantilever sheet pile wall and anchored sheet pile wall. The length and spacing of the anchors considered in the numerical models were 6 m (19.7 inches) and 4 m (13.1 inches), respectively. All material properties were the same as those for preceding Cases 1-8.

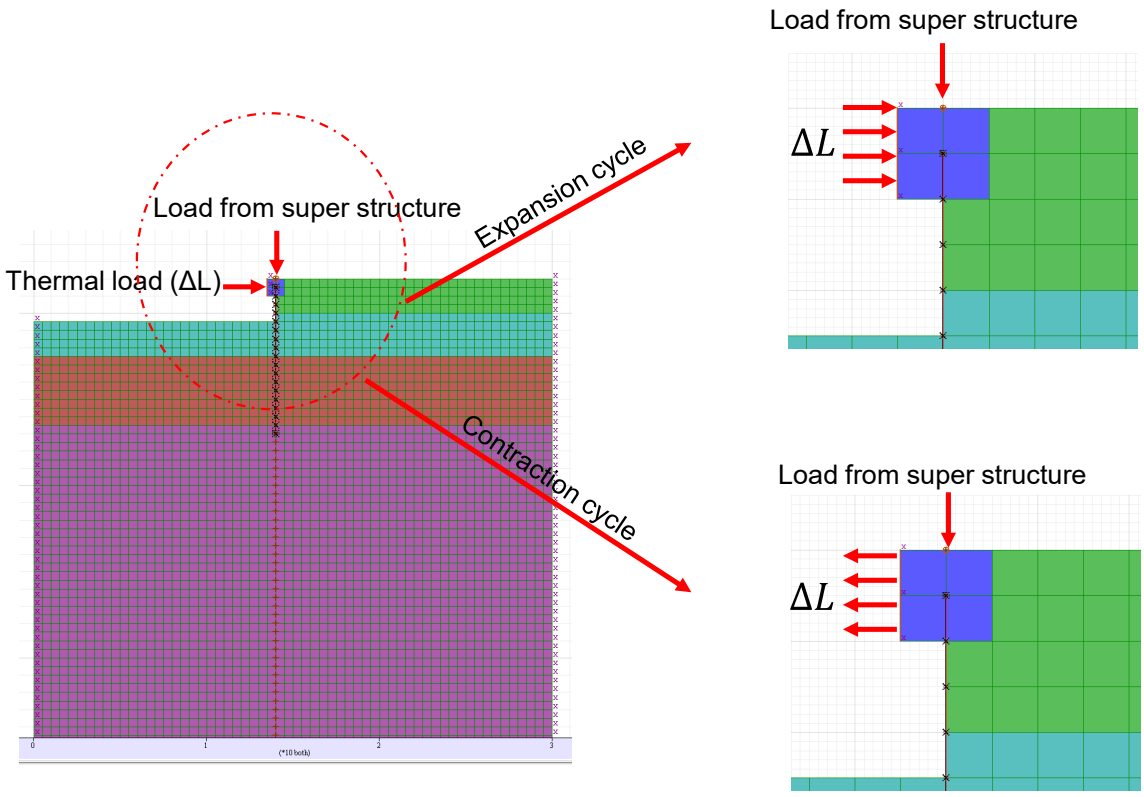

Figure 6.47 Case 9: Comparison of the abutment types (conventional *vs*. semi-integral) and consequent temperature effect.

6.10.2 Results

Thermally-induced expansion and contraction in the superstructure of a semi-integral abutment bridge were observed to affect the horizontal deflection of the sheet pile wall to some extent. For example, in the base condition with a 60 ft span, contraction of the superstructure in winter resulted in the maximum horizontal deflection of the sheet pile of about 0.2 inches larger than that of the conventional bridge. On the other hand, expansion of the superstructure in summer resulted in the maximum horizontal deflection of about 0.2 inches less than that of the conventional bridge. Besides, such an addition (or a deduction) in the maximum horizontal deflection due to the thermal loading decreased when the sheet pile wall was anchored (Figure 6.48). A similar trend was observed for the extreme condition with a 100 ft span (Figure 6.49).

Overall, the influence of thermal loading on the semi-integral abutment bridge during seasonal temperature fluctuations appeared to increase or reduce the maximum horizontal deflection of the sheet pile wall by ±0.2-0.3 inches for the bridge-span length investigated in this study (40 - 100 ft). Moreover, such an influence was lessened when the sheet pile wall was anchored. Lastly, the project team did not observe a significant change in the shear force and bending moment imposed on the sheet pile wall when the thermally-induced displacement was applied to the model, as shown in Figures 6.50 to 6.53. Therefore, the factor of safety values against the shear and bending failures were not expected to change dramatically for a semi-integral abutment bridge.

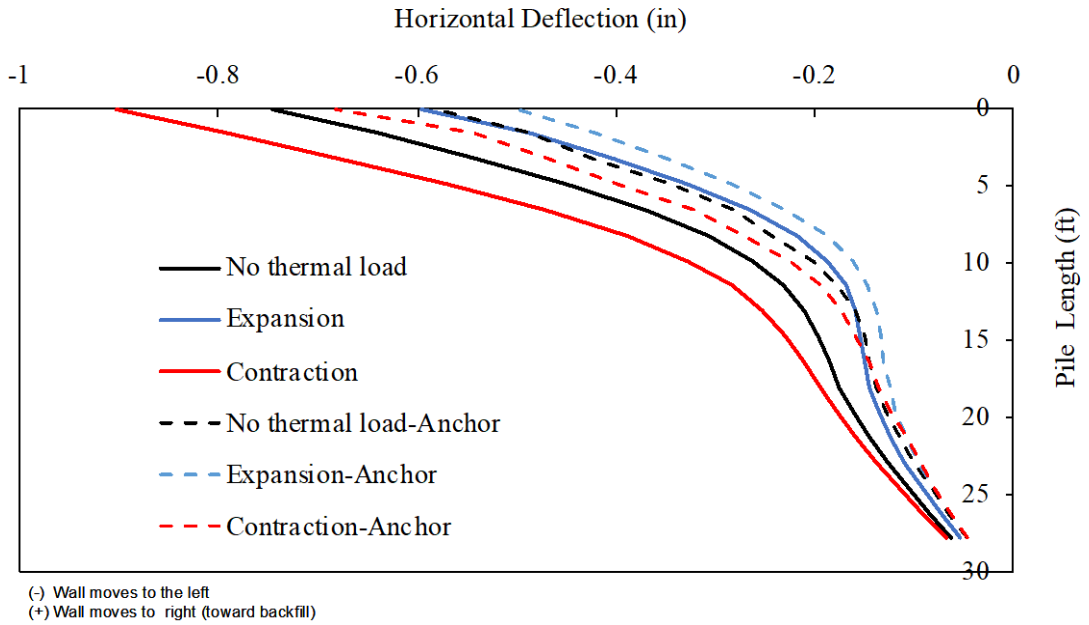

Figure 6.48 Parametric study Case 9: Horizontal deflection of the sheet pile wall for different abutment types (conventional *vs*. semi-integral) and consequent temperature effect (a base condition with a span length of 60 ft and excavation level of 4.9 ft (1.5 m)).

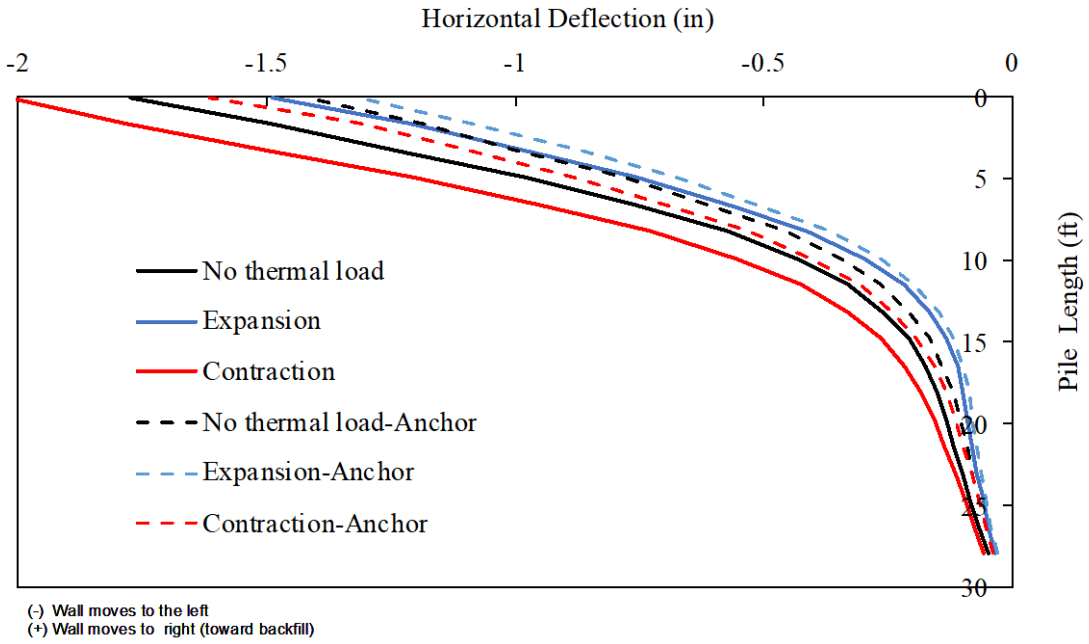

Figure 6.49 Parametric study Case 9: Horizontal settlement of the sheet pile wall for different abutment types (conventional *vs*. semi-integral) and consequent temperature effect (an extreme condition with a span length of 100 ft and excavation level of 8.2 ft (2.5 m)).

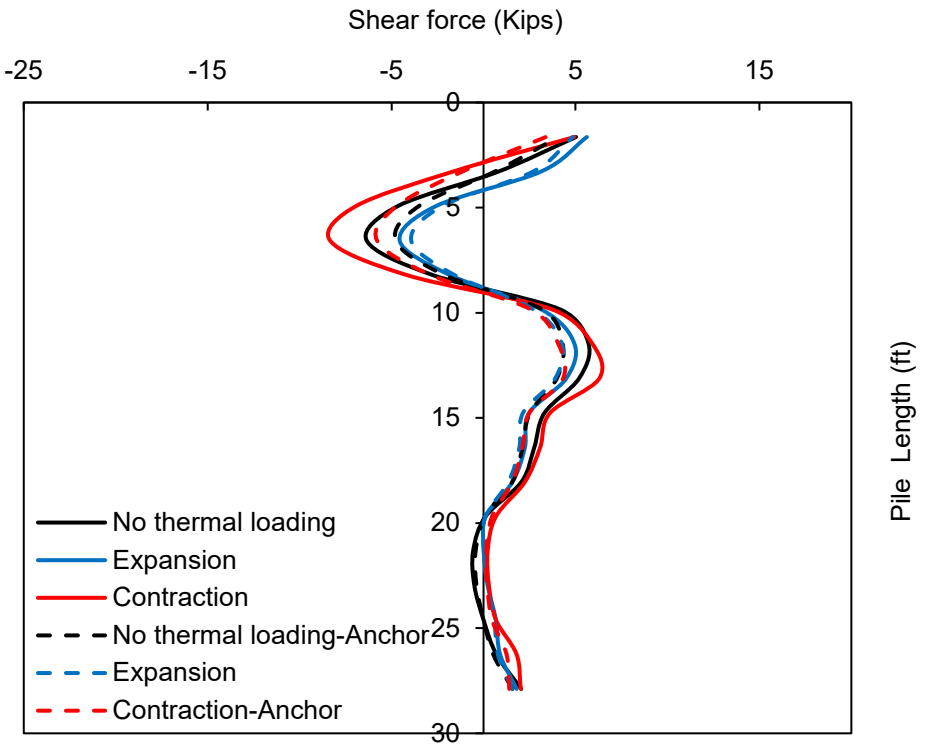

Figure 6.50 Parametric study Case 9: Shear force imposed on the sheet pile wall for different abutment types (conventional *vs*. semi-integral) and consequent temperature effect (a base condition with a span length of 60 ft and excavation level of 4.9 ft (1.5 m)).

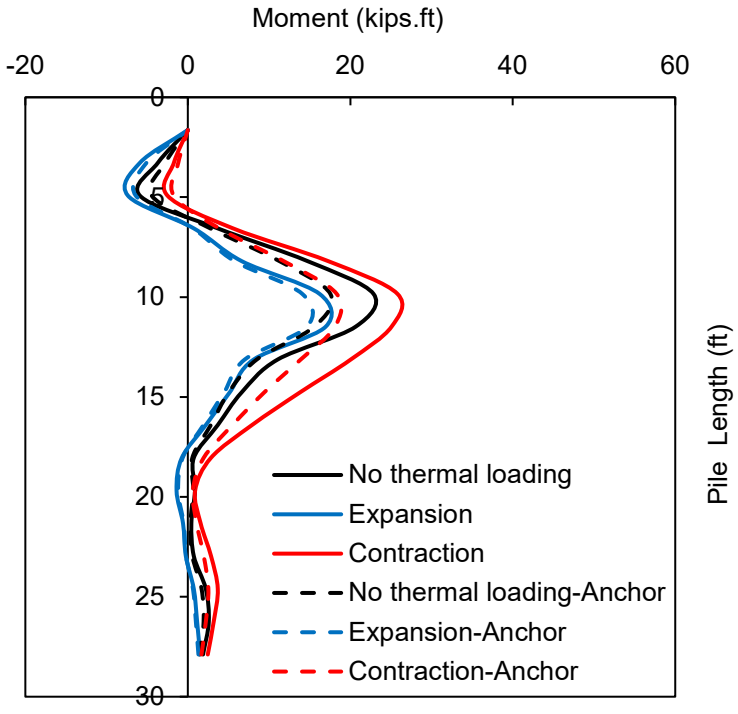

Figure 6.51 Parametric study Case 9: Bending moment imposed on the sheet pile wall for different abutment types (conventional *vs*. semi-integral) and consequent temperature effect (a base condition with a span length of 60 ft and excavation level of 4.9 ft (1.5 m)).

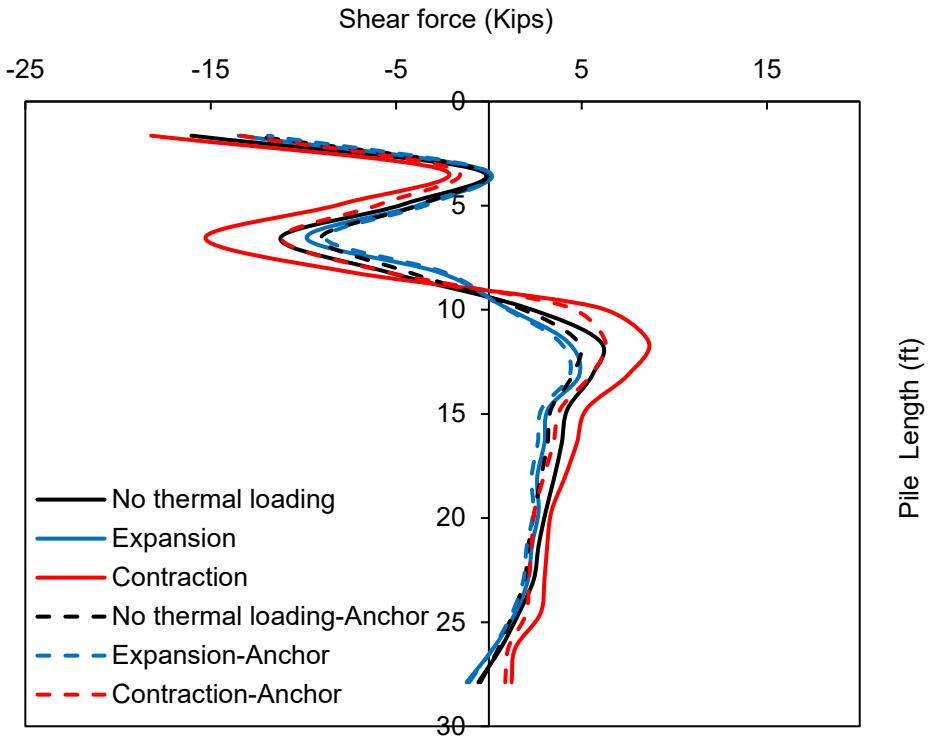

Figure 6.52 Parametric study Case 9: Shear force imposed on the sheet pile wall for different abutment types (conventional *vs*. semi-integral) and consequent temperature effect (an extreme condition with a span length of 100 ft and excavation level of 8.2 ft (2.5 m)).

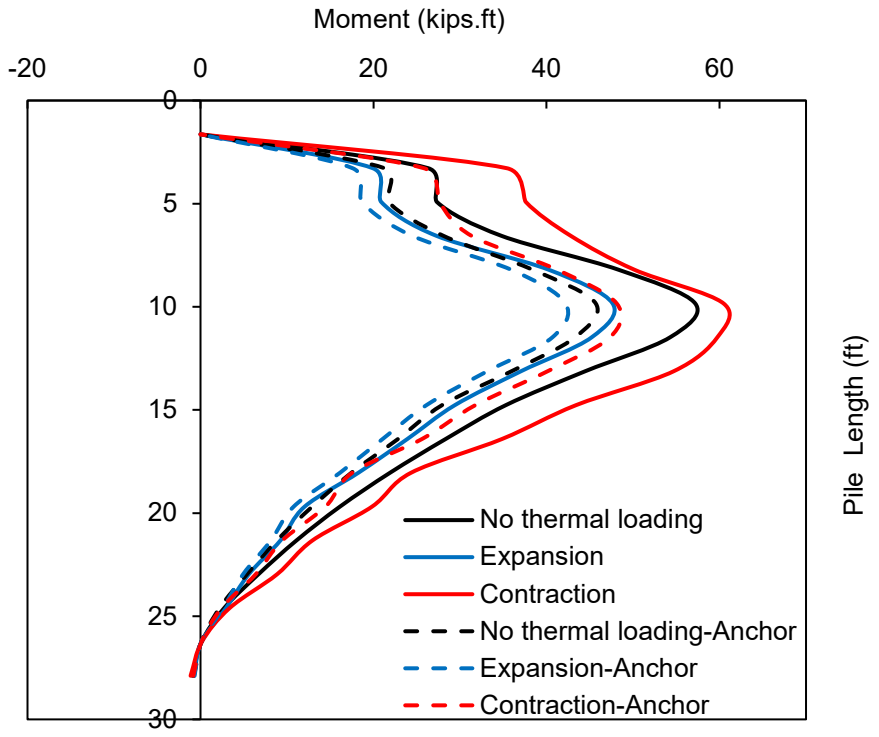

Figure 6.53 Parametric study Case 9: Bending moment imposed on the sheet pile wall for different abutment types (conventional *vs*. semi-integral) and consequent temperature effect (an extreme condition with a span length of 100 ft and excavation level of 8.2 ft (2.5 m)).

6.11 Summary

A summary of parametric numerical study results, including the maximum horizontal deflection, maximum vertical settlement, the factor of safety against shear failure, and the factor of safety against bending failure is presented in Table 6.21. For the selected bridge site and hypothetical treatment of the sheet pile abutment system, salient observations were as follows:

- The cantilever sheet pile wall could have sustained the combined axial and lateral loading with maximum horizontal deflection of less than 1 inch for the bridge span lengths up to 60 feet and excavation levels up to 1.5 m (~5 ft). With the anchored wall, the sheet pile abutment system could have sustained the combined loads even beyond the 60 ft span

length at the reasonable maximum horizontal deflection (1-2 inches). Note that this observation is valid for the selected bridge site and soil condition.

- For all considered case studies in this project, the vertical settlement of the sheet pile abutment system was less than 1 inch.
- For all considered case studies in this project, the factor of safety values against the shear and bending failures were greater than 2.0. Therefore, the serviceability of the sheet pile abutment system, such as horizontal deflection and vertical settlement, was a primary design factor rather than the mechanical integrity of the sheet pile wall.
- Increasing the section modulus (for example, PZ22 → PZ27 → PZ35) could have helped to reduce the horizontal deflection of the sheet pile wall, at the expense of a slight increase in the vertical settlement.
- Increasing the pile length could have helped to reduce both the horizontal deflection and vertical settlement of the sheet pile abutment.
- For the anchored wall configuration, the length and spacing of anchors needed to be carefully designed to ensure that the maximum horizontal deflection of the sheet pile wall did not exceed a predetermined limit.
- Fluctuation of the water level (e.g., submerged *vs*. dry conditions in this study) may have led to substantial differences in the shear force and bending moment imposed on the sheet pile wall, while its impact on the horizontal deflection and vertical settlement of the sheet pile was trivial.
- End-bearing of the sheet pile on the rock may have helped to reduce the vertical settlement of the sheet pile abutment system. However, the maximum horizontal deflection increased up to 50%, compared to the soil end-bearing condition. One possible

mechanism was that the firmer end-bearing condition may have magnified the P-Delta effect when the sheet pile was subjected to the combined axial and lateral loading.

- The influence of thermal loading in the case of the semi-integral abutment bridge during seasonal temperature fluctuations may have increased or decreased the maximum horizontal deflection of the sheet pile wall by ±0.2-0.3 inches for a bridge-span length of 40 - 100 ft. Such an influence could have been lessened when the sheet pile wall was anchored. On the other hand, the factor of safety against shear and bending failures was not significantly affected by the bridge abutment design (that is, conventional *vs*. semi-integral abutment).

The method to estimate the factor of safety against shear and bending failures is described here.

The shear strength (V_r) of a sheet pile was determined following the limit state design:

$$V_r = 0.66\phi F_y A_g \tag{6.5}$$

where ϕ is the resistance Factors ($\phi = 0.9$ in this analysis), F_y is the yield strength of the sheet pile ($F_y = 3.45 \times 10^5\ kPa$ for steel grade 50), and A_g is the cross-sectional area of the sheet pile. The maximum shear force imposed on the sheet pile wall, V_f, was obtained from the numerical simulation. With that, the factor of safety against shear failure, FS_{shear}, was evaluated as follows:

$$FS_{shear} = \frac{V_r}{V_f} \tag{6.6}$$

The bending resistance (Mr) of a sheet pile was determined following the limit state design:

$$M_r = \phi Z F_y \tag{6.7}$$

where Z is the section modulus (m^3/m) of the sheet pile. The maximum bending moment imposed on the sheet pile wall, M_f, was obtained from the numerical simulation. With that, the factor of safety against bending failure, FS_{bend}, was evaluated as follows:

$$FS_{bend} = \frac{M_r}{M_f} \tag{6.8}$$

Table 6.21 The summary of parametric case study results in this project.

Case	Number of simulation	Span length	Dead load (kN/m)	Pile length (m)	Pile type	Excavation level (m)	Anchor and Deadman method		Maximum horizontal deflection (cm)	Maximum vertical settlement (cm)	FS: Shear failure	FS: Bending failure
							length (m)	Spacing (m)				
1	1	40ft (12.2m)	80	8.5	PZ 22	1.5	N/A		1.83	-0.36	60.8	10.8
	2	60ft (18.8m)	120	8.5	PZ 22	1.5	N/A		2.32	0.20	55.1	7.4
	3	80ft (24.4m)	160	8.5	PZ 22	1.5	N/A		3.31	0.69	44.8	4.6
	4	100ft (30.5m)	200	8.5	PZ 22	1.5	N/A		4.78	1.26	35.5	3.1
2	1	60ft (18.8m)	120	8.5	PZ 22	0.5	N/A		1.10	0.17	169.0	17.5
	2	60ft (18.8m)	120	8.5	PZ 22	1.5	N/A		2.20	0.46	61.7	8.2
	3	60ft (18.8m)	120	8.5	PZ 22	2.5	N/A		4.92	0.49	57.6	4.6
3	1	60ft (18.8m)	120	8.5	PZ22	1.5	N/A		2.30	0.20	55.0	7.4
	2	60ft (18.8m)	120	8.5	PZ27	1.5	N/A		2.20	0.27	62.5	9.4
	3	60ft (18.8m)	120	8.5	PZ35	1.5	N/A		2.10	0.27	77.6	13.2
	4	100ft (30.5m)	200	8.5	PZ22	2.5	N/A		10.70	1.60	36.0	2.0
	5	100ft (30.5m)	200	8.5	PZ27	2.5	N/A		7.40	1.82	44.1	3.4
	6	100ft (30.5m)	200	8.5	PZ35	2.5	N/A		6.50	2.10	53.0	4.7
4	1	60ft (18.8m)	80	6.5	PZ 22	1.5	N/A		3.23	1.47	49.7	5.6
	2	60ft (18.8m)	120	8.5	PZ 22	1.5	N/A		2.30	0.22	54.9	7.3
	3	60ft (18.8m)	160	10.5	PZ 22	1.5	N/A		2.01	0.28	59.7	8.7

Y: considering water level,
N: Not considering water level,
FS: factor of safety

Case	Number of simulation	Span length	Dead load (kN/m)	Pile length (m)	Pile type	Excavation level (m)	Anchor and Deadman method		Maximum horizontal deflection (cm)	Maximum vertical settlement (cm)	FS: Shear failure	FS: Bending failure
							length (m)	spacing (m)				
5	1	60ft (18.8m)	120	8.5	PZ 22	1.5	N/A		2.30	N/A	56.0	7.5
	2	60ft (18.8m)	120	8.5	PZ 22	1.5	4.5	4m	2.20	N/A	59.6	8.3
	3	60ft (18.8m)	120	8.5	PZ 22	1.5	4.5	8m	2.10	N/A	59.6	8.3
	4	100ft (30.5m)	200	8.5	PZ 22	2.5	N/A		10.70	N/A	35.9	2.0
	5	100ft (30.5m)	200	8.5	PZ 22	2.5	4.5	4m	7.50	N/A	48.6	3.1
	6	100ft (30.5m)	200	8.5	PZ 22	2.5	4.5	8m	6.50	N/A	53.8	3.6
6	1	60ft (18.8m)	120	8.5	PZ 22	1.5	N/A		2.30	N/A	56.0	7.5
	2	60ft (18.8m)	120	8.5	PZ 22	1.5	2	6m	2.20	N/A	61.0	8.6
	3	60ft (18.8m)	120	8.5	PZ 22	1.5	6	6m	2.10	N/A	58.9	8.2
	4	100ft (30.5m)	200	8.5	PZ 22	2.5	N/A		10.70	N/A	35.9	2.0
	5	100ft (30.5m)	200	8.5	PZ 22	2.5	2	6m	7.30	N/A	49.5	3.2
	6	100ft (30.5m)	200	8.5	PZ 22	2.5	6	6m	6.60	N/A	54.3	3.7
7	1	60ft (18.8m)	120	8.5	PZ 22	1.5	N/A		2.30	0.22	56.0	7.4
	2	60ft (18.8m)	120	8.5	PZ 22	1.5	N/A		2.60	-0.37	42.9	4.9
	3	100ft (30.5m)	200	8.5	PZ 22	1.5	N/A		4.80	0.34	35.5	3.1
	4	100ft (30.5m)	200	8.5	PZ 22	1.5	N/A		5.00	1.24	28.7	2.6
8	1 (sand)	60ft (18.8m)	120	8.5	PZ 22	1.5	N/A		2.32	0.22	56.0	7.4
	2 (rock)	60ft (18.8m)	120	8.5	PZ 22	1.5	N/A		4.80	0.21	40.1	3.9
	3 (sand)	100ft (30.5m)	200	8.5	PZ 22	1.5	N/A		4.03	1.26	35.5	3.1
	4 (rock)	100ft (30.5m)	200	8.5	PZ 22	1.5	N/A		7.54	0.65	75.2	2.5

Y: considering water level, N: Not considering water level, FS: factor of safety

Chapter 7 Conclusions and Recommendations

7.1 Conclusions

Several preceding research and projects in the USA and Europe suggested that steel sheet pile walls could be a viable axial load-bearing foundation for a bridge abutment. Numerous benefits can be achieved when sheet pile walls are used as the main elements to sustain the axial and lateral loading, such as saving construction time and cost, and aesthetic advantages. In this research, the project team quantitatively evaluated the sheet pile-sand interface parameters using the team's large-scale direct shear testing setup. The test results were used as the input parameters to assess the bearing capacity of sheet piles in the field test and numerical study. The large-scale direct shear test results showed good agreement with the literature in terms of the submerged *vs*. dry condition comparison. With an internal frictional angle of backfill sand at 34° and a relative density of 70%, the resultant sheet pile-soil friction angle was obtained as 27°, which was about 4/5 of the internal friction angle of soil.

The project team conducted static axial loading tests with a down-sized test sheet pile at the controlled test site. Soil characterization and in-situ tests were conducted to estimate the bearing capacity of the sheet pile by analytical, SPT-based, and CPT-based methods. The ultimate bearing capacity of the test sheet pile obtained from three separate static loading tests was consistently in the range of 35 kN to 37 kN (7.87-8.32 kips). Analysis based on the strain-gauge measurements showed that the pile shaft carried most of the load (70% to 75%), while the tip resistance contributed up to 25% of the total bearing capacity. The CPT-based method resulted in a good match with the field test data, while the analytical method and SPT-based method appeared to slightly over- and under-estimate the side frictional resistance, respectively. Nonetheless, all predictions were comparable to the static loading test results. The result from the

numerical modelling was also in agreement with the field test data. In the field test, sheet piles were not plugged due to a specialized pile installation process to protect strain gauges.

Upon the completion of large-scale direct shear tests and down-sized field loading tests, the project team conducted a numerical parametric study of the sheet pile abutment system for several design factors. The numerical simulation model was validated for the case of axial loading alone, lateral loading alone, and combined axial and lateral loading for the parametric study. For the selected bridge site and hypothetical treatment of the sheet pile abutment system, salient observations were obtained as follows:

- The cantilever sheet pile wall sustained the combined axial and lateral loading with maximum horizontal deflection of less than 1 inch for bridge-span lengths up to 60 feet and excavation levels up to 1.5 m (~5 ft). With the anchored wall, the sheet pile abutment system sustained the combined loads even beyond the 60 ft span length at the reasonable maximum horizontal deflection (1-2 inches).
- For all considered case studies in this project, the vertical settlement of the sheet pile abutment system was less than 1 inch.
- For all considered case studies in this project, the factor of safety values against the shear and bending failures were greater than 2.0. Therefore, the serviceability of the sheet pile abutment system, such as horizontal deflection and vertical settlement, was a primary design factor rather than the mechanical integrity of the sheet pile wall.
- Increasing the section modulus (for example, PZ22 → PZ27 → PZ35) can have helped to reduce the horizontal deflection of the sheet pile wall, at the expense of a slight increase in the vertical settlement.
- Increasing the pile length could have helped to reduce both the horizontal deflection and vertical settlement of the sheet pile abutment.

- For the anchored wall configuration, the length and spacing of anchors needed to be carefully designed to ensure that the maximum horizontal deflection of the sheet pile wall did not exceed a predetermined limit.
- Fluctuation of the water level (e.g., submerged *vs*. dry conditions in this study) may have led to substantial differences in the shear force and bending moment imposed on the sheet pile wall, while its impact on the horizontal deflection and vertical settlement of the sheet pile was trivial.
- End-bearing of the sheet pile on the rock may have helped to reduce the vertical settlement of the sheet pile abutment system. However, the maximum horizontal deflection increased up to 50%, compared to the soil end-bearing condition. One possible mechanism was that the firmer end-bearing condition may have magnified the P-Delta (P-Δ) effect when the sheet pile was subjected to the combined axial and lateral loading.
- The influence of thermal loading in the case of the semi-integral abutment bridge during seasonal temperature fluctuations may have increased or decreased the maximum horizontal deflection of the sheet pile wall by ± 0.2-0.3 inches for a bridge-span length of 40 - 100 ft. Such an influence could have been lessened when the sheet pile wall was anchored. On the other hand, the factor of safety against shear and bending failures was not significantly affected by the bridge abutment design (that is, conventional *vs*. semi-integral abutment).

In conclusion, the sheet pile abutment system can be a reliable option to support the combined axial and lateral loading for short-span bridges. Bridge design elements, such as the span length, excavation depth, sheet-pile type, sheet-pile length, adoption of anchors and Deadman concrete, need to be carefully checked to meet the criteria relating to the horizontal

deflection and vertical settlement of the sheet-pile wall, as well as the factor of safety against shear and bending failures of the sheet-pile wall.

7.2 Recommendations for Future Work

Based on the research findings from the down-sized field tests, numerical studies, and literature reviews, recommendations for future work can be made as follows:

- A sheet pile wall is a group of sheet piles. Most preceding studies focused only on the bearing capacity of a single sheet pile, not sheet pile rows. A full-scale static loading test with sheet pile rows may be beneficial to add confidence to the bearing capacity of the sheet pile abutment system.
- Most literature and this research conducted static loading tests of sheet piles on sand. Other soil conditions, such as silty or clayey soils, need to be examined to better understand how sheet piles may behave in different soil situations. Upon the study results, revised prediction methods based on either CPT, SPT, or analytical calculations, need to be suggested to facilitate the design of the sheet pile abutment system in different geologic regions.
- Other failure criteria of the sheet pile, such as a buckling failure, should be investigated.
- The concept of pile plugging also needs to be examined further in depth to better estimate the bearing capacity of sheet piles. The plugging phenomenon may occur when the sheet piles are driven into the soil (Figure 7.1). Consequently, it may increase the tip bearing resistance of the sheet pile.

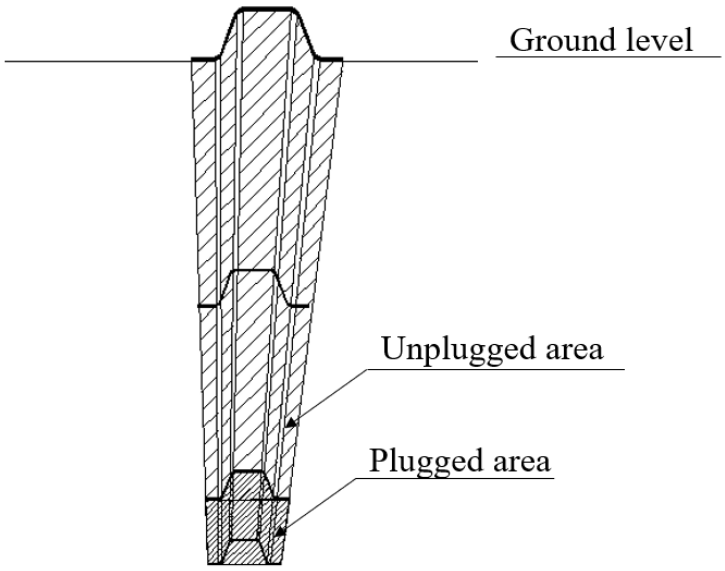

Figure 7.1 An example of the unplugged and plugged area in the sheet pile.

- The side frictional resistance appears to be a primary contributor to the axial load bearing capacity of a sheet pile. When soil is excavated at one side, the lateral movement of the sheet pile from the backfill soil may result in both the active and passive soil zones along the sheet-pile length. It may make the distribution of side frictional resistances quite complex. With that, the side friction along the active zone of the sheet pile may be neglected up to the point of stability, similar to the approach in some literature. However, with the anticipated increase in the sheet pile length to support the axial load, active and passive zones are likely to exist for both the front and back of the sheet-pile wall. More in-depth studies are warranted to better understand the mobilization of side frictional resistances in such a case.

Considering all these factors, more field loading tests with an actual scale of sheet pile are recommended to confirm the validity of the sheet pile abutment system. First, it is needed to investigate the drivability of the sheet piles by using an impact hammer vs. a vibratory hammer.

PDA tests can be performed during the driving of sheet piles with an impact hammer to ensure quality assurance (QA) and quality control (QC). To ensure the effectiveness of the PDA method for assessing the pile installation and generating bearing resistance of the pile, its applicability must be verified for the purpose of QA/QC. A CPT test is also recommended to compare the CPT-based prediction of the bearing capacity. The project team recommends conducting the combined axial + lateral loading tests at a field test site to corroborate the findings on the horizontal deflection and vertical settlement of the sheet pile from this study. Several instrumentations, including the horizontal and vertical LVDTs, pressure cells in both front and behind the sheet-pile wall, and multiple strain gauges mounted along with the sheet-pile length, are recommended for such full-scale field loading tests. In addition, the P-Delta effect needs to be further analyzed by using the anticipated field test data. Lastly, it is recommended to compare the PDA test results and CPT-based predictions with the field loading test data to help the quality control of sheet piles for an application to short-span bridges in Nebraska.

References

ASCE. (1996). “Design of sheet pile walls” Technical Engineering and Design Guides as Adapted from the US Army Corps of Engineers, no. 15.

ASTM. (2015). ASTM C136-06 - Standard test method for sieve analysis of fine and coarse aggregates.

ASTM. (2017). ASTM A572/A572M-12 - Standard specification for high-strength low-alloy Columbium-Vanadium structural steel.

ASTM. (2020a). ASTM D1143/D1143M-20 - Standard test methods for deep foundation elements under static axial compressive load.

ASTM. (2020b). ASTM D5778-20 - Standard test method for electronic friction cone and piezocone penetration testing of soils.

ASTM. (2021). ASTM D5321/D5321M-20 - Standard test method for determining the shear strength of soil-geosynthetic and geosynthetic-geosynthetic interfaces by direct shear.

ASTM. (2022). ASTM D1586/D1586M-18e1 - Standard test method for standard penetration test (SPT) and split-barrel sampling of soils.

Bowles, J. E. (1977). Foundation Analysis and Design, 750pp.

Burke, M. P. (1994). “Semi-Integral Bridges: Movements and Forces” Transportation Research Record (TRR) 1460, TRB, National Research Council, Washington, D.C., pp. 1-7.

Bustamante, M. and Gianeselli, L. (1991). “Predicting the bearing capacity of sheet piles under vertical load” In Proceedings of the 4th International Conference on Piling and Deep Foundations, Stresa, Italy, pp. 1-8.

Carle, R. and Whitaker, S. (1989). “Sheet piling bridge abutments” In Deep Foundations Institute Annual Meeting, Baltimore, Maryland, pp. 1-16.

Chung, H. I., Kim, B., Oh, I. K., and Yoo, J. (2004). "Application of steel sheet pile embedded retaining wall as a bridge abutment" Geotechnical Engineering for Transportation Projects, 2, pp. 2186-2194.

Das, B. M. (1994). Principles of Geotechnical Engineering, PWS-Kent. Boston. MA.

Davisson, M. T. (1972). "High capacity piles" Proc. Innovations in Foundation Construction, 52.

Day, R. A. and Potts, D. M. (1993). "Modelling sheet pile retaining walls" Computers and Geotechnics, 15(3), pp. 125-143.

Evans, R., White, D., and Klaiber, W. (2012). "Modified sheet pile abutments for low-volume road bridges." Final Report, Iowa Highway Research Board (IHRB) TR-568.

Federal Highway Administration (2009). "Bridge scour and stream instability countermeasures – Experience, selection, and design guidelines" Third Edition, Report FHWA-HHI-09-111, Hydraulic Engineering Circular (HEC) No. 23, U.S. Department of Transportation, Washington, D.C., 255 p.

Federal Highway Administration (2012a). "Evaluating scour at bridges" Fifth Edition, Report FHWA-HIF-12-003, Hydraulic Engineering Circular (HEC) No. 18, U.S. Department of Transportation, Washington, D.C., 340 p.

Federal Highway Administration (2012b). "Stream stability at highway structures," Fourth Edition, Report FHWA-HIF-12-004, Hydraulic Engineering Circular (HEC) No. 20, U.S. Department of Transportation, Washington, D.C., 328 p.

Itasca (2016). "FLAC-Fast Lagrangian Analysis of Continua," Version. 8.0, Itasca Consulting Group, lnc.

Liao, S. S. and Whitman, R. V. (1986). "Overburden correction factors for SPT in sand" Journal of Geotechnical Engineering, 112(3), pp. 373-377.

Lichtenstein Consulting Engineers (2001). “Manual for condition evaluation and load rating of highway bridges using load and resistance factor philosophy” National Cooperative Highway Research Program (NCHRP) Project C12-46 Web Document, 28.

Mansur, C. I. and Hunter, A. H. (1970). “Pile tests-Arkansas river project.” Journal of the Soil Mechanics and Foundations Division, 96(5), pp. 1545-1582.

McShane, G. (1991). “Steel sheet piling used in the combined role of bearing piles and earth retaining members.” In Proceedings of the 4th International Conference on Piling and Deep Foundations, Stresa, Italy (Vol. 112, p. 113).

Meyerhof, G. G. (1976). “Bearing capacity and settlement of pile foundations.” Journal of the Geotechnical Engineering Division, 102(3), pp. 197-228.

Meyerhof, G. G. (1956). “Penetration tests and bearing capacity of cohesionless soils.” Journal of the Soil Mechanics and Foundations Division, 82(1), 866-1.

Mullins, G. and Stokes, M. (2009). “Influence of cantilever sheet pile deflection on adjacent roadways: final report” June 2009 (No. BD-544-40). University of South Florida.

Nebraska Department of Roads, Bridge Division. (2016). “Bridge office policies and procedures, BOPP 2016” Last updated: December 2016.

Nottingham, L. and Schmertmann, J. (1975). “An investigation of pile capacity design procedures.” Final Report D629 to Florida Department of Transportation, Department of Civil Engineering, University of Florida.

Nucor Skyline (2022). Technical product manual.

Nucor Skyline (2021). Steel sheet pile bridge abutment technical design manual. Published in partnership with Michael Baker International.

Panchal, J. P., McNamara, A.M., and Goodey, R.J. (2020). “Sheet pile groups as an alternative foundation solution to cast-in-situ concrete piles,” International Journal of Physical Modelling in Geotechnics, 20(2), pp. 83-96.

Peck, R. B., Hanson, W. E., and Thornburn, T. H. (1974). Foundation Engineering. John Wiley & Sons. Inc, New York.

Rahman, M. M. (2020). “Foundation design using standard penetration test (SPT) N-value.” Bangladesh Water Development Board.

Razmi, J., Ladani, L., and Aggour, S. M. (2014). “Finite element simulation of pile behaviour under thermo-mechanical loading in integral abutment bridges.” Structure and Infrastructure Engineering, 10(5), pp. 643-653.

Rybak, J. and Żyrek, T. (2013). “Experimental validation of sheet pile and combined pile axial capacity computation.” In 11th Slovak Geotechnical Conference Water Effects on Geotechnical Constructions, pp. 3-4.

Schmertmann, J. H. (1978). “Guidelines for cone penetration test: performance and design (No. FHWA-TS-78-209).” United States. Federal Highway Administration.

Song, C.-R., Al-Ostaz, A., Cheng, A. H.-D., and Mantena, P. (2012). “Structural, material, and geotechnical solutions to levee and floodwall construction and retrofitting.” Final report submitted to DHS/SERRI.

Sotiropoulos, F. and Diplas, P. (2017). “Scour at the base of retaining walls and other longitudinal structures,” NCHRP 24-36 Final Report, Transportation Research Board, Washington, D.C., 143 p.

Steel Construction Institute. (1998). “Design guide for steel sheet pile bridge abutments.” United Kingdom.

Sylvain, M. B. (2019). “A study on soil-structure interaction of axially loaded sheet piles” (Doctoral dissertation, The University of North Carolina at Charlotte).

Sylvain, M. B., Pando, M. A., Whelan, M. J., Rice, C. D., Ogunro, V. O., Park, Y., and Koch, T. (2017). “Case history of a full scale axial load test of sheet piles,” ASCE Geotechnical Frontiers, GSP 279, pp. 355-365.

Taenaka, S., Otani, J., Tatsuta, M., and Nishiumi, K. (2006). “Vertical bearing capacity of steel sheet piles.” 6th International Conference on Physical Modelling in Geotechnics - Physical Modelling in Geotechnics, pp. 1-6.

Underwood, C. A. (2020). “The use of steel sheet pile as permanent building foundation walls: lessons learned over 15 years of design in Minneapolis, Minnesota, USA.” In Geo-Congress 2020 (pp. 68-77). Reston, VA: American Society of Civil Engineers.

Underwood, C. A. and Greenlee, R. M. (2010). “Steel sheet pile used as permanent foundation and retention systems-design and construction,” In Earth Retention Conference 3 (pp. 129-136).

Yandzio, E. (1998). “Design guide for steel sheet pile bridge abutments.” SCI-P-187, The Steel Construction Institute, Berkshire, UK.